Regulated systems of I-SceI expression for in-depth studies of the biological effects of DSBs and DSB clusters

Inaugural-Dissertation

zur

Erlangung des Doktorgrades

Dr. rer. nat.

der Fakultät für Biologie

an der

Universität Duisburg-Essen

vorgelegt von

Mohammad Sharif Mortoga Hasan

aus Bandarban, Bangladesch

July, 2020

DOI: 10.17185/duepublico/73597
URN: urn:nbn:de:hbz:464-20211122-081921-7

Die der vorliegenden Arbeit zugrunde liegenden Experimente wurden am Institut für Medizinische Strahlenbiologie am Universitätsklinikum Essen durchgeführt.

1. Gutachter: Prof. Dr. Georg Iliakis

2. Gutachter: Prof. Dr. Verena Jendrossek

Vorsitzender des Prüfungsausschusses: Prof. Dr.Dominik Boos

Tag der mündlichen Prüfung: 20.11.2020

The output of your PhD is not your thesis. The output is YOU!

Anonymous!

This PhD thesis work is dedicated to my beloved parents and all my well-wishers!

TABLE OF CONTENTS

List of commonly used abbreviations

53BP1	p53 binding protein
γ-H2AX	phosphorylated H2AX at S139
Aa	Amino acid
ADP	Adenosine diphosphate
alt-EJ	Alternative end joining
ATM	Ataxia telangiectasia mutated kinase
ATP	Adenosine triphosphate
ATR	ATM and Rad3 related kinase
BLM	Bloom syndrome protein
bp	base pair
BRCA1/2	Breast cancer susceptibility protein1/2
BSA	Bovine serum albumin
CDK	Cyclin-dependent kinase
Chk1/2	Checkpoint kinase 1
CHO	Chinese Hamster Ovary
CR	Chromosomal rearrangements
CLSM	Confocal laser scanning microscopy
CMV	Cytomegalovirus
c-NHEJ	classical non-homologous end joining
CO_2	Carbon dioxide
CSR	Class switch recombination
CRs	chromosomal rearrangements
CtIP	C-terminal binding protein interacting protein

Da	Dalton
DAPI	4',6-diamidino-2-phenylindole
DDR	DNA damage response
DEQ	Dose equivalent
DMEM	Dulbecco's modified eagle's medium
DMSO	Dimethyl sulfoxide
DNA	Deoxyribonucleic acid
Dna2	DNA replication helicase/nuclease DNA2
DNA-PK	DNA-dependent protein kinase
DNA-PKcs	Catalytic subunit of DNA-PK
DR	Dose response
DSB/s	Double strand break/s
DSBR	Double-stranded break repair
dsDNA	Double stranded DNA
DTT	1,4-Dithiothreitol
EDTA	Ethylene diamine tetraacetic acid
EdU	5-ethynyl-2´-deoxyuridine
e.g.	*exempli gratia*
et al.	*et alii ('and others')*
Exo1	Exonuclease 1
eV	Electron Volt
FACS	Fluorescence activated cell sorting
FBS	Fetal bovine serum
FDR	Fraction of DNA released

GFP	Green fluorescent protein
GC	Gene Conversion
Gy	Gray (J/kg), unit of ionizing radiation dose
HEPES	4-(2-hydroxyethyl)-1-Piperazineethanesulfonic acid
HJ	Holiday Junction
HR(R)	Homologous recombination (repair)
i.e.	*id est* (‘it is’)
IF	Immunofluorescence
IR	Ionizing radiation
IRIF	Ionizing radiation induced foci
KAP1	KRAB (Krüppel-associated box) domain associated protein 1
LET	Linear energy transfer
MDC1	Mediator of DNA damage checkpoint protein 1
MMEJ	Microhomology mediated end joining
Mre11	Meiotic recombination 11
MRN complex	Mre11/Rad50/Nbs1 complex
Nbs1	Nijmegen breakage syndrome (Nibrin)
NHEJ	Non-homologous end joining
PARP	Poly (ADP-ribose) polymerase
PAXX	Paralog of Xrcc4 and Xlf
PBS	Phosphate-buffered saline
PFA	Paraformaldehyde
PFGE	Pulsed-field gel electrophoresis
PI	Propidium iodide

PI3K	Phosphoinositide 3-kinase
PIKK	Phosphoinositide 3-kinase-related protein kinase
Plk1	Polo-like kinase 1
PMT	Photomultiplier tube
P/S	Penicillin and streptomycin
PTIP	PAX transactivation activation domain-interacting protein
Puro	Puromycin resistance gene
RAP80	Receptor-associated protein 80
RE	Restriction enzyme
RIF1	RAP1-interacting factor 1
RNF8/168	Ring finger protein 8/168
ROS	Reactive oxygen species
RPA	Replication protein A
rpm	revolutions per minute
SDSA	Synthesis dependent strand annealing
Ser	Serine
SSA	Single strand annealing
SSB	Single strand break
ssDNA	Single stranded DNA
SQ/TQ	Serine or threonine followed by glutamine
Wt	Wild-type
XLF	Xrcc4-like factor
XRCC1/2/3/4	X-ray cross-complementing protein 1/2/3/4

List of figures

List of tables

I Introduction

Deoxyribonucleic acid (DNA) is the fundamental carrier of genetic information in all-living organisms. It is constantly exposed to a myriad of endogenous as well as exogenous damaging agents, which pose great threat to the integrity of the genome. On a daily basis each cell in human body confronts thousands of DNA lesions. As a consequence, many breaks can occur in the structure of DNA including DNA double strand breaks, single strand breaks, base damage and sugar lesions. Of all types of lesions, DSBs are the most deleterious lesions, which if left unrepaired or mis-repaired can result in adverse biological effects such as genomic rearrangements and carcinogenesis. To faithfully protect the cells from such threats and ultimately maintain genome integrity, cells have evolved various DSB repair pathways that are coordinated with the cell cycle. Homologous recombination repair (HRR) and classical non-homologous end joining (c-NHEJ) are the major pathways contributing to the removal of DSBs (JR, MR, and SJ 2012). While HRR is active only in late S and G2 phase, c-NHEJ pathway dominates throughout the entire cell cycle particularly in G0 and G1 cell cycle phases. In absence of HRR and/or c-NHEJ, cells instead repair DSBs using a back-up pathway termed as alternative end joining pathway (alt-EJ) (Iliakis, Mladenov, and Mladenova 2019). In our present study, we focus on DSB repair pathways involved in repair in G0 phase of the cell cycle. Furthermore the role of one of resection components, CtIP in mediating repair of both DSB lesions and chromosome breaks, is emphasized. Finally, we delineate via a biological model system the mechanism of high-LET irradiation in eliciting adverse biological consequences.

1 Ionizing radiation

Ionizing radiation (IR) is an energetic radiation process in which deposited energy is sufficient enough to expel one or more tightly bound electrons from an atom or a molecule. A prominent feature of IR is its ability to release a significant amount of energy in a location dependent manner. The amount of energy released per ionization event is approximately 33 electronvolts (eV). Such an ionizing event is more than enough to break a strong chemical bond, for example, the bond energy associated with C=C is about 6.24 eV. Ionizing radiations are of two types: electromagnetic radiations and particulate radiations. X-rays and γ-rays are considered as electromagnetic radiations, whereas protons, α-particles, neutrons and heavy charged ions belong to particulate types of radiation.

Radiation density of particulate radiation is described by its physical quantity; linear energy transfer (LET), a unit (keV/μm) by which the deposited energy in ionizing events per unit length of particle track is measured. This physical parameter is defined as the amount of energy transferred into the material by ionizing particles per unit length along the track. Depending on the speed and charge of the particles, LET can vary significantly. Owing to the limited interactions per tract of the secondary electrons produced, X-rays and γ-rays are considered as low-LET radiation. X-ray and γ-rays are also referred to as indirectly ionizing modality as they lose their energy to produce secondary electrons in order to generate damage. On the other hand protons, α-particles, neutrons and heavy charged ions belong to high-LET radiation because they produce dense ionizations along with their radiation track. Because of their sufficient kinetic energy and their potential to distort the atomic structure in the absorbing material, they are referred to as densely ionizing radiation modality (Hall and Giaccia n.d.; Hill 1999).

In radiation biology, the unit to measure the quantity of ionizing radiation is gray (Gy), which is a derived unit of ionizing radiation in the International System of Units (SI). It measures the amount of energy absorbed per unit of mass of the exposed matter (organ or tissue) and is defined as joules per kilogram (J/Kg). One Gy (1 Gy) of absorbed dose is defined as the absorption of one joule of energy by one kilogram of exposed matter. Equal doses of different types of irradiation are not equivalent in manifesting adverse biological effects to exposed human tissues or tumors. Given that, at the same radiation dose, the biological effects of high-LET radiations are in principle higher than those of the low-LET radiations. Alpha particle or α-particle for a given absorbed dose of 1 Gy will produce greater harm compared to X-rays. This increased efficacy is associated with inherent characteristics of high-LET radiation to deposit most of its energy within a small volume and ultimately cause complex biological damage (Goodhead and Nikjoo 1989).

1.1 Physical properties of ionizing radiation

X-ray photons as a form of electromagnetic radiation engage in interactions with the absorbing material electrons either by Compton interaction or by photoelectric interaction. The former one is the main cause of scattered radiation in absorbing material due to the interaction of photon with the loosely bound outer shell electron. Following interaction of photon with orbital electron, photon imparts part of its energy to the electron (known also as Compton electron) as kinetic energy that propels the electron from the outer shell of the atom. The resultant incident photon with its altered direction in the absorbing material will have a

different wavelength as well as a different but reduced energy. Owing to the change in the direction of the photon, this form of absorption is therefore known as a scattering process. While liberated electrons have the potential to travel and cause ionization events, scattered photons with reduced energy can take part in further interactions. These electrons including those produced by further interaction of scattered photons and produced electrons are known as secondary electrons. At high X-ray energy , the Compton-scattered radiation is much more predominant than photoelectric interaction and is the most dominant interaction mechanism in human tissues that are irradiated in the diagnostic and therapeutic range (30 keV to 30 MeV) (Hall and Giaccia n.d.).

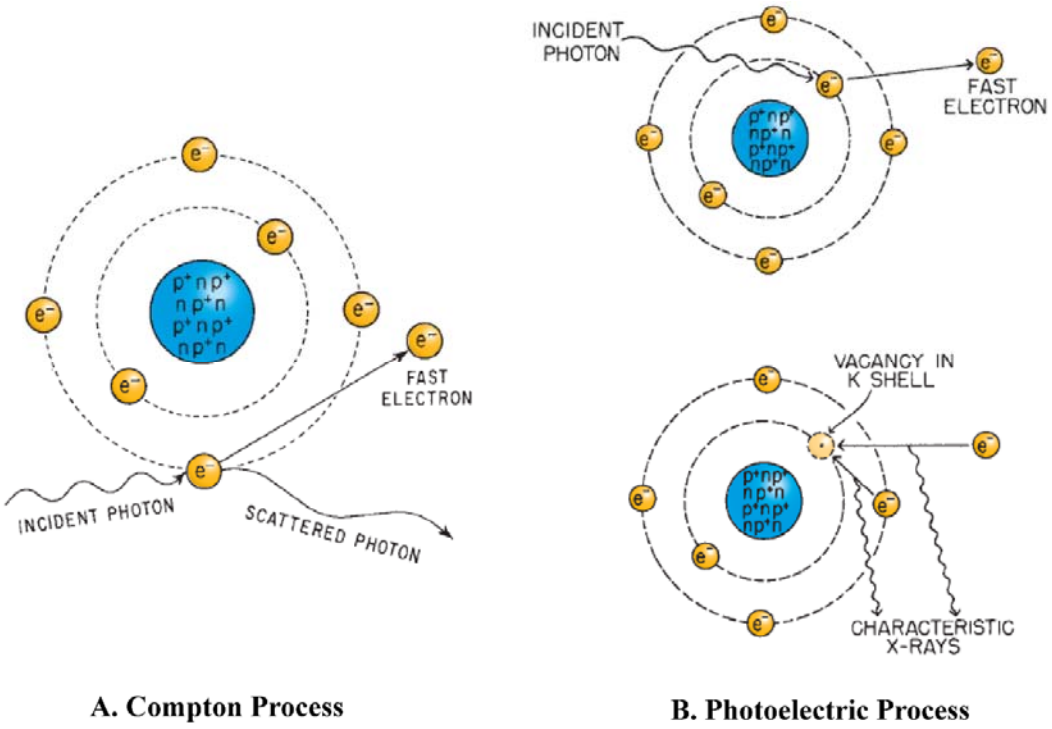

Figure 1 Schematic depiction of absorption of an X-ray photon by (A) Compton scattering and (B) the photoelectric process. In Compton interaction (A), incident X-ray photons interact with weakly bound orbital electrons of an atom of the absorbing molecule. Part of the photon energy is imparted to the electron as kinetic energy. The incident photon, deflected from its original path, moves along on its path with longer wavelength and reduced energy. On the other hand, photoelectric effect (B) involves interaction between the photon and a tightly bound planetary electron of an atom of the absorber. During the interaction, photons transfer the entire energy to inner shell electrons (K shell) that, in turn, ejects them from the atom (B: top panel). An electron from an outer orbit or from outside the atom fills the vacancy left in atomic shell (change of energy level in electrons) and releases a photon, whose energy is characteristic to the atom (B: bottom panel). Image Source (Hall and Giaccia n.d.).

By contrast, in the low X-ray energy regime, the photoelectric interaction is more probable. In this process, the photon bounces off the tightly bound electron in one of the atomic shells most probably in the inner shell of the absorbing material. The energy absorbed from the photon is equivalent to the kinetic energy of the liberated electron and binding energy of the electron combined. Liberated electrons are known as photoelectrons. In order to stabilize the atom, an electron either from the outer shell or from outside the atom fills the vacancy in the inner shell. The drop in energy of the filling electron is emitted as characteristic radiation (X-ray photon) that depends on the binding energy of the electrons involved. Identical to Compton process, electrons with fast kinetics are produced in this form of interaction which can further ionize the constituents of the absorbing materials thereby inducing biological damage.

The adverse biological effects of radiation results in principle from damage in DNA and the action of radiation can be of direct or indirect depending on the form of radiation modality. In the event of high-LET radiation such as neutrons or α-particles, direct action of radiation is the dominant process. Indirect action of radiation, on the other hand, causes damage to the target cells by interacting with other atoms or molecules (mostly H_2O) in the cell. This indirect mode of action generates reactive oxygen species (ROS) that have the capability to diffuse and damage other biomolecules. In the case of DNA, IR may lead to the formation of different lesions, such as DNA double strand breaks (DSBs), single strand breaks (SSBs), base or sugar backbone damages.

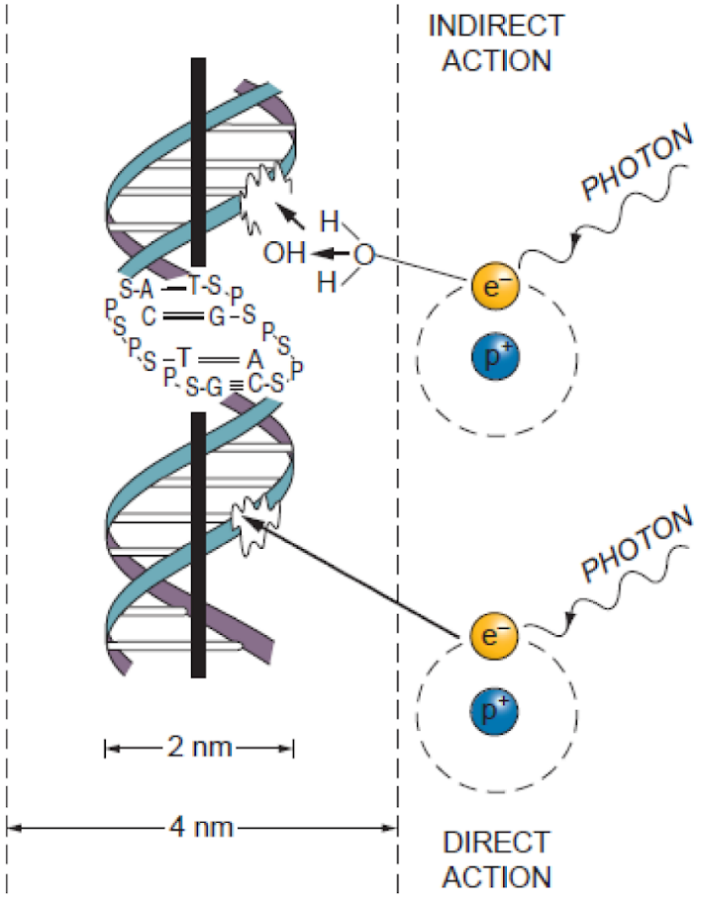

Figure 2 Schematic illustration of direct and indirect actions of radiation on the DNA. In direct action of radiation, a secondary electron resulting from absorption of an X-ray photon hits directly the DNA to produce an effect (breaks the chemical bonds), whereas in indirect form of radiation, hydroxyl radical (OH·) produced from an interaction between secondary electron and water molecule causes indirect damage to the DNA. The DNA helix has a diameter of about 20 Å (2 nm). It is estimated that free radicals produced in a cylinder with a diameter double that of the DNA helix can affect the DNA. Indirect action is dominant for sparsely ionizing radiation, such as X-rays. S, sugar; P, phosphorus; A, adenine; T, thymine; G, guanine; C, cytosine. Image source (Hall and Giaccia n.d.).

In indirect form of radiation, formation of highly reactive hydroxyl radical (OH·) follows a two-step reaction. In the first step, water molecule (H_2O) present in the cell interacts with a photon released from X-or γ-ray and ultimately becomes ionized. This reaction is expressed as:

$$H_2O \rightarrow H_2O^+ + e^-$$

In this particular reaction, H_2O^+ is an ion radical and is electrically charged since it has already lost an electron. Owing to its inherent charged status and having an unpaired electron, H_2O^+ shows characteristics of an ion as well as of a free radical. The ion radical of H_2O in the following step reacts with another water molecule thus forming the hydronium-cations and highly reactive hydroxyl radical (OH·). The reaction is as follows

$$H_2O^+ + H_2O \rightarrow H_3O^+ + OH\cdot$$

The final product; hydroxyl radical, diffuses to the target molecule of the cell, DNA. It is estimated that about two thirds of the X-ray damage to DNA in mammalian cells is caused by indirect action of radiation.

1.2 Induction of DNA damage

Cells are continuously exposed to various intrinsic and extrinsic DNA damaging agents which cause DSBs. DSBs pose a great threat to the survival of the cell and are a major driver of genomic instability. In addition to generating DSBs, irradiation results in damaged nucleotides, base damages and single strand breaks (SSBs). Irradiation of a cell with 1 Gy of X-rays theoretically generates approximately 20-40 DSBs, 1000 SSBs and more than 1000 base damages (Hall and Giaccia n.d.; Ward 1985). Despite the severity of these DNA lesions, the cell nevertheless can engage multiple repair mechanisms to protect its genome integrity. Not surprisingly, the degree of DSB complexity is mainly dependent on the parameter of LET. It is widely known that biological effects of DSBs derived from high-LET are more complex than that produced by low-LET. Other than creating single DSBs, high-LET radiation modality generates also DSB-clusters; a phenomenon where multiple DSBs are located in close proximity. This poses more threats to the survival of the cell as it may cause chromatin destabilization locally thereby undermining the processing of DSBs. The associated vital factor is indeed the event of cluster of ionization, which renders the degree of complexity and causes biological damage. As such, DSBs generated within clusters of ionization can differ greatly between sparsely ionizing radiation (low-LET) and densely ionizing radiation (high-LET) (Iliakis et al. 2019; Schipler and Iliakis 2013).

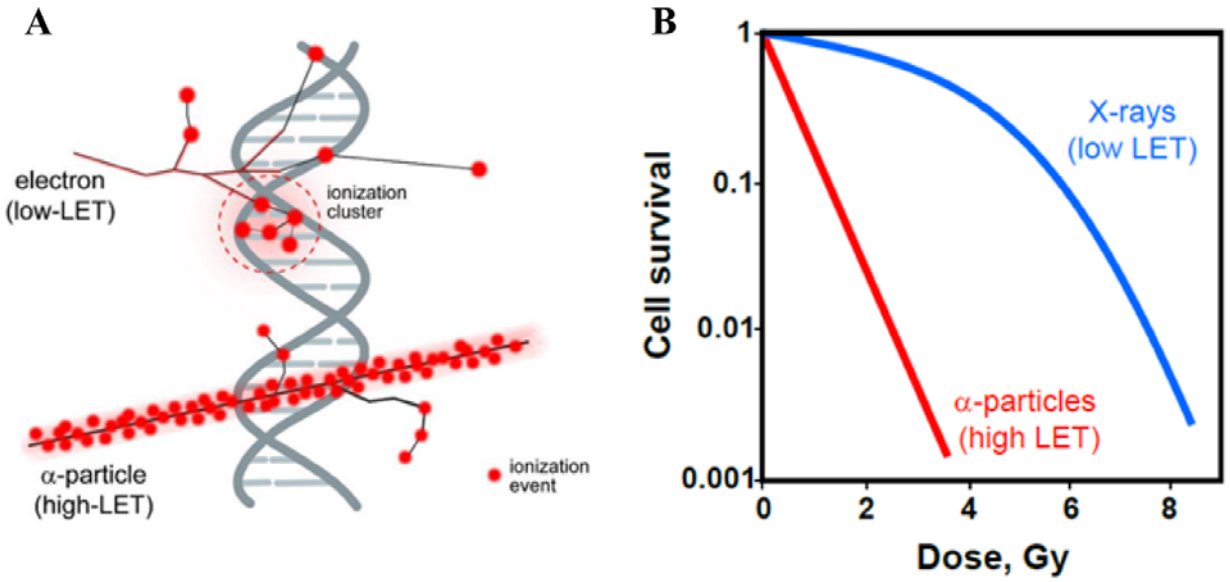

Figure 3 DNA damage induction by low and high LET radiation. (A) Generation of ionization clusters by low and high LET radiation. In the event of ionizations, IR localizes along the radiation track. Note that high LET radiation produces more clustered DNA damage as the density of ionizations is very high (see the ionization event for α-particle). Schematic is adapted from (Iliakis, Mladenov, et al. 2019). **(B)** Survival curve plot following exposure of cells to low and high LET radiation modality. Graph is adapted from (Iliakis et al. 2019).

In the current study, radiation of both modalities (low-LET: X-rays and high-LET: α-particles) were used to generate DNA damage in cells and study the DSB repair mechanisms. Moreover, I-SceI homing endonuclease; a biological means of generating DSBs mimicking the biological effect of high-LET has also been extensively used in our biological rodent model system. In the system integration of multiple I-SceI cutting sites in the genome in close proximity that result in clustered I-SceI induced DSBs mimics the effect of high-LET (Schipler et al. 2016).

1.2.1 DNA double-strand break – a potential threat for genomic stability

Maintenance of genome stability, supported by efficient and accurate repair of DNA lesions, is fundamental for cellular homeostasis and survival in cells of eukaryotes. Yet continuous exposure of cells to various environmental and endogenous DNA damaging agent's imbalance their genomic integrity and continuity of DNA molecules thus creating breaks in the DNA structure. DSBs are the most deleterious lesions and are formed in cells exposed to DNA damaging agents like ionizing radiation (IR) and anti-cancer drugs. Moreover, they also form in a variety of physiological processes including transcription, meiosis, V(D)J recombination, immunoglobulin heavy chain class switch recombination (CSR) and at collapsed replication forks during DNA replication (Alt et al. 2013). Consequently, cells have

evolved internal repair mechanisms to act on these detrimental breaks and they are activated once DSB inducing agents pose threats to the cells. This mechanism is known as DNA damage response (DDR). If left unrepaired or in case of misrepair event, it leads to gross chromosomal rearrangements thus trigger the formation of deletions, mutations and importantly, chromosomal aberrations, which may result in genomic instability, an evolving hallmark of cancer cells. As such, failure in efficient repair of DSBs will lead to the development of various human syndromes and is often associated with ageing, neurological disorders, developmental defects, immunodeficiency and cancer (Cornforth and Bedford 1993; Iliakis et al. 2004; Jackson and Bartek 2009).

1.3 Forms of DSBs and their level of complexity

DNA double strand breaks (DSBs) can be induced by means of exploiting routinely used restriction enzymes (such as I-SceI) or through IR (high or low LET). I-SceI is a restriction enzyme with 18bp non-palindromic sequence, which can be artificially integrated into the genome thus DSBs at the I-SceI sites can be introduced. Restriction endonucleases (REs) generated DSBs can create ends that are of blunt or staggered. While RE-induced DSBs disrupt the double-stranded DNA molecule without altering its nucleotides chemically, DSBs induced by IR distort DNA structure by altering chemically minimum of two constituent building blocks (nucleotides) in opposite strands and is directly ascribed to the ionization event within an ionization cluster. Owing to the presence of chemically altered residues at the DSB ends and their incompatibility for ligation require end-processing. IR generated DSBs therefore require end processing prior to end joining. Moreover, the process of irradiation results in damaged nucleotides, base damages and single strand breaks in the vicinity of DSBs thus adding more complexity to the lesions.

Hence, DSBs are of different categories. Therefore in the following section we will address various types of DSBs that can be created by means of biological, chemical or physical methods.

1.3.1 T1-DSB: Nuclease generated DSB, a simple form of DSB with ligatable ends

DSBs generated by restriction endonucleases (REs) disrupt the phosphodiester moiety and retain phosphate at 5´ (5´-phosphate) and hydroxyl at 3´ (3´-OH) in the DNA molecule, thus guarantee the formation of ligatable termini (Bryant and Johnston 1993; Obe and Natarajan 1985). As a consequence, RE-generated breaks can either have blunt or protruding ends. Therefore, rejoining the breaks by reforming the phosphodiester bond is, in principle, possible. Thus, RE induced DSBs are the simplest forms of DSB as they disintegrate the

continuity of DNA structure without chemical and structural alterations (illustrated in figure 4). Despite its simplicity in mediating ligation, the length of sticky ends and type (3-´or 5´-) can significantly affect the DSB processing efficiency. While DSB ends with protruding ends are easy to re-ligate, blunt ended DSBs are comparatively difficult to repair (van Gent and van der Burg 2007; Pfeiffer, Goedecke, and Obe 2000). Restriction endonucleases are frequently used in molecular biology to create DSBs of variable length by integrating their recognition sequence into the genome, for example, *I-SceI* homing endonuclease. This approach has gained significant attention in the light of a defined biological model system to study the detrimental biological effects of simple or complex forms of DSBs and the pathways involved in their elimination (Schipler et al. 2016).

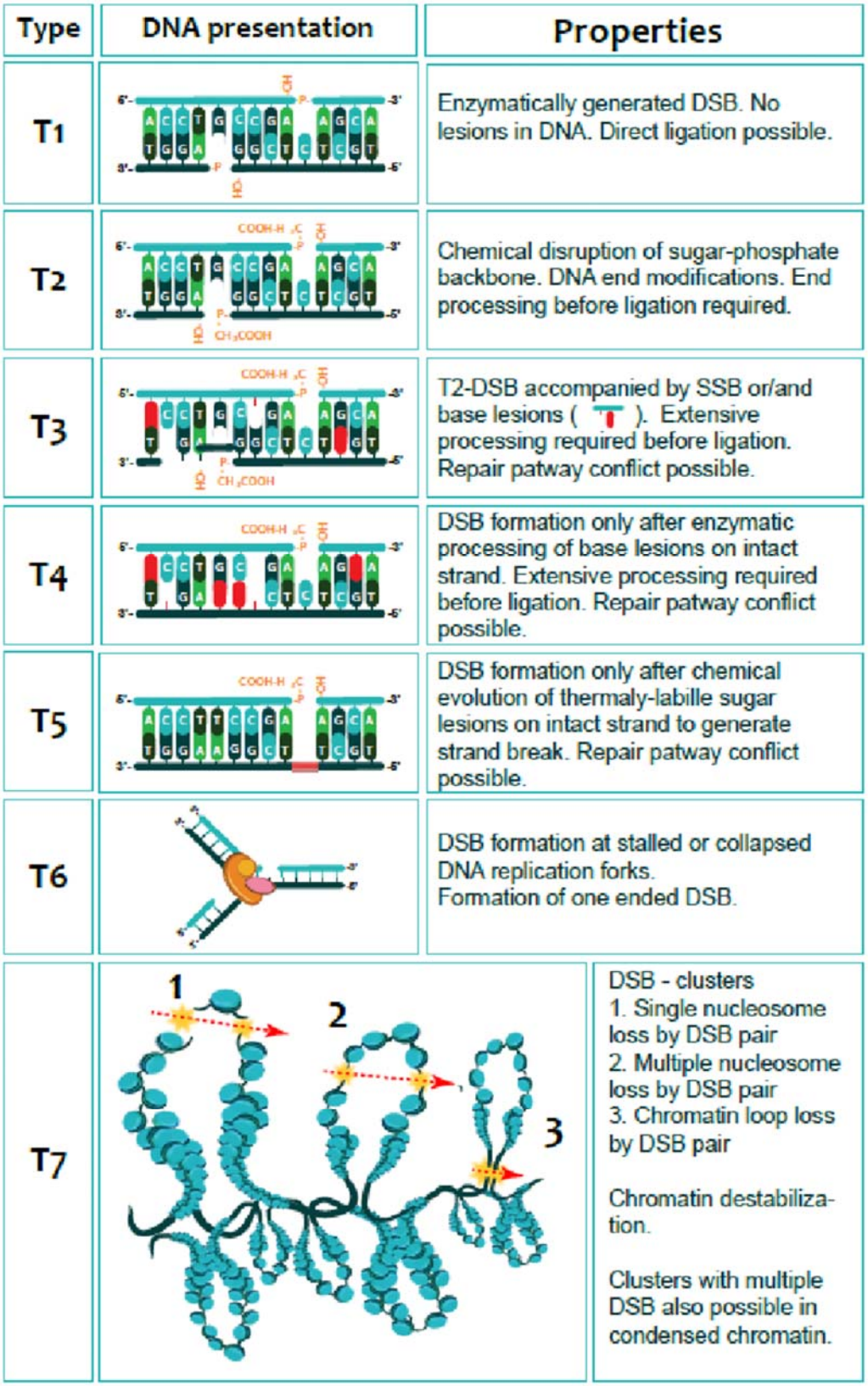

Figure 4 Schematic illustration of concepts utilized in the classification of DSBs according to their degree of complexity. Image source (Mladenov, Saha, and Iliakis 2018).

1.3.2 T2-DSB: Irradiation induced DSBs, simple DSBs with modified ends

Unlike RE-induced DSBs, DSBs generated by IR are likely to be distinct and characterized by chemically modified DNA termini due to the disruption of the sugar moiety. They typically bear modified and unligatable 3´damaged sugar in the form of phosphoglycolate (3´-CH_3COOH) and a 5´hydroxyl group (5´-OH) thus affecting the integrity of the DNA molecule (Povirk 2006). In this category of DSBs, complexity is derived via chemical modifications at or near the end and in any of the nucleotide constituents of DNA. As such, direct DNA ligation in these modified ends requires further end-processing steps so that repair can proceed. Moreover, IR induces a wide range of lesions via oxidation reactions (direct loss of an electron from atom or attack of dissociated OH· from radiolysis of water) including sugar and base damages and these lesions outnumbers DSBs by a ratio of 20:1 (Ward 1985). Certain forms of sugar damages can also distort the sugar-phosphate backbone of the DNA and produce thus SSBs. The co-occurrence of two discrete SSBs in opposite DNA strands with exclusion of around 10 nucleotides generates a DSB.

1.3.3 T3-DSB: Irradiation induced complex DSBs, locally multiply damaged sites

As noted above in the text, high-LET results in more complex types of DNA damage. As such, it will potentially comprise more breaks within one or two helical turns of the DNA. The presence of two or more DNA lesions consisting base or sugar damages within one turn of DNA helix increases the biological consequences and thus constitutes the proposed term called clustered damage sites (CDS) or locally multiply damaged sites (MDS) (Ward 1985). These forms of DSBs arise from CDSs and are accompanied with additional chemical modifications.

1.3.4 T4-DSB: Indirect DSB induced by enzymatic processing

In addition to the DNA damage clusters that are formed immediately after irradiation, radiation can also result in non-DSB clusters, which initially do not form DSBs but through processing of a base lesion opposite to an unrepaired SSB or through concurrent processing of two base damages on complementary strands turn into a DSB. This form of indirect DSBs adds another level of complexity. Evidence suggests that this type of clustered DSBs created from incomplete processing outnumbers type-2/type-3 DSBs after their exposure to low-LET radiation by approximately 4:1. The degree of reparability of non-DSB clusters is dependent on their composition, spacing and polarity of the lesions that lie within the cluster (Hada and

Sutherland 2006; Schipler and Iliakis 2013). Reduced or altered activity of glycosylases or nucleases can also leave some lesions within non-DSB clusters unrepaired.

1.3.5 T5-DSB: Indirect DSB induced by complex chemical modifications

IR-generated sugar lesions that are formed immediately are termed as prompt DSBs. Temperature dependent processing of sugar lesions, usually generated within 1 h post irradiation, leads to the formation of delayed DSBs. Temperature above 10°C accelerates the process of chemical modification of sugar lesion significantly. Through this chemical evolution, a non-strand-breaking sugar lesion converts into a more dangerous DNA strand breaking entity. These thermally labile sugar lesions are known as radiation-induced labile sites and can include damage in sugar moiety, abasic sites and base damages (Cheng et al. 2015; Schipler and Iliakis 2013; Satyendra K Singh et al. 2011).

Collectively, these forms of DSBs (T3-DSB, T4-DSB and T5-DSB) with enhanced complexity increase with high-LET compared to low-LET and accounting for compromised processing to a significant degree by pathways involved in DSB repair which renders chromatin destabilization directly or indirectly. Thus, they all are categorized as IR induced complex DSBs.

1.3.6 T6-DSB: Replication fork-associated DSBs

In this category of DSB, DSBs can be generated when a replication fork encounters a DNA lesion. When a replication fork is halted by a SSB, collapse of replication fork will convert SSB into a so-called “one-sided” DSB. Majority of the DSBs that can be attributed to endogenous processes are predominantly associated with DNA replication errors (Cannan and Pederson 2016).

1.3.7 T7-DSB: Clustered DSBs, complex arrangements of non-DSB and DSB clustered lesions

IR can induce more breaks in close proximity of one lesion within the DNA molecule. In such scenarios, involvement of more DSBs creates an additional level of complexity termed as cluster of DSBs. Chances that they can locally undermine the stability of chromatin in location and composition-dependent manner. Clustered DSBs located at distances from around 100bp to few hundred thousand bp will have the potential to destabilize the chromatin and may thus lead to fragment loss (figure 4). Consequently, loss of intervening fragments will lead to a compromised DSB processing and poor repair outcome which may give rise to deletions and exchange-type chromosomal aberrations formation. This form of clustered DSB

is best suitable for the explanation of increased efficacy for high-LET radiation. Indeed, substantial evidence from well-established mathematical modeling demonstrates that the probability of DSB cluster induction increases because of enhanced ionization clustering, a physical characteristic of high-LET radiation modality. Moreover, the size of the generated fragments becomes smaller with the increase of LET.

1.3.8 I-SceI homing endonuclease to study the adverse biological effect of DSBs and DSB clusters

I-SceI, encoded in the mitochondrial intron of the yeast *S. cerevisiae,* is a monomeric 235 amino acid homing endonuclease. The 18bp-long recognition sequence, TAGGGATAACAGGGTAAT, is non-symmetrical, absent in mammalian cells and has very high sequence specificity, which makes it an attractive tool in molecular biology to generate *in vitro* site specific DSBs thus allowing detailed studies of DSB repair mechanisms (Honma et al. 2007). The sequence is non-symmetrical, absent in mammalian cells and has very high sequence specificity.

Various fluorescence reporter assays have been previously reported to analyze functionality of DSB repair pathways by introducing a DSB into a defined site using I-SceI. As such, I-SceI induced DSBs are created either by transient transfection of I-SceI expression vectors or by controlled translocation of constitutively expressed I-SceI from the cytoplasm into the nucleus. Consistent with this, DSB repair pathway specific I-SceI based reporter assays in U2OS cell line have been extensively used. For example, DR-GFP-U2OS cells harbor a copy of the DR-GFP reporter which is used for the functional analysis of HRR function. Similarly, EJ5-GFP-U2OS cells harbor a copy of the EJ5-GFP reporter to measure the efficiency of c-NHEJ pathway. The EJ2-GFP-U2OS and SA-GFP-U2OS cells harbor reporter for alt-EJ and SSA efficiency respectively (Bennardo et al. 2008; Gunn and Stark 2012; Mladenov, Staudt, et al. 2019; Mladenova, Mladenov, and Iliakis 2016). A successful exploitation of I-SceI in CHO rodent cell line (CHO10B4) has previously been successfully performed in our lab with a view to investigating the adverse biological effects associated with enzyme induced DSBs of different complexity (Anon n.d.; Schipler et al. 2016).

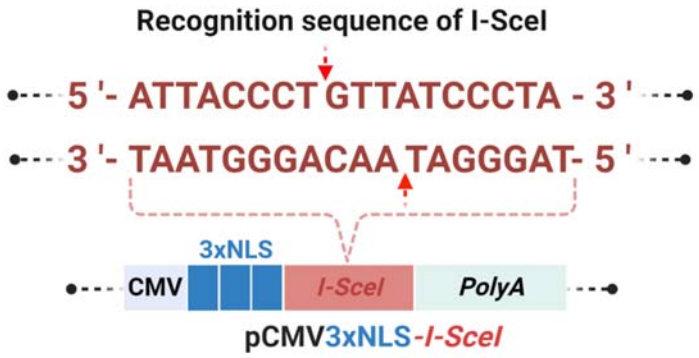

Figure 5 Schematic representation of I-SceI cleavage site and expression vector. 18bp-long non-palindromic recognition sequence of I-SceI endonuclease. Double strand break at the site, indicated by red arrows, yields a 4-bp overhang at the 3´end. **(Upper Panel)** I-SceI expression vector, pCMV3xNLS-ISce-I that is frequently used for transient transfection and expression of I-SceI.

2 Cellular mechanisms of DNA damage signaling and repair

2.1 Multistep signaling activation of DSBs

Recruitment of DDR factors to the DNA lesions follows a sequence to coordinate the DNA repair. Upon DSB induction, cellular DSB ends are rapidly sensed by primary damage sensors namely MRN complex, KU70/80 heterodimer and Poly (ADP-ribose) polymerases 1 (PARP1) and their binding activates the signaling cascade responsible for DNA repair. Initial binding of MRN complex to DSBs is mediated through its globular domains consisting of dimerized RAD50 and MRE11 subunits. Owing to its high abundance and high affinity for DSBs, it is likely that KU70/80 binds DNA ends faster than MRN. However, the interaction between MRN and KU70/Ku80 and their initial recruitment at the DSB remains unclear. The third DNA damage sensor, PARP1 is activated after binding to DSBs and is a central enzyme in Poly (ADP-ribosyl)ation (PARylation) of proteins at DNA damage sites. Evidence shows that PARP1 can compete with KU for DSB binding to promote alt-EJ (Polo and Jackson 2011; RS et al. 2008; Wang et al. 2006).

Following sensing the DNA lesions, three prominent members of the family of phosphotidylinositide-3-kinase related kinases (PIKKs) predominantly play role as a signal transducer. PIKKs comprise the family of Ser/Thr-protein kinases which show sequence similarity to phosphatidylinositol-3 kinases (PI3Ks). Ataxia telegiectasia mutated kinase (ATM) has key roles in phosphorylating a plethora of substrates participating in DNA damage repair pathway. In non-irradiated cells, ATM is held inactive as dimer. However, upon irradiation an event of auto-phosphorylation at serine residue of 1981 causes dimer

dissociation that triggers kinase activation of ATM (CJ and MB 2003). The recruitment of ATM to the DSB is mediated through its interaction with MRN complex. ATM is then acetylated by an acetyl transferase Tip60. ATM phosphorylates histone variant H2AX on serine 139 (known as γ-H2AX) which serves as a marker for DSBs (CH et al. 2003). Ataxia-telangiectasia and Rad3 related kinase (ATR) is another important member of the PIKK family that is activated upon DSB induction. Contrary to ATM which requires a DSB for activation, the initial signal for the recruitment of ATR is the presence of replication protein A (RPA) coated single-stranded DNA (ssDNA) which is recognized by its stable binding partner ATRIP (ATR-interacting protein). Loading of Rad9-Rad1-Hus1 (9-1-1) complex and binding of ATR activator topoisomerase binding protein 1 (TOPBP1) facilitate ATR-mediated phosphorylation and activation of checkpoint kinase 1 (Chk1) (Y 2003). ATM and ATR kinases can alone phosphorylate more than 700 target proteins involved in DSB signaling and repair. Besides sharing many downstream targets, ATM is thought to exclusively target Chk-2, while ATR activates Chk-1 to trigger checkpoint activation. In contrast to ATM and ATR, which are involved in DNA damage sensing and checkpoint activation, DNA-PKcs, the catalytic subunit of the DNA-dependent protein kinase (DNA-PK) holoenzyme is directly involved in DSB repair by c-NHEJ. DNA-PKcs relies on Ku70/80 to direct it to DSB ends and trigger its activation (Fernandez-Capetillo et al. 2002).

A plethora of mediator proteins is actively involved in maintaining the DNA damage signaling which is amplified by the transducer proteins. Notably, phosphorylation of H2AX by ATM leads to chromatin relaxation which is then followed by sequential recruitment of many other downstream DNA damage signaling proteins involved in the DNA repair process including MDC1, RNF8, L3MBTL2, RNF168, 53BP1, BRCA1 and many more (Doil et al. 2009; Nowsheen et al. 2018; Smeenk and Mailand 2016).

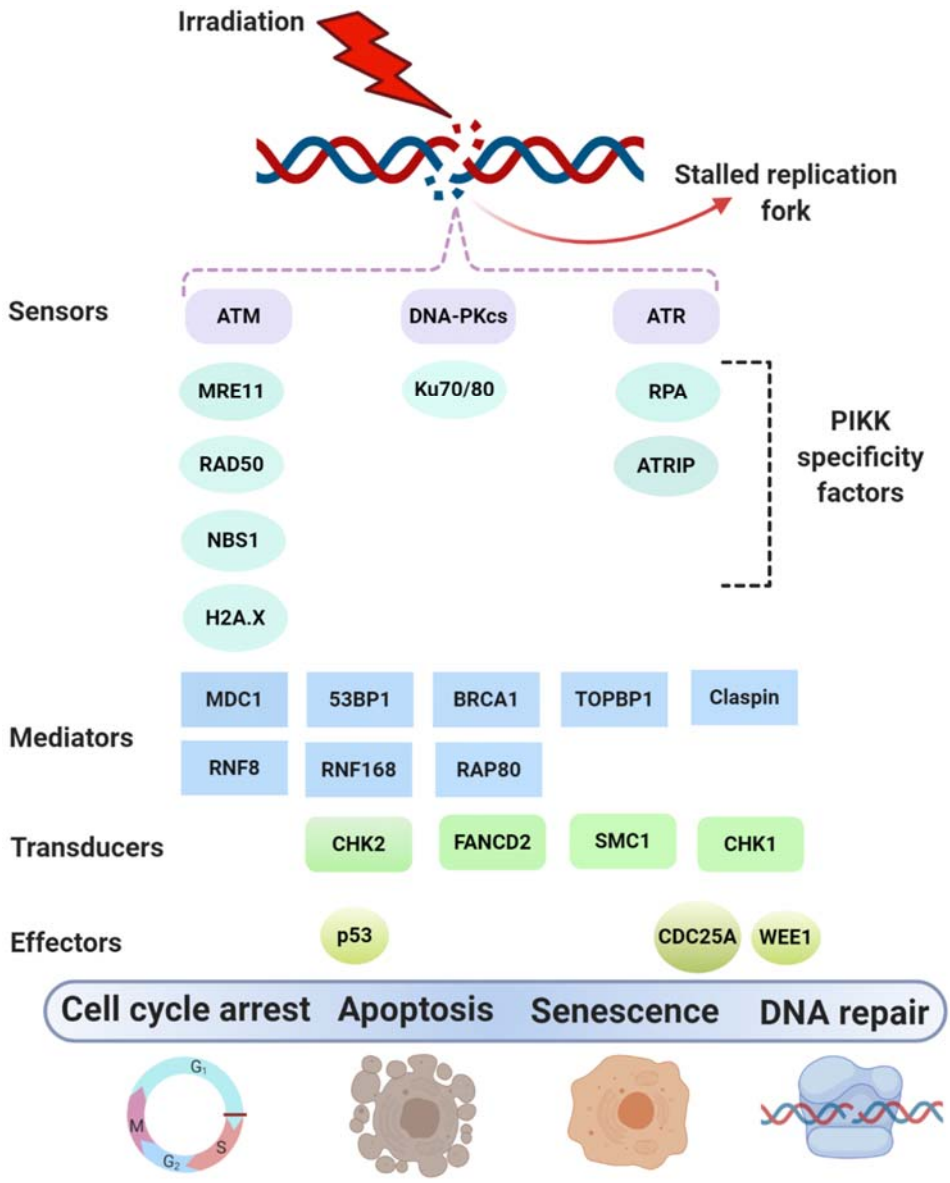

Figure 6 Schematic illustration of DNA damage-signaling and the proteins involved. Following damage induction, DNA lesions are recognized by sensors (e.g ATM). Mediator proteins amplify DNA damage signaling. After that proteins including Chk2 serve to transduce the initiated DNA damage signals. Finally, effectors (e.g tumor suppressor p53) initiate cellular responses including apoptosis, senescence or cell cycle arrest/delay to allow cells repair their damaged DNA. Image has been adopted and modified from (Bohgaki, Bohgaki, and Hakem 2010).

At the effector level, the DDR interfaces with the cell cycle checkpoints. In particular, the activation of G2/M checkpoint following damage induction restricts progression of cells into mitotic phase thus preventing the propagation of damaged DNA to the daughter cells. ATM and ATR have been shown to play prominent roles in G2-M cell-cycle arrest in response to DSBs. Recent reports from our lab implicated also the role of DNA-PKcs in checkpoint control

(Mladenov, Fan, Dueva, et al. 2019; Mladenov, Fan, Paul-Konietzko, et al. 2019). The activated two kinase signaling cascades, the ATM-Chk2 and ATR-Chk1, subsequently inactivate the Cdc25 phosphatases via phosphorylation that restricts mitosis-promoting activity of the cyclin B-CDK1 complexes resulting in G2 arrest (Peng et al. 1997; Xiao et al. 2006). Several studies provide strong evidence for efficient G2/M checkpoint activation by a sensitivity threshold of 10-20 DSBs, *i.e.* below this threshold DSB level, G2-M arrest is undetectable (Deckbar, Jeggo, and Löbrich 2011; Syljuåsen et al. 2006).
If the above-mentioned sequential events ensure successful DNA repair, cells can enter the cell cycle. If the DNA damage cannot be eliminated, cells instead can initiate senescence or programmed cell death in the form of apoptosis or autophagy (Jackson and Bartek 2009).

2.1.1 DNA damage response and cellular signaling

To respond efficiently to radiation-induced DNA damage, eukaryotic-cells have evolved an intricate system of cellular response known as DNA damage response (DDR) that sense, signal and repair DNA lesions. A number of associated cellular events after sensing the damage is then initiated within the cells to properly regulate cell cycle progression and repair of DNA breaks. Components of DDR are classified as sensors, transducers, mediators and finally effectors. These molecular components use a multitude of post-translational modifications like phosphorylation, ubiquitination, SUMOylation, acetylation, PARylation and methylation of repair factors to ensure an efficient and accurate localization, modulation and clearance of DNA repair factors (Bekker-Jensen and Mailand 2011).

2.1.2 Ubiquitination signaling (RNF8/RNF168) mediated recruitment of 53BP1 at damaged chromatin

It is widely known that in eukaryotes, DNA damage signaling is largely governed by a variety of post-translational modifications (PTMs) of proteins, for example, phosphorylation, methylation, acetylation, ubiquitination, sumoylation (small ubiquitin-like modifiers) and neddylation. Ubiquitin is a small (8.6 kDa) regulatory protein in eukaryotes. Ubiquitination is a reversible post-translational modification involving covalent attachment of one or more ubiquitin (Ub) molecules to the substrate protein (Lysine, K). Ubiquitination regulates numerous functions in DNA damage repair pathway in the context of chromatin regulation and protein degradation. A critical function of ubiquitin is to maintain the balance between two major pathways, c-NHEJ and HR, in S and G2 phases of the cells. Ubiquitin-dependent covalent modifications involve a complex cascade of three distinct enzymes: E1, which is an

ubiquitin-activating enzyme, E2, that is an ubiquitin-conjugating enzyme, and a third enzyme, E3 ubiquitin ligase (Scheffner, Nuber, and Huibregtse 1995).

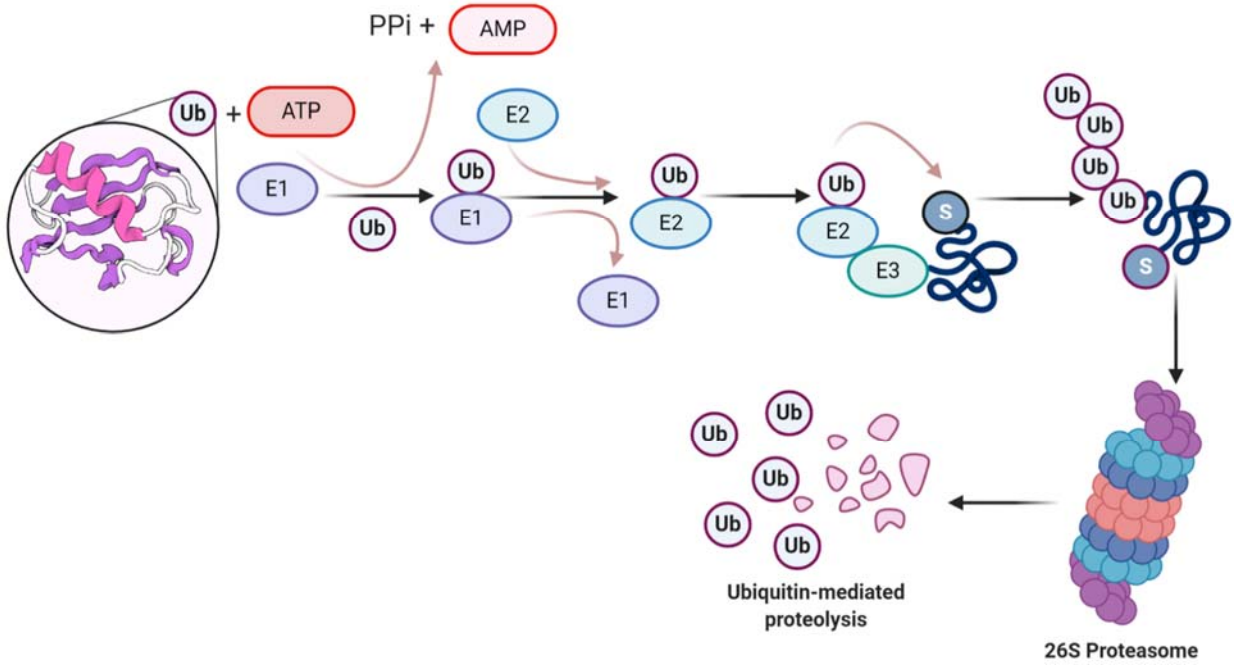

Figure 7 A schematic outline of ubiquitination reaction cascade involving three sets of enzymes. E1 are involved in ubiquitin activation, E2 in ubiquitin conjugation and E3, an ubiquitin ligase. Schematic is adapted and modified from (Nowsheen, Deng, and Lou 2019).

The concerted action of these proteins sequentially catalyze the activation, conjugation and ligation reactions thus leading covalent attachment of multiple ubiquitin molecules to lysine residues of substrate proteins for example, histones (H2A and H2AX) (Mailand et al. 2007). Biochemical studies show that ubiquitin is at first activated by E1 in an ATP-dependent manner and subsequently forms a thioester linkage between ubiquitin C-terminal and E2 catalytic cysteine residue. At the last step E3 ubiquitin ligase catalyzes formation of an isopeptide bond between carboxy terminal of ubiquitin substrate and the lysine (K) residue on the target protein. This ubiquitination cascade can either monoubiquitinate; conjugating a single ubiquitin molecule or polyubiquitinate; formation of ubiquitin chain by conjugating multiple ubiquitin molecules, to the substrates. As a result, ubiquitinated mostly polyubiquitinated proteins are then directed to the proteasomal system for degradation. Of all, Lys48-linked poly ubiquitin chain is the most common signal for 26S proteasome complex that is responsible for most of the regulated proteolysis in the cell (Hershko and Ciechanover 1998). E3 ligases are known as writers of DSB-associated histone ubiquitination and confer majority of the substrate specificity to the ubiquitination cascade. RNF8/168 are two important

E3 ligases owing to the presence of RING (Really Interesting New Gene) finger domain. Moreover, there are some reported ubiquitin-binding effectors functioning as readers and E2 ligases are known as readers. In contrast, deubiquitinases, the deubiquitinating enzymes (DUBs), are considered as erasers of DSB-induced histone ubiquitination (Smeenk and Mailand 2016).

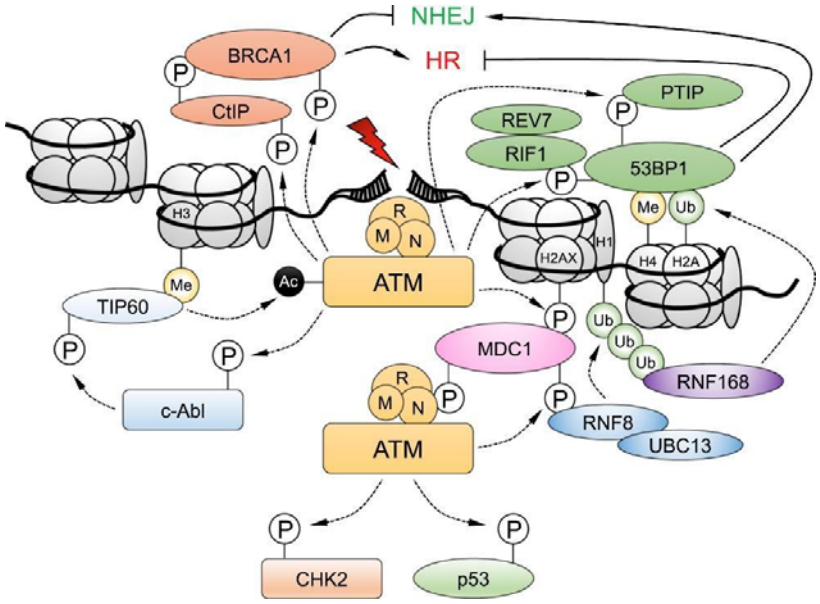

Figure 8 ATM activates the ubiquitin signaling cascade on damaged chromatin. Activated by MRN at DSB sites, ATM phosphorylates histone H2AX and MDC1 to initiate RNF8/168 mediated ubiquitination-signaling cascade that in turn facilitates 53BP1 recruitment. ATM dependent phosphorylation of 53BP1 further stimulates recruitment of its effectors that are antagonized by BRCA1 and CtIP in a complex mechanism. P, phosphorylation; Me, methylation; Ub, ubiquitination; Ac, acetylation. This schematic has been adapted from (Blackford and Jackson 2017).

Tumor suppressor p53 binding protein 1 (53BP1) is an important regulator of DSB signaling as it promotes c-NHEJ and inhibits HRR. Upon induction of DSBs, 53BP1 rapidly forms large foci near DNA lesions. The signaling cascade starts-off with the detection of DSB ends by MRN complex, which triggers the activation of ATM by auto-phosphorylation (Carson et al. 2003). Subsequently, ATM phosphorylates histone H2AX on S139 in the region surrounding the DSBs, thus forming γ-H2AX foci. The mediator of DNA damage-check-point 1 (MDC1) then localizes to DSB sites by binding to γ -H2AX via its tandem BRCA1-C-terminal (BRCT) domains and is phosphorylated by ATM (Fernandez-Capetillo et al. 2002; Rogakou et al. 1998). The phosphorylation of MDC1 promotes the recruitment of two E3 ubiquitin ligases ring finger protein 8 (RNF8) and 168 (RNF168) in conjunction with the E2 conjugating enzyme UBC13 (ubiquitin conjugating enzyme E2 N) and HERC2 (HECT and RLD domain-containing

E3 ubiquitin protein ligase 2). ATM phosphorylation at TQXF motif on MDC1 is recognized by forkhead-associated (FHA) domain of the ubiquitin ligase RNF8 thus promoting RNF8 recruitment to the damaged chromatin. On the other hand, RING domain located at C-terminal recognizes the E2 ubiquitin ligase, UBC13 and mediates UBC13- RNF8-driven K63 ubiquitylation that triggers recruitment of downstream DSB effectors. Besides binding to phosphorylated MDC1, FHA domain of RNF8 interacts with ATM-phosphorylated HERC2, an E3 RING ligase thus forming complex comprised of MDC1-RNF8-HERC2. In addition to stabilizing the RNF8-UBC13 interaction, HERC2 helps maintain sufficient level of RNF8 to trigger DSB induced downstream ubiquitination (Bekker-Jensen et al. 2010).

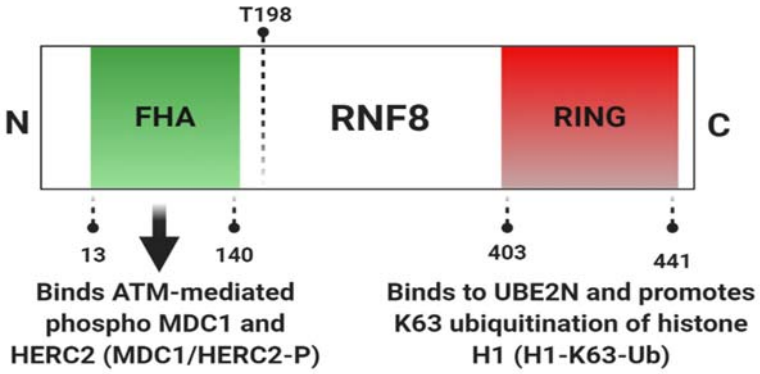

Figure 9 Organization of RNF8 domain. FHA, forkhead-associated domain; N, N terminus; C, C terminus. This schematic has been adopted and modified from (Orthwein et al. 2014).

As a result, RNF8 is the first ligase to be recruited to the site of damage in an ATM-dependent manner. There are contradictory results about the target molecules of this ubiquitin ligase. Earlier report shows that RNF8 polyubiquitinates linker histone H1 that triggers the assembly of RNF168 to the modified histones (Mailand et al. 2007). However, a recent report demonstrates that upon DNA damage histone H1 is mono-ubiquitinated and binds instead a polycomb group-like protein L3MBTL2 as a missing link between RNF8 and RNF168. Consistent with this, RNF8 ubiquitinates L3MBTL2 at K63-specific chains and forms ubiquitin chains at damaged sites, which then facilitates anchoring of second E3 ubiquitin ligase, RNF168. After binding to the ubiquitin chain, RNF168 (mono) ubiquitinates its key substrate histone H2A on K13 and/or K15 to form H2AK13Ub and H2AK15Ub at DSB sites. This ubiquitination, together with H4K20 methylation, promotes 53BP1 recruitment in which 53BP1 interacts directly with H2AK15Ub through its ubiquitination-dependent recruitment (UDR) motif. The Tudor domain of 53BP1 recognizes dimethylated H4 at Lys20 (H4K20me2) thus triggering the relocation of 53BP1 to the sites of DSB. Besides recognizing H4K20me2,

53BP1 Tudor domain has been shown to be recognized by L3MBTL and JMJD2A. ATM-dependent phosphorylation of 53BP1 at N-termini mediates recruitment of RIF1 and PTIP (Luijsterburg and van Attikum 2012; Mailand et al. 2007; Nowsheen et al. 2018). The RING domain of RNF168 is not essential for their recruitment at DSBs and is dependent on two ubiquitin-binding motifs, MIU1 and MIU2 instead (Doil et al. 2009).

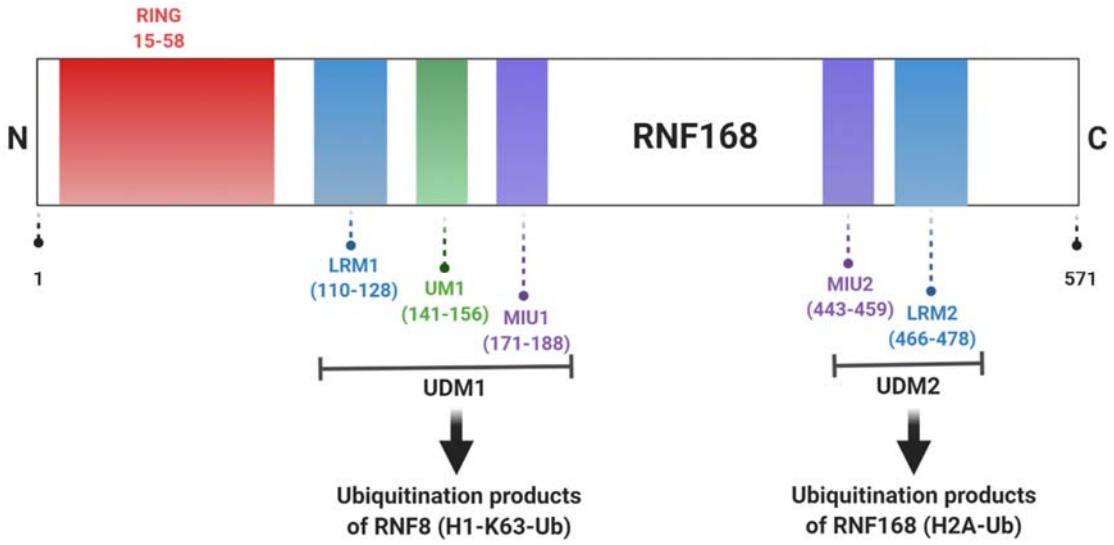

Figure 10 Composition and reported functions of ubiquitin-dependent DSB recruitment modules (UDM1 and UDM2) in RNF168 gene. It has three major regions: at N-terminus, RING domain and UDM1 are located, and at C-terminal region, cluster of protein-interacting motif 2 (UDM2) is located. The domain structure is adopted and modified from (Thorslund et al. 2015).

This coordinated signaling of two ubiquitin ligases promotes further recruitment of two important downstream pathway-deciding regulators, BRCA1 and 53BP1. With an existing antagonistic relationship between them, while BRCA1-BARD1 direct the pathway toward HR by mediating H2A K125/K127/K129 mono-ubiquitination, pro c-NHEJ factor; 53BP1 diverts the pathway toward c-NHEJ by H2AK13/K15Ub ubiquitination. Mono-ubiquitination of H2A mediated by BRAC1-BARD1 promotes 53BP1 displacement thus leaving DSB sites accessible for DNA end resection factors. After retention at DSB sites, 53BP1 acts as a scaffold protein that anchors further downstream effector proteins like PAX transcription activation domain interacting protein (PTIP) , Rap1 interacting factor 1(RIF1) and the REV7-Shieldin-CST complex thus protecting DSB ends from being resected (Chapman et al. 2013; Hustedt and Durocher 2017). 53BP1 and its effectors are the key negative regulators of DNA end resection, promoting c-NHEJ pathway.

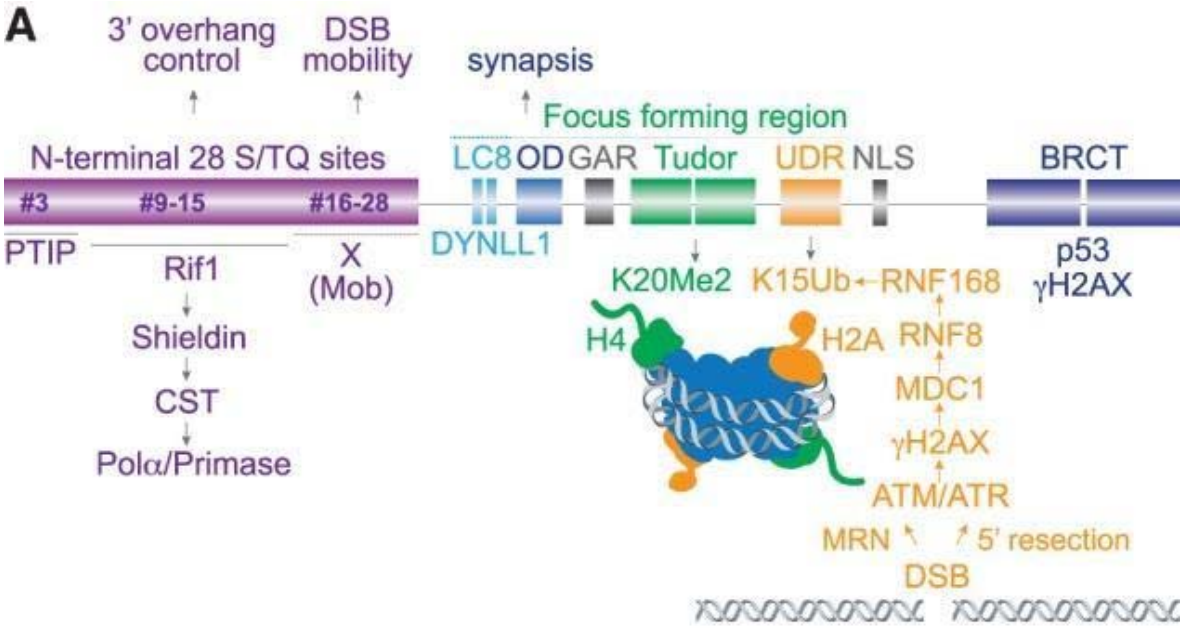

Figure 11 Schematic diagram of functional domain structure of 53BP1 and its interacting partners. Twenty-eight Ser/Thr-Gln (S/T-Q) sites located in N-terminus (violet) promotes binding of its downstream effector proteins PTIP, the RIF1/Shieldin/CST/Polα/primase axis and as of yet unidentified factor (X) which mediates DSB mobility function, and is ATM phosphorylation dependent. BRCT (BRCA1 carboxy-terminal) domain in C-termini binds to p53. Retention of 53BP1 to DNA lesions requires the Focus Forming Region (FFR). It consists of an oligomerization domain (OD), a glycine-arginine-rich (GAR) motif, a tandem Tudor motif that binds to dimethylated Lys20 of histone (H4K20me2) and an ubiquitination-dependent recruitment (UDR) motif that interacts with ubiquitinated H2AK15, for what signaling proteins ATM, MDC1, RNF8, RNF168, 53BP1 are recruited hierarchically to chromatin areas surrounding DSBs. Domain structure is adapted from (Mirman and de Lange 2020).

Based on the above described observations, E3 ubiquitin ligases RNF8 and RNF168 function as damage sensors upstream of 53BP1 signaling in cells exposed to DNA damage. As such, ubiquitin signaling as well as their fine balance is essential to ensure efficient and accurate DSB repair.

2.2. Mechanisms of cell signaling to repair DNA double strand breaks (DSBs)

As a part of DDR, cells of higher eukaryotes engage four mechanistically distinct pathways to remove the sustained DSBs and maintain genome integrity. Each pathway uses a discrete molecular mechanism to process the persistent DNA damage. In the following sections a detailed overview of each repair pathway along with their molecular apparatus, stepwise processing of DSB lesions and how DDR is influenced by damage complexity (simple or complex type of DSBs) is broadly discussed. Moreover, cell cycle specific involvement and

regulation have also been a focus of the discussion.

2.2.1 DNA end resection mediated by CtIP at DSBs and its role in alternative end joining

Vertebrate C-terminal-binding protein interacting protein (CtIP), is a 5´to 3´endo-nuclease and a key regulatory component of DNA end resection (Sartori et al. 2007). CtIP orthologs are evolutionarily conserved. Research focused on its ortholog in fission yeast (Ctp1), budding yeast (Sae2) and plant (Com1) demonstrate functions similar to that of CtIP. CtIP was identified as a cofactor for the transcriptional repressor of CtBP (carboxy-terminal binding protein) and interacting partner of tumor suppressor proteins Rb (retinoblastoma protein) and BRCA1 (breast cancer type 1 susceptibility factor) (Fusco, Reymond, and Zervos 1998; Wong et al. 1998). In G1 phase, CtIP activates its own promoter as well as the promoters of E2F/Rb target genes such as Cyclin D1. Binding of CtIP to E2F-responsive promoters causes repression of Rb, which in turn allows S-phase gene expression and progression from G1 to S phase(Liu and Lee 2006). Two CDK consensus phosphorylation sites in CtIP have been identified. In S and G2 cell cycle, CDK-dependent phosphorylation of CtIP at S327 promotes its binding with the C-terminal BRCT domain of BRCA1 as well as MRN and is important for localization of CtIP at damaged sites. Consequently this association triggers the ubiquitination process of CtIP by N-terminal ubiquitin-ligase activity of BRCA1(Yu et al. 2006). On the other hand, phosphorylation at T847 regulates DNA end resection during HR (figure 13). The CDK-dependent CtIP phosphorylation is required for the subsequent phosphorylation at T859 by ATM. Consistent with this, the ATM phosphorylation sites, S664 and S745, are likely to be dispensable for CtIP recruitment to DSBs. Indeed, several lines of evidence implicate CtIP in alternative resection-directed DSB repair pathways (MMEJ/alt-EJ) during G1 phase (Yun and Hiom 2009).

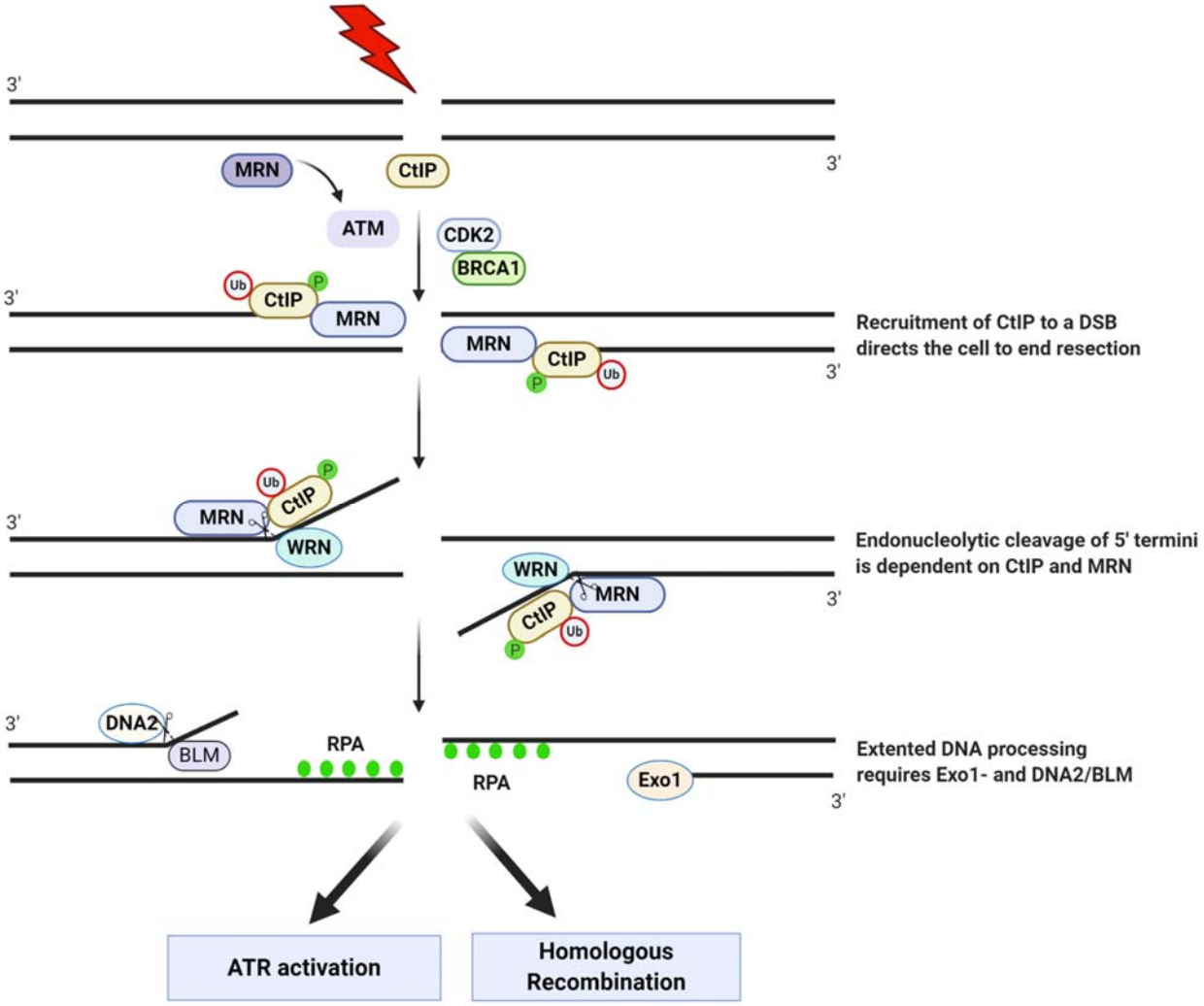

Figure 12 CtIP and MRN complex in DSB end resection. Upon damage induction, both CDK and ATM phosphorylate CtIP which triggers its recruitment to DNA damage sites. BRCA1 mediates CtIP ubiquitination. MRN, stimulated by CtIP, initiates DNA end resection by creating an endonuclease nick proximal to the 5´end of the break. Helicase activity of WRN influences this initial end-processing of DSB and is crucial for long-range resection activities by Exo1 and Dna2/BLM. Replication protein A (RPA) coats the generated ssDNA, which activates checkpoint protein kinase ATR and thus homologous recombination-mediated DSB repair. The illustration has been adapted and modified from (You and Bailis 2010).

Evidence suggests that CtIP physically interacts with MRN and regulates its function in end resection. Thereby, CtIP promotes the nuclease function of MRE11 where it first creates a nick in close proximity of 5´-termini of the DNA break, which then follows a 3´-5´exonucleolytic trimming of DNA towards the break. Following this, the combined action of helicases (WRN, BLM) helicases and nucleases (Dna2 and Exo1) carry out long-range resection to generate long 3´ssDNA tails which are rapidly bound by hetero-trimeric replication protein A complex

(RPA). Subsequently Rad51 recombinase displaces the bound RPA protein to initiate strand invasion and homology search to complete HR (Anand et al. 2016; Andres and Williams 2017; Deshpande et al. 2016). Alternatively, if HRR is compromised, alt-EJ or SSA that profit from resected DNA, can take place. (Mladenov, Staudt, et al. 2019).

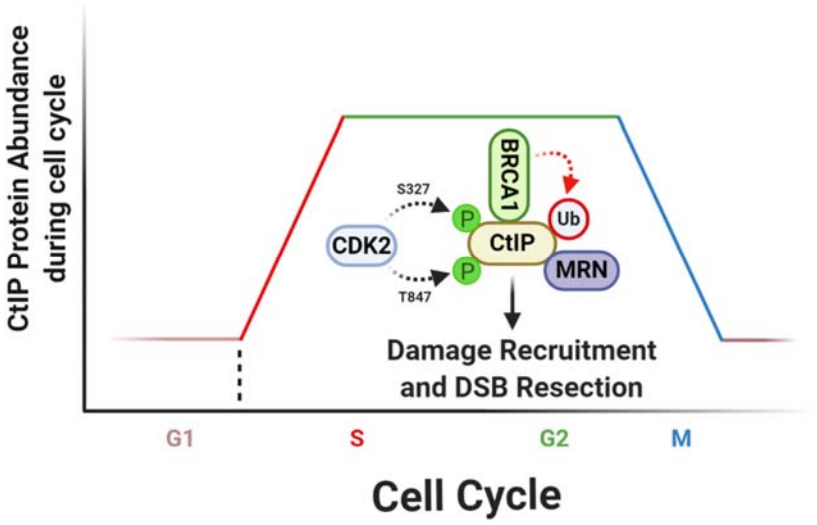

Figure 13 CtIP protein levels during the cell cycle. CtIP expression oscillates during cell cycle and is regulated by post-translational modifications. CtIP protein level is low in G1 and high in S, G2 and M phases. CtIP function in HRR is mediated through CDK2 and BRCA1-dependent modifications. Phosphorylation of CtIP at S327 by CDK2 promotes its interaction with BRCA1 and MRN and directs its localization to damaged chromatin. On the other hand, CDK2-mediated phosphorylation of CtIP at T847 stimulates its function in resection. This illustration is adapted and modified from (You and Bailis 2010).

CtIP, with its 897 amino acid residues, contains several functional domains that serve its essential functions in DNA damage response. CtIP homodimerization via its putative N-terminal coiled-coil motif (residues 45-160) is essential for both localization to DSBs and end resection. The middle region of CtIP contains several motifs: PLDLS motif which interacts with CtBP transcriptional repressor and a direct DNA binding motif, which contains two lysine residues (K513 and K515) that are critical for its DNA binding activity. Furthermore, the DNA binding motif also contains a PCNA-binding module stretching from 515 to 537 residues. The C-terminus of CtIP, sharing sequence homology with budding yeast ortholog Sae2, contains two phosphorylation sites, T847 and T859 that are important for DNA end resection (Barton et al. 2014; Peterson et al. 2013). Upon damage induction, both Cyclin dependent kinases (CDKs) and polo like kinases (Plks) phosphorylate CtIP at T847 in S and G2 phases, while the apical kinases ATM and ATR phosphorylate it at T859 (Peterson et al. 2013).

Interestingly, a previous report also showed phosphorylation of CtIP at T847 and S327 in G1-phase cells by Plk3. Recent reports demonstrate CDK2 independent limited resection in G1 phase of the cell cycle (Barton et al. 2014; Liu et al. 2019).

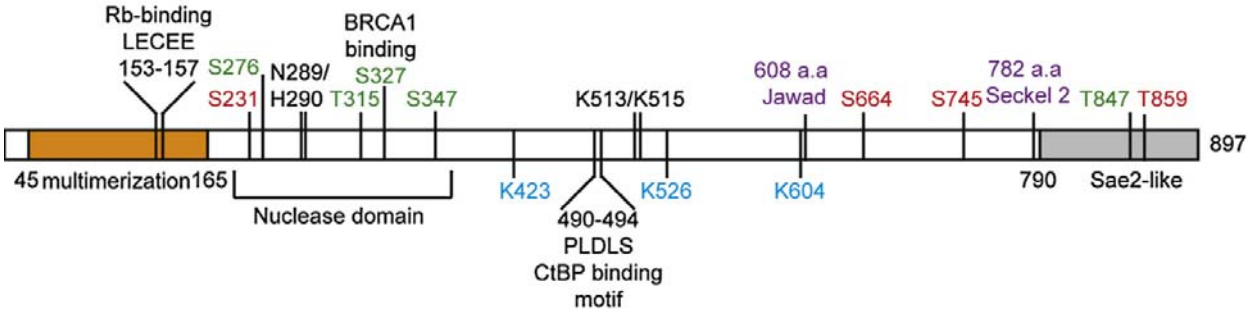

Figure 14 Schematic representation of CtIP protein domain structure. The N-terminus contains a multimerization domain (amino acids 45-165, orange) and an Rb consensus binding site (153-157). A CtBP-binding motif is located in the middle. The C-terminal Sae2-like region (amino acids 793-897, grey) comprises MRN binding domain and is conserved from yeast to humans. Phosphorylation at S327 (green) by CDK mediates its association with BRCA1 and is important for its recruitment to damaged chromatin, BRCA1-mediated ubiquitination. The 509–557 region of CtIP has DNA-binding activity. K513 and K515, two conserved key lysine residues in vertebrates, are indispensable for both DNA binding activity and recruitment at damage chromatin. Acetylation target residues K432, K526 and K604 are shown in blue. The two phosphorylation sites (S664 and S745, red) of checkpoint protein kinase ATM are conserved in vertebrates. Domain structure is adapted from (Makharashvili and Paull 2015).

2.2.2 Classical non-homologous end joining (c-NHEJ)

The dominant pathway for DSB repair is classical non-homologous end joining (c-NHEJ). In contrast to HRR, c-NHEJ instead seals the two DNA ends without the requirement of sequence template and is putatively error-prone (Mladenov et al. 2016). A key enzyme in c-NHEJ is DNA-PK holoenzyme, a serine/threonine kinase. It is composed of DNA-dependent protein kinase catalytic subunit (DNA-PKcs) and DNA tethering Ku heterodimer (Ku70/80) (Blier et al. 1993; Downs and Jackson 2004). Upon its assembly at DSB sites, DNA-PKcs phosphorylates several target proteins including some of c-NHEJ factors Ku, XRCC4, XLF, H2AX, Kap1, 53BP1 and the DNA end-processing factor, Artemis (Drouet et al. 2006; Stiff et al. 2004). In response to DNA damage, DNA-PKcs undergoes auto-phosphorylation at its PQR and ABCDE clusters. This auto phosphorylation event facilitates repair of DSBs (Uematsu et al. 2007). Owing to its very large size around 450kDa, it functions as a molecular scaffold for the recruitment of additional factors like X-ray repair cross-complementing 4 (XRCC4), ligase 4 and XLF (XRCC-like factor protein). C-NHEJ is very fast and can efficiently

eliminate DSBs from the genome with half time of approximately 10-20 minutes. Despite its fast repair kinetics, the ensuing repair is error-prone and is associated with small sequence alterations around the break. Since c-NHEJ ensures template-independent rejoining of DSBs, it operates throughout all the cell cycles (Goodarzi and Jeggo 2013; Symington 2016). Accumulating evidence reveals the involvement of the core c-NHEJ component, DNA-PKcs in end processing activity (Deshpande et al. 2020; Mladenov, Fan, Dueva, et al. 2019; Mladenov, Fan, Paul-Konietzko, et al. 2019). Artemis is the major nuclease that has already been shown to regulate processing of complex DSB ends (e.g; hairpins) during V(D)J recombination and is facilitated by ABCDE cluster phosphorylation of DNA-PKcs (Yannone et al. 2008).

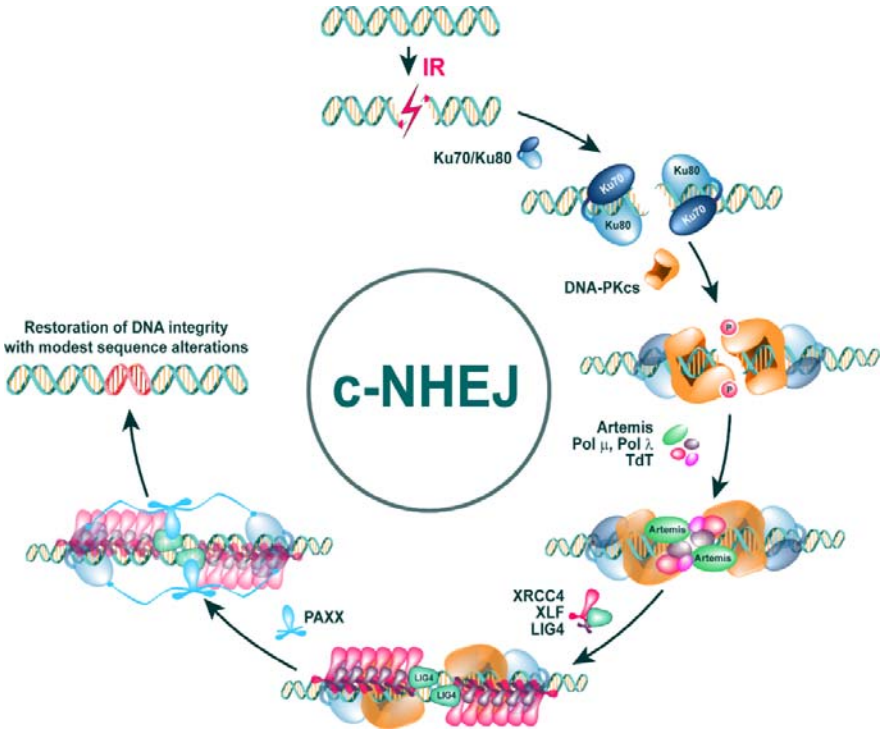

Figure 15 Classical non-homologous end joining (c-NHEJ) with the key components. See the text (2.2.2) for detailed description. This figure has been adapted from (Mladenov et al. 2016).

2.2.3 Homologous recombination repair (HRR)

Homologous recombination repair (HRR) pathway is evolutionarily conserved in eukaryotes. It faithfully repairs the DNA lesions by using the sister chromatid as a template to restore the original sequence in an error-free manner to its original state. Owing to its dependence on homologous DNA template, this pathway is active exclusively in S and G2 phases of the cell cycle. Proteins that play significant role in HRR are RAD51 and its 5 paralogs (XRCC2,

XRCC3, RAD51B, RAD51C and RAD51D), RAD52, BRCA1, BRCA2, MRN complex and CtIP (Chun, Buechelmaier, and Powell 2013). An inevitable step for HRR mediated repair is DNA end resection, which generates 3´- single stranded DNA (ssDNA) overhang at the vicinity of DNA breaks which is necessary for strand invasion and homology search to ensure faithful repair. Mre11-Rad50-NBS1 (MRN) complex and CtIP, collectively known as resection ensemble, initiate resection (Makharashvili and Paull 2015; Paull 2015). Stimulated by CtIP, MRE11 from MRN complex starts-off its primary function by creating a nick in the vicinity of DNA breaks which then followed by simultaneous removal of the DNA adducts and loading of (BLM) helicase together with Exonuclease 1 (Exo1) and/or DNA2, which has both 3´endonuclease and helicase activities. The nuclease function of resection factors process the free DNA ends to expose single-stranded DNA (ssDNA) overhangs and are rapidly coated by replication protein A, RPA thus facilitating the process of DNA resection (Mehta and Haber 2014; Symington 2016). Loading of strand exchange recombination enzymes, Dmc1 and Rad51, on to the RPA-coated ssDNA is then followed and is coordinated by BRCA1-PALB2-BRCA2-DSS1 proteins(Zhao et al. 2015; Zhou and Paull 2013). The Rad51 nucleoprotein filament subsequently mediates the strand invasion and coordinates its annealing to the homologous region present in sister chromatid to form Holliday Junction (HJ) (Ip et al. 2008). Since one sister chromatid uses the sequence of other sister chromatid as a template to correct the missing information, this pathway is often known as homologous recombination repair sub-pathway of gene conversion (GC).

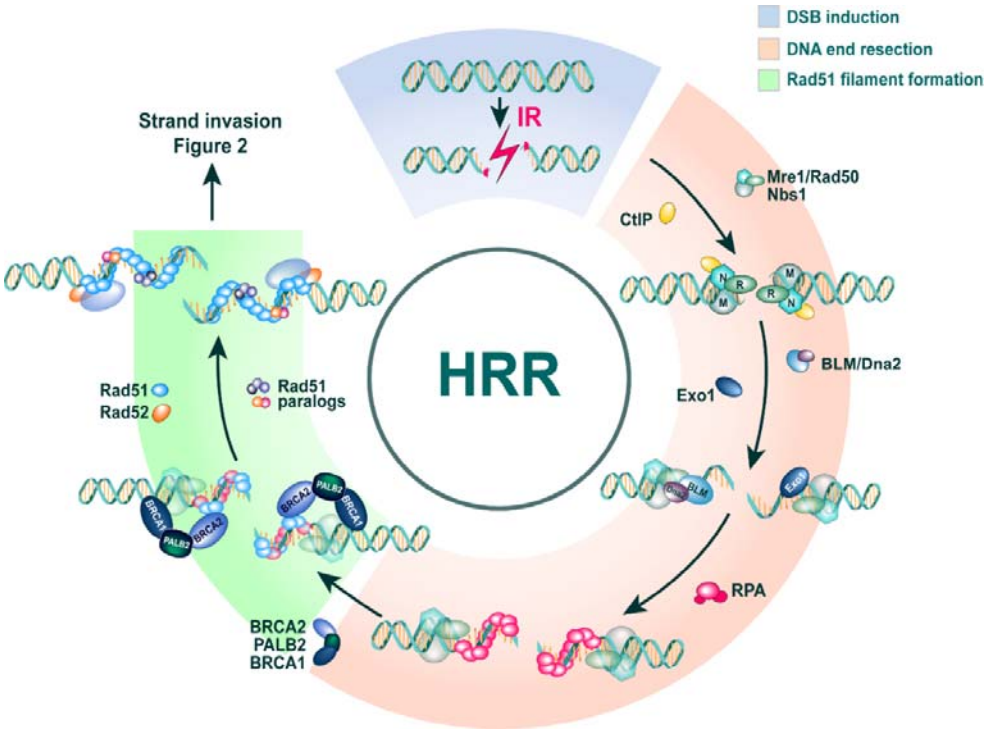

Figure 16 Schematic representation of homologous recombination pathway. Figure is adapted from (Mladenov et al. 2016).

2.2.4. Alternative end joining (alt-EJ)

When any of these two major repair pathways are not functional, cells employ a back-up pathway known as alternative end joining (alt-EJ) to resolve DSBs. DSB repair by alt-EJ was observed for the first time during class-switch recombination (CSR) in c-NHEJ deficient lymphocytes (Yan et al. 2007). Until now, no alt-EJ specific key components have been described. Alt-EJ functions and re-joins the two ends of DNA independently DNA-PK. The repair kinetics of alt-EJ is slower than that of c-NHEJ (DiBiase et al. 2000; Nevaldine, Longo, and Hahn 1997; Wang et al. 2006). However, many of the proteins involved in the HRR and SSA pathway (PARP1, MRE11, NBS1, CtIP, XRCC1, and LIG3) are co-opted by this alternative pathway for DSB processing. One of the first factors implicated in this pathway is Poly (ADP-ribose) Polymerase 1 (PARP-1) by virtue of having high DNA end binding affinity (Beck et al. 2014; Haince et al. 2008; Truong et al. 2013; Wang et al. 2006; Zhang and Jasin 2011). An interesting aspect of alt-EJ is the involvement of the nuclease ensemble (MRN complex and CtIP) that coordinates the resection process. Subsequently, end-processing that exposes micro-homologies (~10bp long) facilitates the alignment of DNA ends for ligation using DNA ligases (LIG1 and LIG3). Therefore alt-EJ is often referred as microhomolgy-

mediated alternative end joining (MMEJ) (Liang et al. 2008; Paul et al. 2013). Recent findings suggest that polymerase theta (Pol θ) encoded by the *POLQ* gene appears to be a new player in alt-EJ. With its intrinsic polymerase and helicase features, Pol θ stabilizes the annealing of the two 3´ssDNA overhangs (Ceccaldi, Rondinelli, and D'Andrea 2016). Altogether, alt-EJ contributes to large deletions and the formation of chromosomal translocation. It is therefore inherently error-prone and a mutagenic pathway. Like c-NHEJ, alt-EJ operates in all cell cycle phases but with increased functional activity in G2 phase. The limited activity of alt-EJ in G1 phase is attributed to the reduced expression of CtIP, a key protein in DNA resection apparatus. Earlier evidence including our lab demonstrated that alt-EJ is compromised in cells entering plateau phase of growth (Averbeck et al. 2014; Liu and Huang 2016; Sartori et al. 2007; Satyendra K. Singh et al. 2011).

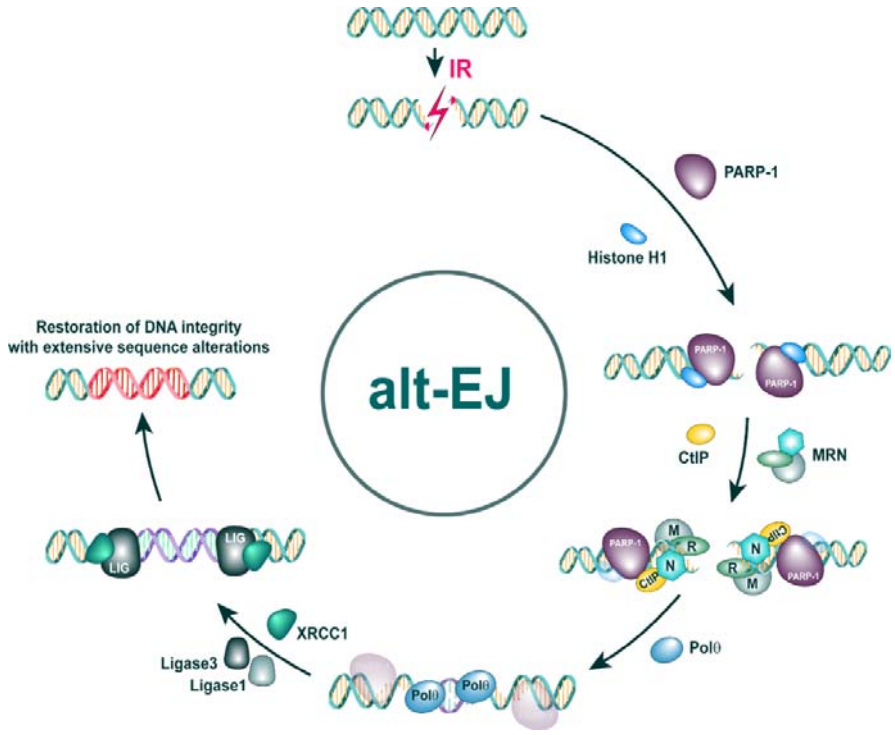

Figure 17 Schematic overview of alternative end-joining mechanism denoting the key factors involved. See the text for description. Figure adapted from (Mladenov et al. 2016).

2.2.5 The role of DNA-PKcs in alternative end joining

Despite its prominent role in classical NHEJ, emerging evidence demonstrates a hitherto unknown role of DNA-PKcs in end processing during homologous recombination. However, the underpinning mechanisms of how it simultaneously regulates and coordinates both end-ligation and end-processing are not fully explored. Numerous studies from the lab of Tanya

Paul show that together with MRN and ATM, DNA-PKcs regulates DNA end resection. They observed that in the presence of DNA-PK, MRN complex promotes resection by recruiting Exo1, which in turn enhances DNA-PK's auto phosphorylation (Deshpande et al. 2020; Symington 2016). They further demonstrate that persistent possession of DNA-PK as adducts at the broken DNA ends stimulates the nuclease activity (first endonuclease, then exonuclease) of MRN. Thereby CtIP phosphorylation plays a critical role in MRN activity. Emerging evidence suggests that in addition to its well-established role in DNA end-joining, DNA-PK also facilitates the processing of DNA ends. Interestingly, studies based on its domain structure revealed an antagonistic relationship between two important amino acid clusters, ABCDE and PQR. DNA end processing is promoted by phosphorylation of the ABCDE cluster but is inhibited by PQR cluster phosphorylation (Meek et al. 2007). DNA-PKcs exerts its dual functions in a sequential manner where it first performs ligation through DNA end tethering followed by initiation of end processing and therewith a transition from c-NHEJ to homologous recombination (Deshpande et al. 2018; Zhou and Paull 2013).

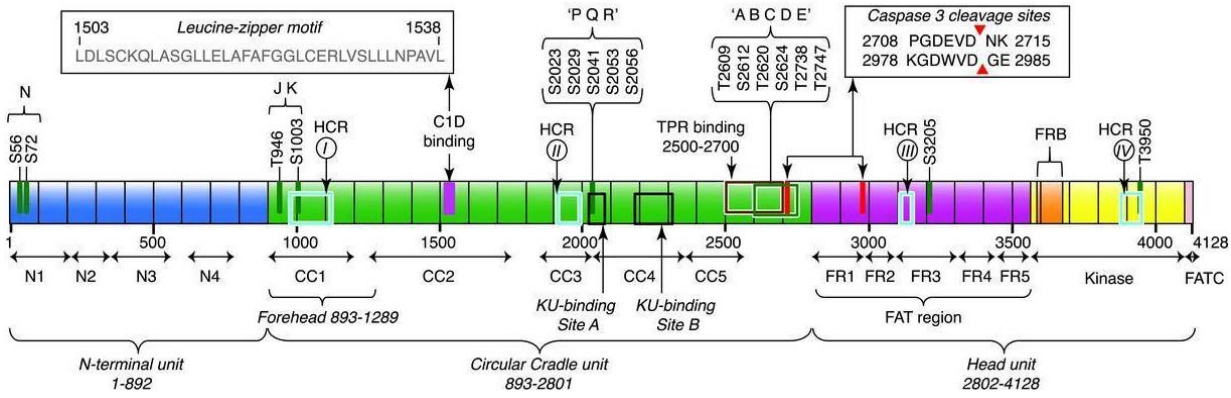

Figure 18 DNA-PKcs domain organization. The N-terminus (blue) consists of four super secondary structures (N1 to N4). The circular cradle unit (green) is composed of five super secondary α-helical structures (CC1 to CC5). The Head region (purple and yellow) is comprised of FAT region (FR1 to FR4), Kinase, FRB, and FATC regions. Highly conserved regions (HCRs), Ku80 binding area (Sites A and B) and interacting sites for other proteins, auto-phosphorylation sites, and caspase 3 cleavage sites are depicted above in the schematic. This domain structure has been adapted from (Sibanda et al. 2017).

2.2.6 Single-strand annealing (SSA)

Another pathway that functions on a similar principle as HRR is known as single-strand annealing (SSA). Emerging evidence suggests that this pathway has key roles in yeast and in higher eukaryotes. While GC exclusively relies on homology present in the sister chromatid, SSA utilizes the homologous regions that exist at either side of the DSB within the

same DNA molecule to bridge the DSB ends. Processing of DNA lesions in the SSA pathway often yields short or long stretches of RPA-coated ss-DNA which is a pivotal step in this pathway (Morrical 2015). Thus the bidirectional resection proceeding until homologous sequences are revealed results in deletions of up to a few hundred to thousand base pairs. Consequent loss of intervening sequence results in large deletions, mutation and possibly also translocations. Therefore SSA is a highly error-prone pathway. Unlike HRR, which requires Rad51 for strand invasion and annealing, SSA utilizes Rad52 (Bhargava, Onyango, and Stark 2016; Stark et al. 2004). Furthermore, Rad51 recombinase is shown to negatively regulate SSA. In HRR-deficient cells, SSA functions as one of the back-up pathways to repair DSBs that are not processed by c-NHEJ. Owing to its dependence on sequence homology and end-processing, this pathway is predominantly active in S and G2 phase of the cell similar to GC (Mortensen et al. 1996; Reddy, Golub, and Radding 1997).

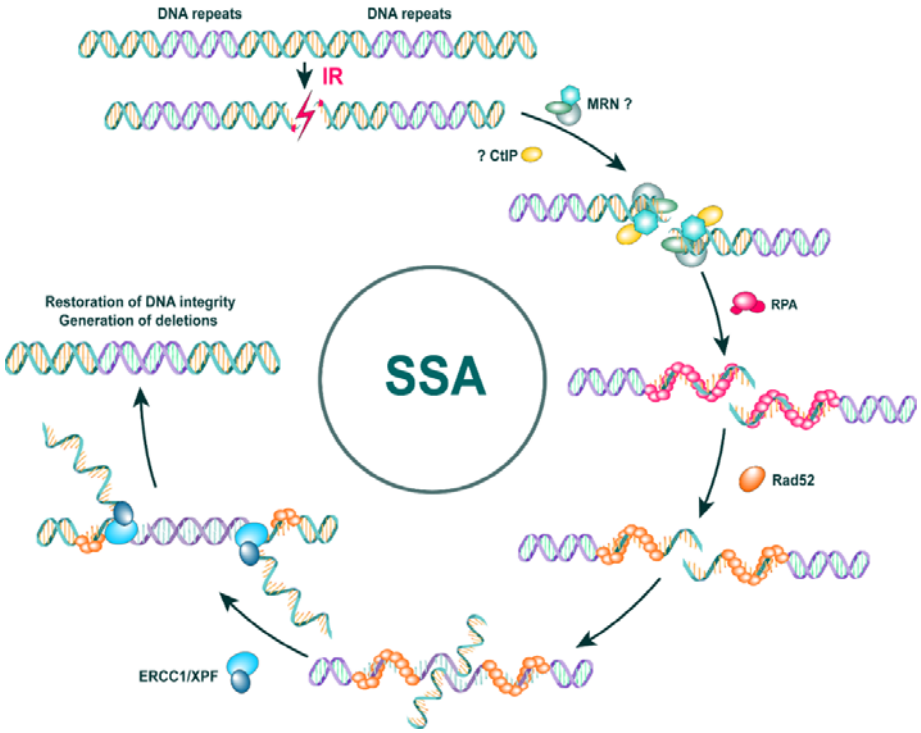

Figure 19 Graphical overview of SSA pathway the showing involvement of Rad52. Figure is adapted from (Mladenov et al. 2016).

As outlined above, each of these pathways shows differences in repair fidelity, speed and efficiency in processing DSBs as well as their dependence on the cell cycle. Despite HRR, which operates in an error-free manner owing to the presence of sister chromatid, rest pathways are inherently error-prone and are associated with sequence alterations at the DSB synapse thus contributing to the formation of chromosomal aberrations. Pathways that

function through end-processing are HRR, SSA and alt-EJ. Contrary to end-processing, c-NHEJ is the only pathway that synapses the broken DNA ends together.

A graphical illustration featuring the parameters defining the DSB repair pathway choice, their in-between coordination as well as operational requirement and hierarchy is therefore summarized in the figure 20.

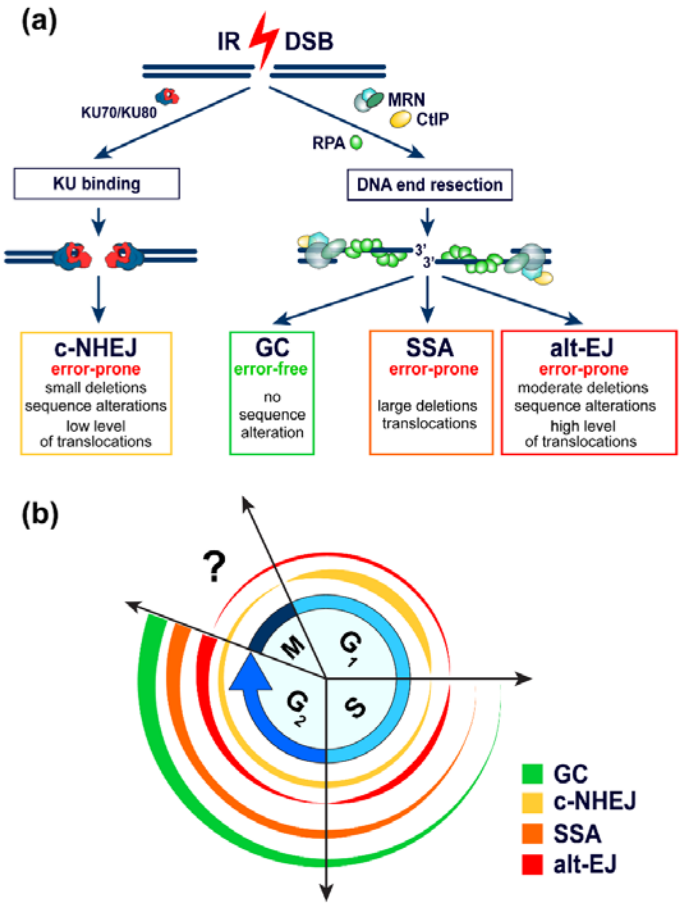

Figure 20 Parameters determining DSB repair pathway choice and hierarchy. (A) DSB repair pathways dependent or not on DNA-end resection. C-NHEJ is dependent on DNA-PK holoenzyme and operates with very fast kinetics, attenuating resection of DSB ends thereby preventing the engagement of resection-dependent pathways. Except GC, which is error-free, the remaining resection dependent pathways are inherently error-prone and frequently associated with genomic rearrangements. **(B)** Coordination of GC, c-NHEJ, SSA and alt-EJ within the cell cycle. Figure is adapted from (Iliakis et al. 2019).

2.3 DSB repair and its coordination with the cell cycle

Eukaryotic cells have evolved a magnificent cell cycle regulatory network. It includes numerous proteins whose activation and inactivation through ordered molecular events tightly control the transitions from one cell cycle phase to another and finally ensue cellular division.

In eukaryotes, the cell cycle is comprised of five distinct phases: three gap phases namely G_0, G_1 and G_2, S-phase and M-phase. A period in the cell cycle in which cells exist in quiescent state is known as G_0 phase. While in G_0 phase cells remain in a quiescent state, synthesis of RNAs as well as proteins concurrently occur in G_1 and G_2 phases. In DNA synthesis phase in other word S-phase, cells duplicate their genetic material. In the last phase denoted as M-phase, cells undergo mitosis, in which replicated chromosomes are segregated into separate nuclei and cytokinesis, in which two daughter cells are formed. Following M-phase cells reenter G1 phase to start anew cell cycle. Since G_0, G_1 and G_2, S occur between mitoses they are therefore collectively referred as interphase (Alberts n.d.; Humphrey and Brooks 2004). In the following section, how cells coordinate DSB repair with the cell cycle phases will be discussed.

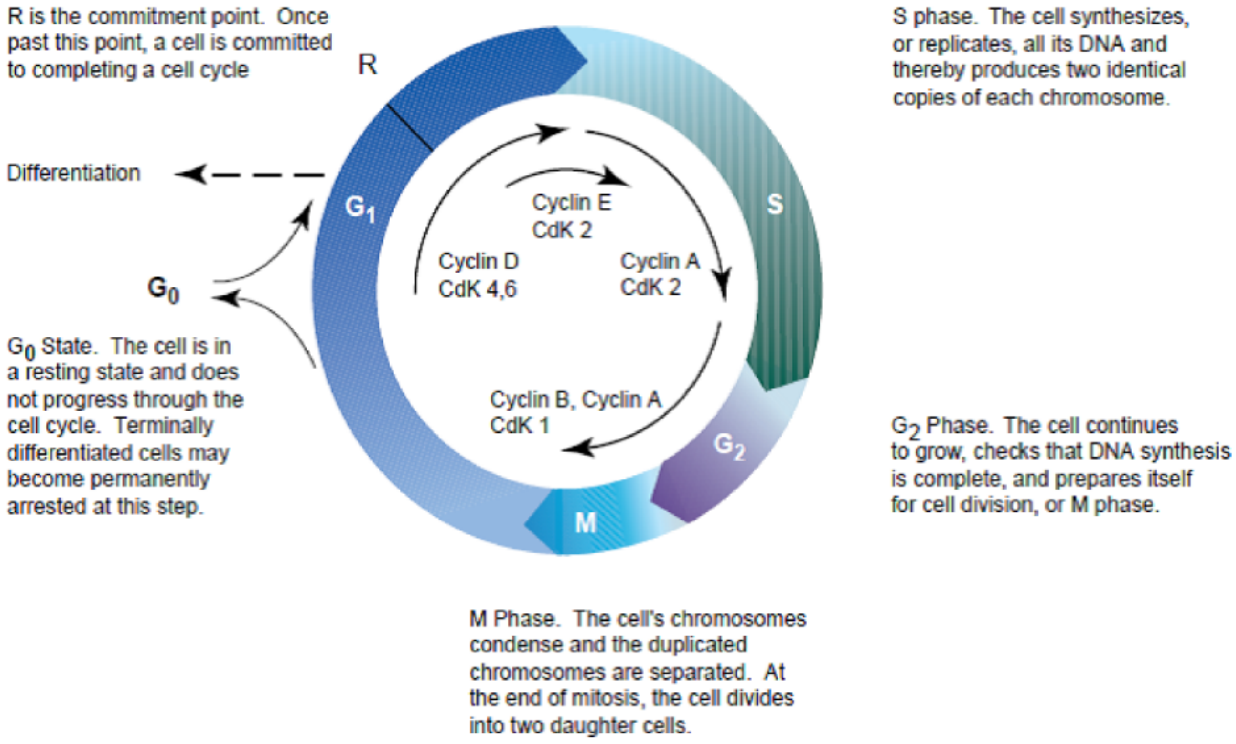

Figure 21 The eukaryotic cell cycle. Image source (Reynolds and Schecker 1999).

2.3.1 DSB repair throughout G1, S and G2 phases

In order to repair DNA breaks, cells have evolved specialized repair pathways that have different outcome depending on the cell cycle phases in which they are active. In G1 phase, c-NHEJ is the predominant pathway of repair choice when no sister chromatid as a template exists. Besides it being the dominant pathway in G1 phase, it remains also active in S- and

G2-phase. However, emerging evidence now convincingly showed that in G1 cells repair can also be mediated via alt-EJ. Owing to the absence of sister chromatid, HRR pathway is not functional in this phase of the cell cycle. Contrary to G1 phase, all repair pathways are functionally active in S and G2 phases of the cell cycle. However, because of the availability of sister chromatid, HRR is predominantly active and functional in late S and G2 phases where the level of expression of pro-HRR factors such as RAD51 and CtIP is high as well (RD and M 2000). Notably, both HRR and c-NHEJ pathways are not mutually exclusive and both have been shown to be active in S as well as in G2 phases. Conversely, putative genes centrally involved in c-NHEJ were found to be regulated independently of the cell cycle. The existing competition between BRCA1 and 53BP1 to promote either HRR or c-NHEJ pathway in S/G2 phase is a decisive step for repair of breaks to take place (Daley and Sung 2014). Identical to c-NHEJ, alt-EJ is functional throughout the cell cycle with a marked increase in its activity in G2 phase (H et al. 2001; Wu, Wang, Wu, et al. 2008).

Progression through the various phases of the cell cycle is normally coordinated by distinct checkpoints. Cells in general have G1/S, intra-S and G2/M checkpoints that in response to X-rays or other DNA damaging agents stop cells from dividing. Cyclin-dependent kinases (CDKs) are the key regulators of cell cycle progression and show their prominent roles in phosphorylating a myriad of proteins involved in distinct cell cycle phases (MB and J 2004). Perhaps the most enigmatic aspect of the checkpoint proteins is their periodic activation in various phases of the cell cycle. Besides governing entry into each cell cycle phase, CDKs are sequentially regulated by cyclins D, E, A and B too. In mammalian cells, the main cell cycle CDKs (CDK1, CDK2, CDK4 and CDK6) pair with particular proteins called cyclins. Each cyclin protein synthesized at a discrete phase of the cell cycle complexes with CDKs thus governs the cell cycle progression. In G1 phase of the cell cycle, CDK4/6 partners with Cyclin D. CDK1/2 pairs with cyclin E and cyclin A, in which the former complex has a role in transition from G1- into S-phase and the latter is important for S-and G2-phase progression. Finally, CDK1 couples with cyclin B that mediates the progression of cells through mitosis. Expression of cyclin B fluctuates throughout cell cycle where it is weak in early- to mid-S phase and high between late-S and G2 phase. Similarly, while the activity of CDK is generally low in G1, from S phase onwards it rises progressively until it reaches maximum upon mitotic entry, see figure 21 (Hydbring, Malumbres, and Sicinski 2016; Lanz, Dibitetto, and Smolka 2019; Suryadinata, Sadowski, and Sarcevic 2010).

2.3.2 DSB repair in stationary, G0 cells

As mentioned in the above section, cells can cease the active cell cycling process or can exit the cell cycle either temporarily or permanently depending on insufficiency of factors like mitogens or growth factors. Consequently, cells enter a state of quiescence known as G0 that is physiologically distinct from interphase- and M-phase. Cells mimicking G0 phase by either by serum deprivation or contact inhibition are routinely used. Upon serum replenishment (addition of mitogens and growth factors), cells reenter the cell cycle. Biochemical studies showed that G0 phase is accompanied by inactivation of CDKs via proteolysis of cyclin subunits - a process already initiated in the preceding late M-phase. Owing to the absence of CDK activity, transcription of genes associated with cell cycle progression is greatly diminished. However, in response to specific stimulation either by substances like mitogens or damage induction, cells may activate the proliferation activity which results in resumption of cell cycle progression (Alberts n.d.).

Pathway-specific involvement and their functional regulation in terms of DSB sensing in G0 have recently been implicated and drawn significant research interest. The dominant pathway in G0 cells is c-NHEJ. Besides c-NHEJ, another pathway with slower kinetics known as alt-EJ is also functional and plays significant role in repair when c-NHEJ is absent. This pathway is growth state dependent and is shown to be greatly compromised upon growth arrest in G0 phase of the cell cycle (Windhofer, Wu, and Iliakis 2007). However, cells deficient in DNA-PKcs show an alt-EJ independent DSB repair regulation. In the present study we put our emphasis on the growth state dependence of alt-EJ and the underlying mechanism for this response.

2.3.3 Pathway contribution to the processing of chromosomal aberrations

Adverse biological effects including mutations, chromosomal aberrations, mitotic inactivation and cell death are associated with DNA damage. IR in particular induces lesions that in turn through failure in repair or re-joining of wrong DNA end lead to chromosomal aberration formations, which feed carcinogenesis. Chromosomal translocation is a multistep process and their presence positively correlates with high frequency of cell killing. Thus DSBs are types of lesions that have the potential to the formation of chromosomal aberrations (Iliakis et al. 2004; Radford 1985). Upon damage induction by IR, a small subset of DSBs with slow repair kinetics has the potential to convert into either chromosomal (G1) or chromatid (G2) breaks. These breaks can be analyzed either using classical cytogenetic technique in metaphase or in G1, G2 by employing Premature chromosome condensation (PCC)

technique. Of two types aberrations induced by IR, cells irradiated in G1-or G0-phase of the cell cycle will result in chromosome-type aberrations, whereas chromatid-type aberrations arise from S-or G2-phase irradiated cells. However, cells irradiated in early S-phase may give rise to both chromosome and chromatid-type aberrations (Bailey and Bedford 2006).

The ability of cells to faithfully repair DSBs also depends on repair pathway involvement and their inherent propensities for DSB processing. Since unrepaired or mis-repaired DSBs lead to the formation of chromosome aberrations, a comprehensive understanding of the repair pathway mechanisms leading to chromosome aberration formation is of paramount importance.

The availability of sister chromatid as a repair template makes HRR a prominent pathway in S/G2 phase and breaks formed in these phases are preferentially repaired by it. Thus HRR is considered to be error-free pathway. However, chances are there that HRR, in a wild-type background, can give rise to chromosomal rearrangements (CRs) and failed HRR results in increased frequency of CRs. Owing to its template-dependent nature, the chance of forming CRs lies in its requirement for sequence homology and in this way, inappropriate template choice accounts for CRs. Moreover, improper template choice can also give rise to unequal sister chromatid exchanges including duplications or deletions. Taking into account its faithful nature of repair, studies however suggest that HRR is unlikely to produce large amount of CRs and in that HRR is very efficient in their suppression. Studies focused on HRR component mutant cells convincingly showed that factors like BRCA1, CtIP, RAD51 and its paralogues display enhanced frequency of CRs (Soni et al. 2014).

Contrary to HRR, DSB rejoining by c-NHEJ is not mediated through homologous template and making them susceptible for illegitimate mis-joining to form translocation. Owing to its fast kinetics, c-NHEJ with the help of DNA-PK complex preferentially joins the ends very quickly thus minimizing mis-joining events. In support of this notion, frequent formation of CRs in $Ku70^{-/-}$, $Ku80^{-/-}$, $Lig4^{-/-}$, or $XRCC4^{-/-}$ cells have already been demonstrated by numerous studies. A study focused on DNA-PKcs showed that chemical inhibition of DNA-PKcs kinase activity and therewith its auto-phosphorylation resulted in enhanced level of abnormal joining and translocations suggesting a suppressive role of c-NHEJ factors in formation of CRs *per se* (Iliakis et al. 2004; Lieber 2010). A competitive relationship between HRR and c-NHEJ, however, exists and in that c-NHEJ disruption leads to increased HRR-dependent repair.

If c-NHEJ and HRR pathways fail, a third pathway known as alt-EJ leading to chromosomal rearrangements comes to the fore. Owing to its comparatively slow kinetics and high half-life

of DSB ends, DSB ends generally have a longer time-frame to mis-join. Thus, the presence of persistent unrepaired DSBs substantially increases the frequency of translocation formation. Experimental results derived from LIG3 deficient cells show a significant decrease in translocation frequency and usage of microhomology, a signature of alt-EJ (D et al. 2011). Similarly, CtIP depletion performed in mouse cells show a substantial decrease both in chromosomal translocation formation and microhomology usage, hinting involvement of CtIP in their formation (Zhang and Jasin 2011). Thus alt-EJ now is considered to be a critical contributor to translocation frequency and genomic instability.

2.4 Chromosome condensation in M-phase and Interphase

In physiological circumstances, chromosomes condense in mitotic phase. However, uncoupling the mitotic events can perform chromosome condensation outside of mitosis. The phenomenon is termed as 'premature chromosome condensation (PCC). Factors collectively known as mitosis/maturation-promoting factor (MPF) mediates the key phosphorylation events associated with chromosome condensation in cells during the onset of M-phase. Exploitation of MPF factors to condense interphase chromosome for the detection of chromosome breaks have drawn significant research interest. Following the first report of PCC observation, Johnson and Rao demonstrated the correct interpretation of PCC. In their experiment, fusion of synchronized interphase cells (G1, S and G2) with inducer mitotic cells was mediated via Sendai virus and they observed that the appearance of condensed chromosome was dependent on the cell phase of interphase cells in which they were at the time of fusion (H and AA 1967; JOHNSON and RAO 1970). Based on their observations, they reached to the following conclusions:

1. Nuclei in G1-phase produced univalent chromosomes (single-chromatid morphology)
2. G2-phase nuclei showed bivalent chromosomes, and
3. Nuclei in S-phase converted to a 'pulverized' appearance which is comprised of both univalent and bivalent chromosomes

They concluded that the interphase chromosome was condensed 'prematurely' following their fusion with mitotic chromosomes and hence they coined the phenomenon as 'premature chromosome condensation'. Upon fusion between interphase and mitotic cells, accumulated MPFs in mitotic nuclei come in contact with interphase chromosomes and force them to condense prematurely. PCC had been considered as a valuable tool for chromosome analysis in radiation biology and cytogenetics. PCC can be achieved by means of viruses

(e.g Sendai virus), by chemicals (polyethylene glycol, PEG) or by drugs (Calyculin A or Okadaic acid). First successful PEG-fusion mediated PCC induction was reported by Pantelias and Maillie (Pantelias and Maillie 1983).

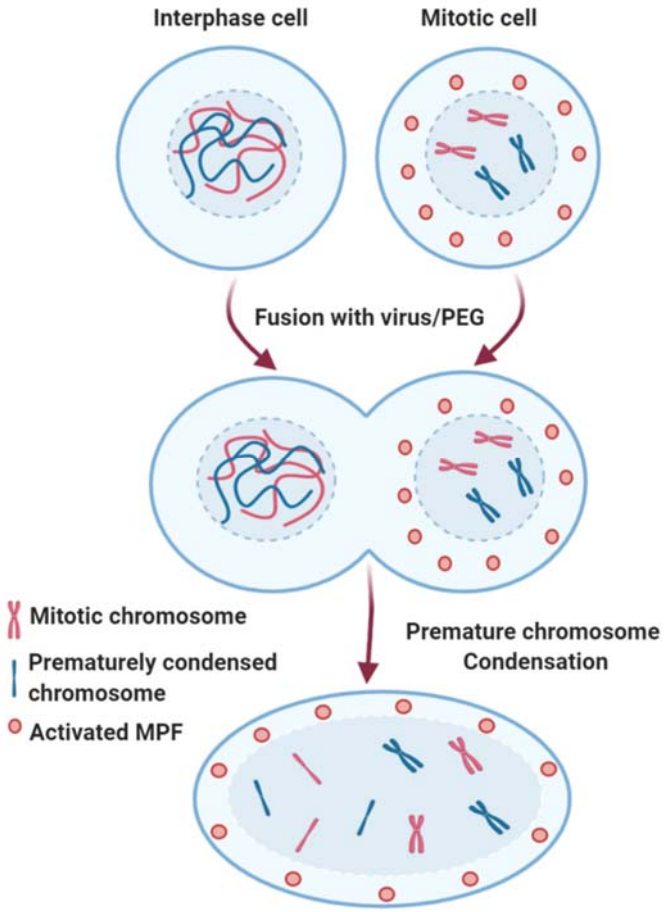

Figure 22 Mechanism of fusion-induced PCC. Fusion, in general, is achieved by either chemicals or virus. The illustration has been adapted and modified from (Gotoh and Durante 2006).

2.4.1 Molecular Mechanisms of Chromosome Condensation

Condensation of chromosome in mitosis is a multistep process in which several key factors like condensing, cohesion, lamina, microtubules, histone H1, aurora kinase and topoisomerase-2 have been identified and shown to play significant role in the condensation process (Ball Jr. and Yokomori 2001; Maton et al. 2005). Yet, the entire mechanism remains unknown. MPF is a complex of p34cdc2/Cyclin B that regulates the cell cycle progression and mitotic events. The dephosphorylated form of p34cdc2/cyclin B complex (activated MPF) mediates chromosome condensation and via PCC-fusion in interphase cells. Aided by cdc25, a cell cycle checkpoint protein and phosphatase, p34cdc2/cyclin B regulates onset of mitosis

and is activated by dephosphorylation at tyrosine (T15). The activity of cdc25 is regulated by auto-phosphorylation and/or dephosphorylation and shows sensitivity to PP1 and PP2A (type 1 and 2A protein phosphatase). Okadaic acid and calyculin A, specific inhibitors of PP1 and PP2A, influence the activity of cdc25 and p34cdc2/cyclin B (Figure 23), thus promoting the premature entry in mitotic stage (Kinoshita et al. 1993; Kumagai and Dunphy 1992). A key factor that preferentially affects the MPF activity is the cellular concentrations of cyclins, in particular cyclin B. The expression of cyclin B oscillates throughout the cell cycle where it is generally low in G1, from S phase onwards it rises gradually until it reaches maximum in G2 which corresponds also the MPF activity (Dorée and Galas 1994). Thus PCC inducing drugs either calyculin A or okadaic acid will induce PCC preferentially in G2-phase, followed by S-phase and only few in G1-phase. Fusion-induced PCC has been studied extensively to measure kinetics of DNA repair in G0 cells following irradiation, whereas calyculin A was used to measure G2 kinetics.

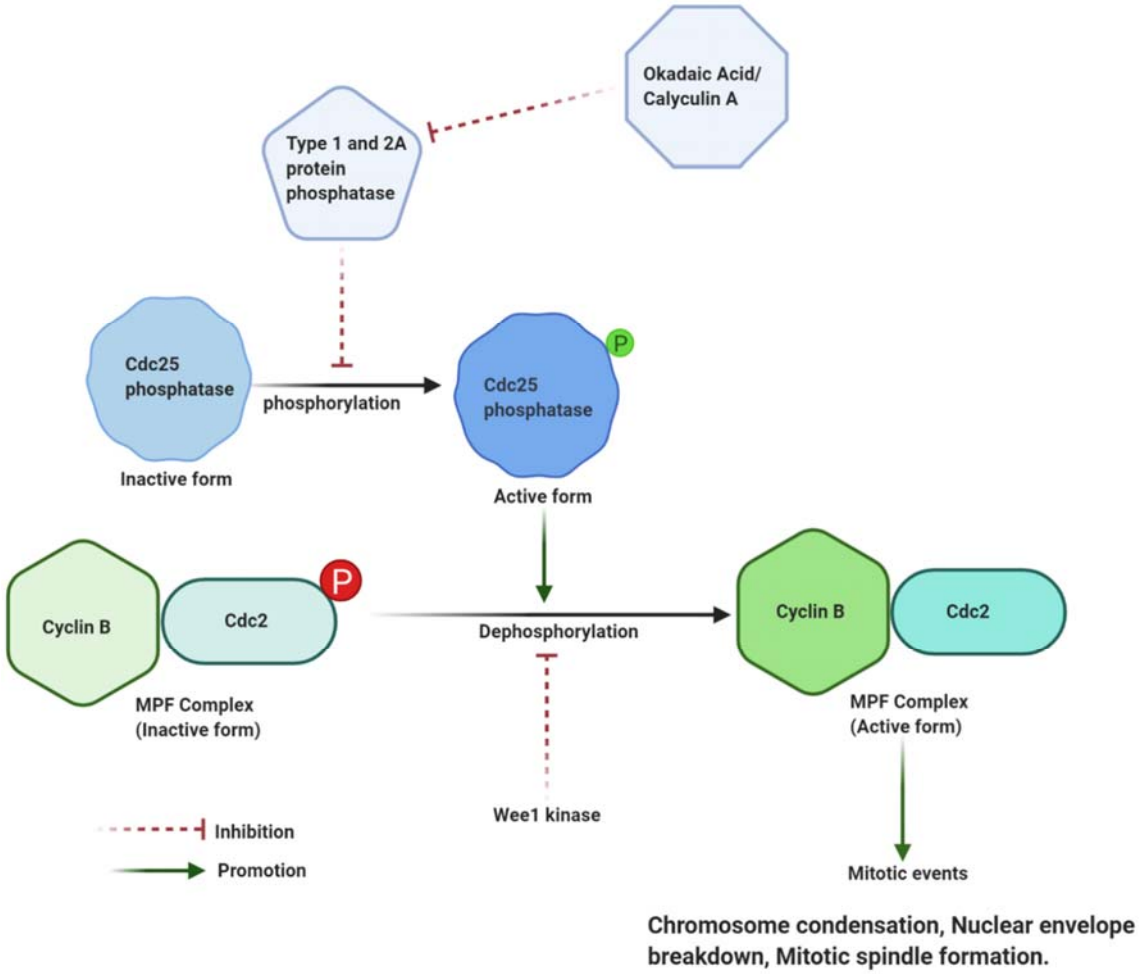

Figure 23 Mechanism of chromosome condensation. This schematic illustration has been adapted and modified from (Gotoh and Durante 2006)

II Aim of the thesis

The overarching objective of this research work is to investigate the functional role of DNA end resection component, CtIP in alternative end joining (alt-EJ) pathway to process DSBs in exponentially growing and plateau phase cells (G1) carrying mutations in components of classical non-homologous end-joining (c-NHEJ) as well as in their wild type counterpart following ionizing radiation. More importantly, we wished to find out the pivotal role of CtIP mediated alt-EJ in the processing of chromosomal breaks especially in G_1-phase cells. Yet, a striking feature of alt-EJ is its marked efficiency-reduction observed when cells enter a quiescent stage in the plateau-phase of growth and we reckoned that it is due to the reduced activity of resection apparatus during G_1/G_0 phase of the cells. Previous studies from our lab show that cells mutant in c-NHEJ factors like Ku70/80, Ligase 4 (Lig-4), X-ray repair cross-complementing protein 4 (XRCC-4) exhibit a compromised DSB processing in G_0 phase of the cell cycle hinting that alt-EJ pathway depends on growth state of the cells (Iliakis 2009).
Remarkably, only DNA-dependent protein kinase catalytic subunit (DNA-PKcs) deficient cells fail to show this efficiency reduction in alt-EJ during quiescent stage and the mechanism underlying this phenomenon remains enigmatic. Thus, our focus was to investigate the dependence of alt-EJ on growth-state especially in DNA-PKcs deficient Chinese hamster ovary cell lines and to further address the underlying regulatory mechanism based on two important questions. The first question pertains to a functional alt-EJ in DNA-PKcs deficient cells entering a quiescent stage. The latter is being an active resection of DSB ends in cells that lack DNA-PKcs activity.
It has been demonstrated that MRE11, the nuclease component of MRN complex, is required for the inception of resection at a DSB and has been implicated in alt-EJ. It remains unknown whether DNA-end processing by nuclease ensemble (MRE11 and CtIP) is an essential requirement for alt-EJ for IR induced DSBs. Thus we further investigated how these two resection elements regulate alt-EJ in DNA-PKcs mutant cells as well as in their wild type counterpart. Most importantly, in this study we investigated the functional role of alt-EJ in repair of chromosome breaks at interphase visualized in irradiated G_0 wild type (CHO10B4) and c-NHEJ mutant cell lines (IRS-20 and XRS-6) derived from Chinese hamster ovary (CHO) by examining premature chromosome condensation (PCC) breaks.
Moreover, in a separate project, in an effort to study the biological consequences of DSBs and DSB clusters, we used a biological model system where I-SceI homing endonuclease generates DSBs. Previous study from our lab shows an increased efficacy of DSB clusters

in cell killing and chromosomal aberration formation that mirrors the adverse biological effects of high-LET radiation modality. Moreover, an excellent observation of persistent 53BP1 signaling in clones sustaining I-SceI-induced complex-DSBs was monitored in a dynamic nuclear event in live cell imaging. Consistent with this, we further investigated enhanced 53BP1 signaling in complex forms of DSBs by employing indirect immunofluorescence in fixed cells.

Moreover, recruitment of 53BP1 to destabilized chromatin is mediated through sequential and concerted activation of ubiquitin-mediated signaling initiated by RNF8 and RNF168. However, the role of ubiquitination in differential 53BP1 signaling between simple DSBs and complex DSBs remains largely unexplored. To gain significant insights into the role of E3 ubiquitin ligase cascade composed of RNF8 and RNF168 in I-SceI induced simple-DSBs and DSB-clusters of increasing complexity, we studied how they regulate the DNA damage response (DDR) signaling between simple and complex-form of DSBs. Therein, we also characterized the role of RNF8 and RNF168 in chromosomal translocation formation in clones allowing the regulated expression of *I-SceI* with a particular emphasis on simple-DSBs.

Since 53BP1 and the two E3 ligases RNF8 and RNF168 function through c-NHEJ pathway, we further measured the distinct effect of high-LET and low-LET irradiation in cell killing following their genetic depletion.

III Materials and Methods

1 Materials

If not stated otherwise chemicals, oligonucleotides, enzymes, media and antibodies used were of highest purity grade.

Table 1. 1 Chemicals

Chemicals	Provider
Acetic Acid	Carl Roth GmbH + Co. KG, Germany
Ammonium persulfate (APS)	Do
Ascorbic Acid	Do
Agarose low melt	Thermo Scientific
4’,6-diamidino-2-phenylindole (DAPI)	Serva, Germany
B-Mercaptoethanol	Sigma Aldrich, Germany
Boric Acid	Carl Roth GmbH + Co. KG, Germany
Bovine serum albumin (fraction V) (BSA)	Sigma Aldrich, Germany
Bromophenol blue	Do
Chaetocin	Sigma Aldrich, Germany
Click-iT® EdU Alexa Fluor®647 Imaging Kit	In-house made
Copper(II) sulfate pentahydrate	Sigma Aldrich, Germany
Crystal Violet	Merck Millipore, Germany
Cy5 dye	Thermo Scientific, Germany
4’,6-diamidino-2-phenylindole (DAPI)	Serva, Germany
D(+)-Saccharose	Carl Roth GmbH + Co. KG, Germany
Dimethyl sulfoxide (DMSO)	Sigma Aldrich, Germany
Ethanol	Sigma Aldrich, Germany
Ethylene diamine tetraacetic acid (EDTA)	Carl Roth GmbH + Co. KG, Germany
Ethidium bromide (EtBr)	Do
Fetal bovine serum (FBS)	Gibco Life Sciences
Formaldehyde	Merck Millipore, Germany
Gelatin from cold water fish skin	Sigma Aldrich, Germany

Glycine	Carl Roth GmbH + Co. KG, Germany
Hepes	Do
Hydrochloric acid (HCl)	Carl Roth GmbH + Co. KG, Germany
Isopropanol	Do
LE standard Molecular Biology grade	7Bioscience GmbH
Low melting agarose	Carl Roth GmbH + Co. KG, Germany
Potassium Chloride, KCL	Do
Methanol	Do
Non-essential amino acids (NEAA)	Biochrom, Germany
Non-Fat dry milk	Carl Roth GmbH + Co. KG, Germany
Page Ruler, Prestained Protein Ladder	Fermentas, Thermo Scientific, Germany
Paraformaldehyde (PFA)	Do
Phosphate-buffered saline (PBS)	Carl Roth GmbH + Co. KG, Germany
Poly ethylene Glycol (PEG)	Sigma Aldrich, USA
PromoFluor Antifade	PromoKine, Germany
Propidium iodide (PI)	Sigma Aldrich, Germany
Rotiphorese® Gel 30 (37,5:1), 30% acrylamide/bis-acrylamide solution	Carl Roth GmbH + Co. KG, Germany
Sodium azide	Carl Roth GmbH + Co. KG, Germany
Sodium bi Carbonate($NaHCO_3$)	Do
Sodium chloride (NaCl)	Do
Sodium dodecyl sulfate (SDS)	Do
Sodium Hydrooxide (NaOH)	Do
Sucrose	Sigma Aldrich, Germany
TEMED	Carl Roth GmbH + Co. KG, Germany
Tris (hydroxymethyl)aminomethane (Tris)	Do
Triton X-100	Do
Trypsin	Biochrom, Germany
Tween-20	Carl Roth GmbH + Co. KG, Germany

Table 1. 2 Buffers and solutions

Solution	Compounds	Application
Fixation solution (3% PFA)	3% PFA (Paraformaldehyde) 2% Sucrose 1x PBS	Flow Cytometry
Fixation solution (2% PFA)	2% PFA (Paraformaldehyde) 2% Sucrose 1x PBS	Immunofluorescence
PBG (Blocking buffer)	0.2% Gelatin 0.5% BSA (fraction V) 1x PBS pH 7.4	Immunofluorescence/ Flow Cytometry
PBS (1x)	137 mM NaCl 10 mM Na_2HPO_4 2.7 mM KCl 1.76 mM KH_2PO_4 pH 7.4	Miscellaneous
P-solution (Permeabilization solution)	0.2% Triton X-100 1x PBS	Flow Cytometry
P-solution (Permeabilization solution)	100 mM Tris, pH 7.4 50 mM EDTA 0.5% Triton X-100	Immunofluorescence
HEPES buffered medium	5 mM NaHCO3 20 mM HEPES Serum-free growth medium	PFGE
Lysis Buffer	10 mM Tris, pH 7.6 100 mM EDTA 50 mM NaCl 2% NLS dH_2O	PFGE

	0.2 mg/ml Proteinase-K before use	
Washing Buffer	10 mM Tris, pH 7.6 100 mM EDTA 50 mM NaCl dH_2O	PFGE
RNase Buffer	10 mM Tris, pH 7.6 100 mM EDTA 50 mM NaCl dH_2O 0.1 mg/ml RNase before use	PFGE
5X TBE (PFGE running buffer)	890 mM Tris 890 mM Boric Acid 10 mM EDTA dH_2O	PFGE
Bradford Solution	0.5 mg/ml Coomassie 25% EtOH 42.5% Phosphoric Acid dH_2O	Western Blot
SDS-PAGE Running Buffer (10X)	0.025M Tris 0.192M Glycine 0.1% SDS dH_2O	Western Blot
Electrode/Transfer Buffer	0.025M Tris 0.175M Glycine 20% Methanol dH_2O	Western Blot
TBS (1X)	50 mM Tris, pH 7.6 150 mM NaCl	Western Blot
PCR Lysis Solution	67 mM Tris-HCL (pH 8.8) 16.6 mM Ammonium sulfate	PCR

	5 mM β-Mercaptoethanol 6.7 mM $MgCl_2$ 6.7 µM EDTA (pH 8.0) 1.7 µM SDS 100 µg/ml proteinase K	

Table 1. 3 Media for cell culture

Growth medium	Company
Dulbecco's Modified Eagle Medium (DMEM)	Sigma-Aldrich
McCoy's 5A Medium	Do
Minimum Essential Medium (MEM)	Do
RPMI 1640 Medium	Do

Table 1. 4 Cell lines and primary cell culture

Cell line	Species	Cell type	Mutation (m) /Knock-out (KO)	Growth medium	Serum
CHO10B 4	Chinese Hamster Ovary (CHO)	Immortalized fibroblasts (Ovarian)	Wild type	McCoy's 5A	5%
Irs20	Do	Do	DNA-PKcs (m)	McCoy's 5A	5%
XRC1-3	Do	Do	DNA-PKcs (m)	McCoy's 5A	5%
Xrs6	Do	Do	Ku80 m	MEM	10%
Irs1SF	Do	Do	XRCC3	McCoy's 5A	5%
D-U2OS	Human	Osteosarcoma	53BP1 KO	McCoy's 5A	10%
U2OS 282C DR-GFP	Human	Osteosarcoma	HRR reporter	McCoy's 5A	10%
A549	Human	Adenocarcinoma	Wild type	McCoy's 5A	7%
U2OS	Human	Adenocarcinoma	Wild type	McCoy's 5A	10%
CHO-1xS.D8	CHO	Clonal cell	I-SceI sequence integrated	Do	5%

CHO-4xS.R12	CHO	Clonal cell	I-SceI sequence integrated	Do	5%

Table 1. 5 Antibiotics

Antibiotics	Final Concentration	Company
Ampicillin	100 µg/ml	Carl Roth GmbH + Co. KG, Germany.
G-418 sulfate	300 µg/ml	Capricorn Scientific GmbH, Germany
Kanamycin	50 µg/ml	Carl Roth GmbH + Co. KG, Karlsruhe, Germany.
Penicillin/Streptomycin	100 µg/ml each	PANTM Biotech GmbH, Germany
Puromycin	2 µg/ml	Carl Roth GmbH + Co. KG, Karlsruhe, Germany.

Table 1. 6 Inhibitors

Name	Description	Final Conc. (µM/ml)	Incubation time(h), pre-IR	Cell lines	Company
Bortezomib (PS-341)	Potent 20S Proteasome inhibitor	2	4 and 12	CHO10B4	Selleck Chemicals
Gibco® KaryoMAX® Colcemid™ Solution	Arrest cells in metaphase by preventing spindle formation during mitosis	0.1µg/ml	No IR, 4 and 2	Do	Gibco™ Invitrogen Corporation
Mirin	MRE11 exonuclease inhibitor	50	1	CHO10B4, IRS-20	Santa Cruz Biotechnology
NU7441	Potent and selective DNA-PKcs inhibitor	5	1	CHO10B4, XRS-6	Tocris Bioscience, USA
Nocodazole	Inhibits polymerization of microtubules	40	10-12	CHO10B4	Sigma Aldrich, Germany

PFM01	MRE11 endonuclease inhibitor	100	1	CHO10B4, IRS-20	Tocris Bioscience, USA
PJ34	Parp-1/2	10	1	CHO10B4, XRS-6	Calbiochem
6-OH-DOPA	Rad52	10	6	Do	Sigma Aldrich, Germany

Table 1. 7 Enzymes

Enzyme	Company
Proteinase-K Molecular biology grade	Blirt S.A., Poland
RNase A (Ribonuclease A)	Applichem GmbH, Germany

Table 1. 8 Ladder and loading dye

Name	Company
DNA loading dye (6x)	Thermo Scientific
Gene Ruler 100bp plus DNA ladder	Do
Gene Ruler 1kb DNA ladder	Do
PageRuler Prestained Protein Ladder	Do

Table 1. 9 Primary Antibodies

The conditions in different methods are indicated (FC: Flow cytometry and IF: Immunofluorescence).

Antibody	Host species	Type	Dilution	Incubation time	Company
53BP1 (H-300)	rabbit	polyclonal	1:400 (IF)	1.5 h (IF)	Santa Cruz Biotechnology
γ–H2AX	mouse	monoclonal	1:400 (IF)	1.5 h (IF)	Abcam
FKBP12 Antibody (H-5)	mouse	monoclonal	1:100 (IF)	1.5 h (IF)	Santa Cruz Biotechnology
RPA	mouse	monoclonal	1:200 (FC)	1.5 h	In-house made, IFMSB, UK-Essen

H3pS10	rabbit	polyclonal	1:5000 (FC)	1.5 h	Abcam
CtIP	mouse	monoclonal	1:200 (WB)	Overnight(WB)	Santa Cruz Biotechnology
GAPDH	mouse	Polyclonal	1:6000 (WB)	Overnight	Merck Millipore
GAPDH	rabbit	Polyclonal	1:6000 (WB)	Overnight	Merck Millipore

Table 1. 10 Secondary Antibodies

The conditions in different methods are indicated (FC: Flow cytometry and IF: Immunofluorescence).

Antibody	Host species	Type	Dilution	Incubation time	Company
Alexa Fluor® 488 Anti-mouse	goat	polyclonal	1:400 (IF,FC)	1 h (IF)	Invitrogen
Alexa Fluor® 488 Anti-rabbit	goat	polyclonal	1:400 (IF,FC)	1 h (IF)	Invitrogen
Alexa Fluor® 568 Anti-mouse	goat	polyclonal	1:400 (IF)	1 h (IF)	Invitrogen
Alexa Fluor® 568 Anti-rabbit	goat	polyclonal	1:400 (IF)	1 h (IF)	Invitrogen
Anti-rabbit-IRDye680	goat	polyclonal	1:10000	1 h (IF)	Li-COR Biosciences
Anti-rabbit-IRDye800	goat	polyclonal	1:10000	1 h (IF)	Li-COR Biosciences
Anti-mouse-IRDye680	goat	polyclonal	1:10000	1 h (IF)	Li-COR Biosciences
Anti-mouse-IRDye800	goat	polyclonal	1:10000	1 h (IF)	Li-COR Biosciences

Table 1. 11 Plasmids

Plasmid	Description
pGFP-53BP1	Expresses 53BP1-GFP fusion protein
pEGFP-kap1	GFP expressing plasmid
pCMV3xNLS-ISceI (pI-SceI-3xNLS)	I-*Sce*I expressing plasmid
pVB-GFP-Puro	GFP-tagged I-SceI expressing plasmid

Table 1. 12 Oligonucleotides

All siRNAs and primers were purchased from Eurogentec unless otherwise stated. PCR primers for flanking the region of I-SceI integration sites were designed in-house and synthesized by Eurogentec. Primers were provided in 100 µM concentration.

siRNA	Sequence
CtIP	siCtIP-1: 5´-GUGCAAGGUUUACAAAUAA-3´
	siCtIP-3: 5´-AGAAUACUCUCCAGGAAGA-3´
RNF8	haRNF8-1: 5′-UGCGGAGUAUGAAUAUGAA-3
	siRNF8-MS1: 5´-GGACAAUCAUGGACAACAA-3´
RNF168	siRNF168-MS-1: 5′-GGAGAAGUGAGAUGGAAGA-3′
	siRNF168-MS-2: 5′- GAAGUGAGAUGGAAGAACA-3′
Primer	**Sequence**
Sceinsert460ASFwd	5´-GACTGTGCCTTTAAACAGC-3´
Sceinsert460ASRev	5´-ACTTTCCACACCCTAACT-3´

Table 1. 13 Major laboratory equipment and applications

Instrument	Application	Company
Analytical Digital Balance Scale, BP 110	Balancing	Sortorius, Gottingen,Germany
Laborklav 55-195	Sterilization	SHP Steriltechnik AG,Germany
Centrifuge, Biofuge Fresco	Centrifugation	Heraeus, Germany
Centrifuge, Multifuge 3S-R	Do	Heraeus, Germany

Centrifuge, Rotanta 460R	Do	Hettich, Germany
Confocal laser scanning microscope TCS SP5	Microscope (Optical Imaging)	Leica Microsystems, Germany
Cooling Unit, DC10-K20	Cooling	Thermo Fischer Scientific, Germany
Coulter counter, Multisizer 4e	Particle sizing and counting system	Beckman Coulter, Germany
Electrophoresis chambers, Horizon	Gel Electrophoresis	Life Technologies, USA
Electrophoresis Power Supply, EPS 301	Gel Electrophoresis	Amersham, GE Healthcare, USA
FluorImager, Typhoon 9400	Gel Scanning	Molecular Dynamics, Germany
Flow cytometer Gallios	Cell cycle analysis and GFP-based transfection efficiency	Beckman Coulter, Germany
Heating unit	Heating	Oehmen, Germany
Inverted microscope LH50A	Microscope	Olympus, Germany
Laminar flow hood, HeraSafe	Biological Safely Cabinet	Heraeus, Germany
Magnetic stirrer, MR Hei-Standard	Stirring	Heidolph, Germany
MCO-18 O2/CO2 incubators	CO_2 incubator	Sanyo, Germany
Molecular Imager VersaDoc	Imaging and Gel Scanning	Bio-Rad, USA
Micro Centrifuge, IR	Centrifugation	Carl Roth, Germany
Minishaker MS1	Shaker	IKA, Germany
Nanodrop	DNA and RNA concentration measurement	Thermo Scientific, Germany
Nucleofector	Cell Transfection	Lonza Cologne GmbH, Germany
Odyssey® infrared imaging system	Western blots with infrared fluorescence detection	LI-COR Biosciences, Germany
O_2/CO_2 Incubator, MCO-18AIC/MCO-18M	CO_2 incubator	Sanyo, Japan
Mettler Toledo FE20/EL20	pH Meter	Mettler-Toledo GmbH, Giessen, Germany
Pipetboy		Falcon, Germany

Pipettes, Rainin Pipet-Lite		Mettler Toledo, Germany
PTB dosimeter	Radiation dosimeter	Physikalisch-Technische Bundesanstalt, Germany
Rocky shaker	Shaker	Oehmen, Germany
Slide drying bench	Heating	Electrothermal, Germany
Sonicator, RK225H	Protein extraction	Sonorex, Bandelin, Germany
Typhoon Scanner	Scanning (Laser Scanner)	GE Healthcare, USA
Thermomixer	Mixing	Eppendorf, Germany
Amersham™ Typhoon™ Biomolecular Imager	Scanning (Laser Scanner)	GE Healthcare, USA
UV Spectrophotometer	Protein conc. measurement	Shimadzu Corp., Japan
Vacuum gas pump	Vacuum system	VWR, Germany
Vortexer, IKA MS 3 basic	Vortexing	IKA, Germany
Water bath, GFL 1092	Heating	Oehmen, Germany
X-ray control unit, Xrad320	Irradiation	PXi, USA
X-ray generator, ISOVOLT Titan	Do	General Electrics, USA
X-ray tube, MXR320	Do	Comet, Switzerland

Table 1. 14 Software's

Software	Company
Adobe Creative Suite 6	Adobe Systems Inc., USA
Image Quant 5.0	GE Healthcare, Germany
Imaris 8.1.2/9.5.1	Bitplane AG, Switzerland
Kaluza 2.1	Beckman Coulter, USA
Leica Application Suite Advanced Fluorescence (LAS AF)	Leica Microsystems, Germany
Metafer	Leica Microsystems, Germany
Microsoft Office 2013	Microsoft Coporation, USA
Mendely reference manager	©2020 Elsevier B.V.
SigmaPlot 12	Systat Software Inc. USA

2 Methods

2.1 Cell Culture

All cell lines were maintained at 37°C in a humidified incubator with 5% CO_2. Cells were cultured in tissue culture dishes in corresponding growth medium (listed in table 3.1.5) supplemented with 5% fetal bovine serum (FBS), 2mM glutamine and 1% penicillin/streptomycin. Cells were on a regular basis tested for the presence of mycoplasma using commercially available mycoplasma detection kit. Only mycoplasma negative cells were further subjected to subsequent experiments.

2.2 Cell Passaging and Counting

Cell cultures were visually examined in phase contrast microscope to evaluate optimum confluency (~80%) and absence of bacterial and fungal contaminants, and were passaged in every second day to maintain optimum confluence. Five ml of PBS (1x) was used to wash/remove the residual medium and dead cells. One milliliter of Trypsin-EDTA was then added to the flask and gently swirled and then incubated for 2 mins at 37°C to detach the adhering cells. They were then observed in a phase contrast microscope to confirm detachment of cells. Next, 5ml growth medium containing 5% FCS was added to stop trypsinization, and cells were resuspended with a Pasteur pipette for proper mixing and reducing cell clumping. Cells were counted with coulter Counter (Multisizer™, Beckman Coulter) where 500µl of cell suspension was subsequently mixed with 9.5ml isotone (1:10 dilution) before putting the vessel into the counting apparatus and appropriate number of cells was plated for subculture. Newly thawed cells were passed at least two times before performing experiments.

2.3 Cell Synchronization

For synchronization of CHO cells in G1 phase of the cell cycle, cell cultures were incubated overnight in medium containing 40 ng/ml nocodazole. Subsequently, mitosis-arrested cells were released from the block for 1 h to enter G1 and immediately used for experiments.

2.4 Inhibitor treatment

Inhibitors used for various experiments were dissolved in dimethyl sulfoxide (DMSO). If not otherwise mentioned, cells were treated with respective inhibitors one hour prior to irradiation and kept until the collection of time point for all performed experiments (PFGE and

cytogenetic). Table 1.6 (inhibitors table) shows different concentrations and incubation time with corresponding experiments for drugs used for experiments. All stocks of inhibitors were stored at -20 °C.

2.5 Transfection (plasmid and siRNA) by electroporation

Transfection by electroporation was performed by Amaxa Nucleofector® device (Lonza). Three-five million cells were transiently transfected with 3-5µg plasmid (1:1) in each transfection. siRNAs were delivered also using the same nucleofector device and 20nmol siRNA was used for each transfection with 3-5million cells. Trypsinized cells were centrifuged at 1000rpm for 2 minutes and dissolved in 100µl pre-warmed transfection buffer followed by the addition of the required amount of plasmid or siRNA. This reaction cocktail was then transferred to the electroporation cuvette. According to manufacturer instructions, transfection programs U23, X01, X05 were used for CHO, U2OS, A549 cells, respectively. Post-transfected cells were transferred to pre-warmed media. Transfection with pGFP-53BP1 plasmid was performed to evaluate the transfection efficiency by FACS, which varied between 85-95%. Post-transfected cells were further subjected to downstream processing like immunofluorescence, flow cytometry, western blot, survival assay and pulse field gel electrophoresis (PFGE). Experiments were performed 8hr, 12hr, 18h, 24hr or 48hr post-transfection.

2.6 IR exposure

Cells were irradiated with X-rays using an X-ray machine (“Isovolt 320HS”, Seifert/Pantak, General Electric-Pantak). Tube voltage and current were set to 320 kV and 10 mA respectively and 1.65 mm aluminium filter (GE-Healthcare) was used to absorb “soft” X-rays. The dose rate was estimated to 1.3 Gy/min using an in-field ionization monitor, calibrated with a PTB dosimeter (Physikalisch-Technische Bundesanstalt, Braunschweig, Germany). Radiation dose was determined using Fricke chemical dosimetry. Rotating the radiation table ensured an even irradiation field. Cells were returned to the incubator immediately after IR and collected at different time points post irradiation.

2.7 Genomic DNA extraction

Total DNA extraction was performed following heat extraction method using PCR lysis solution. DNA was extracted from asynchronously maintained CHO clonal cells. Cells in culture dish were first washed with PBS and trypsinized. The collected cells were centrifuged

for 5 min at 4°C and washed once with cold PBS. The cell pellet was resuspended in 200µl PCR lysis solution and incubated for one hour at 37°C followed by deproteinization by Proteinase K for 10 min at 80°C. Finally 5-25 µl aliquots of DNA were used as template to perform PCR reaction for genotyping of CHO clonal cell lines.

2.8 Polymerase chain reaction (PCR)

PCR (Polymerase chain reaction) was performed to amplify DNA sequences. The PCR reaction mixture was set up in a total volume of 20 µl containing of 1-10 ng template DNA, 100 mM dNTP Mix, 1 x PCR-Buffer, 2.5 U Phusion® Polymerase, 0.2 µm of reverse and forward primer and Milli-Q water. The amplification reactions were performed in a Mastercycler-ep-gradient-S thermal cycler (Eppendorf) with the conditions illustrated in Table 1. The PCR fragments were visualized on 1% or 2% agarose gel. The PCR conditions were as mentioned below.

Program		Temperature	Time
Step 1	Denaturation	98°C	30 sec
Step 2	Denaturation	98°C	15 sec
Step 3	Annealing	56°C	15 sec
Step 4	Elongation	72°C	15 sec
Step 5	Elongation	72°C	5 min
Step 6		4°C	Store

Step 2, 3 and 4 were repeated for 35 cycles.

2.9 Agarose gel electrophoresis

Agarose gels were run at 95V for 45 mins in a 1 x TAE buffer. Gene Ruler 1kb Plus DNA Ladder (Thermo Scientific) was used for amplicon size determination. In order to visualize the DNA, the gel was stained for 1 h in 50 ml 1 x TAE containing 1% ethidium bromide (EtBr) with gentle shaking. Finally the gel picture was captured using UV Transilluminator Bio-Doc Analyzer (Biometra).

2.10 Heat-shock transformation of *E. coli*

Transformation was performed using competent *E. coli* strain DH5α. DH5α was thawed on ice in a 1.5-ml tube and gently mixed with 10-50ng of plasmid DNA. The content was gently mixed-up by flicking the bottom of the tube a few times. The content was then placed on ice for 15mins, followed by heat shock for 30 seconds at 42°C and finally placed on ice again for 15 mins. Subsequently, 950µl warmed LB medium (without antibiotics) was added to the microtube followed by 1.5 hours incubation at 37°C in a shaking incubator. Cells were then homogenously spread using a one-way bent inoculation needle onto a 10cm LB agar plate containing ampicillin (100µg/mL) and incubated at 37°C overnight. On the following day colonies were selected for plasmid Midi-prep.

2.11 Midi preparation of Plasmid DNA

Plasmid DNA was purified using GeneJET Plasmid Miniprep Kit (Thermo Scientific) following the manufacturer's recommended protocol. A single colony was selected and picked from the transformed agar plate and used to inoculate 6ml LB media in a 12ml vial. Six microliter of ampicillin was added (1:1000 ratio) and incubated at 37°C in a shaker overnight to obtain a saturated culture. Next day, the cells were pelleted by centrifugation and suspended in 250µl re-suspension solution and transferred to the microcentrifuge tube. Lysis buffer (250µl) was added to liberate plasmid DNA, followed by Neutralization buffer (350) to neutralize the resulting lysate. The mixture was gently inverted 4-6 times. The supernatant was centrifugated for 10min at 13000rpm and transferred to the spin column provided, and centrifuged. The flow through was discarded. Spin column containing absorbed DNA was subjected to two steps of washing with 500µl washing solution and residual ethanol present in the washing solution was removed by brief centrifugation. Finally, the desired plasmid DNA was eluted using 50µl Elution buffer and stored at -20°C until further use. Concentration of purified plasmid DNA was determined using the Tecan M2000 (Tecan®) Photometer. Two µl of DEPC-treated water was used as blank. Two µl of DNA samples was used for the estimation of concentration.

2.12 Preparation of lysate from cell culture and protein quantification

Cells were washed once with ice-cold PBS and lysed in 100µl Radio-Immunoprecipitation Assay (RIPA) buffer containing protease and phosphatase inhibitor. Whole lysates were placed on ice for 15 mins followed by DNA fragmentation in a sonicator (Bio Ruptor® UCD-200TM-EX) and finally placed on the ice for another 15 mins. The sonicated lysate was then

centrifuged at 12000rpm for 15 min at 4°C and the supernatant was transferred to a new microtube. Aliquots were stored at -80°C until further analysis. Protein concentration was determined using colorimetric Bradford assay. At 562nm, absorbance was colorimetrically measured.

2.13 SDS-PAGE and western blotting

For SDS-PAGE a stacking gel of 5% and a separating gel of 10% were prepared. Samples (50-100µg) were mixed properly with protein loading dye (2x Laemmli Solution) to a final volume of 30-40µl and denatured at 95°C for 5 minutes. The samples were shortly spinned before loading onto the SDS-PAGE gel and run at 70V for 15mins. The voltage of the run was increased to 100V thereafter for two hours. Proteins were transferred from gels onto nitrocellulose membranes using Bio-Rad wet transfer system at 100 Volts for 2 h.

The membrane was blocked using 5% w/v skim milk powder in TBS for one hour at RT on a rocking platform. Traces of blocking solution were washed by rinsing with TBS and incubated at 4°C overnight with appropriate primary antibody (1:200-1:1000) on a rocking platform. The blot was then washed thrice for 5-10 min with TBST (0.05% Tween20 in 1X TBS). The membrane was then incubated for 1 hour at room temperature (RT) with the appropriate secondary antibodies conjugated with infrared dyes (IRDye 680LT and IRDye 800CW, Li-Cor BioSciences, USA) that was diluted in TBST solution (1:10,000-1:20,000). Following this, the membrane was washed thrice with TBST for 10 min each at RT. Finally, proteins of interest were detected using Odyssey® Infrared Imaging System.

2.14 Clonogenic survival assay

For the clonogenic survival assay, exponentially growing cells were irradiated with increasing doses of IR, trypsinized immediately and plated in different dilutions according to the dose of radiation delivered. For I-*Sce*I transfected cells, cells ranging from 300-1500 were plated in 60 mm dishes immediately after transfection. Cells plated for survival were grown for 8 days (CHO wild type and clonal derivative cell lines) in a humidified incubator at 37°C and 5% CO_2 and subsequently fixed and stained with 1% Crystal Violet in 70% Ethanol. Colonies were counted either manually using a stereomicroscope. Only colonies that comprised of 50 or more cells were scored.

2.15 Pulsed-field gel electrophoresis

Pulsed-field gel electrophoresis (PFGE) was performed to detect IR-induced DSBs with the

physical separation of fragmented DNA. To evaluate the induction of DSBs at different radiation doses, cells were collected and resuspended in ice-cold serum-free HEPES-buffered cell culture medium to reach a final concentration of $6x10^6$ cells/ml. This cell suspension was then mixed with an equal volume of serum-free HEPES-buffered medium containing 1% low melting agarose (Thermo Scientific). The cell-agarose suspension was then pipetted into glass tubes with a diameter of 3 mm and placed on ice for polymerization. Solidified cell-agarose suspension was extruded from glass tubes and cut into 5 mm long cylindrical pieces (plugs). To obtain dose-response curve, agarose plugs were placed in a 35 mm petri dish containing 2 ml cold serum- free HEPES buffered medium and exposed to 5, 10, 20 and 30 Gy of IR. Non-irradiated controls were also kept on ice. Plugs were immediately placed in cold lysis buffer and incubated at 4°C until repair kinetics plugs were collected for all time points. For the evaluation of DSB repair kinetics, attached cells in the culture dishes were exposed to 20 Gy of IR and incubated at normal cell culture conditions to allow cells to repair IR induced DSBs, until the collection of time points. After each repair time interval, cells were collected and embedded in agarose plugs and placed in cold lysis buffer as described above. For determination of the background-DNA-released, plugs were prepared from otherwise identically treated non-irradiated cells at different time points. All collected plugs in the cold lysis buffer were initially incubated at 4°C for at least 1hour and then at 50°C water bath for 18h. After lysis, the plugs were then washed with washing buffer in a 37°C water bath for 2 h. Then, the plugs were treated with RNase A (0.1mg/ml) at 37°C for another 2 h and loaded in 0.5% agarose gels prepared in 0.5X TBE buffer. Electrophoresis was carried out in Horizon 20x25 boxes with cooled circulating 0.5X TBE buffer to ensure a stable temperature of less than 10°C for 40 h using alternating cycles of 50 V (1.25 V/cm) for 900 sec in the (forward) direction of DNA migration and 200 V (5 V/cm) for 75 sec in the reverse direction. Following electrophoresis gels were stained with 8 µg/ml EtBr for 6 h and washed in dH_2O overnight to remove the excess EtBr. Solutions for PFGE are shown in Table 5. Gels were scanned with Typhoon 9400 imaging device and analyzed using Image Quant 5.0 software. The fraction of DNA released (FDR) from the well into the lane reflects the DSBs present in the cellular genome and is plotted as a function of dose to obtain a dose response (DR) curve. FDR shows a linear increase with the dose of IR, however the dose response can vary depending on the cell type and cell cycle phase (Iliakis et al. 1991). Therefore using DR curves for each set of plugs, we calculated a dose equivalent (DEQ) in Gy for the repair kinetics (RK) data points and this parameter was plotted against repair time. Curve fitting was performed in Sigma Plot 12.5 software using an exponential decay algorithm, assuming a

fast and a slow repair component.

2.16 Cell cycle analysis by FACS

Fluorescence-activated cell sorting (FACS) is a specialized type of flow cytometry that allows cell sorting by assessing fluorescence intensity. Cell cycle distribution was evaluated by measuring the fluorescence intensity propidium iodide (PI) – a DNA intercalating dye that exhibits strongly increased fluorescence when bound to nucleic acids and is membrane impermeant. Thus, for DNA content measurements, cells were fixed and permeabilized in 70% pre-chilled ethanol (EtOH). Fixed cells were stored at 4°C for further use. Before measurement, cells were spun down, EtOH was decanted and the pellet was resuspended in sufficient amount of PI staining solution (40 µg/ml PI, 62 µg/ml RNaseA dissolved in PBS) and the content was incubated for 15-30min at 37°C in a water bath. Samples were then measured in a flow cytometer (Gallios™, Beckman Coulter). To obtain standard histograms 15000 events were counted, and gated based on forward and side scattering. Acquired LMD data files were analysed using the Kaluza® flow cytometry analysis software. Cell cycle analysis using HST files was performed with WinCycle® software.

2.17 Classical cytogenetic

To perform classical cytogenetics, cells were allowed to accumulate at metaphase by adding colcemid (0.1µg/ml) for 2 h before collection. Cells were collected following PBS wash and trypsinization and centrifuged at 1200rpm for 5min. In the following step, cells were treated with a hypotonic solution (75mM KCl) by adding it drop-wise while tapping the tube well enough to dissolve the pellet and mix the cells. Following hypotonic treatment, cells were fixed with fixative solution (3:1, methanol: Glacial acetic acid). After washing the cells twice in fixative, fixed cells were dropped on a (one drop 20µl) glass slide to prepare metaphase spreads and stained with 3% Giemsa stain (dissolved in 1 x Sörensen's buffer) for 6-7 minutes prepared in Sorenson's buffer (1x). The slides were air dried at RT and finally mounted with coverslips using Entellan® (Merck). Scoring criteria included chromatid breaks and gaps with the latter being longer than the chromatid width. Chromosome exchanges were counted as two chromatid breaks. Bright field microscopy (Olympus VANOX-T, Japan) was used for scoring. Alternatively, an automated imaging system (MetaSystems) was used to obtain high quality images of metaphase chromosomes. For searching metaphases the M-Search module of the Metafer software (MetaSystems) was employed using the 10x objective. A classifier was used for M-Search that was specifically configured for the selected

cell line. After performing M-Search, only metaphases with good spreading were selected and captured at a higher magnification (63x oil immersion objective) using the AutoCapt setting of the Metafer software. Images were analyzed using the Ikaros Software. See figure 66 for the CHO metaphase spreads, showing chromatid breaks and chromatid exchanges.

2.18 Cell fusion and premature chromosome condensation (PCC)

Chromosomal aberrations can be visualized during mitosis when chromosomes are condensed. Premature chromosome condensation (PCC) is a sensitive method to detect chromosome breaks in interphase chromosomes. In the present work PCC was employed for chromosome analysis of univalent chromosomes (single-chromatid morphology) in G1/G0 interphase cells. In this method interphase cells (recipient) are fused with inducer mitotic cells and fusion is achieved in particular by the fusing agent polyethylene glycol (PEG). In order to fuse serum-deprived cells, trypsinized cells collected in 14 ml round bottom culture tube were centrifuged at 1100rpm for 5mins. Simultaneously, mitotic cells were collected by shaking-off procedure and were spun down following centrifugation. After that both mitotic and interphase cells were resuspended with 1ml of reaction mixture (1x PBS, 10mM Hepes and Colcemid) and centrifuged with 900rpm for 5mins. Supernatant was removed by decanting the tubes and kept the tubes in the inverted position on tissue until the addition of PEG. After a while, 150 µl of PEG (45%, prepared in PBS and 10mM Hepes) was added straight to the cell pellet while holding the tube upside down and immediately reversed the tubes without further shaking. Next, 1.5ml of the same reaction cocktail (1x PBS, 10mM Hepes and Colcemid, 0.1µg/ml) was added to the tubes and mixed with PEG solution gently tapping the bottom of the tube before centrifugation. Finally, 750 µl of pre-warmed RMPI medium supplemented with 10% serum and colcemid was added carefully so that inducer mitotic cells and interphase recipient cells remain suspended in small aggregations. Samples were incubated at 37^0C for around one hour to allow cell fusion and PCC induction. Of note, in every step during PCC, cells were kept in serum-free medium to restrain them from proceeding through G1/S (interphase cells) and in colcemid to restrict M/G1 transition (mitotic cells). After 1 h of incubation period, chromosome spreads were prepared following standard cytogenetic procedures mentioned in section (2.17). Bright field microscopy (Olympus VANOX-T, Japan) was used for scoring. Standard criteria were used for scoring. For scoring, we specifically used normalized yield of excess PCC fragments following subtraction of breaks of non-irradiated control samples (21 PCC). See figure 40 and result section 1.6.1.1 for detail. Examples of some PCC spreads (irradiated/non-irradiated) are shown in figure 40, 41, 46.

2.19 Immunofluorescence staining

For immunofluorescence staining of γ–H2AX and 53BP1, $0.2x10^6$ transfected cells were plated in 35 mm dishes with 2 ml growth medium. Twelve hours post-transfection the growth medium was removed, cells were washed with PBS and fixed in 2 ml 2% paraformaldehyde PFA for 15 min. Cells were washed again with PBS and permeabilized in 2 ml P-solution (100 mM Tris-pH 7.4, 50 mM EDTA, 0.5% Triton X-100) for 7 min. After washing, cells were blocked in PBG (0.2% gelatin, 0.5% BSA in PBS) at 4 °C overnight. The primary antibody was diluted 1:400 in PBG and 100 µl droplets were pipetted on a Parafilm®. The coverslips were placed with the cells facing the antibody solution and incubated for 1.5 h at RT. After returning the cover slips into the dishes they were washed with PBS (1x) 3 x 10 min at RT. In the next step the cells were incubated for 1h at RT with secondary antibodies conjugated with Alexa Fluor dyes (1:400 dilution) and washed 3 times in PBS ten minutes each. After that coverslips were incubated with 50 ng/ml DAPI (4', 6 diamidino-2-phenylindole) for staining of DNA. Coverslips were then mounted on microscopic slides with PromoFluor antifade reagent (promoKine, Germany). Before scanning, slides were kept for 24 h at RT and finally stored at 4 °C. Scanning of the slides was carried out with a Confocal Laser Scanning Microscope (CLSM) from Leica Microsystems (DMI 6000 B).

2.20 Confocal Microscopy

Fixed cells were analyzed by confocal microscopy using a Leica TCS-SL laser scanning microscope (TCS SP5, Leica Microsystems). The different channels were detected sequentially, and the laser power and detection windows were adjusted for each channel to exclude overlap between different fluorochromes and to avoid signal saturation. Confocal Laser Scanning Microscope (TCS SP5, Leica Microsystems).

2.21 Foci analysis by Imaris

The analysis of the LIF files (three dimensional data sets) that were generated after scanning was performed using the Imaris® software (Imaris 8.1.2/9.5.1; Bitplane). For foci scoring, images of different time points in respective experiments were loaded and foci of cells were counted. Foci were defined as spots of higher intensity than the defined threshold and with minimum size of 0.5 µm. The data was analyzed with Microsoft Excel 2013® and graphs were plotted with SigmaPlot® 12.0.

IV Results

1 The role of CtIP in DSB processing

1.1 CtIP depletion sensitizes the CHO cells to IR

In order to examine the effect of CtIP depletion on cellular survival, we performed clonogenic survival assay in rodent cell line (CHO10B4-wild type) transfected or not with siRNA against CtIP following exposure to different doses (Gy) of IR. It is evident from the result that CtIP depletion resulted in sensitization of the cells towards ionizing radiation (IR) when compared to control siRNA transfected cells. This is consistent with a previous report showing that CtIP depletion in human cells leads to a marked sensitization towards DNA damaging agents (Sartori et al. 2007).

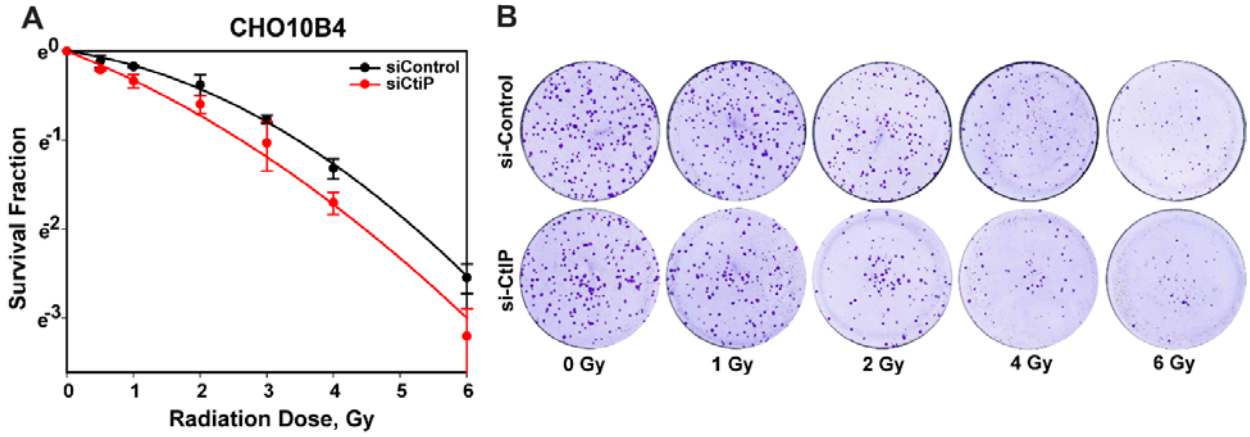

Figure 24 CtIP depletion causes radio-sensitization in CHO10B4 cells. Cells maintained in exponential phase of growth were transfected with siRNAs against CtIP. Twenty-four hours post transfection, cells were irradiated, trypsinized and subsequently seeded again in appropriate numbers to form colonies. **A,** Survival fraction of CHO10B4 cells measured by clonogenic survival assay. Data points shown in the graph represent mean and standard deviation (SD) calculated from three to four independent experiments. **B,** Representative picture of survival dishes from colony formation assay counted at 8 days.

CtIP is an essential component of homology-dependent repair pathway and is restricted to S/G2 phase of the cell cycle. Previous reports convincingly showed a precise role of CtIP in alt-EJ (Bennardo et al. 2008; Lafranchi et al. 2014). In order to establish a connection between CtIP and its role in alt-EJ, we performed similarly clonogenic survival assay using moderate radiation dose (0 to 2 Gy) in CHO mutant cell line - irs1SF, which is of CHO origin but deficient in one of the paralogs of RAD51, XRCC3 thus excluding the relative contribution

of CtIP that is mediated through HRR and exemplifying the role of CtIP contributed via alt-EJ. CtIP-depleted irs1SF cells showed a moderate sensitivity toward irradiation compared to their corresponding control demonstrating a possible functional role of CtIP in alt-EJ (figure 25).

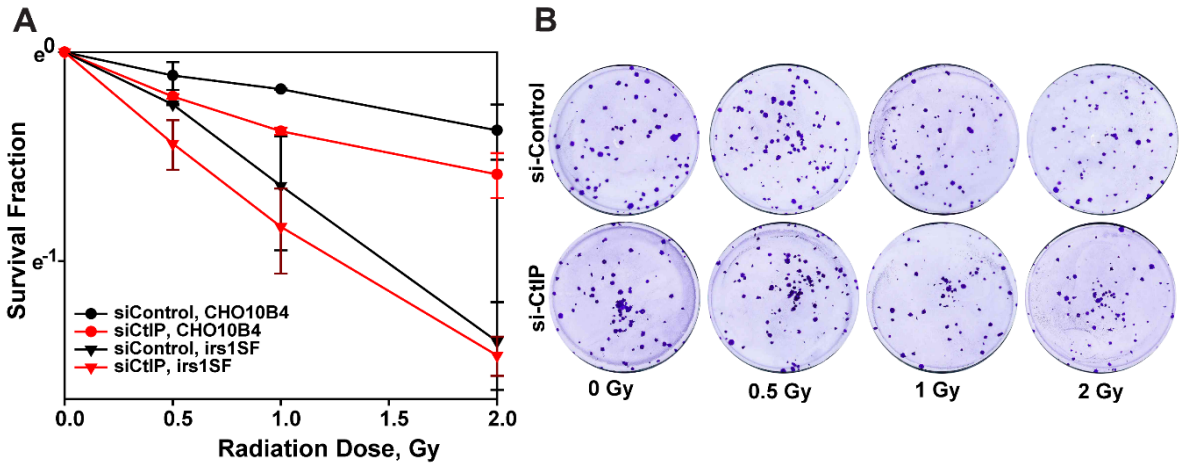

Figure 25 Knockdown of CtIP in HRR deficient cells moderately sensitizes cells to irradiation. Asynchronously growing irs1SF (XRCC3 mutant) cells were transfected with siRNAs against CtIP. Twenty four hours after transfection, cells were irradiated and seeded again in appropriate numbers following trypsinization and allowed to form colonies for 8 days. **A,** Survival fraction of irs1SF cells was measured by colony formation assay and is plotted as a function of radiation dose (Gy). Data points shown in the graph represent mean and standard deviation (SD) calculated from two independent experiments. **B,** Representative dishes from survival assay showing colonies forming after 8 days in different doses as indicated.

CtIP protein level oscillates throughout the cell cycle. While it remains low in resting G0 cells (cells obtained by serum deprivation or maintaining cells in plateau phase of growth) as well as in cycling G1 cells, it increases significantly in S and G2 phases of the cell cycle (Chen et al. 1996; Yu and Baer 2000). In G0/G1 cells, DNA double strand breaks are repaired mostly by non-homologous end joining (c-NHEJ) where homologous recombination repair (HRR) pathway is inherently absent (Lieber 2008). However, cells with mutations in components of c-NHEJ rely on alternative end joining (alt-EJ) that functions as backup not only to c-NHEJ but also to HRR (DiBiase et al. 2000; Wu, Wang, Mussfeldt, et al. 2008; Wu, Wang, Wu, et al. 2008). Since HRR does not take place in G1-phase cells and CtIP mediates alt-EJ in G1 phase of the cell cycle, the effect of CtIP depletion on radiosensitization is possibly through its involvement in alt-EJ. Therefore, we next examined the role of CtIP on alt-EJ repair pathway specifically in G1 cells. Homogenous G1 cells were obtained by releasing nocodazole-arrested mitotic cells for one hour in fresh media. Cell cycle profiles of

nocodazole-arrested and nocodazole-released cells are shown in figure 26. The obtained results show a minor radio-sensitization of G1 population upon CtIP depletion which might be due to the reported low expression level of CtIP in G1 phase, as well as the short duration of G1 phase (1-1.5 hours) in Chinese hamster cells.

Collectively, our experimental evidence suggests a functional role of CtIP in alt-EJ and that the function is not limited to only S/G2 phase, as shown before, but possibly contributes to DSB repair in G1-phase through alt-EJ.

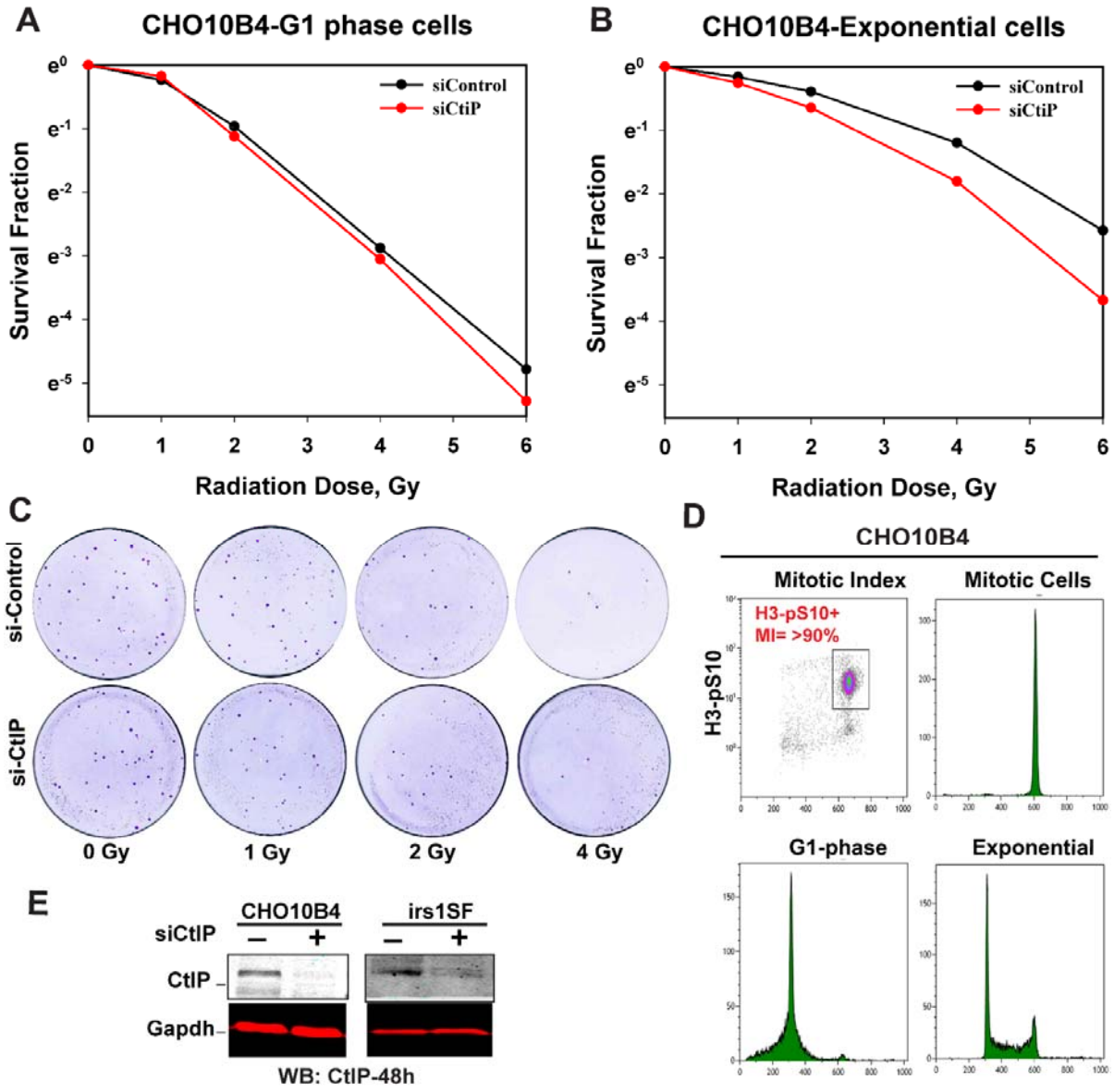

Figure 26 Contribution of CtIP on cell survival in G1 phase. RNA interference knockdown of CtIP was performed in exponentially growing CHO10B4 cells. After that, cells were synchronized in G1-phase as mentioned in description and in parallel, a population of asynchronously growing cells was maintained. (**A and B)** Clonogenic survival assay performed in G1-phase and asynchronously growing cells following RNAi-

mediated CtIP knockdown. **(C)** Representative cell culture dishes showing colonies obtained from experiment performed in G1-phase cells. (**D)** Density plot showing mitotic cells stained with an antibody against phosphorylated Histone H3 at pS10 (H3pS10) positive (mitotic= >90%) cells. Cell cycle analysis shows the histogram for Mitotic cells (nocodazole-arrested), G1-Phase (Cells released 1h after nocodazole arrest) and Exponential (exponentially growing cell population). (**E)** Western blot analysis showing efficient siRNA-mediated knockdown of CtIP in wild type CHO10B4 and irs1SF (XRCC3 mut) cells. GAPDH serves as a loading control. Data shown here are from one experiment.

1.2 CtIP regulates DNA end processing in CHO10B4 cells

Sartori *et al* first reported the essential role of CtIP in DSB end resection (Sartori et al. 2007). Earlier studies suggest the essential role of CtiP in DNA end processing in G2 phase of the cell cycle in which HRR pathway is mainly functional, and further demonstrated marked reduction of end resection in human cells following CtIP depletion. However, CtIP mediated DNA end processing remains hitherto unknown in hamster cell lines. Therefore, we aimed to extend our approach using wild type (CHO10B4) hamster cell line and examined the effect of CtIP depletion on DNA end resection. Towards this, we conducted three-parameter fluorescent-based flow cytometry experiments to measure RPA accumulation at single-stranded DNA that is a surrogate marker for DNA end resection at sites of DSBs. Thereby, pulse of EdU staining served to discriminate replicating S-phase cells (EdU positive) from G2 phase cells (EdU negative). Resection (*i. e.* RPA signal) is analyzed as a function of time after IR. CtIP down regulation caused significant abrogation in DNA end resection in G2-phase cells (EdU negative) as measured by RPA accumulation (figure 27). While Red peak shows RPA accumulation at 0 Gy, G2 cells exposed to 20 Gy show a significant increase of total RPA intensity which reflects presence of ssDNA (figure 27 left panel). In contrast, CtIP-knockdown cells showed marked reduction in RPA70 intensity when compared to control siRNA treated cells at all-time points examined (figure 27 right panel). Hence, RNAi-mediated CtIP down-regulation abrogates resection indicating thus a prominent role of CtIP in DNA-end processing.

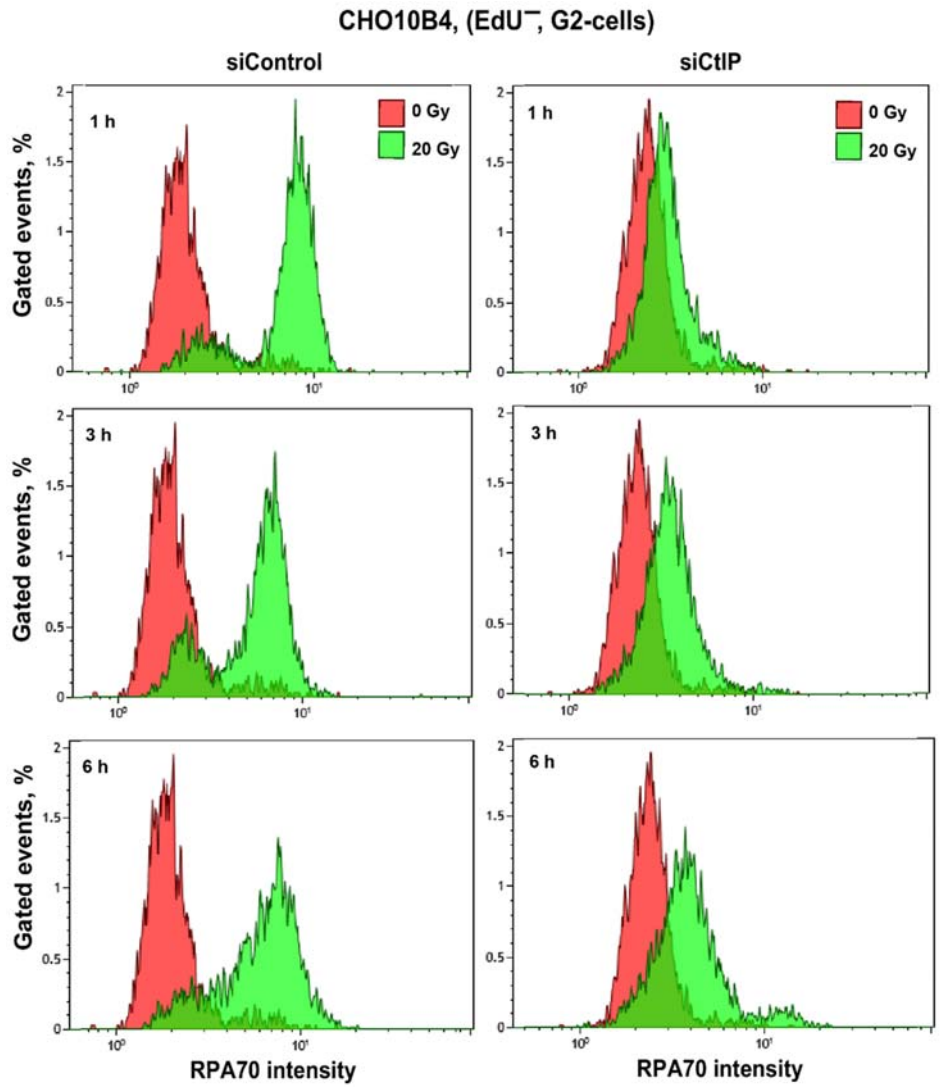

Figure 27 CtIP is a limiting factor for DNA end resection in G2-phase. Histograms showing RPA70 signal intensity measured in G2 phase (EdU-negative) CHO10B4 cells following exposure to IR. The red peak shows chromatin-bound in non-irradiated cells, while the green peak represents RPA signal intensity at 20 Gy. An increase in RPA signal intensity is accompanied by an increase in RPA70 accretion on chromatin thus measures DNA end resection.

A previous report demonstrates the existence of DNA end resection in G1 phase of human cells (Averbeck et al. 2014). However, no such observations have previously been reported in rodent cells. In an effort to explore whether end-processing is indeed essential for G1 cells to repair DSBs, we analyzed similarly RPA signal intensity during G1-phase in CHO cells. Akin to human cells, asynchronously growing G1-phase CHO cells showed resection, which is limited but detectable at 3 h and 6 h after irradiation (figure 28 left panel) and that is absent upon depletion of CtIP suggesting its role in G1 phase of the cells Figure 28 right panel). We

correlate this with the slow kinetics of fraction of alt-EJ that is involved in processing of DSBs and is increased in later time points.

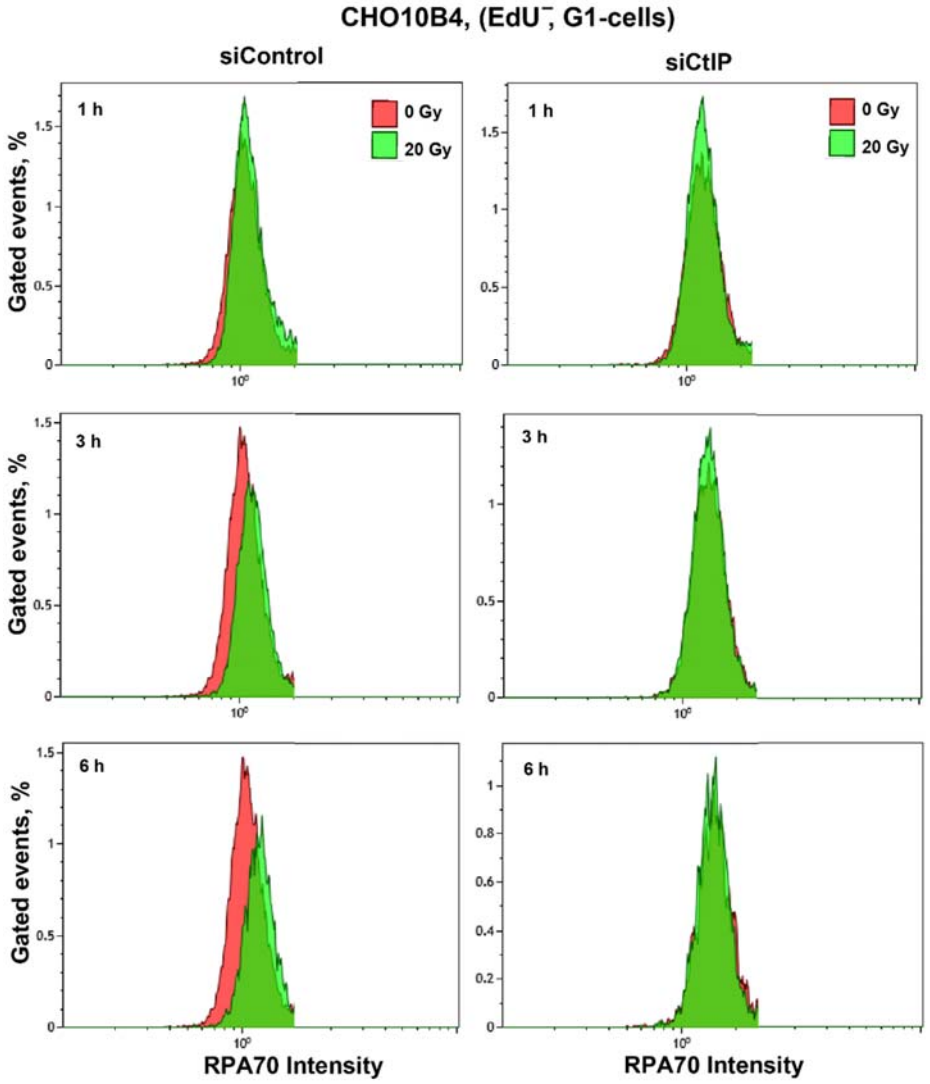

Figure 28 CtIP promotes DNA end resection in G1-phase CHO10B4 cells. Representative histograms showing RPA70 signal intensity in non-irradiated (0 Gy) and irradiated (20 Gy) G1-phase cells at the indicated hours.

Earlier experiments from our lab show an enhanced DNA end resection in G2 phase of the cell cycle particularly in DNA-PKcs deficient cell lines ((Wu, Wang, Wu, et al. 2008) and Dueva 2015, PhD thesis). The mechanism of this hyper-resection is yet unknown. To investigate whether these findings also hold true for rodent cells, we measure the resection in G2 and G1 phase of DNA-PKcs mutant cell line IRS-20. Compared to corresponding CHO wild type cells, IRS-20 cells show marked increase in their level of resection in G2 phase (figure 29 left panel), which is consistent with the results in human cells. However, there is

no detectable effect in resection level at 1 h in G1-phase cells as it was observed for wild type CHO counterpart between CtIP or not depleted cells. However, trace levels of DNA end-resection at 3 h was noted.

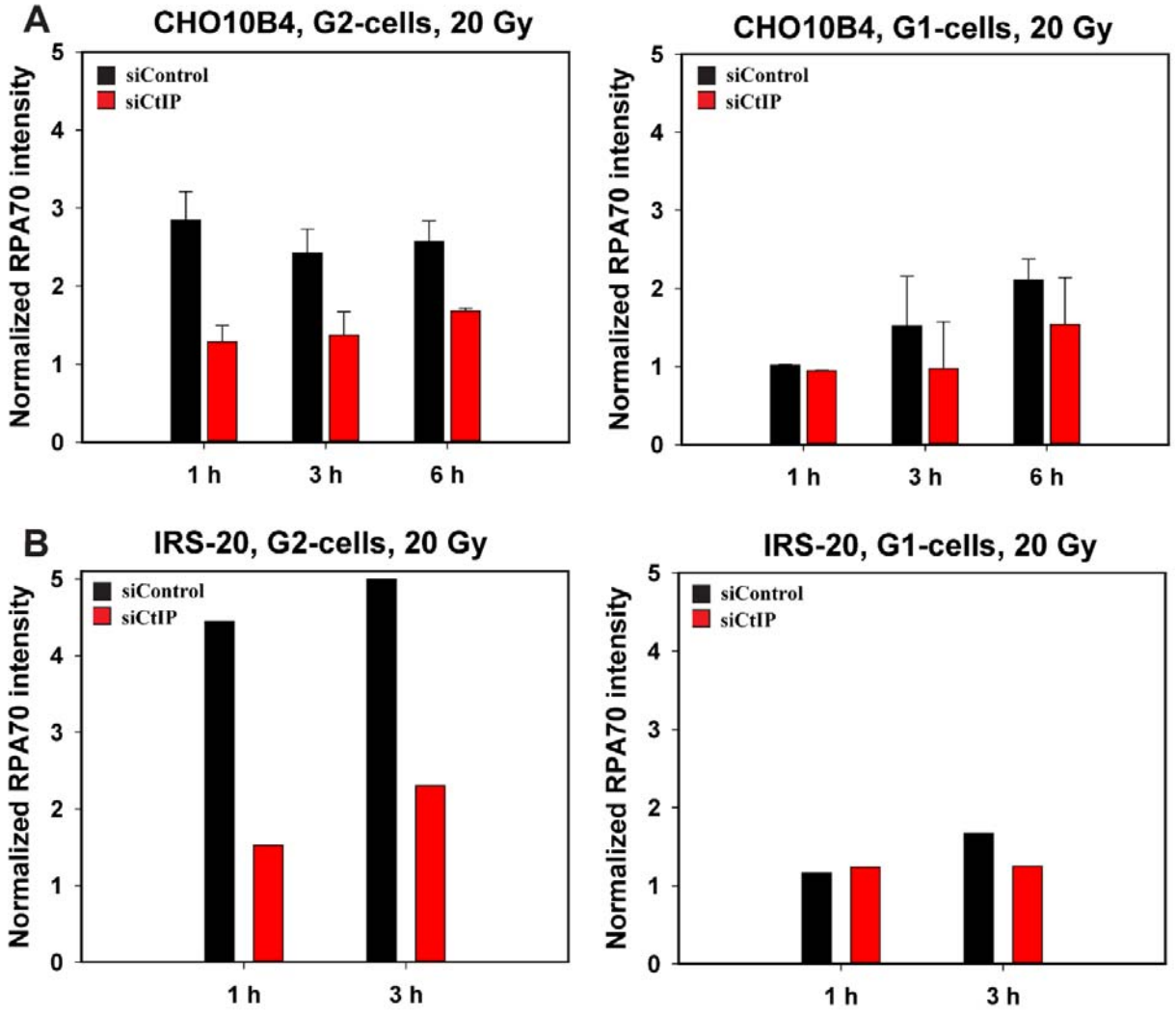

Figure 29 CtIP is a positive regulator of resection in G1 and G2 phase cells. Resection analysis in CHO10B4 (upper panel) and IRS-20 (lower panel) cells transfected with control siRNA (siControl) and siRNA against CtIP (siCtIP) after exposure to 20 Gy of IR analyzed in G2 (left panel) and G1-cells (right panel). Resection was measured by intensity of RPA70 signal in EdU-negative cells (G2 and G1). Data represents mean and standard deviation from two independent experiments (CHO10B4). Data shown for IRS-20 are from a single experiment.

In aggregate these data demonstrate that alt-EJ may benefit from limited DNA end resection particularly in G1 phase of the cell cycle and is mediated by CtIP.

1.3 Alt-EJ in DNA-PKcs deficient cells is growth state independent

It has been convincingly shown that c-NHEJ pathway functions across all phases of the cell cycle, and is independent of cell growth state and growth factor signaling. In contrary, alt-EJ, a pathway that operates as back-up pathway of HRR and c-NHEJ, shows dependence on growth state of the cells. Previous work from our laboratory carried out in wild type cells treated with DNA-PKcs inhibitor, NU7441 and c-NHEJ mutant rodent cells demonstrated that alt-EJ is compromised as they reach the plateau phase of growth and enter a quiescence stage. The underlying mechanism for this suppression of alt-EJ pathway is yet unknown. Interestingly, only DNA-PKcs mutant cells fail to show the reduction in their efficiency in alt-EJ once they enter the quiescent stage – an observation first reported from our laboratory not long ago (Satyendra K. Singh et al. 2011; Singh et al. 2012). Based on these findings we reckoned that alt-EJ in G0/G1 phase may be regulated by CtIP-mediated end-resection. In line with this, our data in section 1.1 (Figure 26) show relatively low cellular sensitivity towards radiation upon CtIP depletion which support the notion of limited CtIP mediated alt-EJ activity in G1-phase of the cells.

Next, we wished to investigate the growth state dependence of alt-EJ in wild type hamster cell line (CHO10B4). To specifically assay for alt-EJ, cells maintained in exponential and plateau-phase of growth (2 and 4 days of serum deprivation), were treated with NU7441 to inhibit c-NHEJ and thus allow alt-EJ as dominant DSB processing pathway (figure 30-A). Whereas DMSO-treated cells efficiently repair DSBs by alt-EJ, a substantial reduction in repair capacity is observed in NU7441-treated cells. This reduction in DSB joining is more pronounced in cells grown in serum free media for 2 days and even further exacerbated in 4 days of growth in plateau phase (Figure 30, A). In marked contrast, DNA-PKcs deficient cell lines IRS-20 and XRC1-3 showed no change in their DSB repair propensity when examined in the plateau-phase of growth. As expected, both cells maintained in exponential state of growth showed the expected repair defect deriving from genetic mutation of DNA-PKcs (figure 30-D and E). However, when analyzed in day 2 and 4, no defect in DSB rejoining was observed in these cell lines, which is opposite from what we observed in their wild type control cells (CHO10B4) (figure 30-D and E). This unexpected observation led us to check the protein level of CtIP in asynchronous and plateau-phase cells. Western blot analysis shows that the level of CtIP is significantly reduced in serum-deprived cells in all cell lines tested (Figure 30, C). While low level of CtIP reflects the repair defect in wild type cells, DSB rejoining activity of DNA-PKcs$^{-/-}$ cells irrespective of their state of growth (exponential/plateau) is not

accompanied by down regulation of CtIP demonstrating alt-EJ is active in DNA-PKcs deficient cells. The marked accumulation of cells in G1-phase upon serum deprivation is confirmed by the cell cycle analysis (Figure 30, B and F).

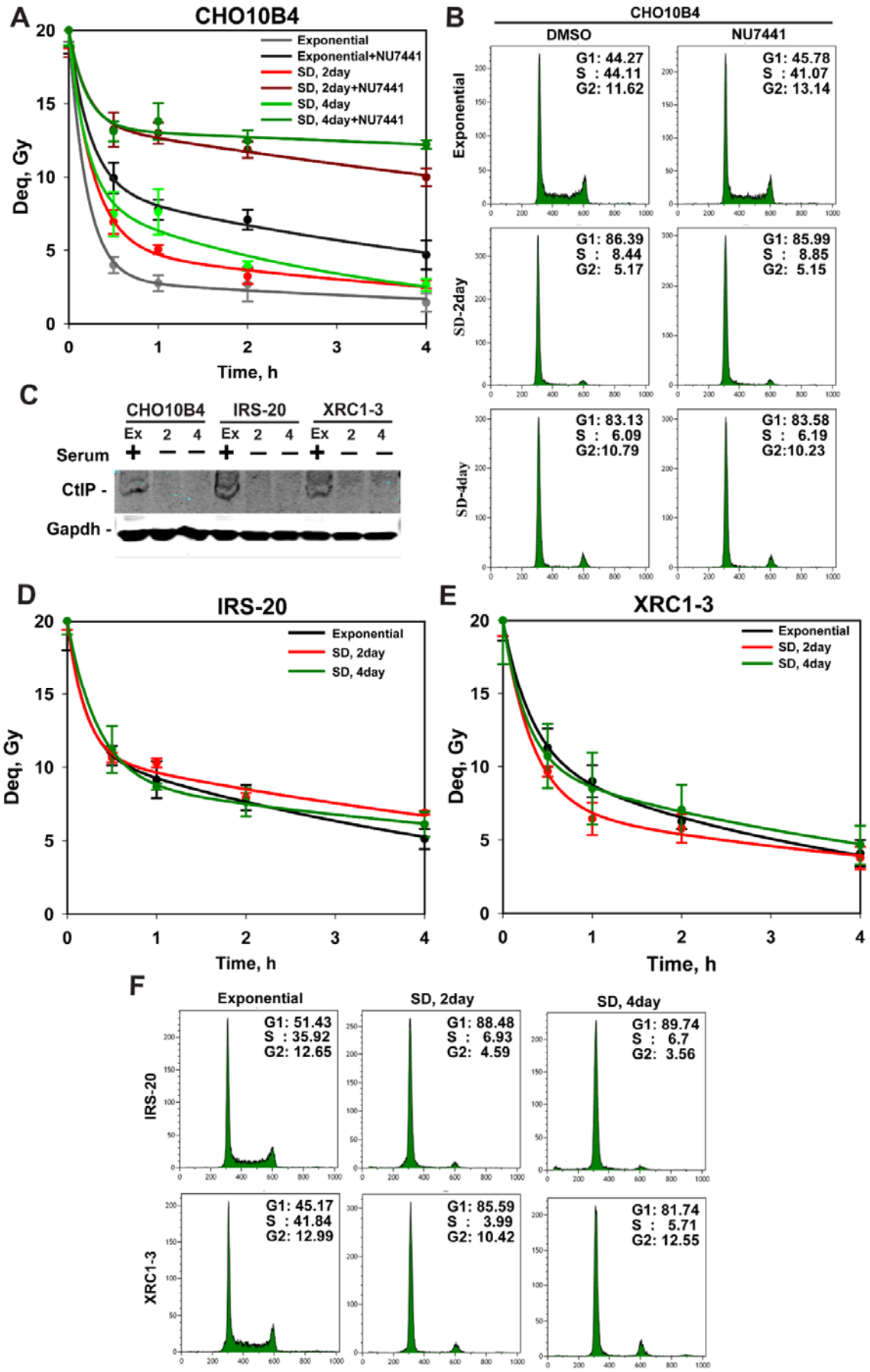
A
CHO10B4
Exponential
Exponential+NU7441
SD, 2day
SD, 2day+NU7441
SD, 4day
SD, 4day+NU7441
Deq, Gy
Time, h
B
CHO10B4
DMSO
NU7441
Exponential
SD-2day
SD-4day
G1: 44.27
S : 44.11
G2: 11.62
G1: 45.78
S : 41.07
G2: 13.14
G1: 86.39
S : 8.44
G2: 5.17
G1: 85.99
S : 8.85
G2: 5.15
G1: 83.13
S : 6.09
G2:10.79
G1: 83.58
S : 6.19
G2:10.23
C
CHO10B4
IRS-20
XRC1-3
Ex 2 4
Serum
CtIP -
Gapdh -
D
IRS-20
Exponential
SD, 2day
SD, 4day
Deq, Gy
Time, h
E
XRC1-3
Exponential
SD, 2day
SD, 4day
Deq, Gy
Time, h
F
Exponential
SD, 2day
SD, 4day
IRS-20
XRC1-3
G1: 51.43
S : 35.92
G2: 12.65
G1: 88.48
S : 6.93
G2: 4.59
G1: 89.74
S : 6.7
G2: 3.56
G1: 45.17
S : 41.84
G2: 12.99
G1: 85.59
S : 3.99
G2: 10.42
G1: 81.74
S : 5.71
G2: 12.55

Figure 30 Differential regulation in alt-EJ dependence on growth state between wild type and DNA-PKcs deficient cells. Cells grown for indicated times (exponential and serum deprived) were subjected to DSB repair kinetics measured by PFGE. Shown results are the average of four determinations from one experiment. **(A and B)** DSB repair kinetics of alt-EJ in CHO10B4 cells (wt) treated or not with NU7441 and cell cycle analysis measured by flow cytometry. **(C and D)** DSB repair kinetics and cell cycle profiles of DNA-PKcs $^{-/-}$ cells analyzed as in (A and B) Results shown are the average of four determinations from one experiment. SD: serum deprived. **(E)** CtIP level by western blot. GAPDH serves as a loading control.

Since DNA-PKcs mutant cells show a repair proficient phenotype under serum-deprivation condition which is attributed to alt-EJ, we next investigated the efficiency of alt-EJ in other c-NHEJ factors mutant cell lines including Ku80 and XRCC4 based on the following questions:

1. Is alt-EJ independent repair proficient phenotype specific for DNA DNA-PKcs$^{-/-}$ cells
2. Is it an discrete property of c-NHEJ mutant cells

Towards this, we performed DSB repair kinetics in asynchronously growing cells as well as in plateau phase XRS6 cells (serum deprived for 2 days). The results in figure 31 show that exponentially growing cells display a compromise in DSB repair as expected. Surprisingly – and differently from what was observed in DNA-PKcs deficient cells, upon serum deprivation (2 days) a marked reduction in repair proficiency is observed. This suggests that the capacity for DSB repair of DNA-PKcs mutant cells in plateau-phase cells is a distinct feature.

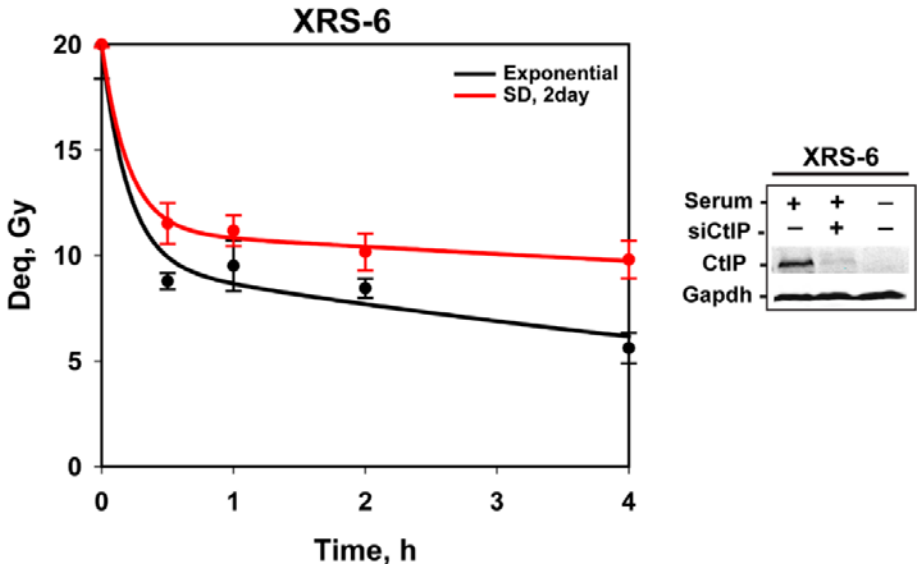

Figure 31 DSB rejoining in KU80 mutant cells (XRS6) is dependent on growth state. DSB rejoining kinetics of XRS6 cells maintained in exponential and serum deprived (2 day) condition. Immunoblot was performed using anti-CtIP antibody and indicates CtIP protein level in exponentially growing cells (depleted with or not siCtIP), as well as in serum deprived cell (3rd lane). GAPDH is a loading control. Results show means and standard error (SE) from four determinations in one experiment.

DNA-dependent protein kinase (DNA-PK), consisting of DNA-PKcs and Ku heterodimer (Ku70/80), first assembles to the free ends of DSBs by recognizing the DSB end and recruits other accessory components of c-NHEJ including XRCC4, ligase 4, XLF (XRCC4-like factor) and APLF prior to ligation (Chang et al. 2017; Jette and Lees-Miller 2015). Of different available c-NHEJ mutants, Lig4 deficient cells show strongest repair deficient phenotype. Since no CHO derivative Lig4 deficient cells are available, we next explored the role of alt-EJ in XR-1 cells, deficient in XRCC4. Results presented in figure 32 show a similar DSB repair capacity which is analogous to Ku80 deficient cells (XRS6) at day 2. An additional reduction in DSB rejoining is noted when growth in stationary phase was maintained for 4 days. Like other c-NHEJ mutant cells, exponentially growing cells showed similar defect in their DSB rejoining capacity. Similar to what was seen in DNA-PKcs$^{-/-}$ and wild type CHO10B4, CtIP protein level in XRCC-4 deficient cell line is markedly reduced in the plateau-phase (day 2 and day 4).

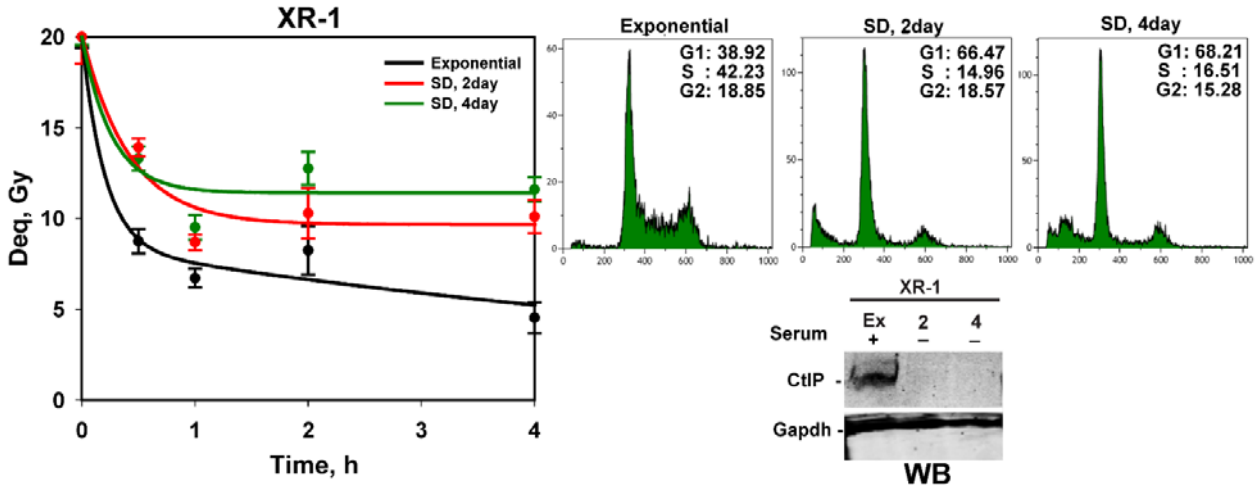

Figure 32 DSB repair capacity in XR-1 cells (XRCC4$^{-/-}$) strongly depends on growth state. DSB repair kinetics of wild type cells maintained in asynchronous (day 2) and in serum deprived condition (day 2 and 4). Corresponding histograms and western blot using the indicated antibodies at indicated time are shown as well. Gapdh serves as a positive control. Shown results are the average and standard error (SE) of four determinations from one experiment.

It suggests, active alt-EJ promotes DSB repair processing in DNA-Pkcs mutant cells and that is absent in other c-NHEJ deficient cells as cells become quiescent. It also further supports the notion that this alt-EJ mediated repair proficiency is independent of CtIP. Yet, the mechanism underlying efficient alt-EJ mediated repair of DSBs in DNA-PKcs deficient cells entering quiescent state is still not fully understood and remains to be further elucidated.

1.4 Functional role of CtIP in alt-EJ mediated DSB repair

As mentioned in the previous section an intriguing characteristic of DNA-PKcs deficient cells is their functional alt-EJ pathway in plateau phase. To test whether this phenotype is dependent on CtIP, we used previously reported siRNA sequences directed against hamster CtIP (K et al. 2015). To begin with, we first explored the role of CtIP in alt-EJ by employing pulse filed gel electrophoresis (PFGE) in exponentially growing CHO10B4 cells after CtIP depletion. As seen in figure 33-A, both DMSO-treated and CtIP-depleted cells show efficient DSB repair utilizing c-NHEJ whereas a compromised repair is observed when cells are treated with NU7441, a potent inhibitor of DNA-PKcs that suppresses c-NHEJ thus allowing alt-EJ to come to the fore. Strikingly, a significant DSB repair defect is observed in cells depleted in CtIP and subsequently treated with NU7441. Our data therefore suggest that CtIP mediated alt-EJ has a primary role in DNA repair and has only recently been investigated by us in hamster cells. Notably, CtIP depletion did not alter the cell cycle distribution profiles of the cells.

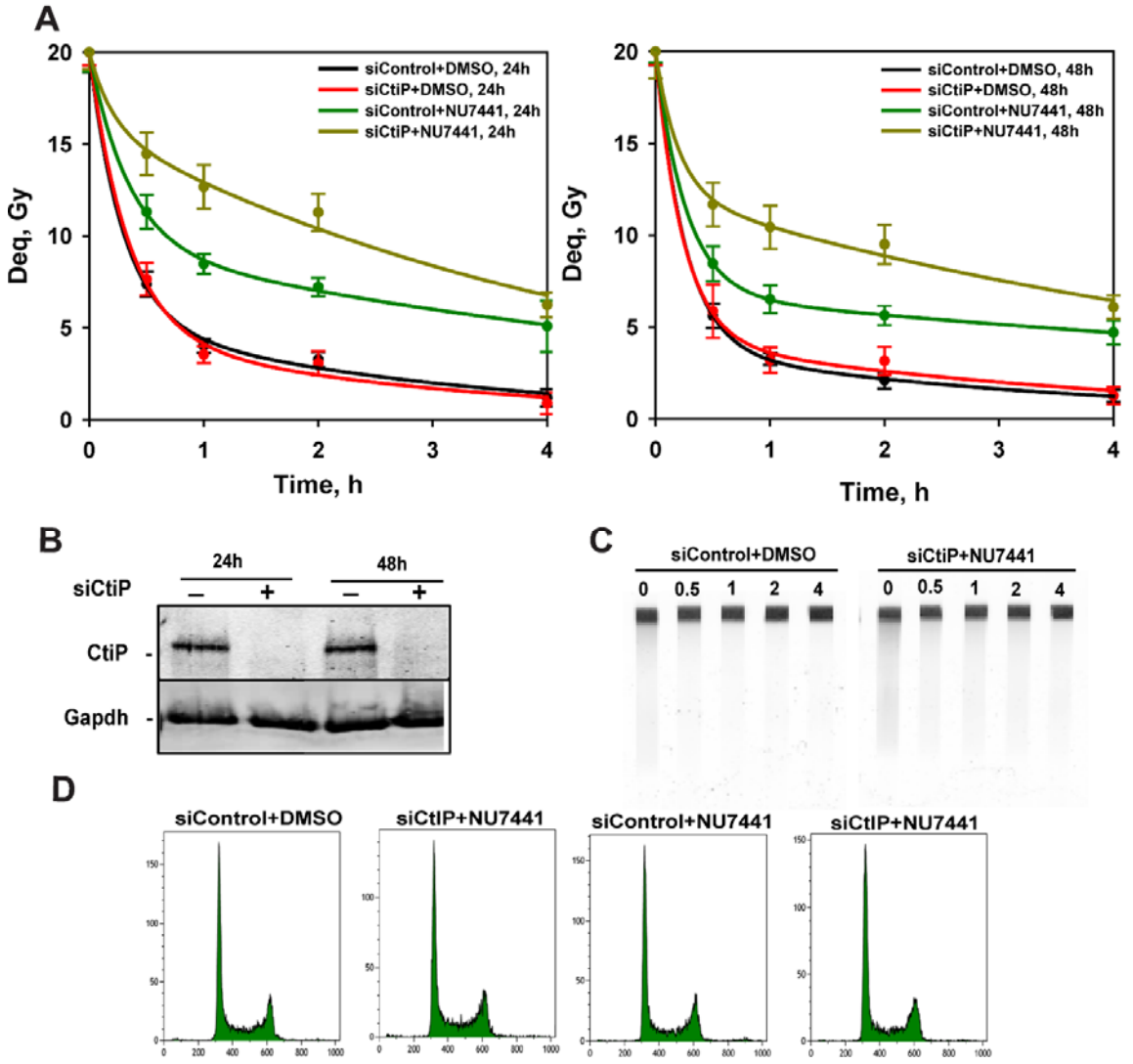

Figure 33 CtIP contributes to DSB repair by alt-EJ. (A) Kinetics of DSB rejoining in asynchronously growing CHO cells following depletion of CtIP for 24 or 48hrs and subsequent treatment with DNA-PKcs inhibitor, NU7441. Kinetics of DSBs repair is plotted as dose equivalent (Deq) as a function of time. **(B)** Western blotting of CtIP protein levels 24 and 48hr after siRNA-mediated depletion. **(C)** Representation of typical PFGE gels and their quantitative analysis as Deq as a function of time. **(D)** Cell cycle profile of CHO10B4 cells. Cells were transfected with siRNA oligonucleotides, and 24 and 48hrs later subjected to propidium iodide staining for cell cycle analysis. Results shown are from three independent experiments.

1.5 Role of CtIP in repair of DSBs in c-NHEJ deficient cells

The striking findings in the role of CtIP in alt-EJ in c-NHEJ competent CHO cells led us to investigate the dependence of c-NHEJ mutant cells on alt-EJ upon CtIP depletion. To study the DSB repair mechanism in c-NHEJ deficient setting, we took advantage of the large repertoire of CHO derived c-NHEJ mutant cell lines available at our laboratory (Wu, Wang, Mussfeldt, et al. 2008). Cell lines mutant in corresponding c-NHEJ components are summarized in table 1.4 in materials and methods section. Most importantly, we started-off our investigation in mutant cells defective in DNA-PKcs. Towards this, we measured the DSB repair kinetics in these cell lines after knocking down CtIP at 24 and 48 h, and exposure of 20 Gy (figure 35-A).

We selected three DNA-PKcs$^{-/-}$ cell lines, IRS-20, XRC1-3 and V3 where we first tested whether DNA-PKcs inhibitor NU7441 has any additional effect than inhibiting the kinase activity of DNA-PKcs. Obtained results with DSB repair kinetics show no additional changes in overall DSB rejoining in these cells pre-treated or not with NU7441 (figure 34).

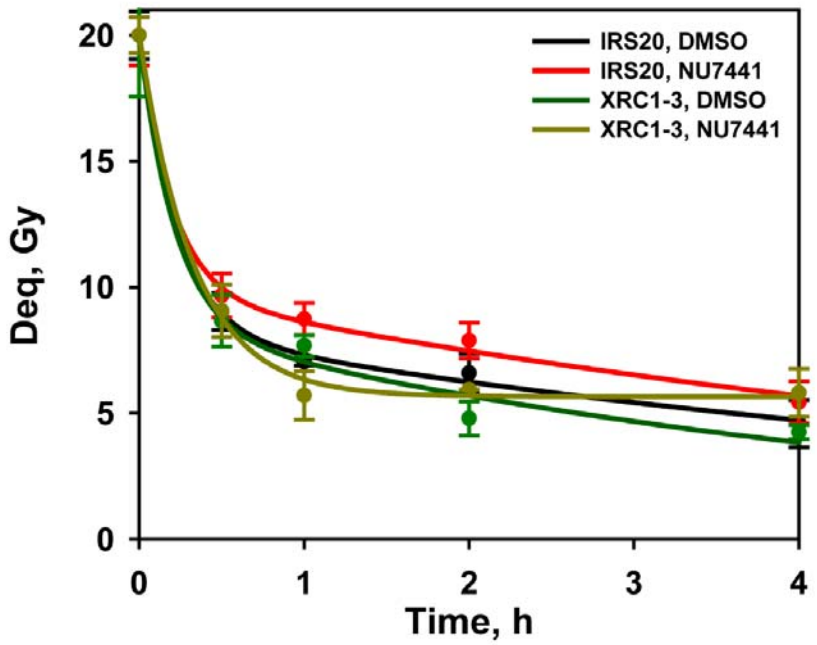

Figure 34 NU7441 has no additional effects on DSB rejoining in DNA-PKcs$^{-/-}$ cell lines. Cells were maintained in exponential state of growth and pre-treated with 5 μM NU7441 for 1 h before exposure to 20 Gy. Shown result is from one experiment and error bars represent standard Error (SE) calculated from four determinations.

We next measured the DSB repair efficiency of DNA-PKcs deficient cell lines maintained in exponential state of growth after knockdown of CtIP. DSB repair kinetics obtained in both cell lines by employing PFGE showed similar repair kinetics implying no additional compromising effects in the processing of DSBs following CtIP knockdown (figure 35-A). It also supports our previous finding from DNA-PKcs deficient human cell lines (unpublished data). No changes in the cell cycle distributions of CtIP knockdown cell were observed (Figure 35-B).

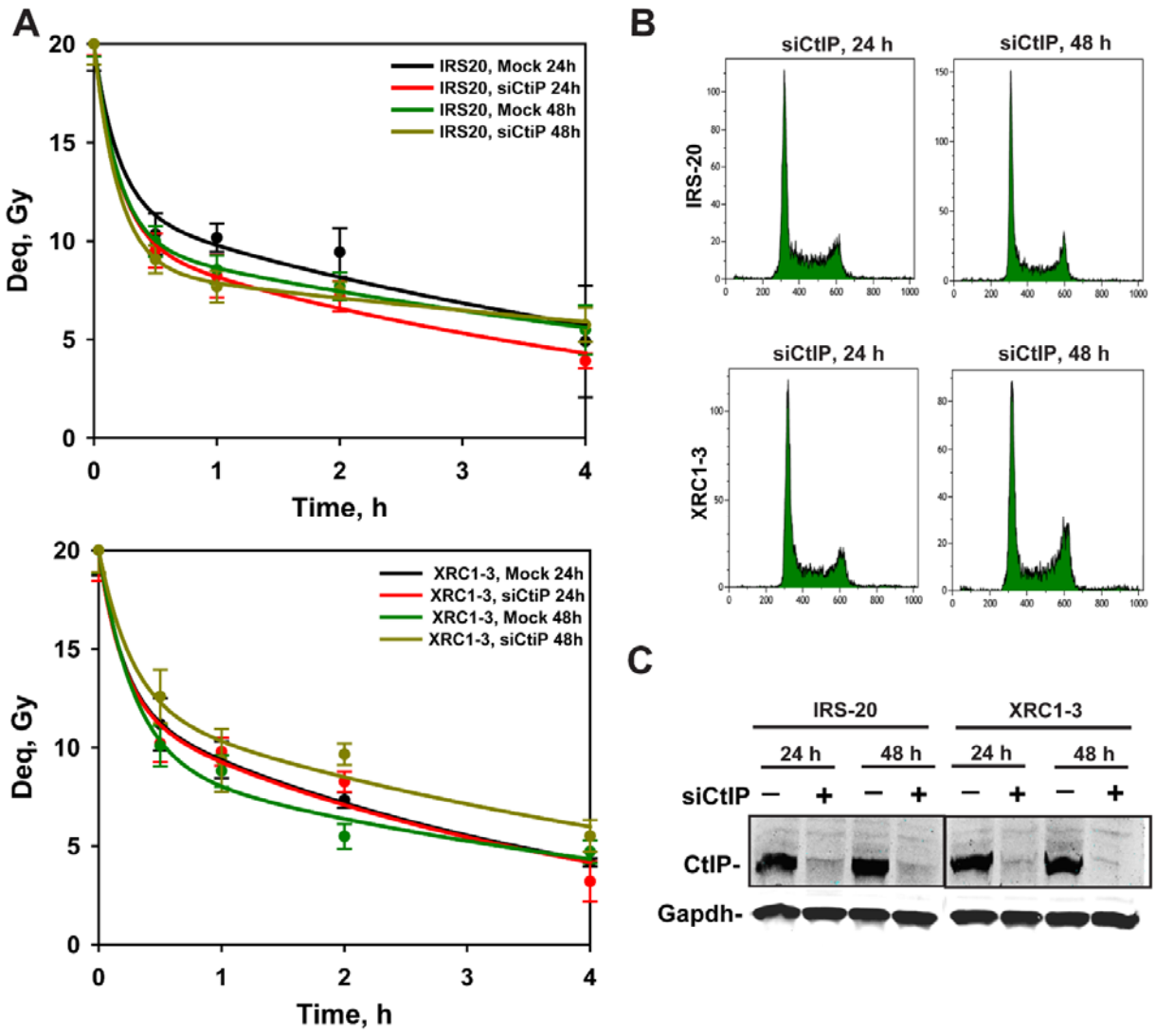

Figure 35 DSB processing in DNA-PKcs mutant cells is independent of CtIP. (A) DSB repair kinetics of two DNA-PKcs cell lines (IRS20 and XRC1-3) measured at 24 h and 48 h following CtIP knockdown. (**B)** Cell cycle profiles following siRNA transfection at the indicated time points**. (C)** Western blotting of CtIP shows efficient down-regulation of CtIP protein level in both cell lines. Obtained results are calculated from two independent experiments with standard error (SE) from at least 8 determinations.

In a similar way, results from another DNA-PKcs null CHO derived V3 cell line showed also similar phenotype like aforementioned two DNA-PKcs mutant cell lines. No qualitative difference in terms of DSB processing efficiency between these three cell lines was observed (figure 36).

This collective finding suggests that knockdown of CtIP in DNA-PKcs mutant cells may not have an impact on alt-EJ efficiency and may thus be regulated by other c-NHEJ factors.

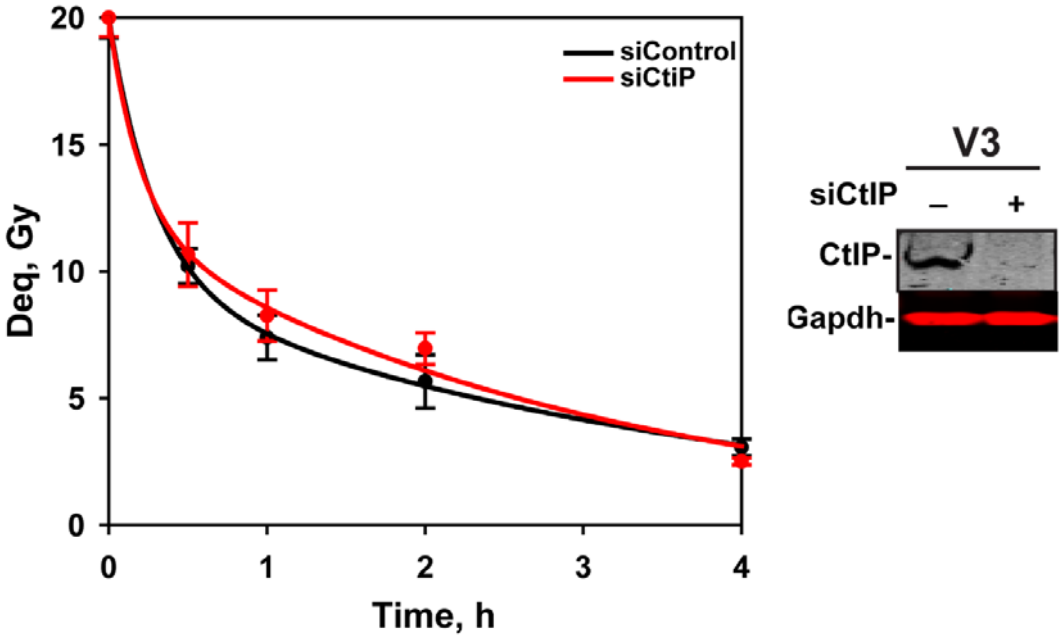

Figure 36 Kinetics of DSB rejoining in exponentially growing DNA-PKcs-deficient (V3 cells). Cells transfected with siCtIP and corresponding siControl were subjected to PFGE 24 h later. Immunoblot was performed using anti-CtIP antibody and indicates efficient down regulation of CtIP protein level upon transfection with siCtIP. GAPDH served as loading control. Results show means and standard error (SE) from four determinations in one experiment.

Since DNA-PKcs' activity depends on Ku70 and 80 subunits, we next sought to investigate the effect of CtIP down-regulation on DSB re-joining in Ku80 deficient cell line, XRS6, where DNA-PKcs is supposed to be present but inactive. PFGE experiments revealed a substantial reduction in DSB processing in cells depleted in CtIP corroborating our findings that CtIP promotes alt-EJ when DNA-PKcs cannot be activated. Notably, concomitant inhibition in CtIP depleted XRS6 cells of DNA-PKcs with NU7441 resulted in additive reduction in alt-EJ efficiency (figure 37-A). No cell proliferation defect is observed in post siRNA-transfected and/or NU7441 treated cells (figure 37-B).

Taken together, these data demonstrate that blocking DNA-PKcs auto-phosphorylation in Ku80 deficient background results in abrogated DSB repair defect. Under these conditions, DSB repair is likely mediated through CtIP dependent alt-EJ.

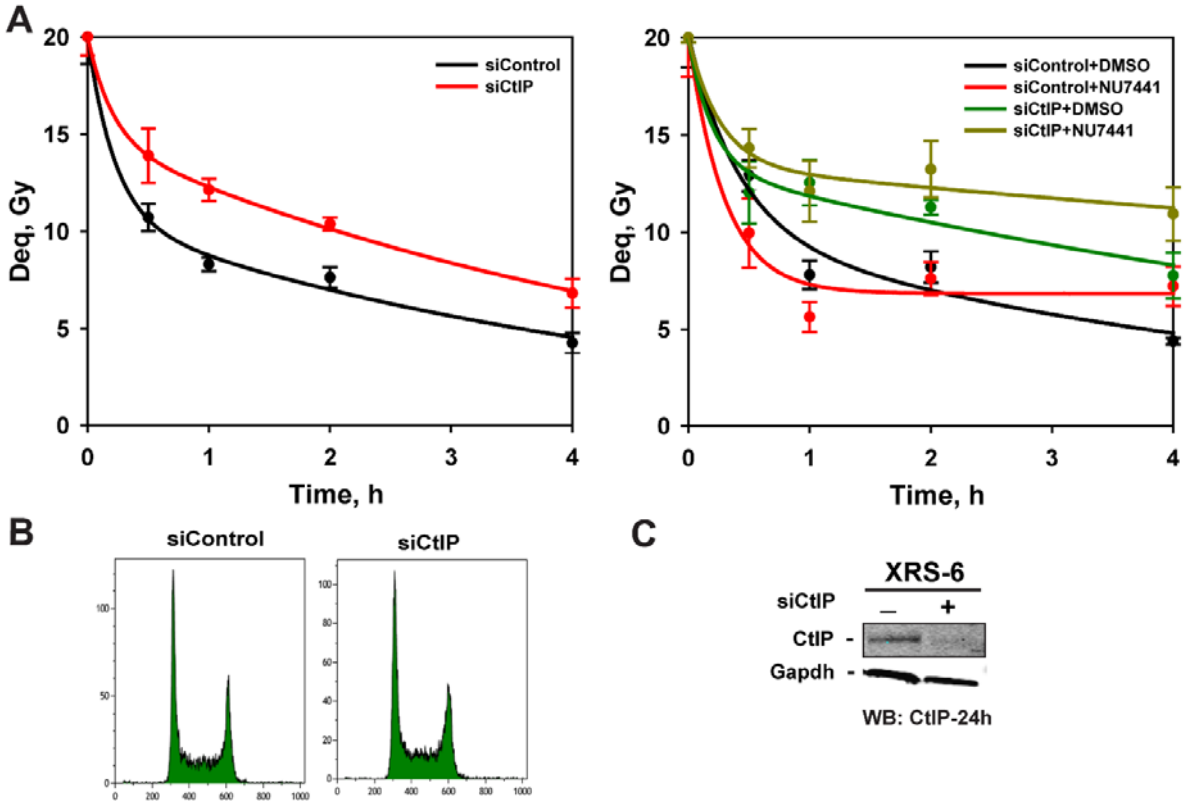

Figure 37 Processing in Ku80-deficient of IR-generated DSBs is dependent on CtIP. (A) (Left panel) DSB repair kinetics in Ku80 mutant XRS-6 cell line upon CtIP depletion. Shown results are from at least 3 independent PFGE experiments and error bars represents standard error (SE) from at least 9 determinations. (Right panel), similarly, in same condition cells were subjected to NU7441 treatment in addition and data shown here are from one experiment. **(B)** Cell cycle distribution of siCtIP transfected cells measured by flow cytometer. (**C)** Western bot for CtIP in Ku80-deficient cell line. Cell lysates were collected 24 h post-transfection. GAPDH is a loading control.

We next selected another c-NHEJ-defective CHO-derived mutant cell line XR-1, which is defective in XRCC4, to further investigate the processing of DSBs in absence of CtIP. Results from PFGE show that in absence of CtIP, XR-1 cells process DSBs with efficiency similar to that of control-siRNA transfected cells (figure 38). This suggests that DSB repair in XR-1 is not restricted to CtIP mediated alt-EJ.

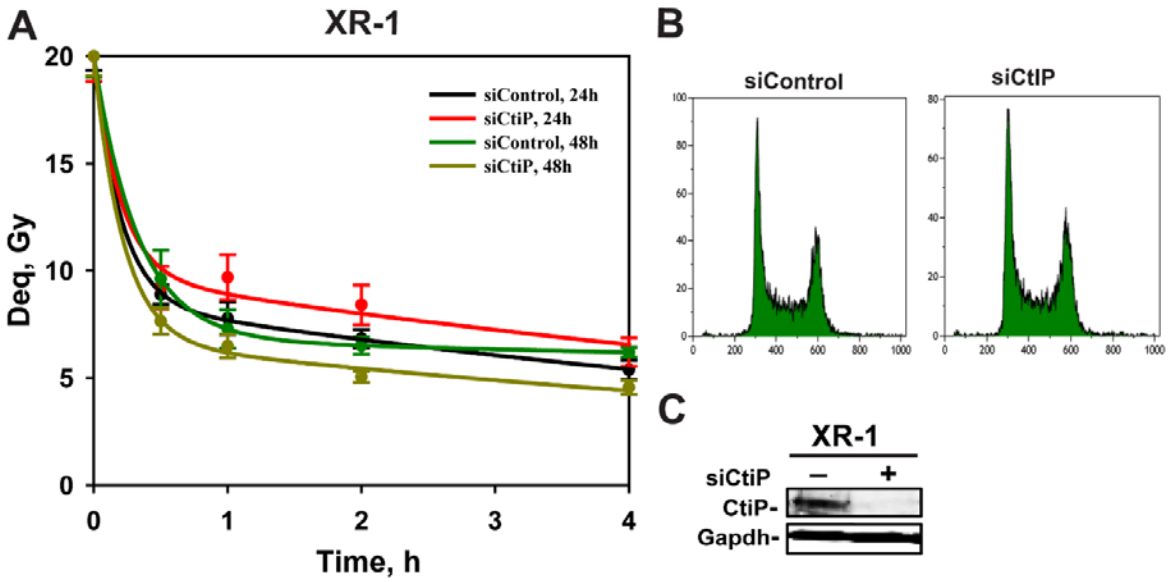

Figure 38 Effect of IR on DSB repair efficiency in CtIP depleted exponentially growing XR-1 cells. (A) Kinetics of DSB repair measured by PFGE in XRCC4 deficient cell line at 24 and 48 h**. (B)** Representative cell cycle histograms upon depletion of CtIP showing no change in the cell cycle profile**. (C)** Western blot for CtIP in XR-1 cells with or without siRNA directed against CtIP**.** Results shown indicate the average and standard error (SE) from two independent experiments and 8 determinations.

1.6 Factors modulating the efficiency of DNA end resection during the G1 phase of the cell cycle

1.6.1 Role of CtIP in initiating end-resection in G1 phase

1.6.1.1 Comparative study of PCC induction procedure in CHO10B4 cell line

Premature chromosome condensation (PCC) has proved to be an unique method for analyzing chromosomal damages in G2 phase and most importantly in G1/G0 phase of the cell cycle (Hittelman and Rao 1975). PCC can be induced by fusing interphase cells with mitotic cells using virus (Sendai virus) or chemical agents such as polyethylene glycol (PEG) (Pantelias and Maillie 1983). However, the degree of cell fusion and PCC induction depends on the growth conditions as well as the sensitivity of cells towards these chemicals, their concentration and incubation time. Hence, these parameters need to be properly optimized for each cell line and fusing agents. In our protocol for CHO10B4 cell line, we employed 45% PEG to mediate fusion between irradiated interphase and non-irradiated mitotic cells.

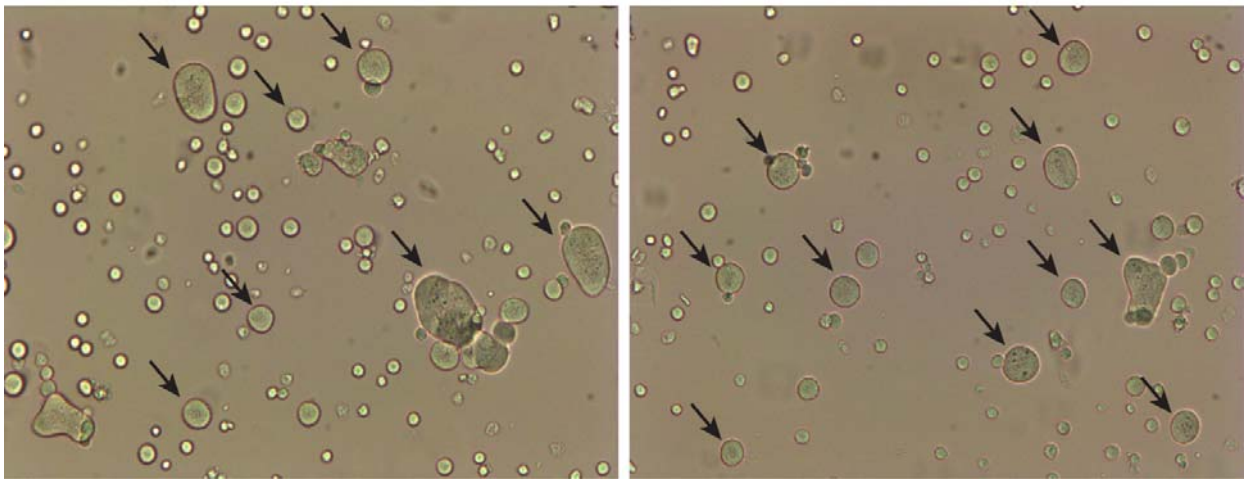

Figure 39 PEG mediates successful fusion between interphase and mitotic CHO cells. Photo-micrographs showing successful fusion between interphase and mitotic cells (indicated by black arrows) by means of 45% PEG (45%). Samples were incubated at 37˚C for 1h to allow PCC induction. Representative fused cells show a distinct morphological appearance (large in size) compared to interphase or mitotic cells.

To obtain optimum PCC indices along with satisfactory cell fusion, we eventually followed the protocol of using 45% PEG concentration and a ratio of 1:1 for interphase-to-mitotic cells for PCC induction in G1 phase of the cell cycle (mentioned in methods section-2.17.2). Since we conducted our experiments in cells that are either serum-deprived or maintained in plateau phase of growth, we therefore checked how PCC breaks formation differs between these two states. One hundred thousand cells were cultured in 3 ml media (60mm culture dish) and 48 h later cells were replenished with serum free medium following a PBS wash, and simultaneously another batch of cells was maintained for growth. After that, PCC induction immediately after irradiation at dose of 6 Gy was conducted in both types of cells for the indicated time points analyzed (1, 2, 4, 7 and 8 days counted following serum deprivation). Figure 39 shows typical examples of non-irradiated and irradiated chromosome spreads of G1-PCC fused with non-irradiated mitotic cells. Whereas non-irradiated PCCs show 21 chromosomes as expected, 12-15 excess chromosome fragments (ECF) are scored in samples processed immediately after irradiation at 6 Gy. Experimental results for chromosomal damage show that the number of G1-PCCc does not vary between serum-deprived and plateau-phase cells suggesting that PCC break formation is irrespective of the growth conditions. Of note, while scoring the PCC numbers, for experimental cells, any S- and or G2-phase-PCCs and most importantly, anaphases were considered as contaminants and consequently excluded from the experiments. As shown in the figure 40, number of scored PCC breaks between experiments at 6 Gy reflect a reproducible trend. For counting

excess chromosome fragments, we especially used yields of excess fragments following subtraction of PCC breaks of control non-irradiated samples (21 chromosomes).

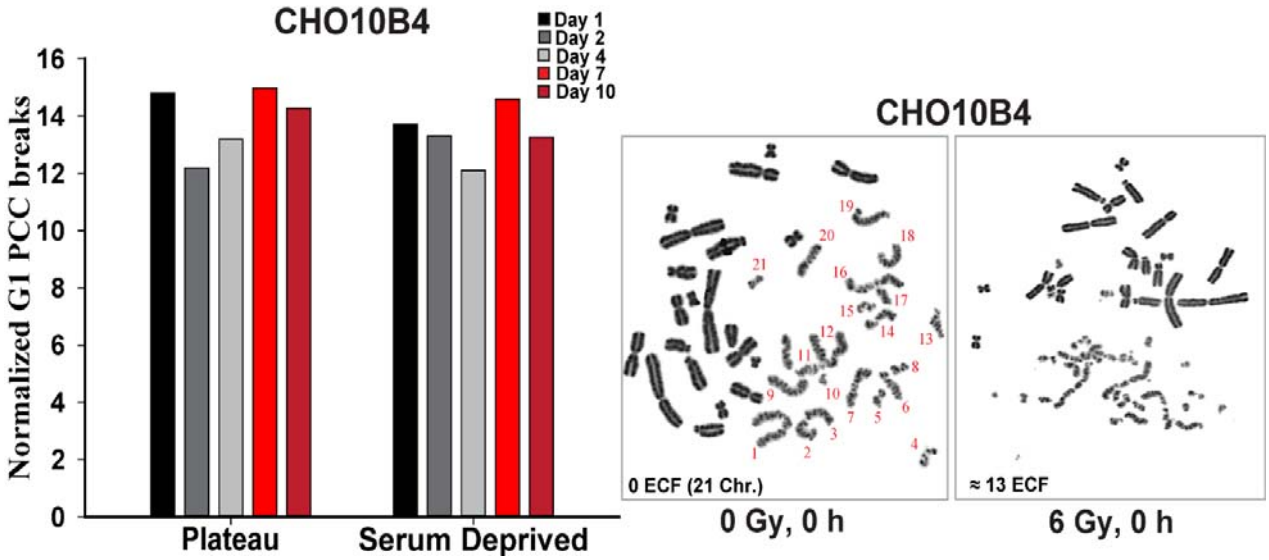

Figure 40 Polyethylene glycol (PEG) mediates fusion between interphase and mitotic CHO cells. Bar graph represents the normalized G1 PCC breaks following subtraction of the G1 PCC of non-irradiated samples (21 chromosomes). Right panel shows the micrographs of G1-PCC from non-irradiated and irradiated (6 Gy) samples. Irradiated sample shows 13 excess chromosome fragment (ECF). The number of chromosomes derived from non-irradiated control PCC is indicated in red and shows 21 chromosomes as expected. Fusion was mediated by means of 45% PEG with an interphase-to-mitotic ratio of one.

1.6.1.2 Repair of PCC breaks requires DNA end resection in G1-phase cells

As mentioned before, earlier research has already investigated the role of CtIP in G2 and S phase of the cell cycle. However, less is known about its role in G1 phase of the cell cycle and its dependence on alt-EJ. To determine whether CtIP can promote alt-EJ dependent end-resection in serum deprived non dividing G1/G0 cells, we examined PCC break formation in CHO wild type and in a set of mutants' defective in DNA-PKcs and Ku-80, upon CtIP depletion. Twenty hours post-transfection of siRNA, cells were serum deprived for next 20 hours, irradiated with 6 Gy and collected at different time points (0, 4 h and 8 h). With our serum deprivation protocol, we could obtain around 90% of G1-arrested cells for the above-mentioned cell lines (figure 42-B). G1-arrested cells following serum deprivation and Mitotic cells obtained with colcemid treatment are shown in figure 42, B. Chromosomes of G1-arrested cells are optically distinct from that of G2 and/or mitotic chromosomes by having

their single-chromatid morphology. To monitor the kinetics of PCC breaks repair, cell fusion at different time points following irradiation at 6Gy of IR was performed. Moreover, efficient CtIP knockdown evident by western blot analysis was achieved for 48 h window after siRNA transfection (Figure 42, C).

In wild type CHO10B4 cells, CtIP knockdown did not show any significant repair defect and a repair of 60% of residual PCC breaks is noted at 4 h. Similar number of chromosome breaks was observed between CtIP depleted and corresponding siControl transfected cells at all-time points analyzed (0, 4 and 8 h). In contrast, depletion of CtIP in DNA-PKcs deficient cell line showed a significant repair defect. Intriguingly, in XRS-6 cell line, which harbors mutant Ku-80, CtIP depletion leads to enhanced chromosomal breaks with 20-21 extra PCC breaks per cell, while the repair kinetics remained unchanged. Control siRNA transfected cells, on the contrary, repaired more than half of their breaks at 8 h. A trend of repair, albeit slow, is noticed in both c-NHEJ mutant cells transfected with control siRNA compared to repair proficient wild type CHO cells. As such, the number of residual PCC breaks at 4 and 8 h is also markedly higher than corresponding CHO wild type cells.

These data in aggregate suggest that CtIP promotes resection in G1 phase for chromosome break repair in c-NHEJ deficient background. Thus, it supports the notion that cells with defects in c-NHEJ utilize alt-EJ to repair PCC breaks, which is enabled by CtIP-dependent end resection.

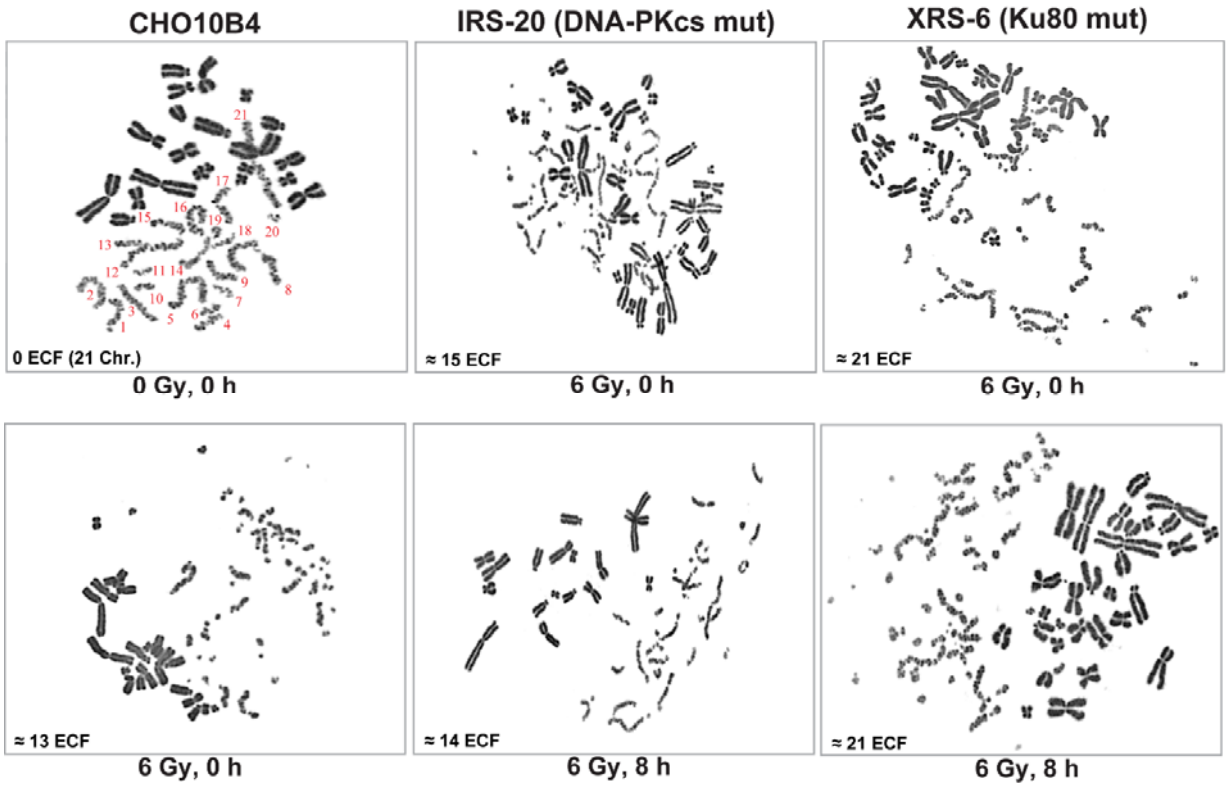

Figure 41 Micrographs of G1-PCC in CHO cells obtained by means of PEG. G1-PCC, shown in the upper left micrograph is non-irradiated representing typical 21 chromosomes and the number of chromosomes is indicated (red). Rest micrographs represent the number of excess chromosome fragments (ECF) as indicated following CtIP depletion and 6 Gy of IR.

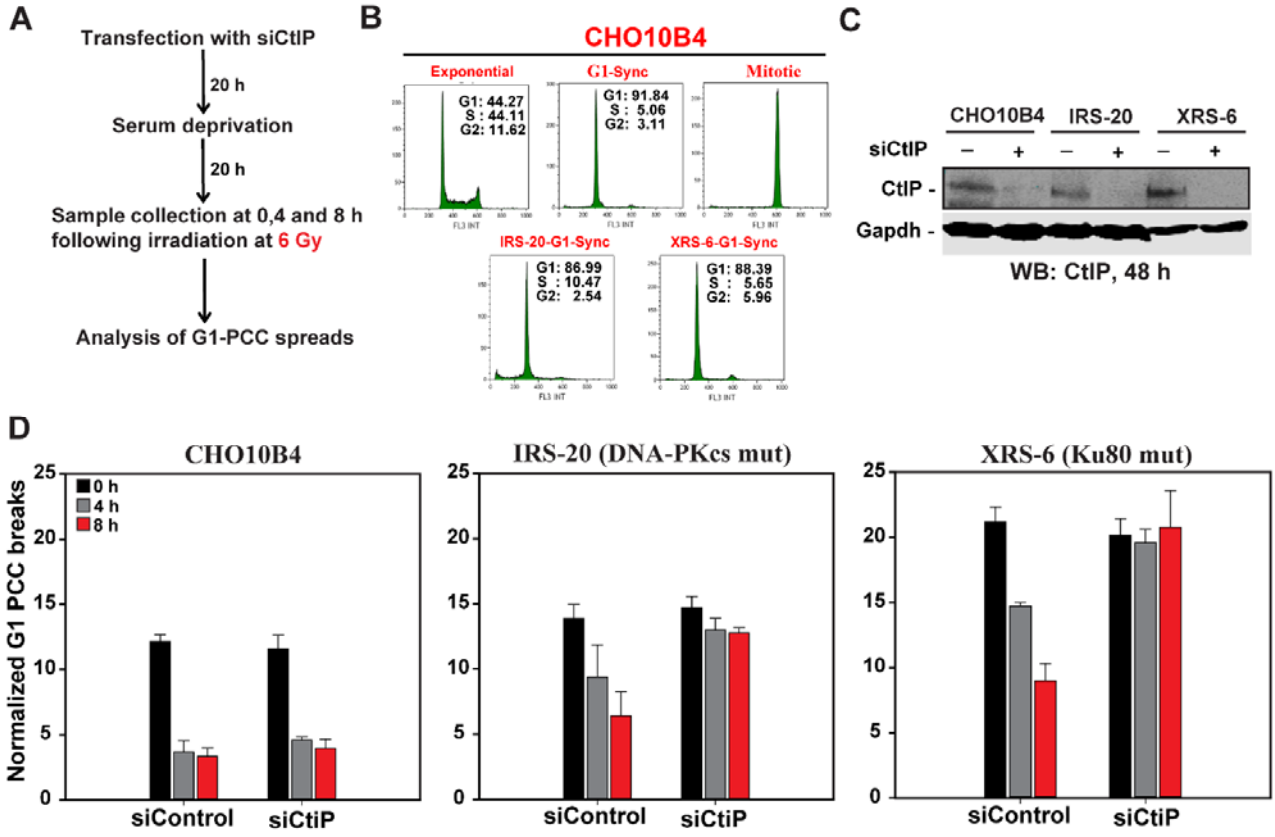

Figure 42 CtIP is indispensable for the repair of G1-PCC breaks in CHO cells. (A) Brief experimental outline of G1-PCC following CtIP knockdown and IR at 6 Gy. **(B)** Representative histograms showing the cell cycle percentage of cells in each population obtained during exponential growth (CHO10B4), Colcemid arrested mitotic cells and G1-synchronized cells. **(C)** Western blot validating efficient knockdown of CtIP analyzed 48 h upon CtIP-depletion. **(D)** Bar graph represents the value of normalized G1 PCC breaks (excess chromosome fragment) in CtIP-knockdown and corresponding siControl transfected cells at the indicated time points. Number of analyzed PCCs range from at least 10 (non-irradiated samples) to 40 (irradiated samples). The mean and standard deviation (SD) shown are from three independent experiments.

1.6.2 Role of Parp and Rad52 in the repair of G1-PCC breaks

The phenotype from previous experiment showing proficiency in repair of chromosome breaks in control siCtIP transfected c-NHEJ mutant cells prompted us to further elucidate the underlying mechanism. While Parp is implicated in alt-EJ, SSA has been shown to be dependent on Rad52. Despite their involvement in different pathways, both Parp and Rad52 are utilized in resection-mediated pathways (Mladenov, Staudt, et al. 2019; Soni et al. 2014). We thus investigated whether pharmacological inhibition of Parp and Rad52 modulates DDR. For DMSO and PJ34 (Parp inhibitor) treated cells, the number of G1-PCC breaks between CtIP-depleted and non-depleted cells remained similar at all-time points analyzed (figure 43-A and C). However, a specific Rad52 inhibitor, 6-OH-DOPA, resulted in a modest effect on

chromosome repair in comparison to DMSO-treated and Parpi-treated samples hinting to the engagement of mutagenic Rad52-driven SSA (figure 43-D). The efficiency in chromosome breaks processing between siCtIP transfected and siControl-transfected cells remained unchanged when treated with NU7441 (figure 43-A). Notably, treatment with NU7441 of wild-type cells showed effects similar to that observed in IRS-20 (DNA-PKcs mutant) cells demonstrating that chemical inhibition of DNA-PKcs recapitulates, in wild-type cells, DNA-PKcs mutant phenotype (43-B and 42-D-middle panel).

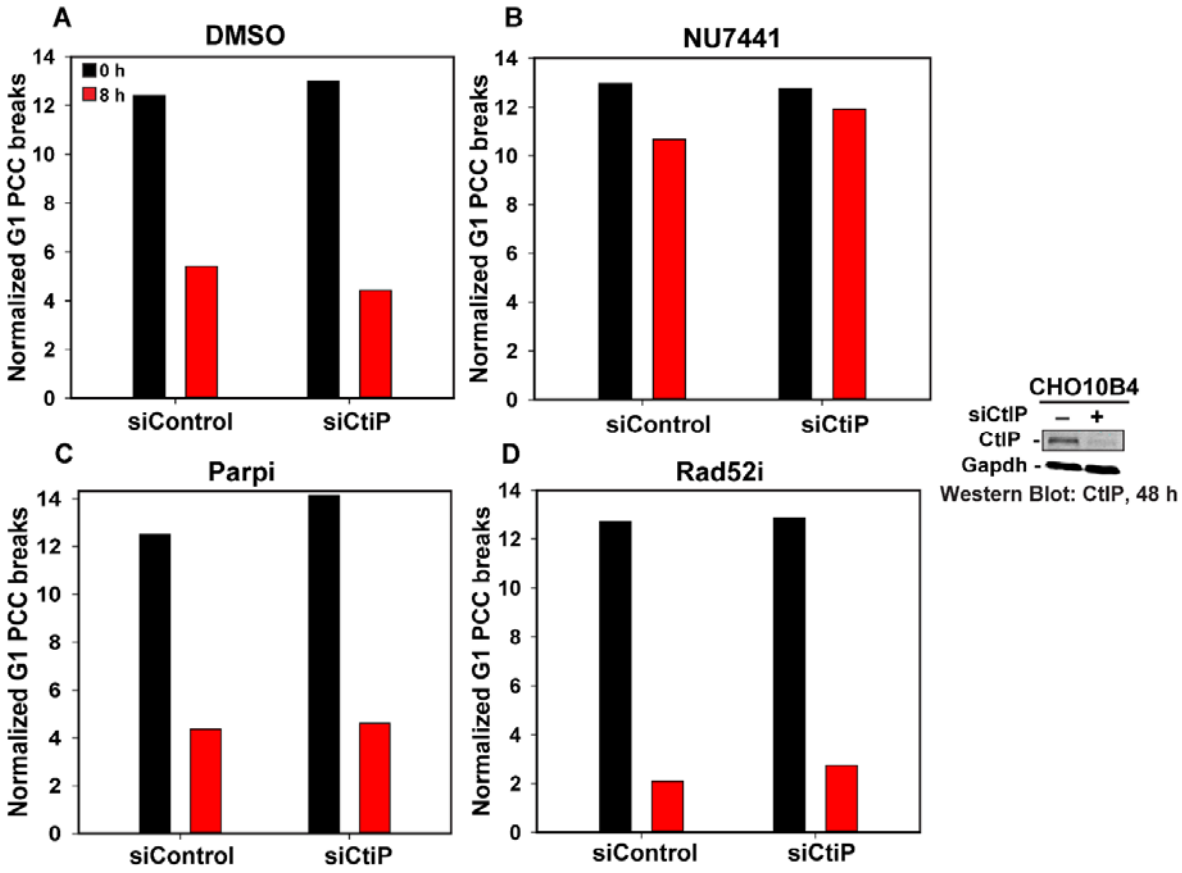

Figure 43 Rad52 and Parp are dispensable for repair of G1-PCC breaks in CHO cells. Analysis of premature chromosome condensation (PCC) in G1 wild type CHO cells (CHO10B4) treated with DMSO, NU7441 (5μM), PJ34 (10μM) and 6-OH-DOPA (10μM) at indicated times following exposure to 6 Gy. Post-irradiated samples were incubated for 1 h for repair and the number of excess chromosome fragments was then scored for analysis. Immunoblot performed at 48 h shows the efficient knockdown of CtIP protein. GAPDH is used as a loading control.

Similarly, we assessed the impact of Rad52 and Parp inhibition in a Ku80 deficient cell line (figure 44). While DMSO-treated cells show efficient chromosome break repair by repairing nearly half of IR-induced chromosome breaks, no reduction in PCC break repair is observed following treatment with PJ34 and 6-OH-DOPA. Surprisingly, inhibition of Rad52 and Parp

shows a strong deficiency in their repair capacity but does not induce more chromosomal breaks in CtIP-knockdown cells. Notably, no effect on cell cycle progression following either siRNA mediated knockdown or treatment with these drugs was observed.

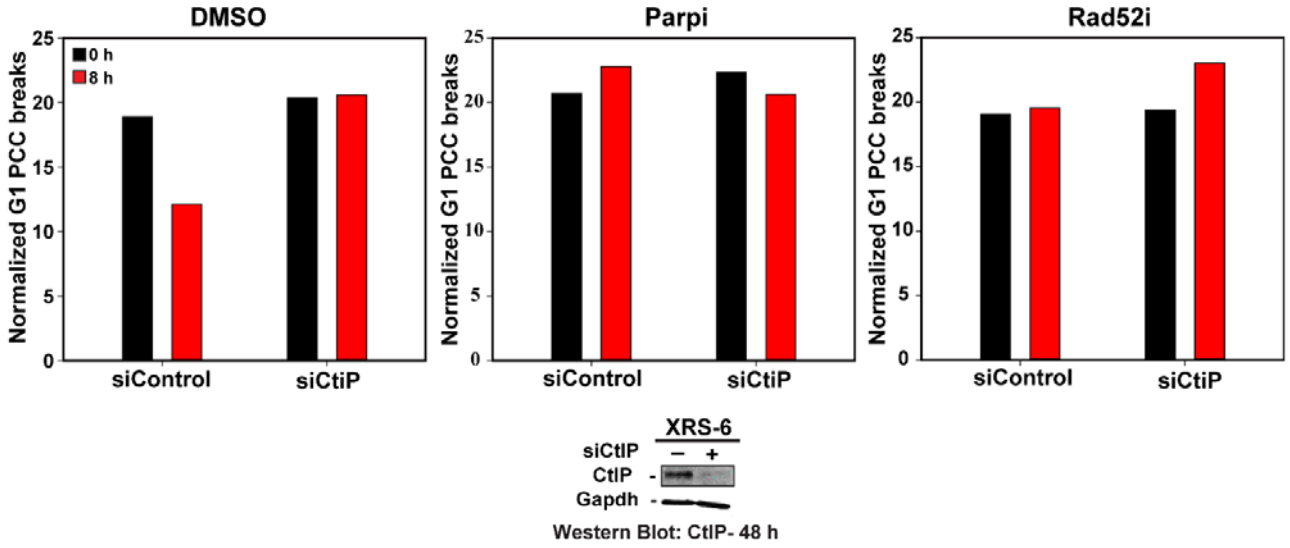

Figure 44 Rad52 and Parp are essential for repair of G1-PCC breaks in Ku80-mutant cells. Premature chromosome condensation (PCC) analysis in Ku80 mutant cells (XRS6) treated with DMSO, PJ34 (10μM) and 6-OH-DOPA (10μM) at indicated time (0 and 8 h) following exposure to 6 Gy of irradiation. Number of chromosomes from non-irradiated samples was subtracted from the irradiated samples. Western blot shows the efficient knockdown of CtIP protein at 48 h. Gapdh is used as a loading control.

1.7 Gradual restoration of CtIP via blocking ubiquitin-proteasome pathway is devoid of its repair-proficient phenotype

Ubiquitin, a 76-amino acid containing protein modifier, is shown to play a crucial role in the degradation of key cell cycle regulatory proteins. This small protein creates mono-or-poly ubiquitination chains by conjugating with substrate proteins and directs them toward proteasome-mediated proteolysis. In line with this, we observed a reduced expression of CtIP protein level in cells maintained in plateau phase of growth (figure 30-C and figure 45-D, lane 2). We thus speculated that ubiquitination might promote CtIP degradation by the proteasome. We inquired whether restoration of CtIP underpins the increased repair proficiency. In order to address this, we treated plateau phase cells with Bortezomib (an ubiquitin-proteasome inhibitor) for 4 h or 12 h with a concomitant inhibition of DNA-PKcs. Surprisingly, by blocking ubiquitin-dependent proteasomal degradation system (UPS), we observed in unperturbed cells a gradual increase in the level of CtIP protein from 4 h (1.7 fold) to 12 h (6.1 fold) compared to DMSO (1.0 fold) treated condition, supporting the notion

that CtIP is negatively regulated by the proteasome system. Remarkably, prolonged (12 h) inhibition of ubiquitin-proteasome pathway by Bortezomib restored CtIP protein to the level observed in exponentially growing cells (8.7 fold) (figure 45-D and E). To evaluate the contribution of CtIP in alt-EJ, we analyzed DSB repair kinetics either with single treatment of NU7441 (1 h) and/or with a dual treatment of NU7441 and Bortezomib (4 or 12 h) before irradiation. As expected, inhibition of DNA-PKcs compromised the repair processing while combined treatment of NU7441 and Bortezomib either for 4 or 12 h showed no additional effect in repair processing (Figure 45, A). It suggests that inhibition of ubiquitin-proteasome pathway does not cause shunting of repair pathway towards resection dependent alt-EJ to process the DSBs.

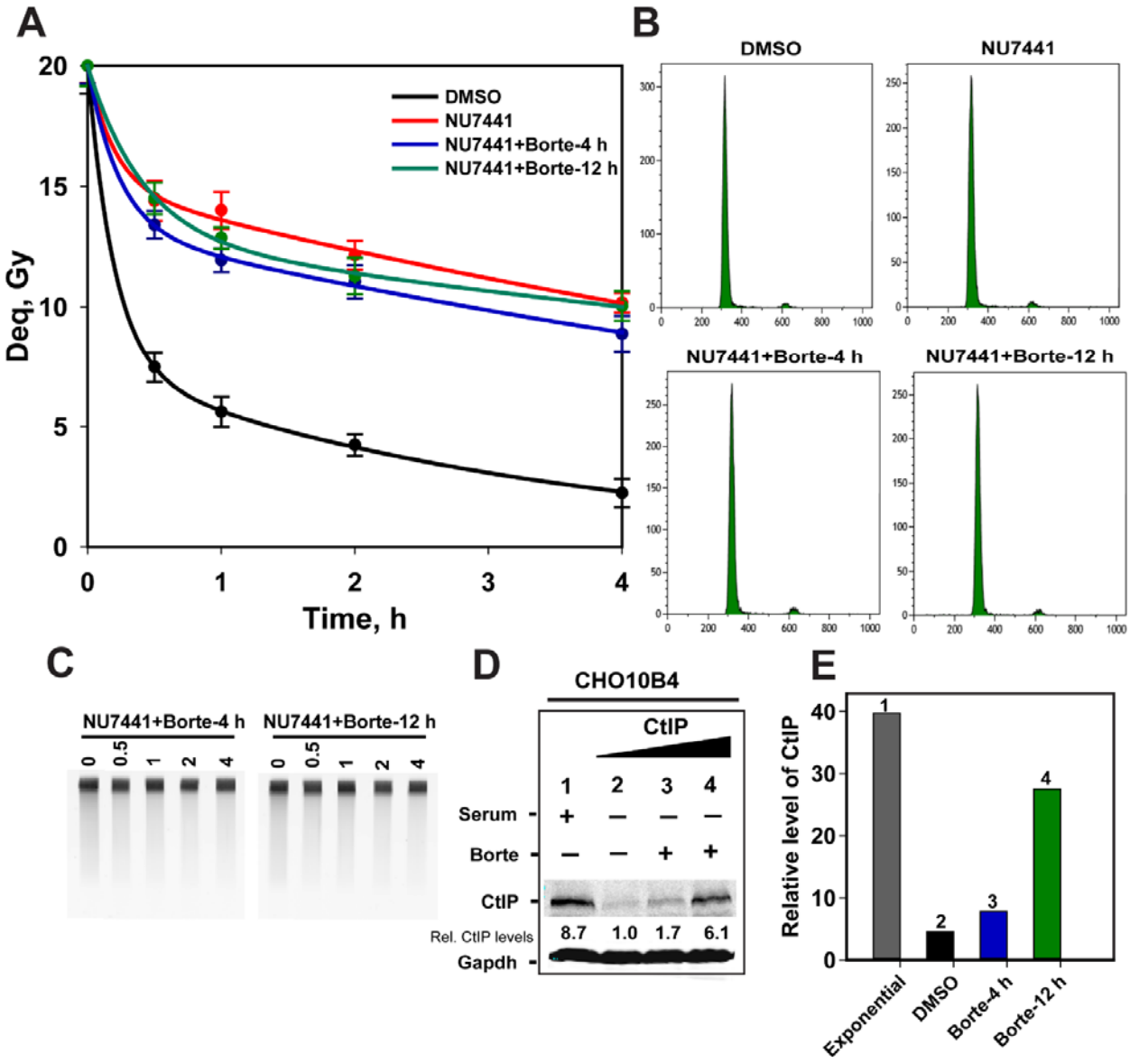

Figure 45 CtIP restoration by blocking ubiquitin-proteasome pathway does not elicit a repair-proficient phenotype. (A) DSB repair kinetics of cells maintained in plateau phase of growth after serum deprivation (3 days) following IR at 20 Gy and measured by PFGE. Cells were either pretreated with NU7441 (1 h) or NU7441+Bortezomib (NU7441+Borte-4 h or 12 h) before IR. (B) Cell cycle analysis of inhibitor and IR treated plateau phase cells using flow cytometer **(C)** Typical PFGE gels of NU7441 and Bortezomib treated samples (4 and 12 h), Numbers denote time points. **(D)** Western blot showing expression of CtIP level as depicted (normalized to DMSO treated) after treatment with NU7441 (5μM) and Bortezomib (μM) as in (A) but without IR. Lanes (1, 2, 3 and 4) represent the condition as written there. The signal intensities of CtIP band shown in fold were quantified by densitometric analysis using ImageJ software and normalized to DMSO treated sample (number 2). **(E)** Quantitative densitometry analysis of relative expression of CtIP in treated samples showing expression level (in fold). The values represent the relative increase of CtIP protein level upon combined treatment with NU7441 (1 h) and Bortezomib (4 h and 12 h) compared to DMSO treated samples and CtIP in

exponentially growing cells were used as control. Shown results represent the mean and standard error (SE) from two independent experiments. Gapdh was used as a loading control.

It is well accepted that interphase chromosome breaks arise from unrepaired DNA double strand breaks (DSBs). In eukaryotic cells, c-NHEJ mainly processes the irradiation induced DSBs. Thus, the rationale is that akin to DSBs, the same pathway also repairs chromosomal breaks. Theoretically, 20-40 DSBs are induced per Gy of irradiation and consequently only 2-4 interphase chromosome breaks are created with the same irradiation dose. It suggests only a subset of DSBs leads to the formation of chromosomal breaks (Terzoudi et al. 2008). Therefore, we performed interphase G1-PCC assay to examine the functional role of c-NHEJ in rejoining chromosome breaks as well as contribution of alt-EJ in c-NHEJ-deficient background. As shown in the figure 46, 1 Gy of IR gives rise to around 2-3 breaks which arise only from the slow and persistent DSBs. Looking at the figure 45-A, it can be postulated that half of the DSBs is rejoined with fast kinetics (10-20 minutes), whereas roughly half of the chromosome breaks is repaired with comparatively slow kinetics (1-2 h). To examine the ultimate contribution and capacity of alt-EJ in processing the DSBs generating chromosomal breaks, we treated the cells with NU7441 to allow the alt-EJ to come to the fore and analyzed the break formation. The results show an increase in the initial outcome of the breaks with a drop in their kinetics of rejoining interphase chromosome breaks (Figure 46). Likewise, an enhanced inhibition in DSB repair was also noticed compared to DMSO-treated control. This implies that in absence of c-NHEJ, alt-EJ repairs a significant amount of both DSBs and DSBs leading to chromosome breaks. Moreover, to investigate how inhibition of ubiquitin-proteasome mediated degradation of CtIP would affect the kinetics of chromosome break formation, we similarly analyzed the chromosome breaks after dual treatment with NU7441 and with Bortezomib. Identical to single treatment with NU7441, dual treatment with NU7441 and Bortezomib showed almost similar, to some extent lesser, kinetics in rejoining chromosome breaks. Thus, the contribution of CtIP-mediated alt-EJ to repair DSBs and chromosome breaks remains speculative.

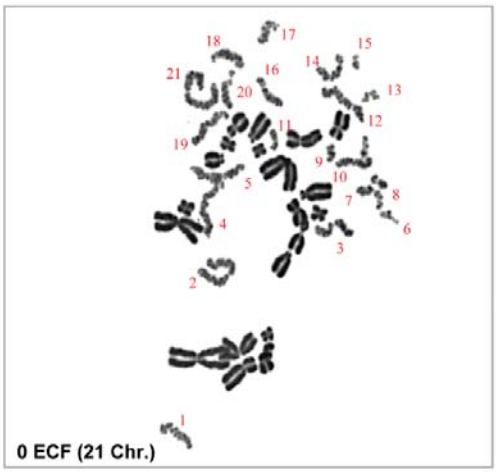

0 Gy 0 h (NU+Borte-4 h)

6 Gy 0 h (NU+Borte-4 h)

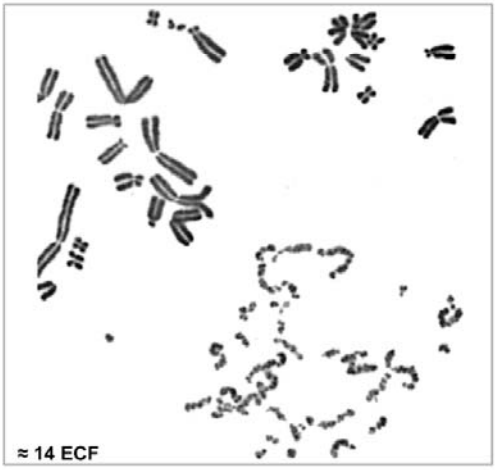

6 Gy 8 h (NU+Borte-4 h)

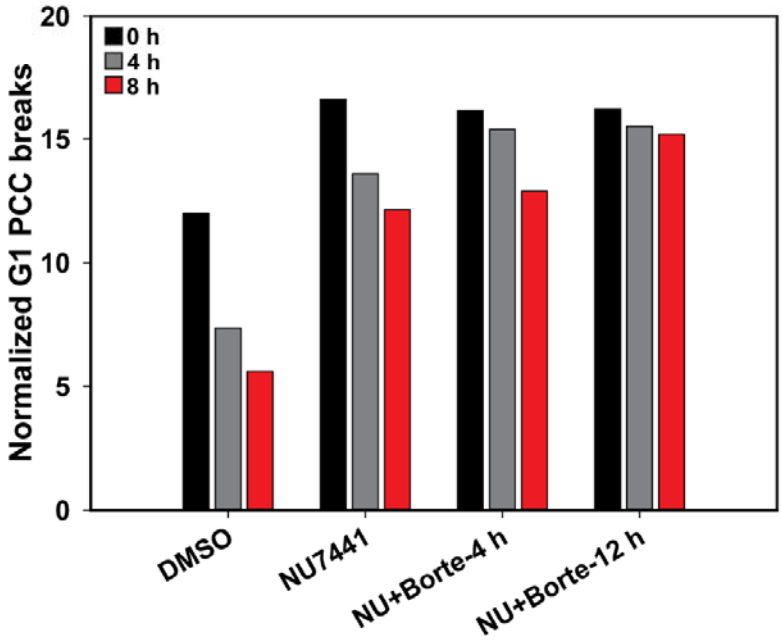

Figure 46 NU7441 and Bortezomib treatment (single or combined) compromise rejoining of chromosome breaks. (Left Panel): Bar graph represents the normalized G1 chromosome breaks after treatment with DMSO, NU7441 (1 h) and NU7441 (1 h) + Bortezomib (4 and 12 h). Cells were irradiated after indicated drug incubation time and samples were collected immediately after irradiation (6 Gy 0 h) and 4 h and 8 h after irradiation at dose of 6 Gy. (Right panel) The micrographs show G1-PCC from non-irradiated but drug treated (0 Gy 0 h) and irradiated as well as drug treated samples (6 Gy at 0 and 4 h). Indicated numbers (red in color) show the number of chromosome (21) obtained using PCC assay. Results are from one experiment.

Based on the above findings, we further enquired how and to what extent resection is regulated in quiescent cells (G0) by looking at RPA signal intensity following ionizing radiation. Obtained results show a significant increase in RPA signal intensity both in wild type and DNA-PKcs deficient cell lines following irradiation at high dose of X-ray (20 Gy) (figure 47). Despite their distinct genetic make-up (DNA-PKcs proficient and deficient), both cell lines elicited similar RPA intensity which is mediated through CtIP. It demonstrates that the fraction of DSBs that are associated with slow repair kinetics may process the breaks (DSBs or chromosome breaks) via resection dependent pathway.

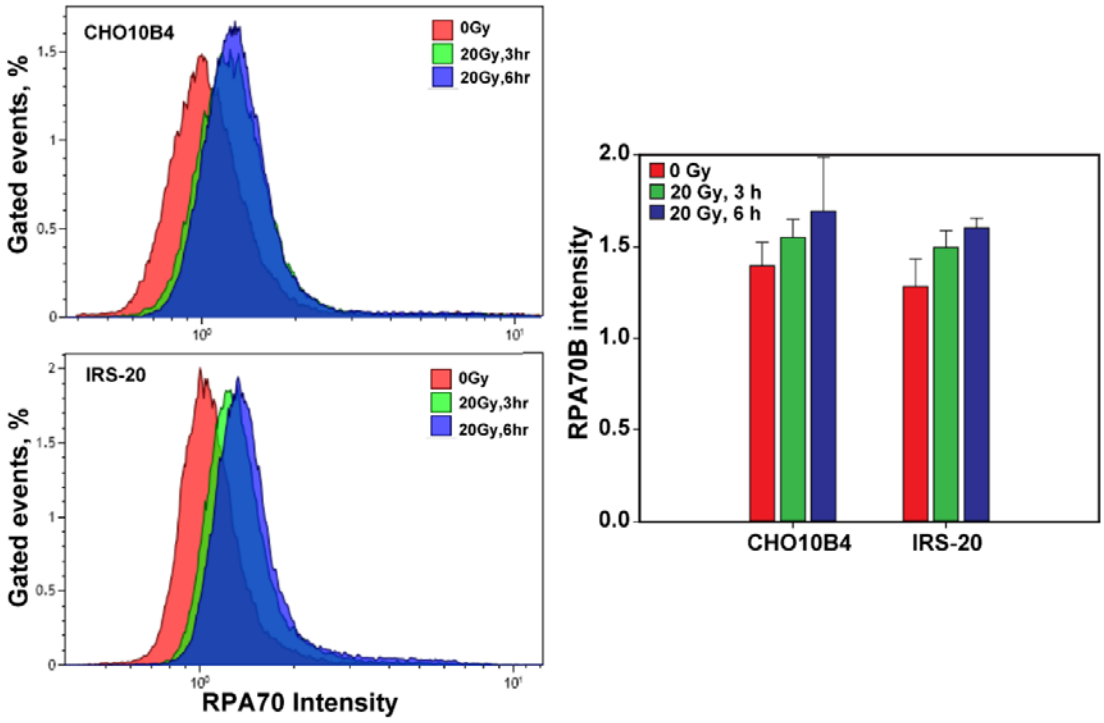

Figure 47 CtIP plays significant role in DNA end resection in quiescent cells. (Left Panel) Representative histograms for wild type (CHO10B4) and DNA-PKcs mutant (IRS-20) cells show the signal intensity of RPA70 measured in EdU negative G1 phase cells. **(Right Panel)** Quantitative analysis of Rpa70 intensity. Shown results represent the mean and the standard deviation from three independent experiments.

1.8 DNA end processing by endo-and-exo nuclease function of MRE11

MRE11, the nuclease component of Mre11-Rad50-Nbs1 (MRN) complex, plays significant role in DSB repair pathways. This nuclease component of MRN complex is likely to be the first nuclease to resect DNA ends and is essential for resection at DSBs of as few as 20bp during alt-EJ (Truong et al. 2013). Research revealed that resection by MRE11 is first initiated by creating a nick in the DNA by MRE11 endonuclease activity and is extended towards the DNA end by 3´→5´exonucleolytic activity of MRE11, which follows a sequence of endo-then-exo. Yet, how its endo- and exonuclease activities regulate DNA repair is unknown.

In order to check whether MRE11 has homologous recombination repair (HRR) uncoupled function in DSB end processing, we tested its role in alt-EJ following irradiation at 20 Gy where HRR is, by default, non-functional (Wu, Wang, Mussfeldt, et al. 2008). We used well-established small-molecule inhibitors of MRE11 with specific inhibitory effects on its endonucleolytic (PFM01) and exo-nucleolytic (Mirin) activities (Shibata et al. 2014). At first we checked this by looking at exponentially growing hamster wild type cell line (CHO10B4) using NU7441 in combination with either single or combined inhibition of endo or exo nuclease function. While inhibition of endo-nuclease activity using PFM01 confers DNA damage sensitivity, blocking of exo-nuclease activity show no effect in DSB processing (Figure 48). Interestingly, simultaneous inhibition of exo-and-endo nuclease activities under the same conditions displays no additional DSB repair sensitivity.

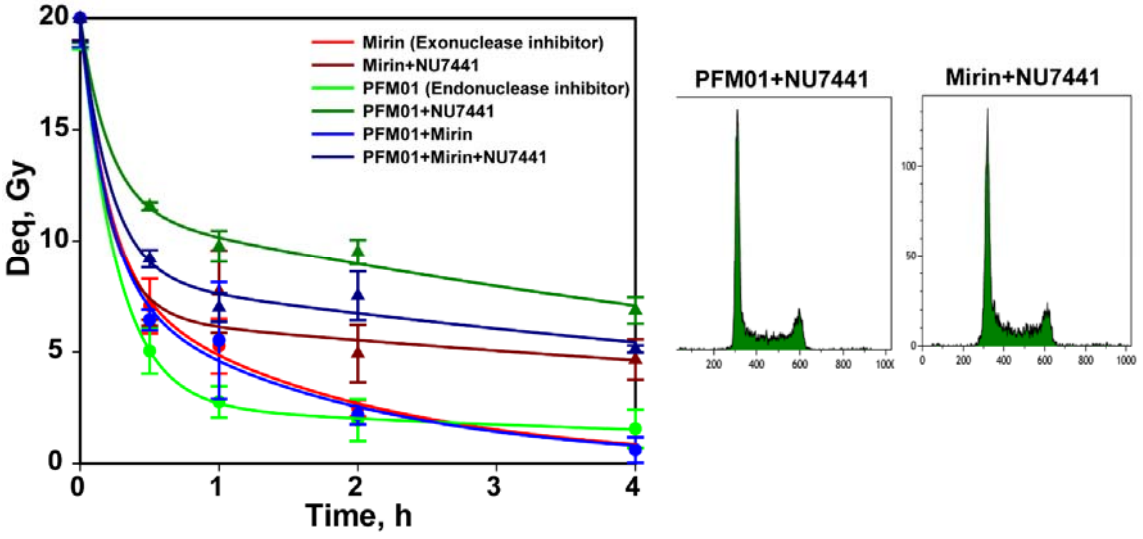

Figure 48 Effects of MRE11 inhibition on alt-EJ. DSB repair was investigated by PFGE in CHO10B4 cells (wild type). One hour before IR, 5 μM of NU7441 and 100 μM of PFM01 or 50μM Mirin was added to the cells.

DSB repair kinetics is shown on the left side and on the right side, cell cycle profile following drug treatment. Results shown are the average and standard error (SE) of four determinations from one experiment.

It is important to note that, DNA end-tethering is functional in cells lacking DNA-PKcs. We performed PFGE in similar experimental setting in one of DNA-PKcs $^{-/-}$ cell lines (IRS-20) to study the role of DNA-PKcs in the regulation of alt-EJ and Mre11-mediated end processing. Inhibition of the nuclease functions of MRE11 (endonucleolytic and exonucleolytic) separate or combined did not show any alteration in alt-EJ activity (Figure 49).

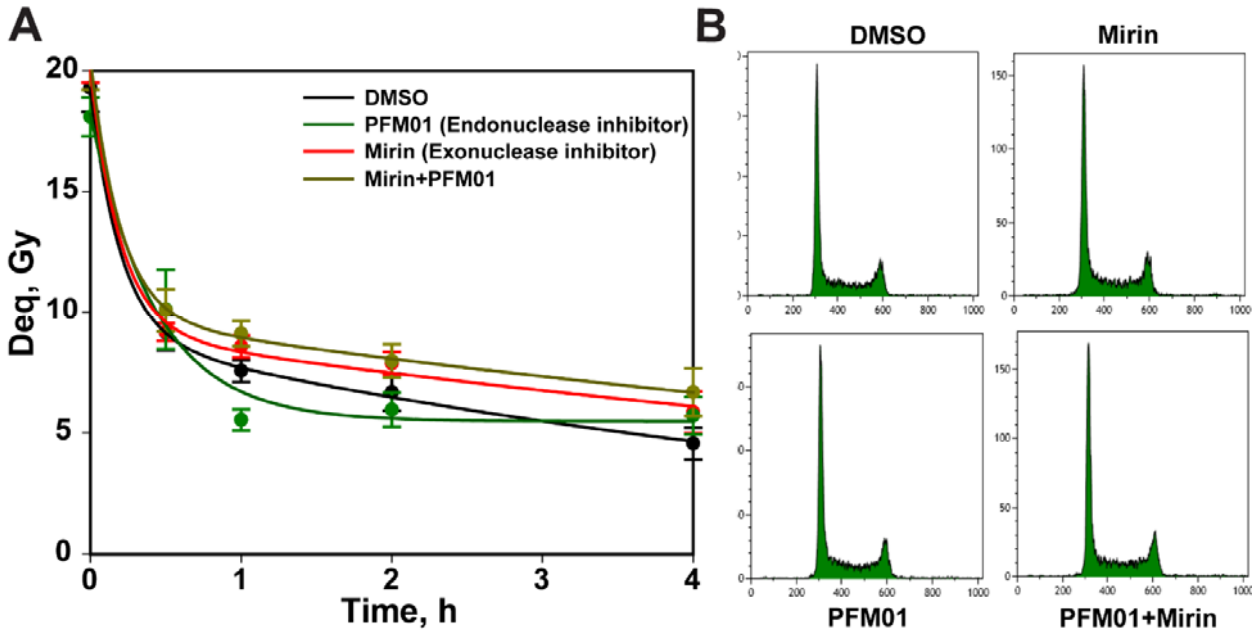

Figure 49 Effects of MRE11 inhibition on alt-EJ in DNA-PKcs mutant cells. Figure shows DSB repair kinetics and cell cycle histograms in DNA-PKcs $^{-/-}$ cells with and without inhibitor treatment. Shown results are the average of four determinations from one experiment. Error bars represent standard error (SE).

Collectively these data reveal that endo- but not exonuclease function of MRE11 promotes alt-EJ of DSB repair.

1.9 Inhibition of Rad52 promotes processing of DSBs by alt-EJ

Rad52 has been shown to play a central role in HRR and single strand annealing (SSA) repair pathway in yeast and mammalian cells (Bi et al. 2004). Both pathways function on similar principle of resecting DNA ends and utilizing homology. Besides, alt-EJ is also resection mediated. But, it utilizes short (microhomolgies) range resection in comparison to SSA, where long-rang resection takes place before annealing the resected ends. SSA in fact, results in extensive resection that is longer than HRR and thus, it is highly mutagenic and results in excessive deletion. Rad52 mediates SSA annealing of homologous stretches on the same

chromatid. On the other hand, Rad51 antagonizes SSA annealing to facilitate the strand invasion thus safeguarding faithful repair by HRR (Bhargava et al. 2016). Recent striking findings from our lab showed that increased DSB loads suppress the overall engagement of HRR in DSB repair and promotes Rad52 involvement (Mladenov, Staudt, et al. 2019). We thus investigated further the involvement of alt-EJ to repair the breaks at high IR dose when activity of SSA is inhibited (by Rad52i). Results summarized in figure 50 indicate a proficient DSB repair kinetics in DMSO treated cells, a marked reduction when treated with NU7441, but a comparative repair phenotype when treated with DL-DOPA, Rad52-specific inhibitor compared to NU7441 treated. It suggests that alt-EJ is engaged in the repair of DSB ends in the absence of both c-NHEJ and SSA

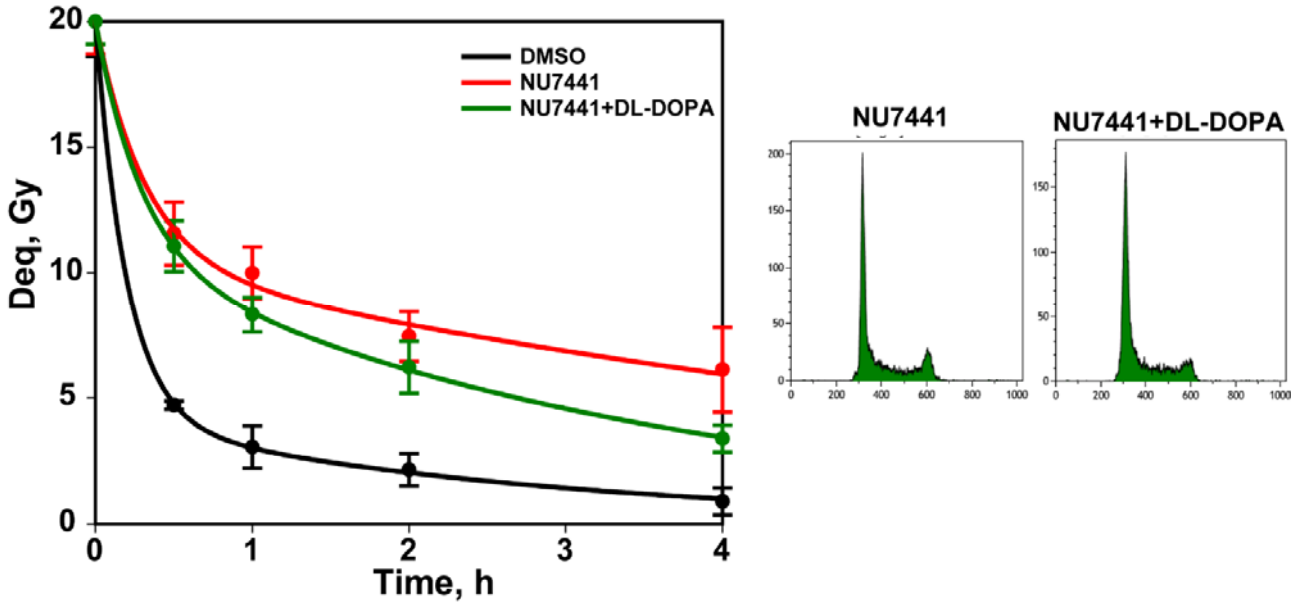

Figure 50 Rad52 inhibition promotes alt-EJ mediated DSB repair. DSB repair kinetics of CHO wild type cells maintained in exponential phase of growth. Before irradiation with 20Gy, cells were pre-treated with the indicated inhibitors. DSB repair kinetics is plotted as dose equivalent (Deq) as a function of time (h). Right panel shows cell cycle profiles of cells treated with NU7441 for 1 h, whereas DL-DOPA was added 6 h before irradiation. Results shown are from two independent experiments.

2 Role of RNF8 and RNF168 ubiquitin ligases in the repair of DSBs and DSB-clusters

2.1 Overview of previously developed biological model systems for clustered DNA double strand breaks (DSBs)

In order for us to study the underpinning mechanisms of DSB-clustering, a feature of densely ionizing radiation modality (high-LET) and the biological consequences thereof, biological model based on rodent cell lines from our laboratory has previously been developed and elaborated (Iliakis et al. 2018; Schipler et al. 2016). Briefly, in this model system, Sleeping-Beauty (SB) DNA transposon technology served as a means of integrating an 18bp-long I-SceI recognition sequence in the genome of CHO cells. By employing this method, we generated different constellations of DSBs in a controlled manner by integrating appropriately constructed vectors in the genomes of cells and achieved high numbers of I-SceI construct integrations (1-20). In figure 51, it represents different I-SceI constellations generated in CHO cells. The simplest form of constellation contains a single I-SceI recognition site and is therefore represented as single-DSB (1xI-SceI-D) where D (e.g. Direct) denotes the direct orientation of the integrated recognition sequence of I-SceI. Next two constructs were created by genetically integrating a pair of I-SceI recognition sites but spaced 200bp apart that generate DSB ends either in compatible (direct, D) or incompatible (reverse, R) orientation. In this configuration, clones that contain compatible DSB ends are denoted as (2xI-SceI-D), whereas incompatible DSB harboring clones are written as (2xI-SceI-R). The constellation, which represents the highest level of DSB clustering, sustains four I-SceI sites that are engineered at an overall distance of 462 bp. The loss of intervening sequence generates DSBs having either compatible or incompatible ends.

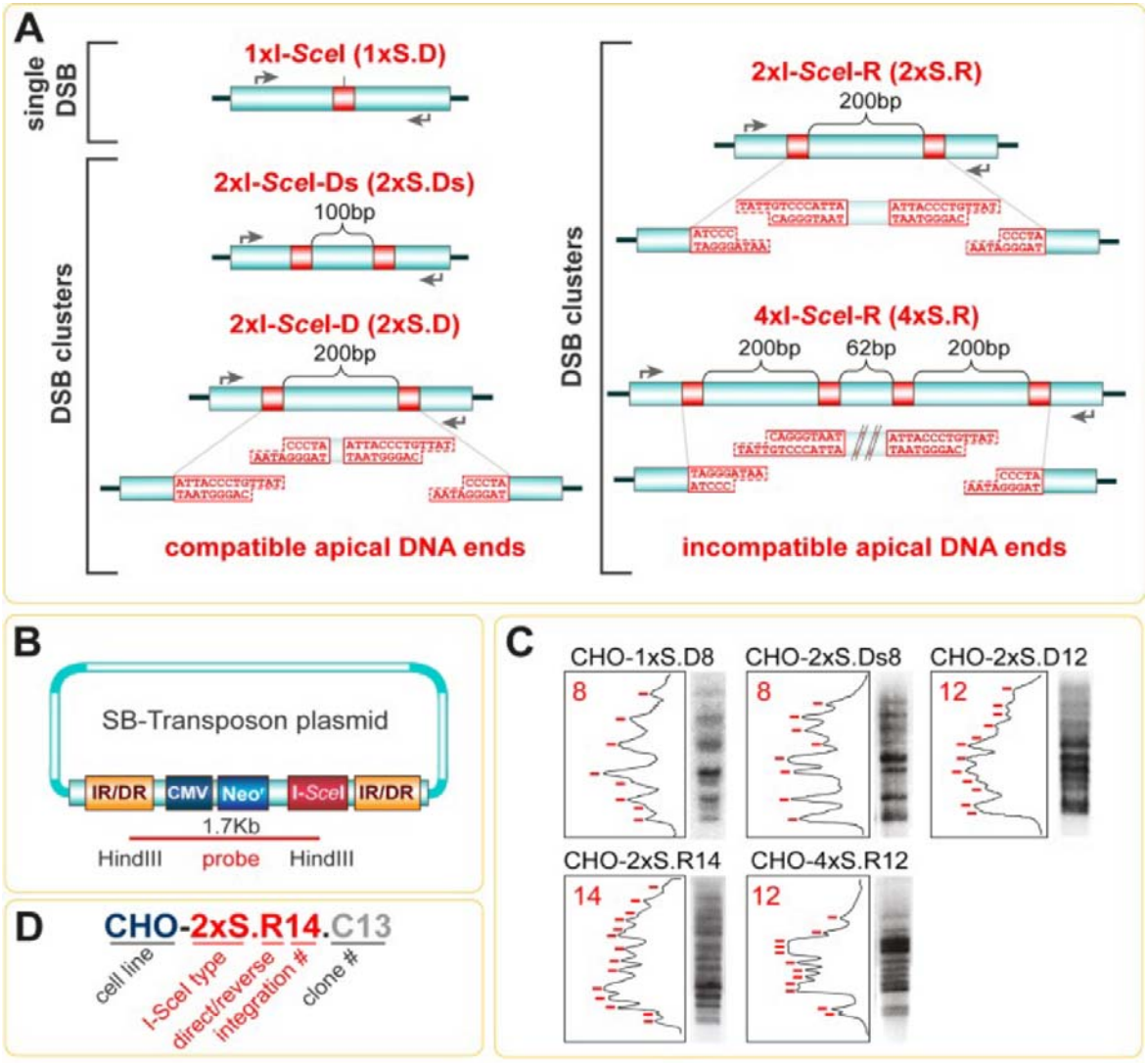

Figure 51 Overview of the approach to generate CHO cell lines carrying different numbers of I-SceI recognition sites allowing induction of simple and complex form of DNA double strand breaks (DSBs). **(A)** CHO clones carrying different combinations of I-SceI sites engineered at specific distances and orientations. Different constellations allowing generation of single-DSBs, of DSB-pairs located at 100 and 200 bp and of DSB quadruplets are illustrated. Red boxex represent the integrated I-SceI recognition sequence. The orientation of I-SceI recognition sites (Direct, D or Reverse, R) in clones harboring 2-4 I-SceI sites is depicted as they generate compatible or incompatible apical DNA ends after the loss of intervening sequence. Grey arrows show the locations of primers used to amplify corresponding DNA segment for junction analysis by sequencing or PCR genotyping. **(B)** Map of the sleeping-Beauty transposon plasmid carrying the I-SceI construct. The transposase binding site comprising the inverted/direct-repeats (IR/DR), CMV-cytomegalovirus promoter, Neo^r-neomycin resistance are highlighted. **(C)** Southern blot analysis of all tested CHO clones after transfection with transposon constructs to confirm their genomic integration. The number of bands corresponds to the number of integrations. The densitometry plots on the left show the quantification basis regarding the number of integrations in each clone. **(D)** Outline of the nomenclature for designating the CHO derived clonal cell lines. The name of the parental cell line (CHO) is followed by the type of the construct used for integration (1xS, 2xS, 4xS), where S

denotes integrated I-SceI sites. After that, the orientation of apical I-SceI sites (D;Direct and R;Reverse) is indicated. The number right after the pattern of orientation (D/R) represents the number of I-SceI integration as evident by southern blotting in the clones. The last part of the designation symbolizes the specific clone (Cx) and is excluded in the description of the results section for simplicity. Ds designates direct orientation of two I-*Sce*I sites separated by a shorter (s) distance of 100 bp—instead of the typical distance of 200 bp used in other pairs. This illustration is adapted from (Schipler et al. 2016).

Constructs comprising varying numbers of I-SceI recognition sequence at different orientations have thus been used to induce simple as well as complex forms of DSBs and to investigate the consequences of DSB clustering on various biological endpoints, such as DDR signaling, genome stability and cell survival.

2.2 PCR based characterization of CHO clones, harboring I-SceI constructs for generation of simple-DSBs and DSB-clusters with increasing complexity

Maintenance of the purity and stability of any cell lines propagated in vitro is a crucial part of cell biology research. Nevertheless, a number of factors like genomic instability associated with continuous propagation in culture, genotypic and phenotypic drift, clonal impurity during isolation of cell line and cross contamination with another cell line have been reported and are often associated with alteration of cell line characteristics and can thus be misleading in terms of drawing conclusions from experimental data (Mitchell et al. 2001). Therefore, phenotypic and genotypic characterization of cell-lines propagated in vitro is warranted. In order to test systematically the genotypic characteristics of commonly used experimental CHO clonal cell lines harboring ISce-I recognition site with defined distance, conventional PCR was performed by amplifying a DNA fragment comprising the clusters using in-house designed primers shown in figure 52-B. Of note, mentioned primers for all integrated I-SceI constructs are common and specific. All PCR products were separated by applying 5µl to a 2% agarose gel followed by electrophoresis for 90min at 70V. Amplified PCR products show clear bands after gel electrophoresis equivalent to the predicted length from the corresponding clonal constructs. Cells harboring a single I-SceI recognition site show a PCR fragment of 240bp (Lane 2). Cells that sustain a DSB cluster in which two I-SceI recognition sites are located with defined distance of 100bp and 200bp show predicted PCR products of 240bp and 480bp respectively. Amplified DNA fragment in clone harboring four-DSB clusters represents a band size of 980bp (Lane 6) as expected. Moreover, plasmids harboring different constellations of I-SceI cassette used to generate the clonal cell lines show representative bands of PCR product shown in lanes 7-13 and were used as positive control.

These results thus confirmed that the I-SceI recognition site is retained in the mentioned clonal cell lines during propagation and maintenance.

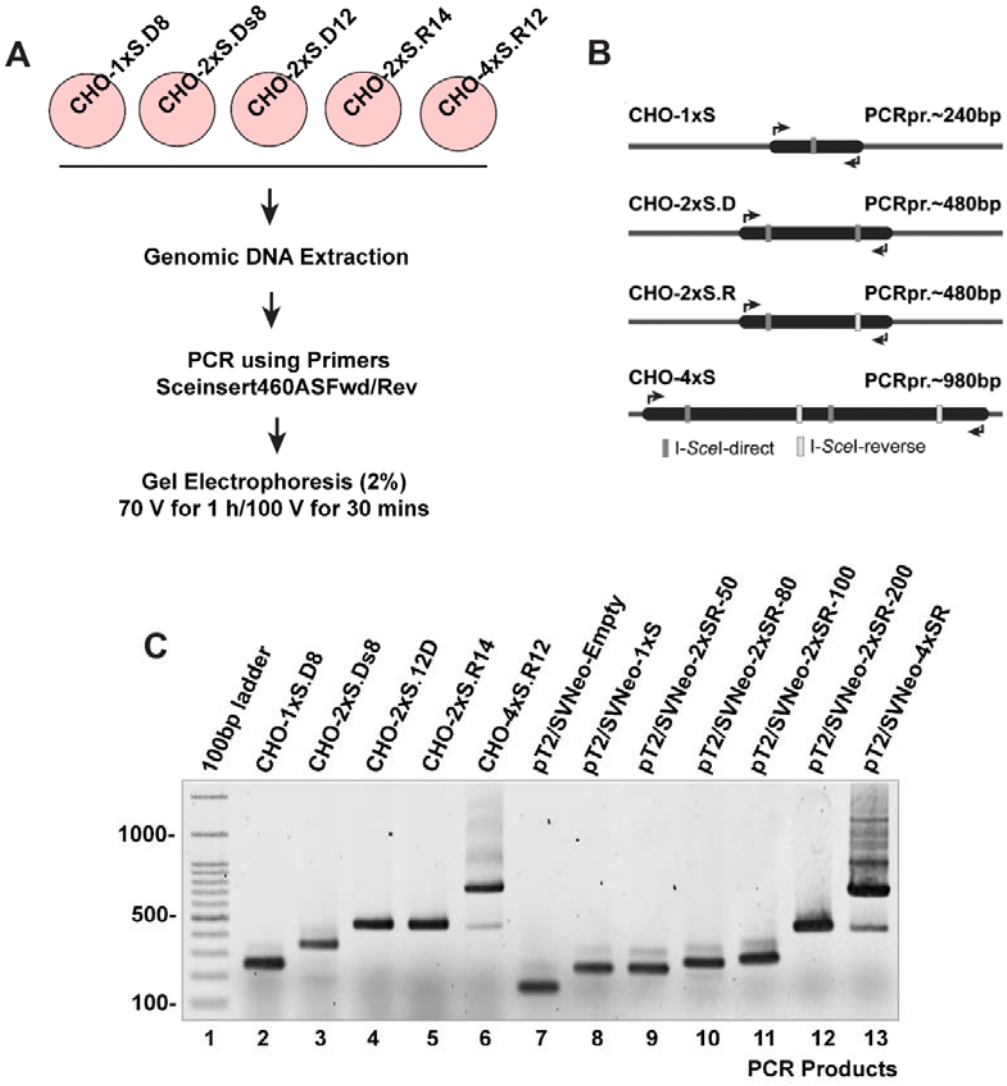

Figure 52 PCR based Genotyping validates the I-SceI recognition sites in the clonal cell lines. (A) Flowchart of brief protocol from genomic DNA extraction to Gel electrophoresis for five clones harboring different constellations of DSB cassettes. **(B)** Schematic representation in CHO clones of I-SceI cassette. PCR Primers used to amplify the region of interest are indicated by black arrows and resulted PCR products indicated can also be seen in figure C. **(C)** Agarose gel electrophoresis (2%) shows the PCR fragments amplified from CHO clones using the primers indicated in figure B. Lanes (2-6) represent the PCR products from CHO clones while plasmids harboring different cassette of I-SceI show the PCR products in lanes (7-13).

2.3 Validation and functional characterization of I-SceI expressing Plasmid pI-SceI-3xNLS

Generation of I-SceI expression construct was kindly provided by Maria Jasin, Addgene plamid # 26477, (C, ME, and M 1998). To amplify and purify the plasmid, midiprep protocol mentioned in methods and material section was followed. At first, eluted pI-SceI plasmid was validated by resolving the plasmid in agarose gel electrophoresis (1%). Figure 53-A shows that with our established lab protocol significant amount of supercoiled plasmid DNA (indicated in black arrow at the bottom) can be recovered. In addition, the efficiency of I-SceI expressing plasmid in generating DNA double strand breaks (DSBs) following transient transfection was confirmed by using DR-GFP reporter construct in U2OS-DR cells. It measures the efficiency of homologous recombination repair (HRR) following DSB induction via I-SceI enzyme. Cellular expression of I-*Sce*I following transient transfection with pI-SceI-3xNLS leads to a site-specific DSB, which is then repaired by HRR using the downstream wild-type GFP sequence as a template, thus resulting in GFP+ cells. Obtained and purified pISce-I plasmid following transfection shows substantial yield of induced GFP^+ cells (~10%) suggesting functional I-SceI expression plasmid. Finally, clonogenic survival assay was performed after expression of I-SceI in one of the corresponding clones namely CHO-4xR.R12. Survival experiment shows significant killing in comparison to mock-transfected cells and thus re-validate the functionality of ISce-I expressing plasmid. All confirmatory experiments were performed in clonal cell line CHO-4xR.R12 as a proof of principle. These experiments confirmed and validated the functionality of the pI-SceI using our established lab protocol and thus were used for subsequent experiments.

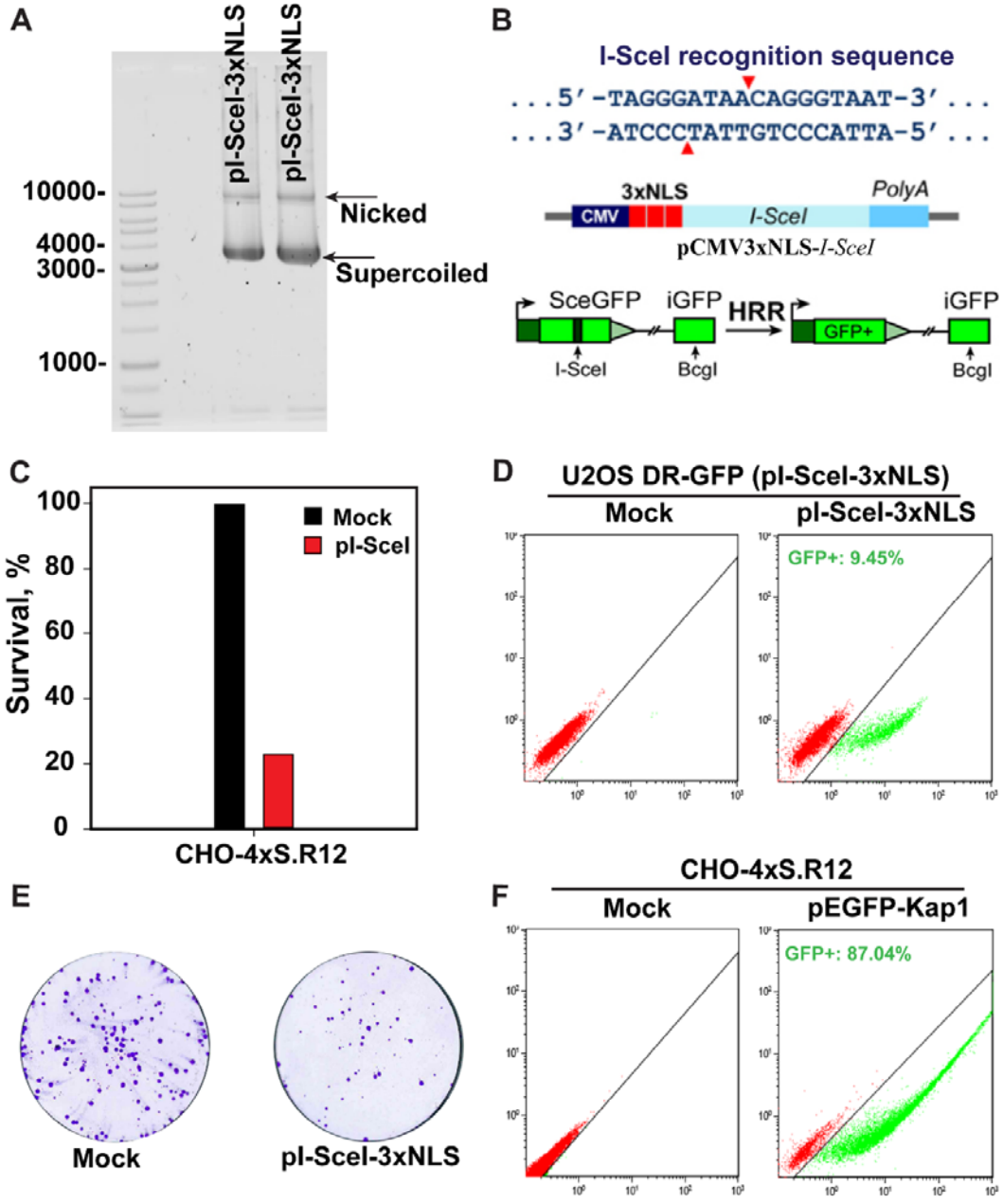

Figure 53 A multi-layered screening workflow for functional pI-SceI-3xNLS plasmid. (A) Gel electrophoresis of pI-SceI-3xNLS resolved in 2% gel showing the expected supercoiled form plasmid DNA (indicated black arrow-bottom) **(B)** Background information about the expression vector I-SceI plasmid **(Top):** Recognition sequence of I-SceI endonuclease is indicated by arrows that results in generation of double strand break and yields a 4-bp 3′ extension, **(Middle):** Domain structure of pCMV3xnls-I-SceI expression vector used in our experimental set-up. NLS stands for nuclear localization signal which ensures the nuclear localization of the expressed enzyme. **(Bottom):** Schematic diagram represents the DR-GFP vector developed to analyze the repair of I-SceI induced DSB by HRR specifically and the experiment was conducted in U2OS-DR-GFP. Schematic has been adapted from (Mladenova et al. 2016). **(C)** Quantification of clonogenic survival following transfection of CHO clonal cell line (CHO-4xS.R12) with purified and optimized I-SceI expression plasmid.

Percentage of survival was calculated using platting efficiency of mock-transfected cells of corresponding clone. **(D)** Flow cytometer analysis in U2OS cells harboring DSB repair reporter substrate (DR-GFP, a reporter of gene conversion-GC events) following transient transfection of purified I-SceI plasmid shows GFP^+ cells (~10%). **(E)** Representative dishes stained with crystal violet from clonogenic survival experiment as in figure (C) One of the clonal cell lines, CHO-4xS.R12, was used as an exemplary for optimization experiments. **(F)** Representative histogram performed by flow cytometer indicates the transfection efficiency measured 24 h after transfection and GFP expressing plasmid, pEGFP was used to measure the transfection efficiency.

2.4 Optimization of knockdown with siRNAs specific for RNF8 and RNF168

2.4.1 RNA interference (RNAi) of RNF8 and RNF168 in parental hamster cells (CHO10B4), after exposure to X-rays

Gene silencing of RNF8 and RNF168 was performed using newly designed RNF8 and RNF168 specific siRNAs respectively. Until now, no specific antibodies raised against RNF8/168 of Chinese hamster origin are available. Therefore, the efficiency of RNF8 and RNF168 knockdown was confirmed by immunostaining of endogenous 53BP1 protein. In control si-RNA treated cells, exposure of cells to IR led to accumulation of 53BP1 in the form of IRIF (ionizing radiation induced 53BP1 foci) at damaged chromatin. In contrast, RNA interference (RNAi) of RNF8 and RNF168 either individually or combined abrogated 53BP1 foci formation at 24 h and 48 h following irradiation at 1 Gy in CHO10B4 cells (Figure 54).

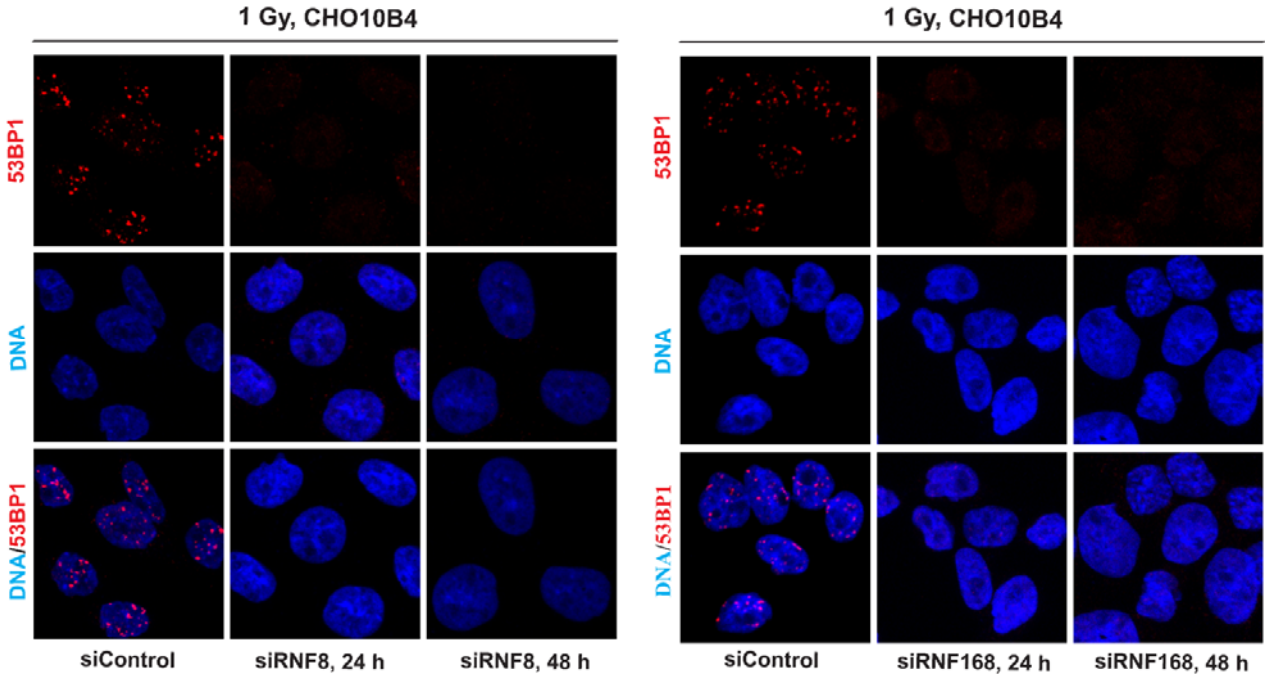

Figure 54 RNF8 and RNF168 knockdown abrogates 53BP1 recruitment to DSB sites. Representative immunofluorescence images showing inhibited 53BP1 foci (red) at the indicated times (24 and 48 h) following

RNAi interference of RNF8 (left panel) and RNF168 (right panel) whereas corresponding siControl transfected cells show accumulation of 53BP1 foci. DNA is counter stained with DAPI. Cells were subjected to 1 Gy of IR and processes for immunofluorescence analysis 1 h later. DNA is counterstained with DAPI.

In an effort to obviate the multiple transfection steps, we extended our approach to the level where we checked the siRNA mediated inactivation efficiency of RNF8/RNF168 at 6 h post-transfection window. We reasoned this for the following rationales:

1. Foci kinetics experiments of γ-H2AX and 53BP1 require the analysis of foci formation at 8 h after transient expression of I-SceI according to our previous published paper and to our follow-up studies (Iliakis et al. 2018; Schipler et al. 2016).
2. Typical siRNA experiments follow a double-transfection protocol where siRNAs are delivered into cells with an initial transfection, which is then followed by a second transient transfection with I-SceI expression plasmid to generate DSBs in absence of targeted protein. Many research groups including us observed that such serial transfection mediates stress and toxicity to the cells and is often associated with variable experimental results (Bennardo et al. 2008; Bindra et al. 2013).

Checking the knockdown efficiency at 8 h of siRNF8/168 based on these above-mentioned two important points was therefore warranted. In this optimization experiment, we evaluated the efficiency of siRNF8 and siRNF168 at different time windows stretching from 6 h till 30 h after siRNA-based transfection. We noticed 53BP1 foci exhaustion upon RNF8/168 down regulation at already at 6 h (figure 55). Considering the toxicity and stress that transfections pose to cells, we followed a single-transfection protocol to deliver simultaneously into cells of both siRNAs and DSB-inducing I-SceI expression plasmid.

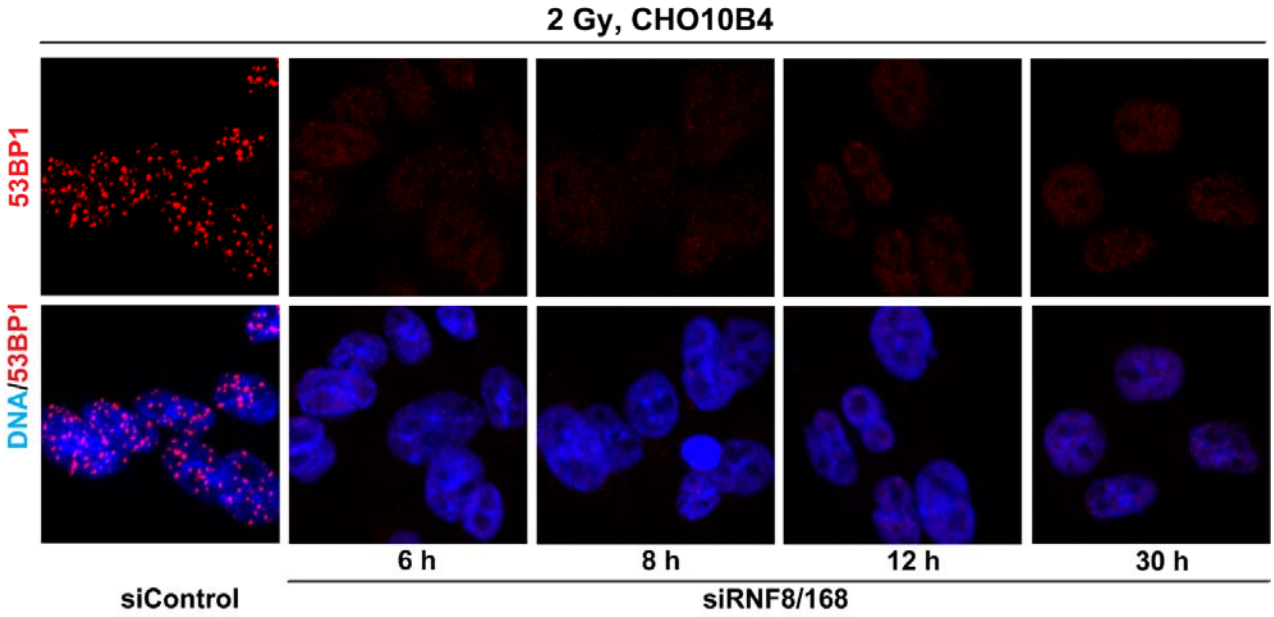

Figure 55 Depletion of RNF8/168 show abrogated formation of 53BP1 foci at 6 h window after transfection with siRNA against RNF8/168.

2.4.2 SiRNA-mediated ablation of RNF8 and RNF168 in CHO derivative clonal cells following expression of I-SceI plasmid

To test in I-SceI transfected clonal cells of the effect of RNF8 and RNF168 knockdown, we similarly studied the effects of siRNA depletion by immunofluorescence analysis of 53BP1 foci formation after transient expression of I-SceI. As outlined above, we followed here optimized single-transfection method to deliver both siRNAs specific to RNF8/168 and I-SceI plasmid into the cells simultaneously. As anticipated, the accumulation of 53BP1 was completely abrogated at 8 h and 24 h by knocking down endogenous RNF8 and RNF168 suggesting RNF8/RNF168 depletion hinders 53BP1 accrual at I-SceI inflicted DSBs on damaged chromatin. This is consistent with the finding from previous experiment performed in the context of IR confirming that siRNA mediated knockdown of RNF8 and RNF168 abrogate 53BPP1 accretion at I-SceI generated DSBs (figure 54 and 55). Figure 56 and supplementary figure 1 show representative images obtained from IF analysis at the time points analyzed for both clonal cell lines. Of note, no change in cell cycle progression was observed after combined transfection of siRNAs and plasmid. Together these results suggest irrespective of IR or I-SceI generated DSBs, siRNA knockdown of RNF8 and RNF168 abrogates the accretion of 53BP1 foci to the damaged DSBs and the types of DSB ends whether chemically modified (IR-generated) and non-modified (I-SceI generated) initiate similar 53BP1 signaling.

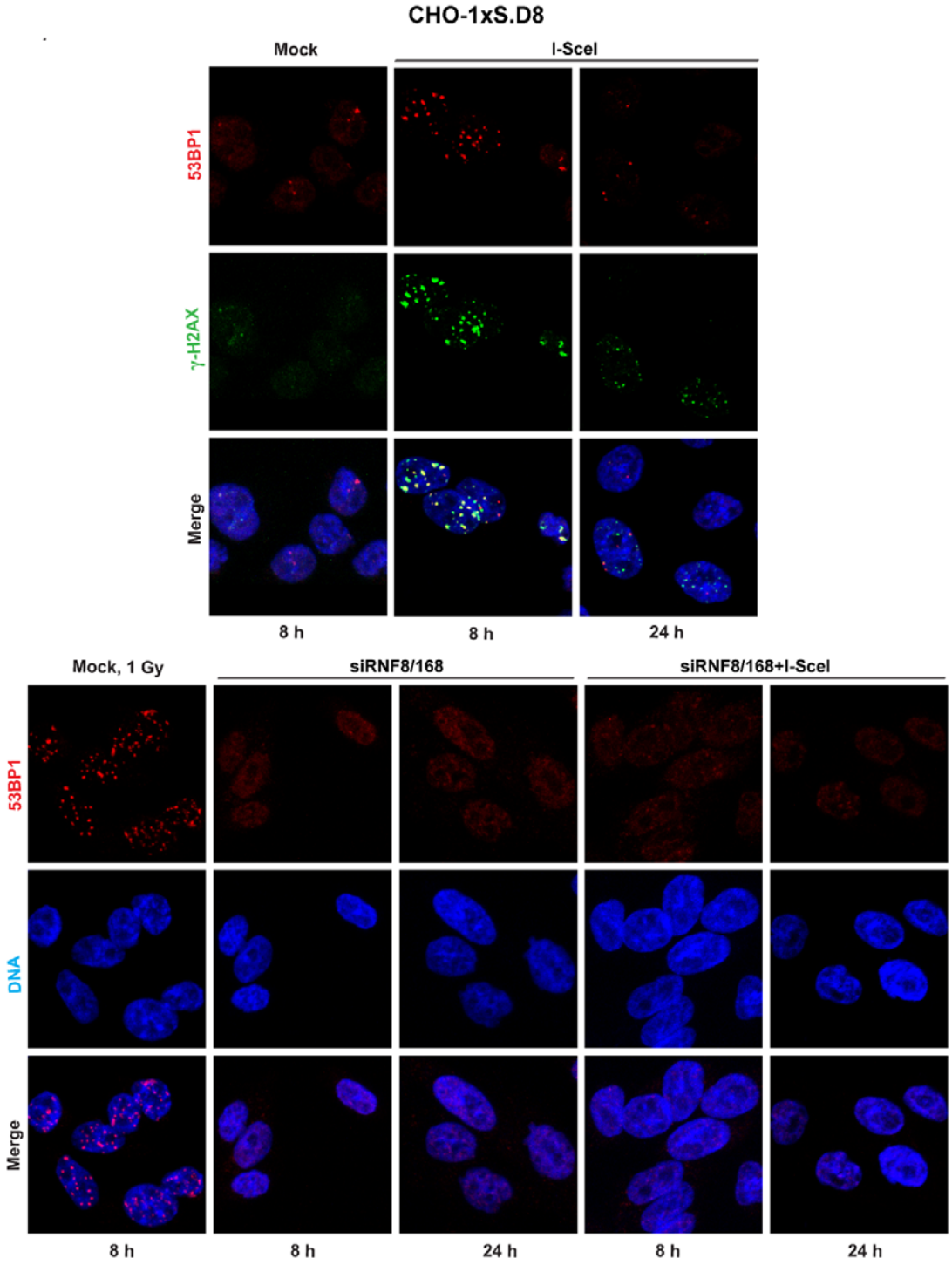

Figure 56 Depletion of RNF8/168 abrogates 53BP1 recruitment to the sites of DSBs generated by I-SceI. Representative images obtained with confocal fluorescence microscope show γ-H2AX (green) and 53BP1 foci (red) in simple DSB clone harboring a single I-SceI recognition site (CHO-1xS.D8) transfected with plasmid expressing I-SceI (pI-SceI-3xNLS). In contrast, 53BP1 foci formation was inhibited in I-SceI transfected as well as in corresponding irradiated cells (1 Gy) upon RNF8/168 knockdown. Corresponding mock-transfected cells instead show IR induced 53BP1 foci retention following their exposure to 1 Gy of irradiation.

2.5 RNF8/RNF168 depleted CHO cells respond distinctly to different radiation modalities

In an attempt to examine the RNF8/168 knockdown effect on cell survival, we performed colony survival assay in CHO cells after efficiently silencing corresponding genes using siRNAs. Cells depleted in RNF8/168 were exposed to different doses of X-ray irradiation. As shown in figure 57-A, compared to their counterparts, down-regulation of RNF8/168 sensitized the cells towards X-ray. This is consistent with previous reports that RNFs are involved in DDR.

Since E3 ligases RNF8 and RNF168 function through c-NHEJ signaling cascade, we investigated whether down regulation of these two components will, if any, show the observed c-NHEJ compromised phenotype. To this end, we induced DNA damage ranging from low complexity using X-rays to high complexity using α-particles. Indeed, clonogenic survival experiments shown in figure 57-A, indicate that compared to control siRNA transfected cells, RNF8/168-depleted cells were killed more efficiently after exposure to low-LET, whereas an opposite scenario was noted when cells were exposed to high-LET, α-particles (compare the red line in figure 57-A). Together these experimental findings indicate that RNF8/168 depletion in cells renders sensitization towards low-LET but not towards complex lesions induced by high-LET irradiation.

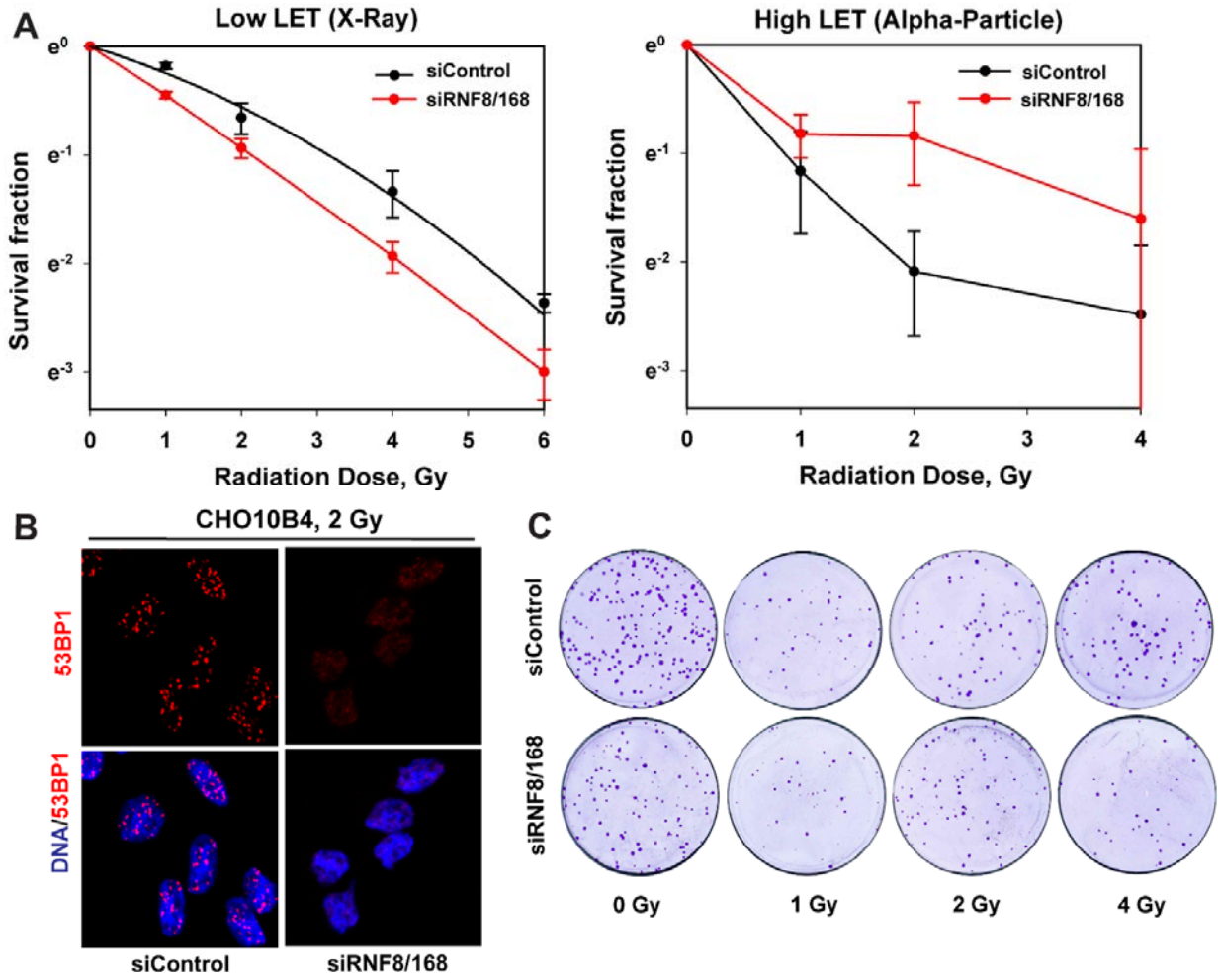

Figure 57 RNF8/168 depletion promotes resistance to high modality radiation (high-LET) in CHO cells. (A) Left panel: Colony survival assay as a function of radiation dose after exposure of CHO cells to low-LET (X-Ray) or high-LET (α-particle) upon siRNF8/168 knockdown. **(B)** IF images show the absence of 53BP1 foci confirming efficient knockdown of RNF8/168 compared to corresponding siControl transfected cells (53BP1 foci in red color) irradiated with 2 Gy of X-ray. **(C)** Representative cell culture dishes showing the colonies formed after 8 days of platting in cells irradiated with high-LET. Twenty-four hours after transfection with indicated siRNAs, cells were immediately platted for survival. Results show the mean and standard deviation from at least two (high-LET) and/or three (low-LET) independent experiments.

2.6 Investigation in simple and complex DSBs clusters of additional IR effects following RNF8 and RNF168 depletion

2.6.1 Survival studies of CHO clones harboring simple-and clustered-DSBs after I-SceI expression and IR

Results based on established clonal cell lines from our lab successfully showed that the number of breaks is associated with the corresponding number of integrated recognition sites

for the rare-cutting endonuclease I-SceI (Schipler et al. 2016). We inquired whether the sustained I-SceI-generated DSBs would increase the DSB loads of the clonal cells following their exposure to IR. To this end, we transiently transfected the clones harboring simple and complex forms of DSBs with a plasmid expressing I-SceI. After 24 h of transfection, cells were exposed to different doses of IR (0, 2, 4 and 6 Gy) and were immediately platted. The results summarized in figure 58 indicate that I-SceI-induced DSBs, in addition to IR-mediated damages (DSBs, SSBs and base damages), do not have additional sensitizing effects on the survival of clonal cells harboring either simple DSBs or clustered DSBs.

Both cells (simple DSBs; 1x and DSB cluster; 4xR) show apparently no change in their survival efficiency following exposure to both IR and I-SceI. However, a modest sensitization in their survival both in simple (CHO-1xD) and complex (CHO-4xR) DSBs following expression of I-SceI can be attributed to their corresponding I-SceI mediated additional killing. However, between the two clones no significant difference in cell killing was noted following transfection either with or not I-SceI. Collectively these results suggest that DSBs induced by restriction enzyme, do not add extra DSB loads to the cells.

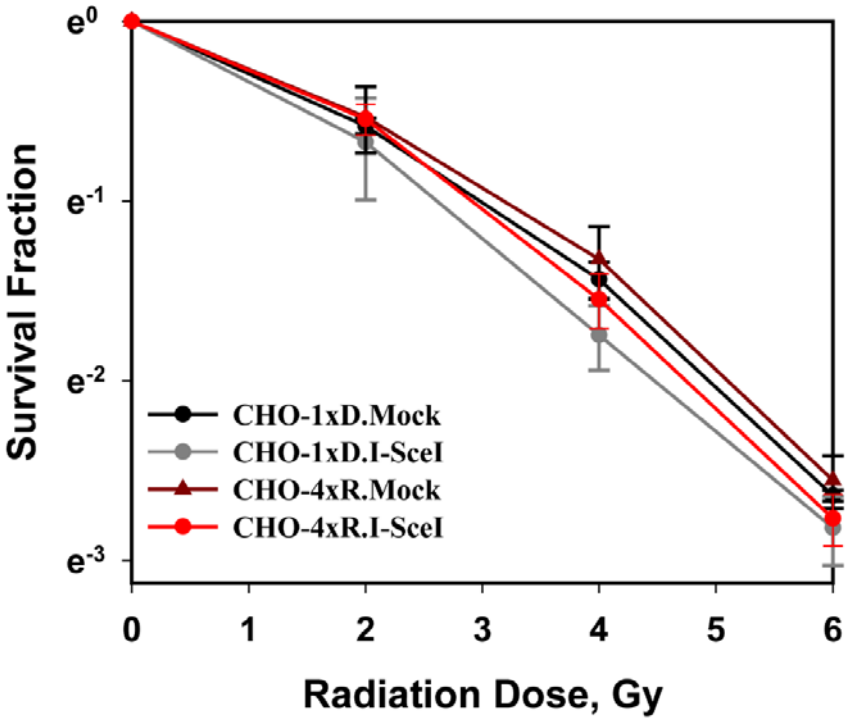

Figure 58 Clonogenic survival of two clonal cell lines harboring simple DSBs (CHO-1xD) and complex DSBs (CHO-4xR). Asynchronously growing cells (around 80% confluent) were transfected with I-SceI expressing plasmid and 24 h post transfection, irradiated cells with different doses (0-6 Gy) were platted in

appropriate numbers for survival. Shown results represent means and standard deviation (SD) from two independent experiments.

2.6.2 Survival studies of CHO clones harboring simple-and clustered-DSBs after I-SceI expression and IR in conditions of depleted RNF8 and/or RNF168 activity

Since our focus is to investigate the mechanistic underpinning of differential RNF8 and RNF168 mediated ubiquitin signaling between simple and complex types of DSBs. We thus extended our experimental approach by looking at whether DSBs induced by I-SceI expression, as measured previously, will affect the cellular survival of these clones with corresponding RNF8/168 knockdown and irradiation exposure. To test the effect of RNF8/168 depletion to the combined DSB-loads created by both ionizing radiation and I-SceI expression, we co-transfected the cells with I-SceI expression plasmid and RNF8/168 specific siRNAs. Twenty-four hour after transfection, cells were exposed to different doses of IR (0-6 Gy) before immediate platting for survival assay.

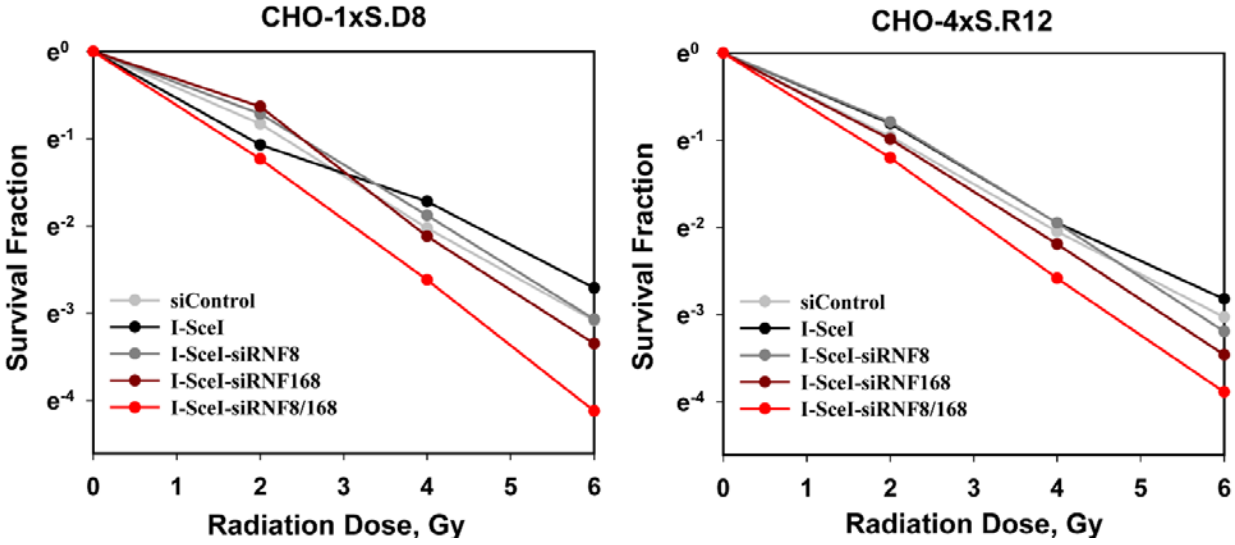

Figure 59 Clonogenic survival assays between two distinct cell lines, simple DSBs (CHO-1xS.D8) and complex DSBs (CHO-4xS.R12). Exponentially growing cells were co-transfected with I-SceI expression plasmids and siRNAs against RNF8/168. Twenty four hours after transfection, cells were irradiated with different doses of IR and seeded again in appropriate numbers following trypsinization and allowed to form colonies for 8 days. The results are from one experiment.

Results presented in Figure 59 show that, both simple and complex DSBs harboring cells responded as expected upon I-SceI expression and gene-specific silencing of RNF8/168. Despite the marked sensitization caused only by combined depletion of RNF8/168 as shown in figure 57-A (left panel), there is no marked additional effects of I-SceI mediated DSB in

both clonal cells following I-SceI expression and/or RNF8/168 depletion combined or separately (figure 59). These data presented here indicate that DSBs generated at integrated I-SceI recognition sites do elicit additional detrimental cellular effects in already irradiated cells and thereby total DSB-load is unaffected.

2.7 Investigation in CHO clones of DSB signaling initiation at conditions where the activity of RNF8 and RNF168 is depleted

2.7.1 RNF8 or RNF168 depletion does not affect the normal level of γ-H2AX foci formation in irradiated CHO cells

Upon induction of damage, γ-H2AX recruits critical downstream DNA damage response factors including 53BP1 and BRCA1 that fine-tune the balance between c-NHEJ and HRR. A process called ubiquitination whereby two-ubiquitin ligases RNF8 and RNF168 regulate their recruitment to the DNA damage sites. We tested therefore if abrogated 53BP1 foci formation upon RNF8/168 down regulation would affect γ-H2AX focus formation. Immunofluorescence images shown in figure 60 and supplementary figure 2 indicate focus formation by the DDR protein γ-H2AX following IR in control-siRNA transfected as well as in siRNF8/168 transfected cells.

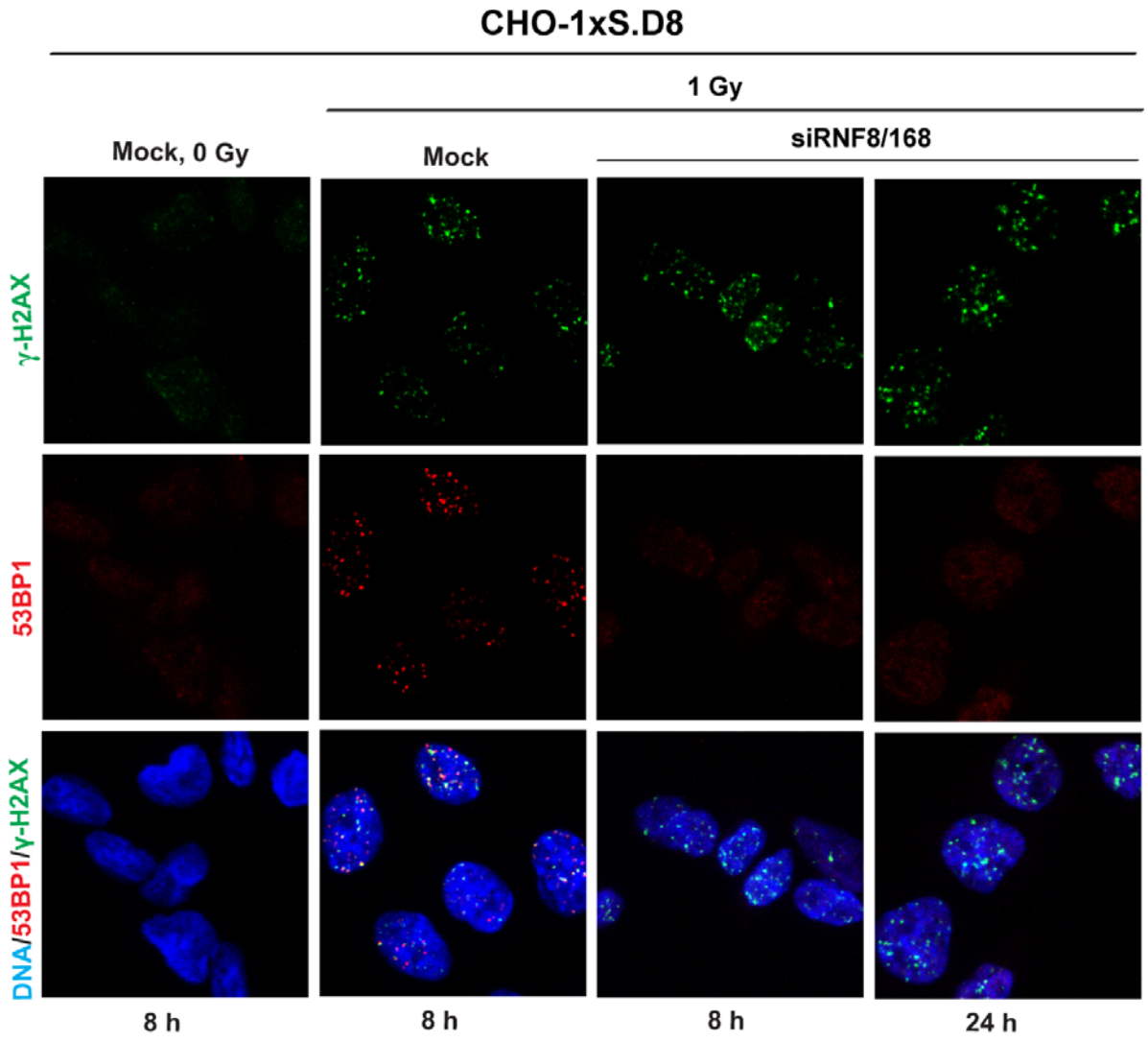

Figure 60 Knockdown of E3 ligases RNF8 and RNF168 does not affect the IR- induced γ-H2AX foci formation at DSB sites. Representative γ-H2AX foci (green) and 53BP1 foci (red) formation at indicated times (8 and 24 h) in cells harboring DSBs of simple type (CHO-1xS.D8). RNF8/168 specific siRNAs abrogated the retention of IRIFs (ionizing radiation induced foci) at damaged chromatin. Twenty-four after transfection with siRNF8/168, cells were irradiated with 1 Gy of dose and were fixed after one hour before staining with indicated antibodies. DNA was counterstained with DAPI (blue).

The level of γ-H2AX foci formation at 8 and 24 h in control siRNA transfected cells (both clonal cells) is similar to the level observed in siRNF8/168 depleted cells (figure 61-A and B). We also compared how cellular response after irradiation between the clones is regulated in terms of 53BP1 foci formation. Results show no variation in 53BP1 foci number between clones harboring simple-or complex-DSBs.

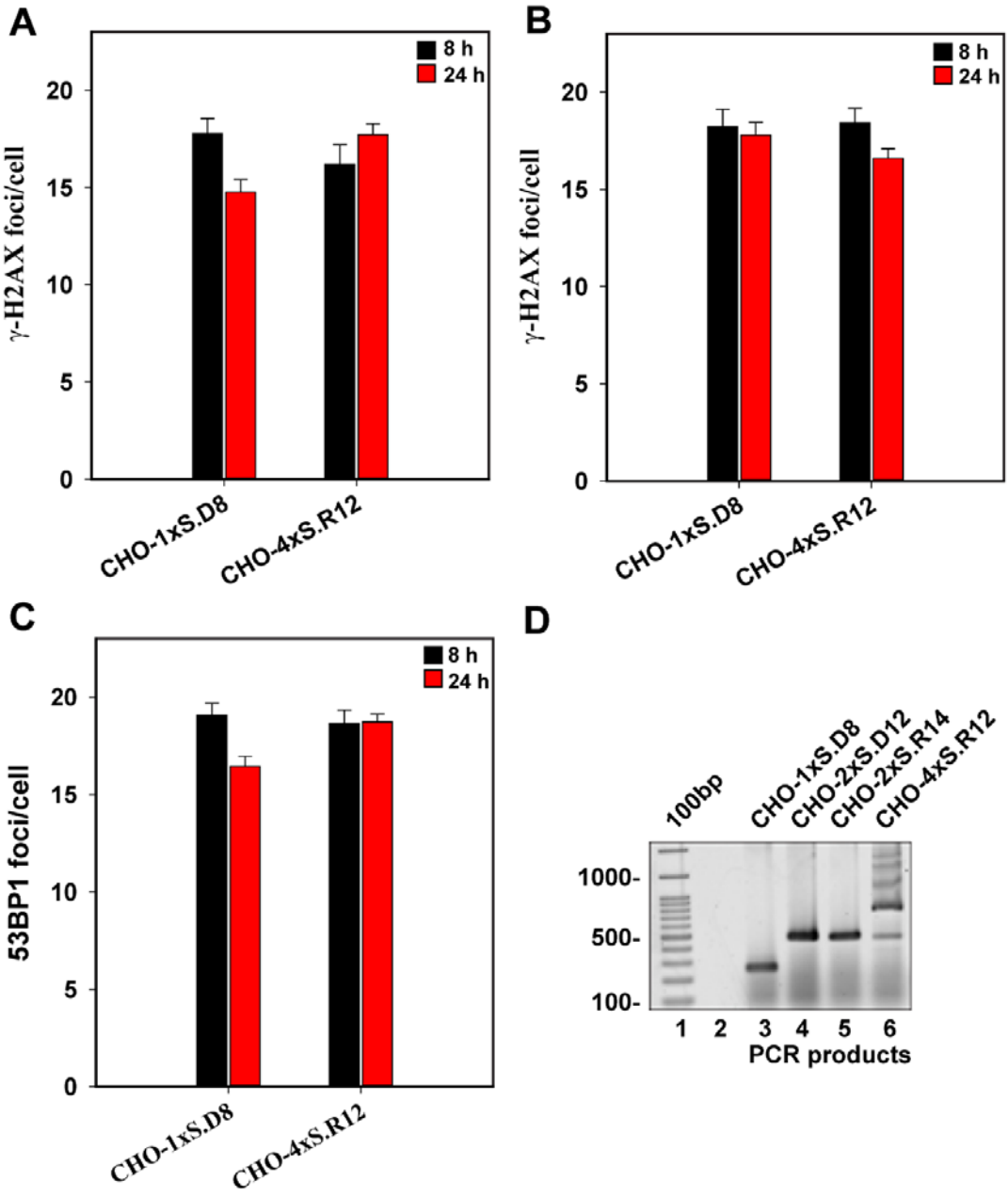

Figure 61 IR-induced γ-H2AX foci formation is unaffected by siRNF8/168 knockdown in both clonal cell lines (simple clone: CHO1xS.D8 and complex-DSB: CHO-4xS.R12). (A) Quantitative analysis showing γ-H2AX foci number per cell in cells after IR with 1 Gy. **(B)** γ-H2AX foci formation same as in **(A)** but after RNAi interference of RNF8/168. **(C)** Quantitative analysis of 53BP1 foci formation in control siRNA transfected clones. **(D)** PCR-Genotyping based validation of retained I-SceI recognition sites during propagation in the experimental clonal cell lines as described in detail in figure 1. Foci number scored in irradiated and siRNA transfected cells is background subtracted.

2.7.2 RNF8 or RNF168 depletion does not affect γ -H2AX foci formation after generation of simple DSBs or DSB clusters in cells expressing I-SceI

Next we measured how the magnitude of γ-H2AX assembly at the I-SceI generated DSB sites is regulated in absence of 53BP1 and its two immediate upstream regulators RNF8/168. To analyze γ-H2AX foci formation after the induction of single-DSBs and DSB-clusters, we co-transfected the I-SceI expression plasmid and siRNAs specific to siRNF8/168. Foci scoring of γ-H2AX in both clones shown in Figure 63 (A and B) indicates that absence of RNF8/168 and 53BP1 does not negatively regulate the localization of γ-H2AX to damaged chromatin and showed the similar level of damage induction relative to their corresponding control-siRNA transfected cells. This observation further strengthens the previous observation where siRNA-directed ablation of RNF8/168 leads to a similar initial DSB signaling measured by γ-H2AX foci formation following IR exposure (figure 61-B). Moreover, siRNA mediated knockdown of RNF8/168 showed a complete abrogation of 53BP1 foci at DSB sites (figure 62 and supplementary figure 3). It is notable to mention that the signaling intensity of 53BP1 foci at later times in cells sustaining clustered-DSBs than in simple-DSBs harboring clones (figure 63-C). A similar observation was first noted in our previous study demonstrating a sustained retention of 53BP1 within the DSB-clustered-flanking chromatin (Schipler et al. 2016).

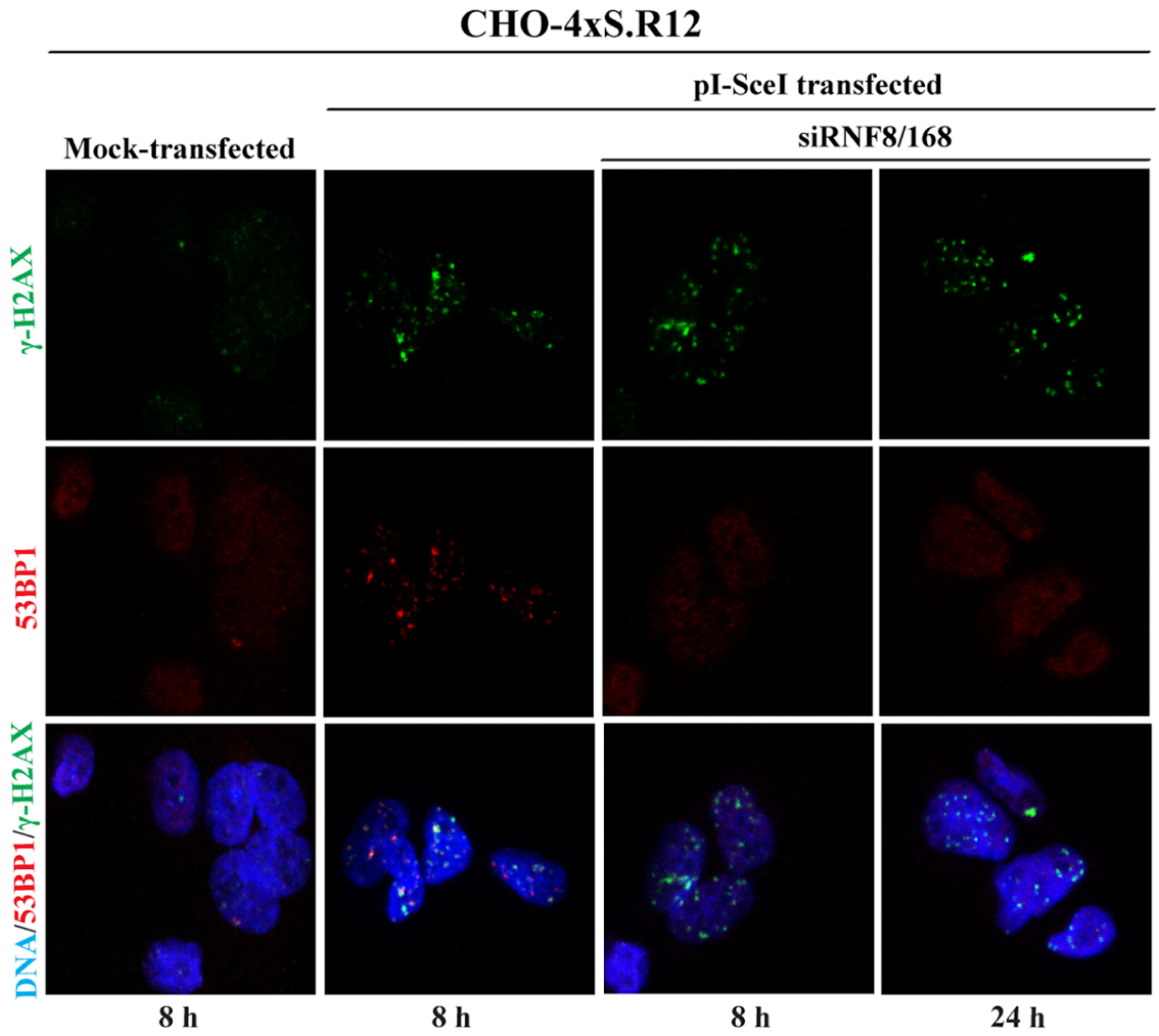

Figure 62 Depletion of RNF8 and RNF168 does not affect I-SceI generated γ-H2AX foci formation at damaged chromatin. IF shows images of γ-H2AX (green) and 53BP1 (red) foci formation at indicated times (8 and 24 h) in CHO clones harboring clustered DSBs (CHO-4xS.R12). Cells co-transfected with siRNF8/168 and pI-SceI were fixed at indicated times (8 and 24 h) and were processed for immunofluorescence with indicated antibodies. DNA was counterstained with DAPI (blue).

These data together with the results discussed above collectively suggest that down regulation of RNF8/168 and their downstream factor, 53BP1 do not impair the preceding formation of γ-H2AX foci at DSB surrounding chromatin.

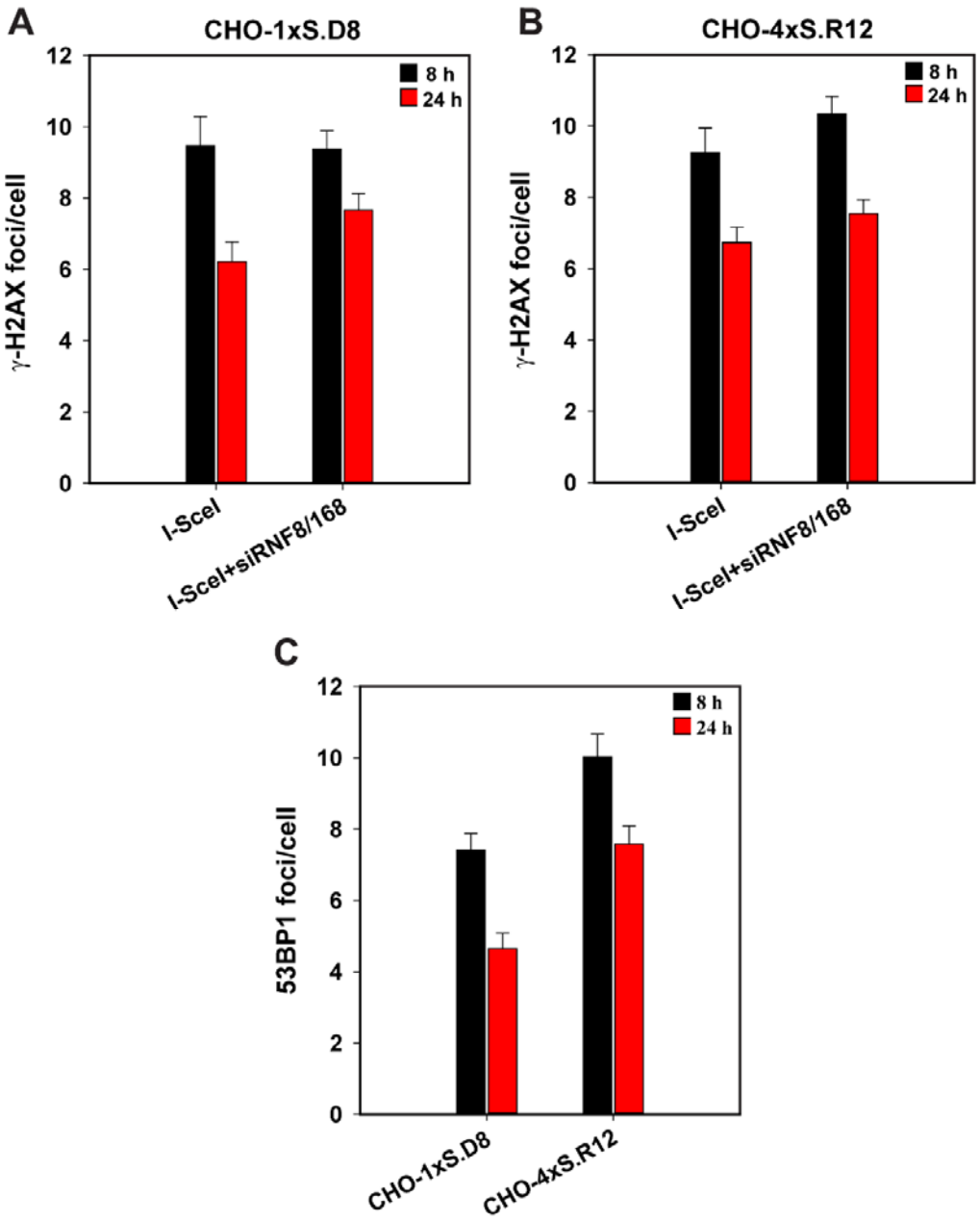

Figure 63 I-SceI generated γ-H2AX foci formation is unaffected by siRNA specific depletion of RNF8/168 in clones (A) Quantitative analysis showing γ-H2AX foci formation in clones sustaining simple-DSBs transfected either with I-SceI expressing plasmid (single) and/or pI-SceI+siRNF8/168 (combined) at analyzed times (8 and 24 h). **(B)** γ-H2AX foci formation same as in **(A)** but for clones harboring complex-DSBs. **(C)** Quantitative analysis of 53BP1 foci formation in both I-SceI transfected clones. The number of foci scored in I-*Sce*I transfected clonal cells is background subtracted.

2.8 DSB end processing of a simple DSB is dependent on c-NHEJ pathway

2.8.1 Ablation of RNF8 and/or RNF168 sensitizes CHO clones to I-SceI-mediated formation of simple DSBs and DSB clusters

Unlike IR, the I-SceI-based model system precludes the contribution of other forms of DNA damage such as SSBs and/or base damages thus making it an excellent system for studying the adverse biological effects of DNA double strand breaks (DSBs) alone. Consistent with this, earlier results utilizing such biological rodent system from our lab demonstrated for the first time that clustered DSBs – a physical characteristic of high-LET radiation modality – indeed have higher propensity for adverse biological consequences compared to simple DSBs (Iliakis et al. 2018; Schipler et al. 2016). Another interesting finding from this study is that simple-DSBs rely on classical non-homologous end joining (c-NHEJ) for their repair, while DSBs with increasing complexity show functional dependence on alt-EJ. Moreover, live-cell imaging experiment indicates that with increasing complexity there is more retention of 53BP1 to the DSBs in such that DSB clusters has heightened 53BP1 signaling due to the delayed dynamics in repair compared to the simple DSBs. We reasoned that cells sustaining clustered lesions display pertinent downstream signaling, compared to simple-DSBs, which are easily ligatable and do not require prolonged damage signaling. In order to gain further insight into the repair mechanism involved in DSBs of simple and complex types, and also the their comparative biological consequences, we looked at the contribution of two downstream repair factors, RNF8 and RNF168. Towards this, we performed clonogenic survival assays following expression of I-SceI with a concomitant knockdown of RNF8 and RNF168 in clones containing simple-DSBs and clustered-DSBs. Figure 64-C shows representative colony formation for both clonal cell lines (CHO-1xS.D8;simple-DSBs and CHO-4xS.R12;complex DSBs) when platted immediately after co-transfection with I-SceI expressing plasmid and/or RNF8/168 targeting siRNAs. Transient expression of I-SceI following transfection with I-SceI expression plasmid results in generation of corresponding DSB-clusters. Summarized in figure 64 shows the obtained results from clonogenic survival experiment. In line with previous observations, cells harboring I-SceI-quadruplets caused increased killing compared to cells with single-DSBs (Schipler et al. 2016). Notably, both clones displayed increase cytotoxicity in absence of RNF8 and that was exacerbated further by down regulation of RNF168. Strikingly, a significant increase in cell killing became evident by co-depletion of RNF8/168, suggesting that absence of these factors in cells sustaining DNA lesions caused more lethal events. These results in aggregate demonstrate that

irrespective of types of lesions, both simple-DSBs and DSB-clusters exhibited comparable sensitivity towards I-SceI induced DSBs in absence of two ubiquitin ligases, RNF8 and RNF168.

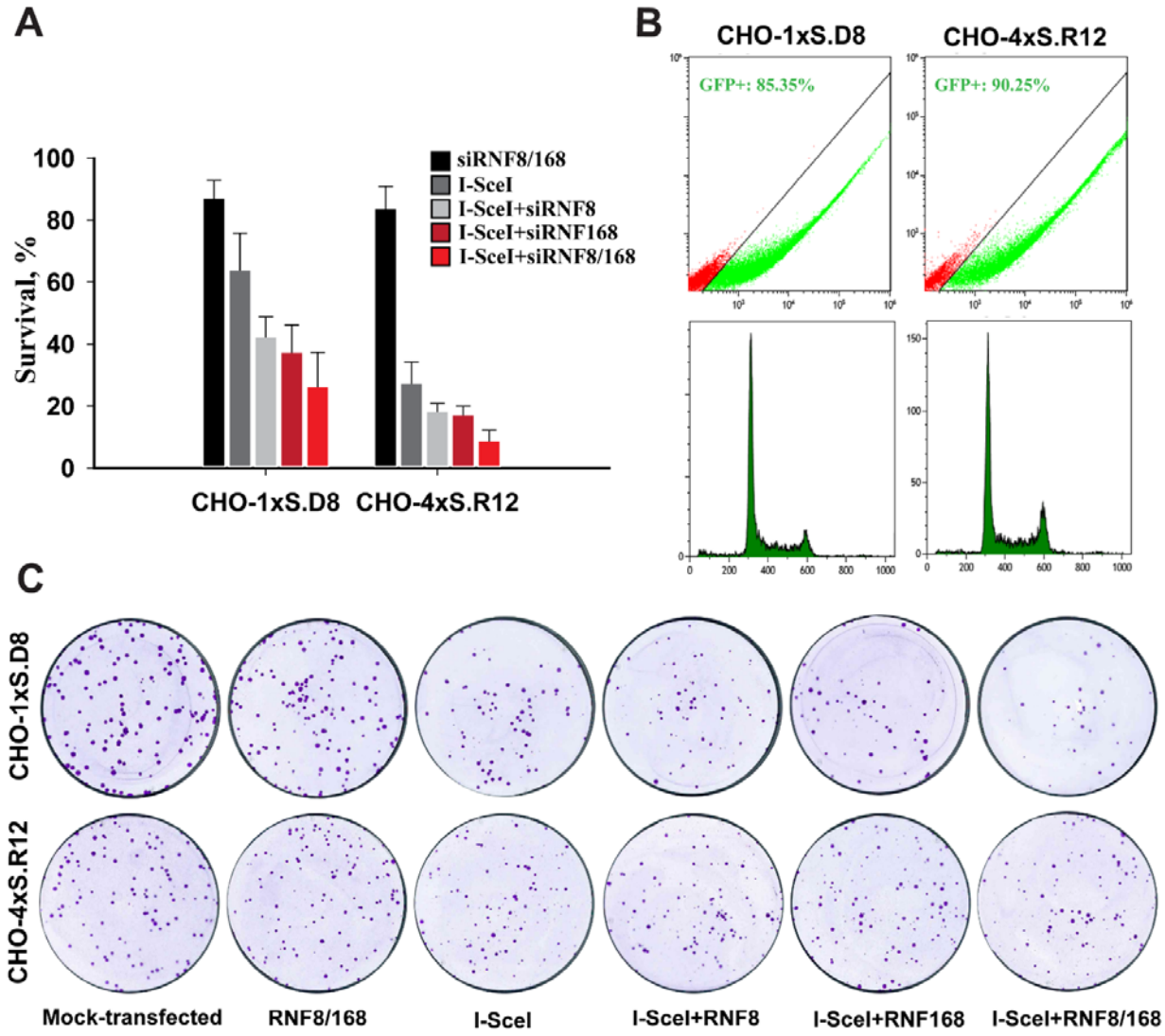

Figure 64 Clonogenic survival assay following depletion of RNF8 and RNF168. (A) Surviving fraction of CHO clones (simple DSBs and DSB clusters) following transfection or not with I-SceI expression plasmid and indicated siRNAs (separate and/or combined). **(B)** Representative histogram shows the transfection efficiency (GFP+ cells) measured after 24 h using GFP expressing plasmid, pEGFP-53BP1 (upper panel). PI staining after 24 h transfection was performed for DNA content analysis to check the cell cycle distribution in experimental clones (lower panel). **(C)** Examples of cell culture dishes stained with crystal violet 8 days after transfection with plasmid I-SceI (pI-SceI-3xNLS) and almost five times more cells were platted for CHO-4xS.R12 clone. Results show the mean and standard deviation (SD) from four independent experiments.

2.8.2 RNF8 and/or RNF168 depletion results in formation of excessive number of translocations in CHO clones harboring I-SceI constructs for simple DSB formation

IR-induced cell killing is linked with the chromosomal aberration formations, an ensuing event following mis-repair of damaged DNA. The extent of cell killing caused by siRNA targeting of RNF8/168 in aforementioned clones led us to investigate further the DSB-processing within DSB-clusters by utilizing cytogenetic approaches. To this end, we analyzed chromosomal translocation formation at metaphase in the above-mentioned clones upon expression of I-SceI and/or corresponding depletion of RNF8/168 separately or combined. Figure 66 shows some representative metaphase spreads obtained from these clones. In case of complex-DSBs, I-SceI-induced DSBs caused more formation of chromosomal translocations compared to single-DSBs and is consistent with previous findings (Iliakis et al. 2018; Schipler et al. 2016). To determine if depletion of RNF8 and RNF168 has additional detrimental effects in the genomic rearrangements, we depleted both factors either individually or combined and assessed translocation formation. Co-depletion of RNF8/168 resulted in 1.8 fold increase in chromosomal translocations in cells that harbor single-DSBs compared to I-SceI alone. In parallel, silencing of RNF8 following expression of I-SceI displayed little increase in chromosome translocation formation although not as much as in the event of RNF168 ablation. Under the same conditions, we also scored chromosomal translocation in clones harboring DSB-clusters (CHO-4xS.R12) and results showed no apparent increase in their formation. We conclude from these experiments that cells harboring simple DSBs rely more on c-NHEJ. Furthermore depletion in simple-DSBs of histone ubiquitin E3 ligases prevents DSB-associated ubiquitination that resulted in less engagement of c-NHEJ pathway and more translocation formation compared to clustered-DSBs.

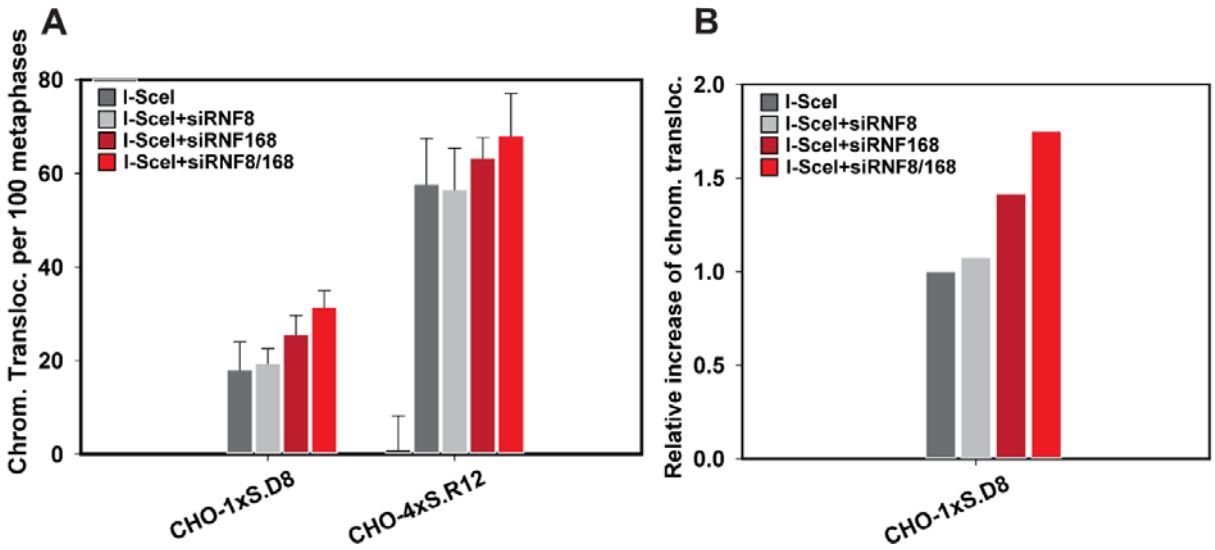

Figure 65 Chromosomal translocations following depletion of RNF8 and RNF168 (**A**) Quantitative analysis of chromosomal translocation formation in both clones. Shown results are the mean and standard deviations from four independent experiments. Number of chromosomal translocations observed in mock-transfected cells were subtracted from I-SceI transfected cells. **(B)** Relative increase in the formation of translocations in simple-DSB harboring clone following expression of I-SceI and knockdown of RNF8 and RNF168 individually or combined. The level of chromosomal translocation in only I-SceI transfected cells was used as basis (1) for normalization. For PCR-Genotyping based validation to confirm the retained I-SceI recognition sites during propagation as well as in experiments in the clonal cell lines as described in detail in figure 1, see supplementary figure 3.

Of note, transfection of individual clonal cells with a GFP-expressing plasmid (pGFP-53BP1) served as a control for transfection efficiency measurement, where only experiments with transfection efficiencies higher than 80% were taken into consideration for the analysis (figure 64-B).

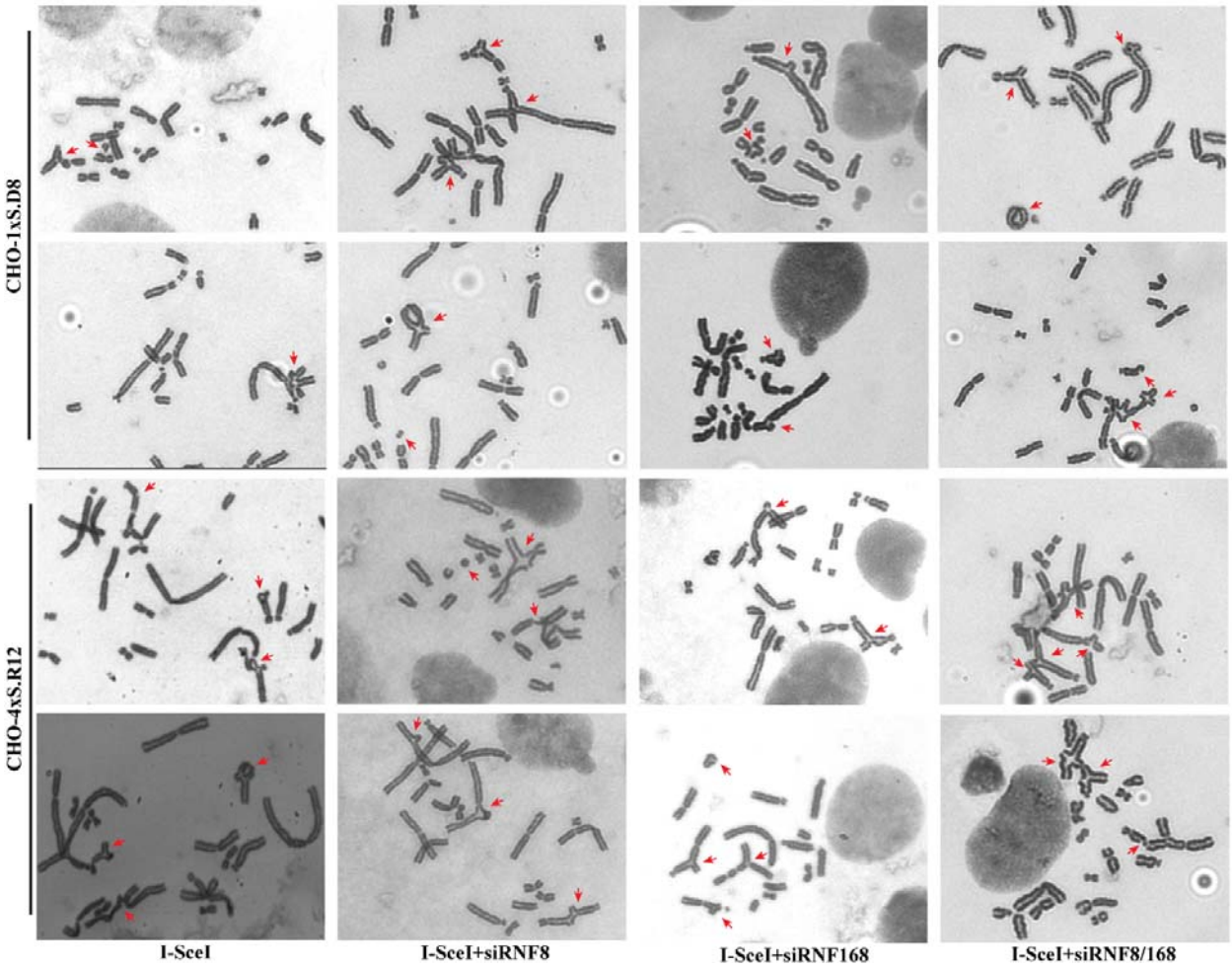

Figure 66 Representative images of metaphases in clones harboring simple (CHO-1xS.D8) and complex (CHO-4xS.R12) DSBs captured after transfection with I-SceI expressing plasmid alone or together with siRNA (individual or combined) directed against RNF8 and RNF168. Red arrows indicate chromosomal aberrations.

2.9 Investigation of physiological relevance of the accumulation of GFP-tagged 53BP1 foci at DSBs and formation of IR-induced DNA damage mediated repair foci

The recruitment of 53BP1 to the sites of DNA DSBs can be visualized either by immunostaining of fixed cells or by monitoring dynamic nuclear events in live cells that ectopically express GFP tagged-53BP1 fusion protein (GFP-53BP1). The expression construct coding for functional 53BP1 fused to green fluorescent protein (GFP) was previously described (Schipler et al. 2016). As mentioned earlier, from the live-cell imaging experiment we observed a heightened 53BP1 signaling in clonal cells harboring DSBs of complex type (Schipler et al. 2016). We therefore investigated our previous findings in a static measurement by employing indirect immunofluorescence method to re-examine the 53BP1 signaling in the form of IRIF in fixed cells. An important fact regarding live-cell imaging

experiments is that the formation of GFP-53BP1 foci is associated with the transient expression of the construct coding for exogenous GFP-53BP1. Therefore the dynamics of the recruitment of both endogenous 53BP1 as well as exogenous GFP-53BP1 foci will differ. Since the mediator protein 53BP1 accumulates in chromatin over a 1Mb of region, it is therefore necessary to investigate the dynamics of assembly of both forms of foci (endogenous and exogenous) to the DSBs and more importantly, to assess the functionality of GFP-bound 53BP1 in response to DNA damage in fixed cells. Thus a comparative and quantitative analysis of both endogenous and exogenous 53BP1 foci is warranted.

2.9.1 Investigation in human 53BP1 knock-out cell lines of physiological relevance of GFP-tagged 53BP1 foci formation

An ideal example of quantitative analysis of exogenous GFP-53BP1 foci corresponding to physiological endogenous 53BP1 protein is to observe the GFP-53BP1 foci formation in 53BP1 knock-out cell line. To explore the function of GFP-53BP1, we transiently expressed into 53BP1 knockout U2OS cells (hereafter D-U2OS) of the plasmid pGFP-53BP1 (target protein 53BP1 fused to GFP) and performed indirect immunofluorescence. Upon irradiation, ectopically expressed GFP-tagged 53BP1 exhibited recruitment to damaged chromatin in the form of GFP-53BP1 foci (figure 67-A). The localization of exogenous GFP-53BP1 to the distorted chromatin recapitulates the damage-induced behavior of endogenous 53BP1. As anticipated, a complete absence of endogenous 53BP1 foci formation evident by immunostaining of 53BP1 protein was observed in this cell line. Additionally, we observed nonspecific background staining of endogenous 53BP1 to the overall formation of GFP-53BP1 foci in D-U2OS cell line. Towards this, we compared the number of GFP-53BP1 foci formation between fixed cells stained or not with endogenous 53BP1 specific antibody. Quantitative analysis showed regardless of antibody (Ab) staining, a similar level of GFP-53BP1 foci formation (figure 67-B). It demonstrates that additional staining of endogenous 53BP1 in D-U2OS cell line does not affect the exogenous formation of GFP-53BP1 foci.

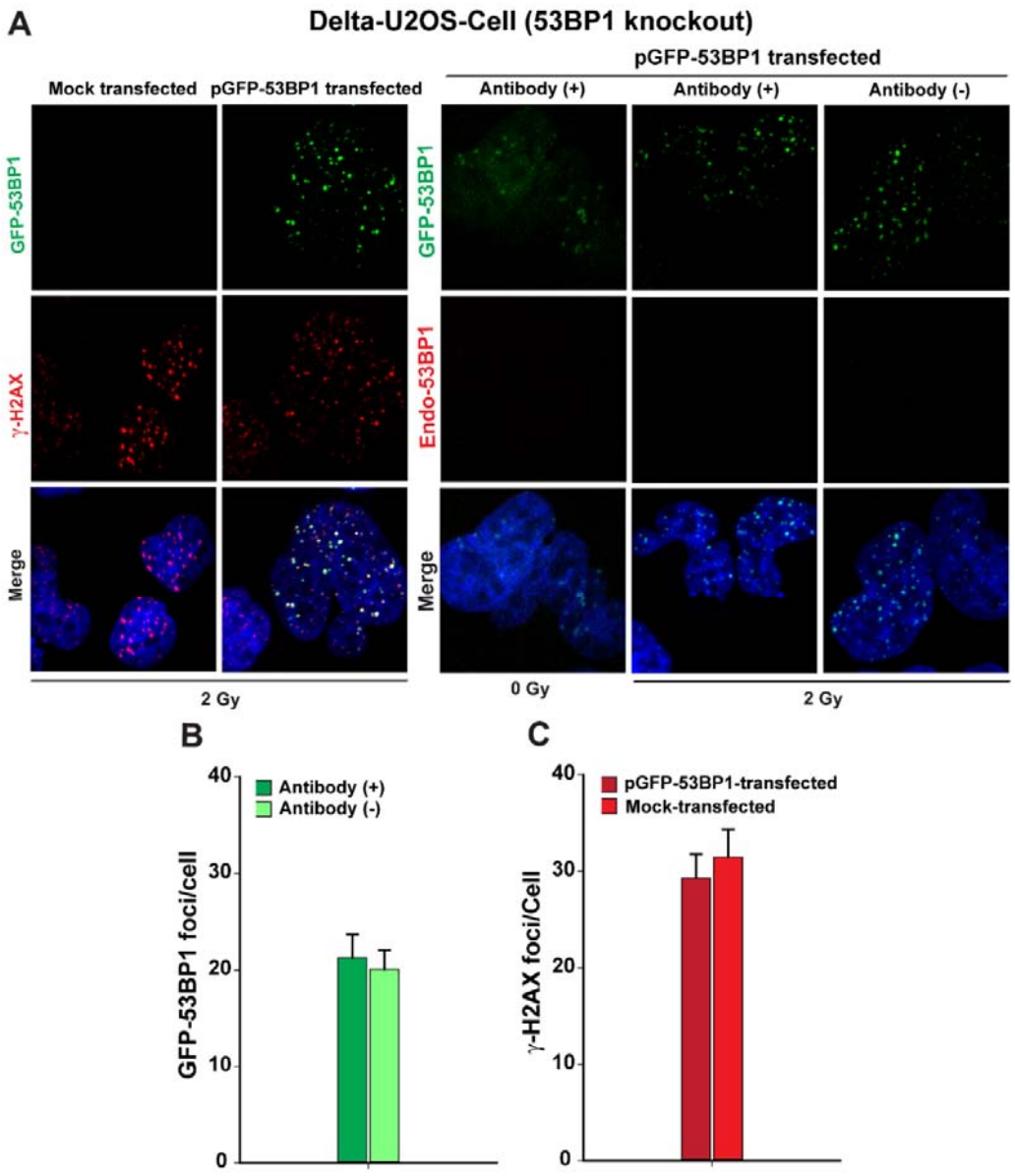

Figure 67 (A) Representative immunofluorescence assay showing images of either GFP-53BP1 foci and/or endogenous γ-H2AX/53BP1 foci in 53BP1 knockout U2OS cell line (Delta-U2OS) after transfecting with GFP-53BP1 expression plasmid as indicated. D-U2OS cells antibody (Ab) stained for endogenous 53BP1 protein does not recognize **(B)** Quantitative analysis of IR-induced 53BP1-GFP foci either stained with or not antibody **(C)** Same as in B but for γ-H2AX foci in pGFP-53BP1 and mock-transfected D-U2OS cells. The number of foci was background subtracted. For representative histogram plots showing transfection efficiency (GFP+ cells) measured after 24 h using GFP expressing plasmid, pEGFP-53BP1, see supplementary figure 5 (upper panel).

To test further if knock-out in D-U2OS cells of endogenous 53BP1 and the ectopic expression of fusion protein GFP-53BP1 influence phosphorylation of γ-H2AX, we checked the formation of γ-H2AX foci after X-ray irradiation. The obtained results showed that absence of

endogenous 53BP1 as well as over expression of GFP-53BP1 did not perturb the preceding formation of γ-H2AX foci within DSB-flanking chromatin and neither mock-transfected nor pGFP-53BP1 transfected cells showed variation in their damage induced γ-H2AX foci formation (figure 67-C). Consistently, analysis of IR-induced γ-H2AX and GFP-53BP1 co-localization showed that approximately 60% of cells exhibited their co-existence in DNA-repair foci at the chromatin mark (figure 68).

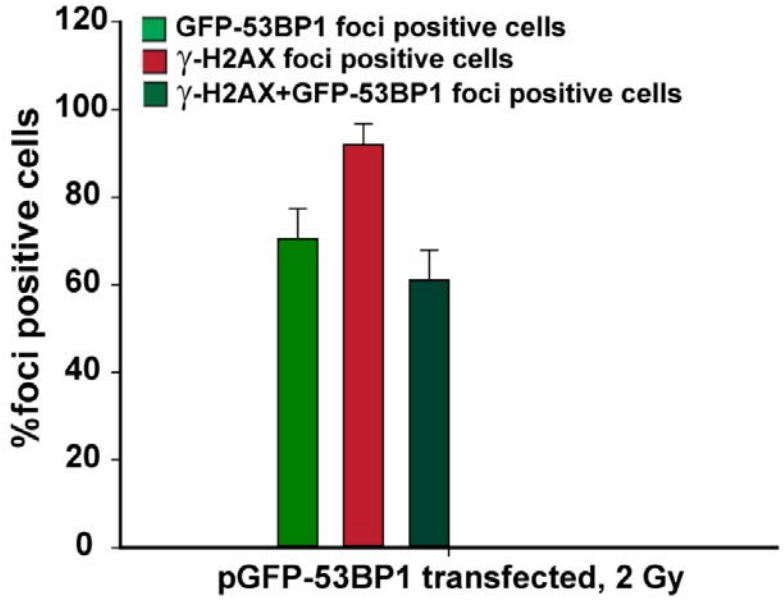

Figure 68 Quantitative analysis of percentage of foci positive cells (either in GFP-53BP1 or γ-H2AX or combined) in D-U2OS cells following transfection with pGFP-53BP1 and irradiation with 2 Gy.

2.9.2 Investigation in 53BP1 proficient human cell lines of physiological relevance of GFP-tagged 53BP1 foci formation

In addition, we also carried out a similar approach using the same fusion plasmid construct pGFP-53BP1 in wild type cells *i.e.* expressing endogenous 53BP1 protein. To do this, we selected two human cell lines of different origin; A549, a human adenocarcinoma cell line and U2OS, an osteocarcinoma cell line. Upon IR, transiently transfected cells, in addition to showing endogenous 53BP1 foci formation, displayed efficient recruitment of GFP-tagged 53BP1 foci to the damaged chromatin (figure 69-A and 70-A). Identical to delta-U2OS cell line, U2OS wild type cell line and A549 cell line exhibited similar level of GFP-53BP1 foci formation regardless of endogenous 53BP1 protein level. However, the level of GFP-53BP1 foci formation in these cells was not comparable to that of endogenous 53BP1 foci formation (Figure 69 and 70).

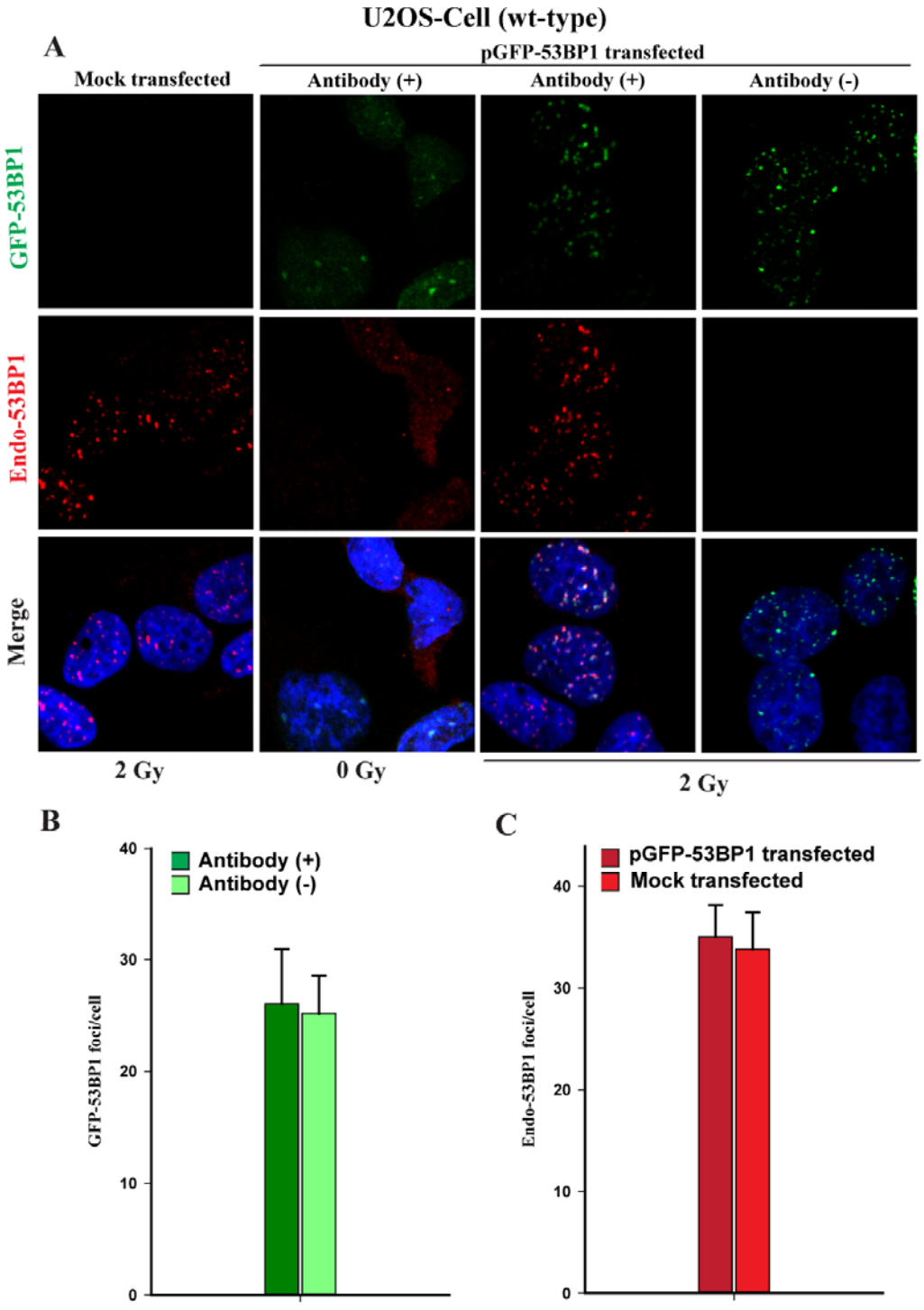

Figure 69 Representative IF images showing GFP-tagged 53BP1 foci (either stained with secondary antibody or not) and endogenous 53BP1 (Red) following irradiation (2 Gy) in pGFP-53BP1 transfected and mock-transfected U2OS wild-type (wt) cells. **(B)** Quantitative analysis of IR-induced GFP-53BP1 foci either stained with or not antibody **(C)** Same as in B but for endogenous 53BP1 foci quantified in mock-transfected and pGFP-53BP1 transfected cells. The number of foci was background subtracted. For representative histogram plots

showing transfection efficiency (GFP+ cells) measured after 24 h using GFP expressing plasmid, pEGFP-53BP1, see supplementary figure 5 (lower panel).

Collectively, these data further strengthen the notion that the means by which IR-induced endogenous 53BP1 foci accumulated at the DSB-modified chromatin is identical to the concomitant recruitment of GFP-53BP1 foci, regardless of cell type.

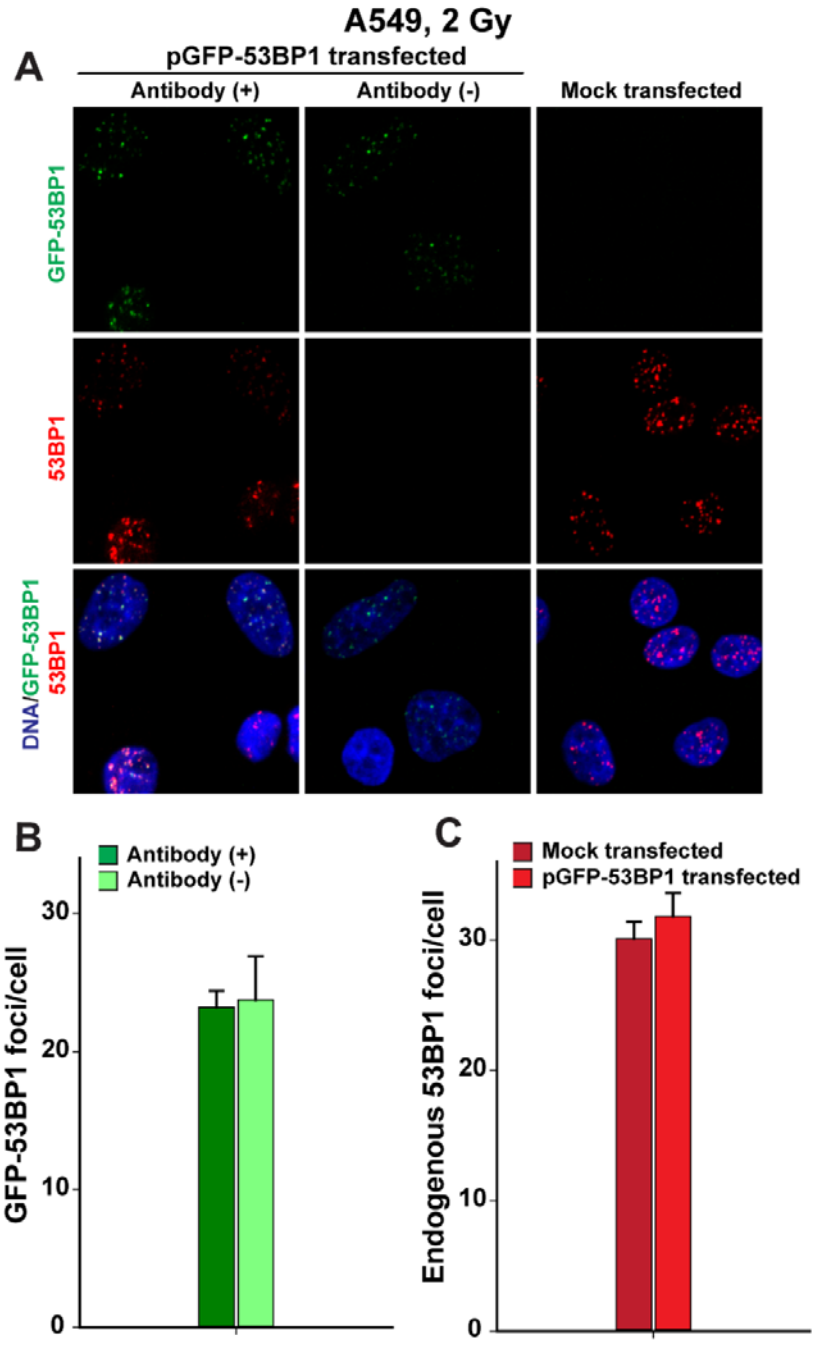

Figure 70 (A) IF images showing GFP-tagged 53BP1 foci and endogenous 53BP1 (Red) following irradiation (2 Gy) in pGFP-53BP1 transfected and mock-transfected A549 cells. **(B)** Quantitative analysis of IR-induced

53BP1-GFP foci either stained with or not antibody **(C)** Same as in B but for endogenous 53BP1 foci in pGFP-53BP1 and mock-transfected cells. The number of foci was background subtracted.

2.9.3 Investigation in 53BP1 proficient hamster cell lines of physiological relevance of GFP-tagged 53BP1 foci formation

In order to validate the ability of the GFP-53BP1 fusion proteins to form foci in CHO10B4 parental cell line, pGFP-53BP1 plasmid expressing a functional GFP-tagged 53BP1 protein was transiently transfected into CHO cells. As expected, similar to endogenous 53BP1 protein, recruitment of GFP-53BP1 foci to IR-induced DSBs was evident (figure 71). Similar to other human cell lines, we did not observe any non-specific effects of endogenous 53BP1 immunostaining on the formation of GFP-fused 53BP1 foci (figure 71-E). We also examined whether foci formed from GFP-53BP fusion proteins overlapped with endogenous 53BP1-decorated chromatin; magnified immunofluorescence image shows their coexistence at IR-treated areas (figure 72).

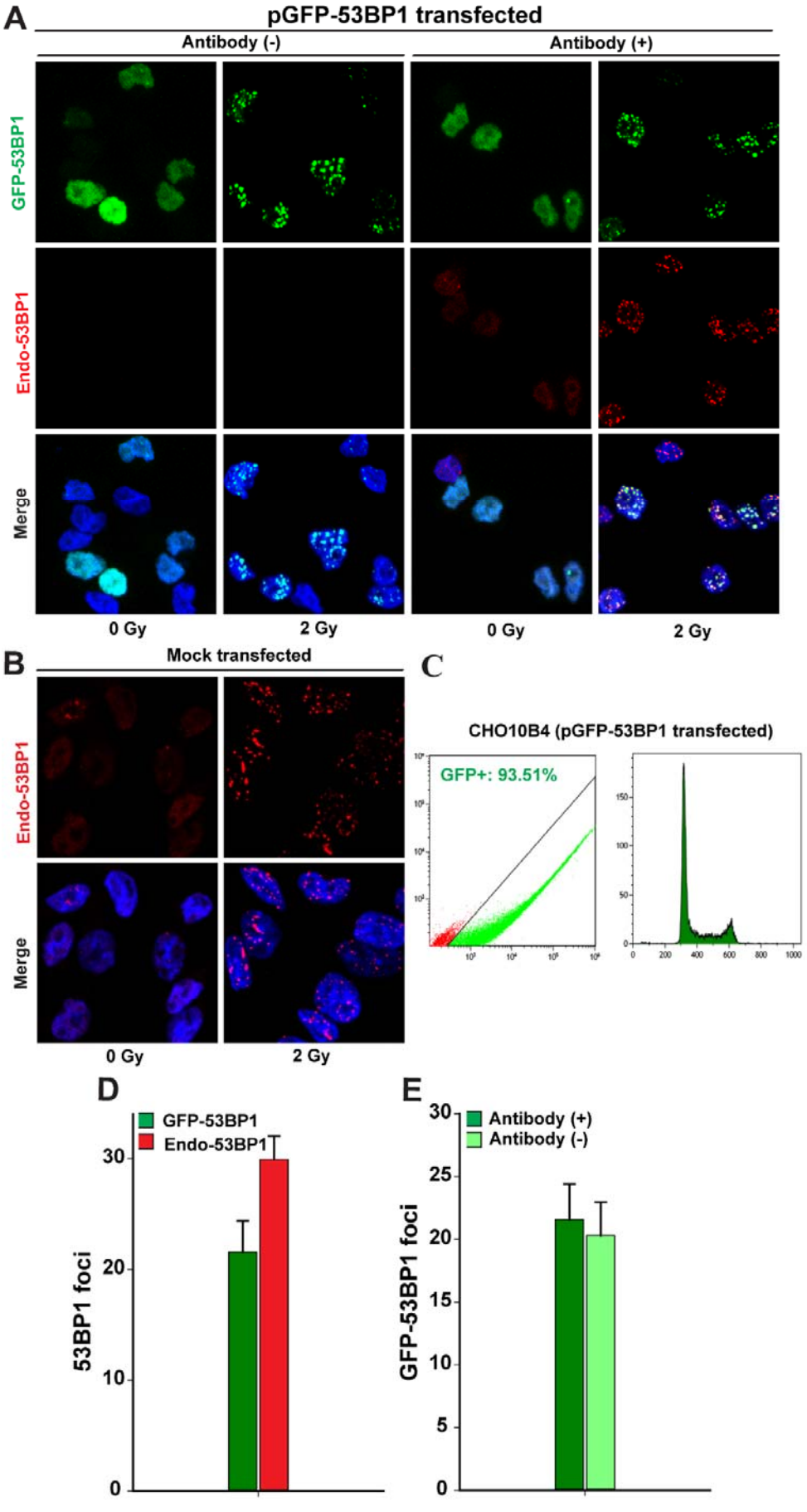
A
pGFP-53BP1 transfected
Antibody (-)
Antibody (+)
GFP-53BP1
Endo-53BP1
Merge
0 Gy
2 Gy
0 Gy
2 Gy
B
Mock transfected
Endo-53BP1
Merge
0 Gy
2 Gy
C
CHO10B4 (pGFP-53BP1 transfected)
GFP+: 93.51%
D
GFP-53BP1
Endo-53BP1
53BP1 foci
0
10
20
30
E
Antibody (+)
Antibody (-)
GFP-53BP1 foci
0
5
10
15
20
25
30

Figure 71 (A) Representative IF images in CHO10B4 cells showing formation of IR-induced GFP-53BP1 foci and endogenous 53BP1 foci following pGFP-53BP1 plasmid transfection. **(B)** Quantitative analysis of GFP-53BP1 and endogenous 53BP1 foci. **(C)** Quantification of IR-induced 53BP1-GFP foci either stained or not with antibody **(D)** Representative histogram shows the transfection efficiency (GFP+ cells) measured after 24 h using GFP expressing plasmid, pEGFP-53BP1 (left panel). PI staining after 24 h transfection was performed for DNA content analysis to check the cell cycle distribution in the experimental cell line (right panel). The number of foci was background subtracted.

2.10 GFP-53BP1 foci co-localize with endogenous 53BP1 and γ-H2AX foci

Co-localization of IR-induced endogenous 53BP1 and ectopically expressed GFP-53BP1 foci at damaged chromatin would indicate that their functional recruitment upon damage induction is mediated through the same DNA damage signaling pathway. In this study, we further investigated whether the more downstream DNA repair protein 53BP1 overlaps with the primary DSB marker, γ-H2AX in 53BP1$^{-/-}$ cells. Analysis of co-existence of both forms of foci in fixed cells shows that almost every IR inflicted DSB exhibited an overlapping of both repair factors. Interestingly, the percentage of GFP-53BP1 foci positive cells is similar to that of both γ-H2AX and GFP-53BP1 foci positive cells indicating that ectopically expressed GFP-fused 53BP1 foci recapitulates the physiological function of endogenous 53BP1 and follows the initial DSB response triggered by H2AX phosphorylation (figure 68 and 72).

We also evaluated in U2OS and A549 cell lines the co-localization of exogenous GFP-53BP1 and endogenous 53BP1 foci. The confocal microscopy images shown in figure 72 indicate their efficient co-localization. Accordingly, in CHO10B4 parental cell line, ectopically expressed GFP-53BP1 foci co-distributed with endogenous 53BP1 foci decorated chromatin region upon irradiation (figure 72).

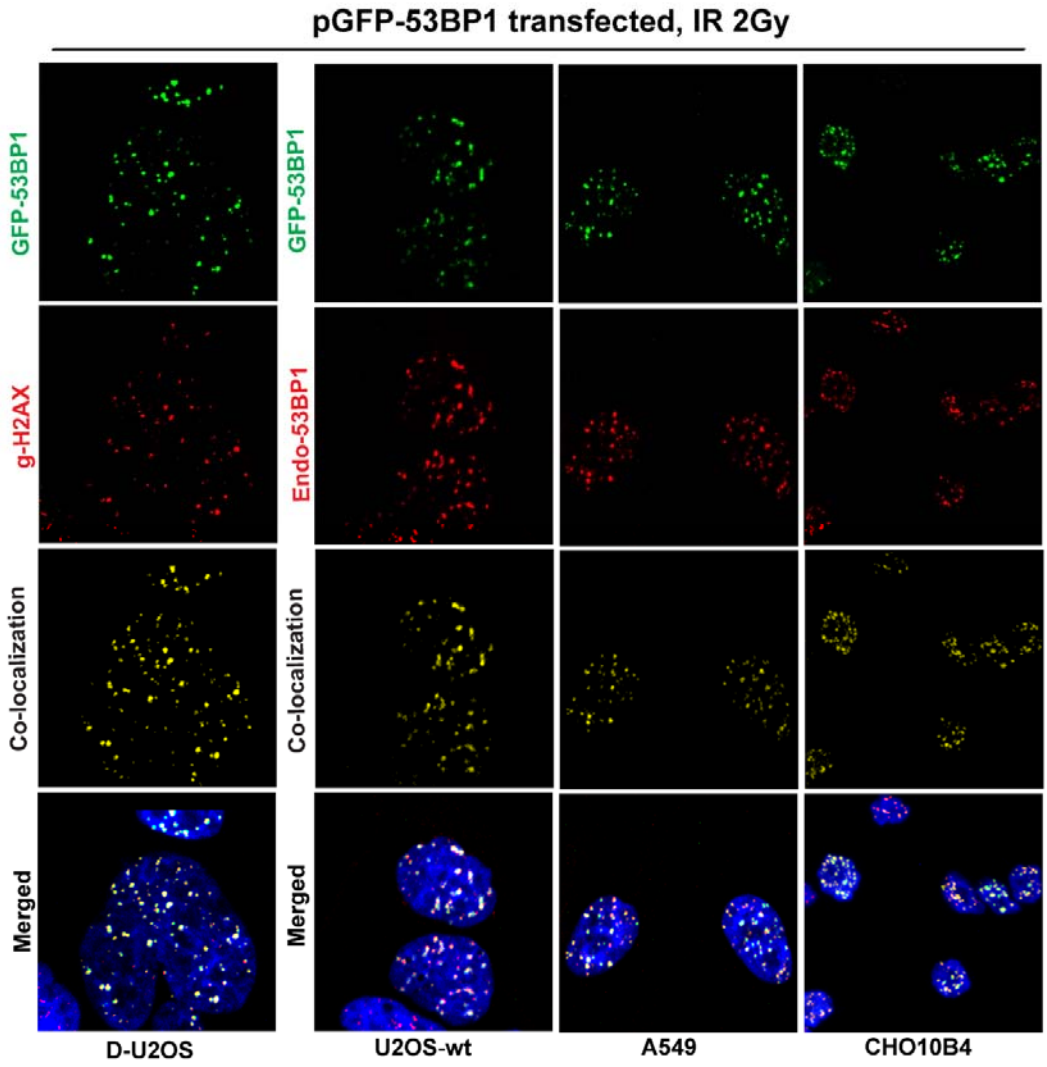

Figure 72 GFP-tagged 53BP1 foci co-localize with endogenous 53BP1 foci in response to IR. Representative fluorescent images showing foci formation of DNA repair proteins γ-H2AX (red), endogenous 53BP1 (red), GFP-53BP1 (green) following IR in 53BP1 knockout cells (D-U2OS cells) and in their corresponding 53BP1 wild type human (U2OS, A549) and CHO cells. Co-localization of GFP-53BP1 foci either with endogenous γ-H2AX or 53BP1 is shown in yellow color. Using Imaris software, images of co-localization were taken (by building a co-localization channel in yellow color). Twenty-four hours after transfection with pGFP-53BP1, Cells were subjected to 2 Gy of irradiation before fixing them for immunofluorescence analysis.

Finally, under the same conditions and following transient expression of I-SceI, we also performed in clonal cells harboring single-DSBs and DSB-quadruplets of confocal image analysis for co-localization using Imaris software. Visualizing the localization of γ-H2AX, endo-53BP1 and GFP-53BP1 foci respectively in response to I-SceI induced DSB breaks in experimental clones showed GFP-53BP1 as well as endo-53BP1 foci co-localized with γ-H2AX (figure 74 left panel). Altogether, these observations indicate that similarly to

endogenous 53BP1, overexpressed GFP-53BP1 forms foci upon damage induction and both types of foci distributed evenly within the damaged chromatin with a pronounced co-localization of both forms of proteins.

2.11 The effect of RNF8 and/or RNF168 depletion on GFP-tagged 53BP1 foci formation in parental hamster cells

To test the direct depletion of GFP-tagged version of 53BP1 by means of RNA interference (RNAi)-mediated gene knockdown of RNF8/168, we co-transfected CHO10B4 cell line with a plasmid construct expressing GFP fusion protein, GFP-53BP1 and RNF8/168 specific siRNAs.

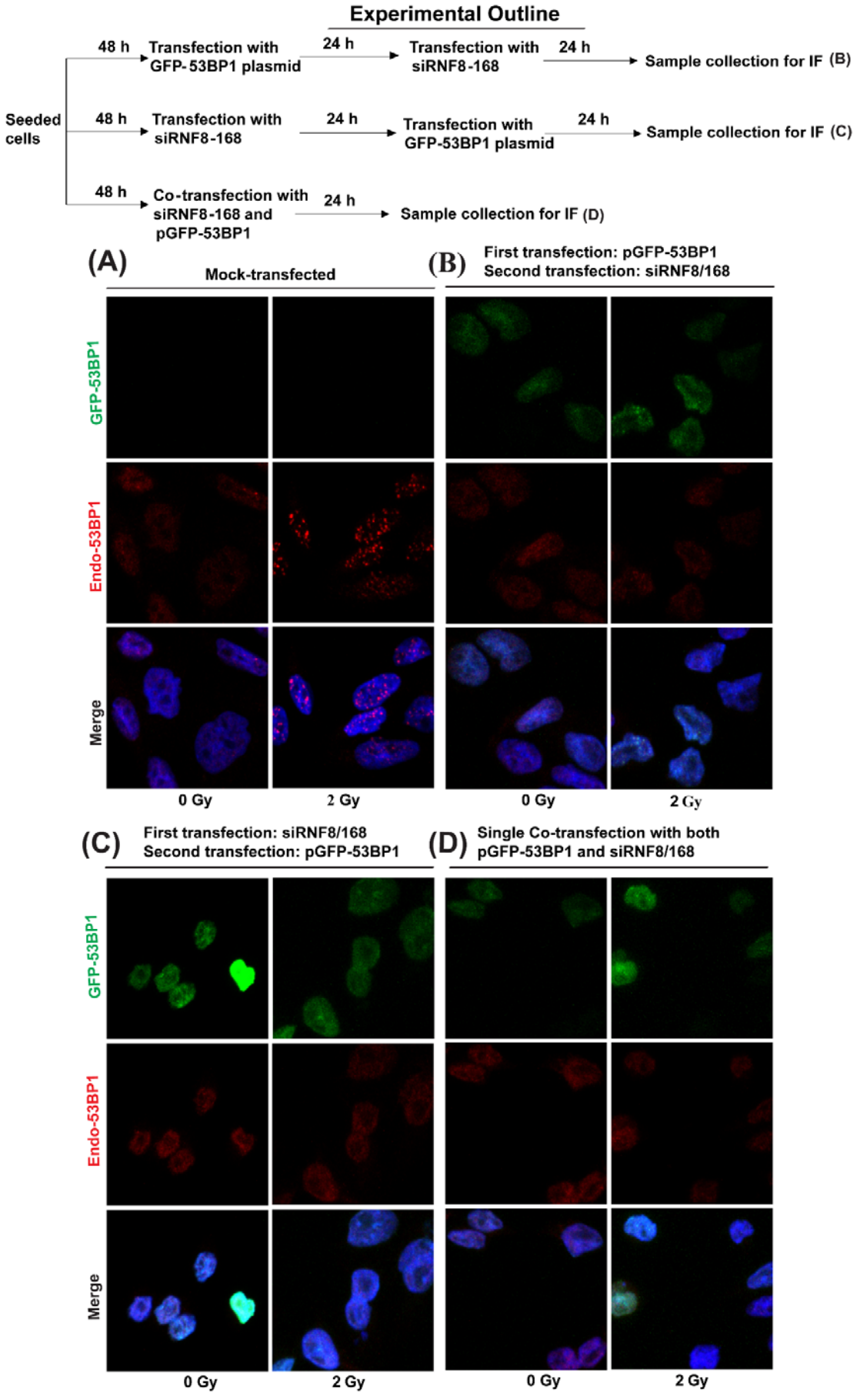
Experimental Outline
Seeded cells
48 h
Transfection with GFP-53BP1 plasmid
24 h
Transfection with siRNF8-168
24 h
Sample collection for IF (B)
48 h
Transfection with siRNF8-168
24 h
Transfection with GFP-53BP1 plasmid
24 h
Sample collection for IF (C)
48 h
Co-transfection with siRNF8-168 and pGFP-53BP1
24 h
Sample collection for IF (D)
(A)
Mock-transfected
(B)
First transfection: pGFP-53BP1
Second transfection: siRNF8/168
GFP-53BP1
Endo-53BP1
Merge
0 Gy
2 Gy
0 Gy
2 Gy
(C)
First transfection: siRNF8/168
Second transfection: pGFP-53BP1
(D)
Single Co-transfection with both pGFP-53BP1 and siRNF8/168
GFP-53BP1
Endo-53BP1
Merge
0 Gy
2 Gy
0 Gy
2 Gy

Figure 73 RNA interference (RNAi) of RNF8-168 abolishes formation of GFP-53BP1 foci. (Upper panel) Outline of the experimental protocol to test the knockdown efficiency of GFP-tagged 53BP1 foci in three combinations. Exponentially growing cells were either (B) first transfected with GFP-53BP1 plasmid then followed by a second transfection after 24 h with siRNAs directed against RNF8/168 or (C) first transfected with siRNAs of RNF8/168 then a second transfection with pGFP-53BP1 or (D) a single transfection to transfect cells with both RNF8/168 specific siRNAs and plasmid for GFP-53BP1. **(Lower panel)** IF images showing abrogation of GFP-53BP1 foci following siRNA mediated gene silencing of RNF8 and RNF168 in accordance with described transfection protocol B,C,D in the upper panel. Cells were treated with 2 Gy of ionizing radiation. Sample collection procedures are the same as in other immunofluorescence experiments.

To that purpose, we checked the recruitment of GFP-53BP1 foci to the sites of DNA damage following irradiation. We tested three different combinations of transfection protocol to optimize the depletion of fusion protein GFP-53BP1 using siRNAs directed against RNF8/168 (Figure 73, upper panel-Experimental outline). In the first two scenarios, we followed a double-transfection protocol where exponentially growing cells were first transfected either with pGFP-53BP1 or siRNF8/168, which was then followed by a second transfection either with RNF8/168, or pGFP-53BP1. In the third case, in order to minimize the transfection related stress as described in section 2.4.1, we followed a single-transfection procedure, where both siRNAs and plasmid pGFP-53BP1 were introduced into cells. With a corresponding absence of endogenous 53BP1, depletion of RNF8 and RNF168 resulted in dramatic abrogation of exogenous GFP-53BP1 foci formation, which is consistent with the previous observation that IR as well as I-SceI induced endogenous 53BP1 foci formation is dependent largely on RNF8/168 (figure 73). In all optimizing conditions, RNF8/168 silencing showed no apparent recruitment of either endogenous 53BP1 foci or GFP-53BP1 foci to DSB-flanking chromatin. In order to mitigate the transfection-related cellular stress, we employed a single-transfection protocol to carry out subsequent experiments. These data collectively demonstrate that 53BP1 foci, either endogenous or exogenous, assemble on damaged chromatin and co-depletion of RNF8/168 abolishes its accrual to the sites of DSBs. To estimate the transfection efficiency, GFP fluorescence activity of GFP coding/expressing plasmid was measured by flow cytometry 24h post-transfection.

2.12 Cluster complexity is a factor in GFP-tagged 53BP1 foci formation in CHO clones harboring I-SceI constructs for simple DSBs and DSB clusters

In CHO10B4 cells, successful ablation of endogenous as well as exogenous 53BP1 foci formation by means of RNA interference of RNF8/168 validates the cell line as a tool to study the dynamics of 53BP1 protein in response to DNA damage especially in the context of I-SceI mediated chromothripsis: an event whereby multiple DSBs locally generated by a catastrophic event causes genomic rearrangements that feed carcinogenesis. Thus we extended our study in clones harboring I-SceI recognition sites representing simple and complex forms of DSBs. In order to investigate the heightened 53BP1 signaling in live cell imaging experiment in DSB clusters compared to simple DSBs (Schipler et al. 2016), we co-transfected both cells with I-SceI expressing plasmid and GFP-53BP1 fusion plasmid and fixed the cells following indirect immunofluorescence (IF) assay. During our indirect IF experiment, we did not observe any foci formation at the earlier time points (8 and 10 h) following expression of I-SceI. Formation of foci was observed at 12 h after I-SceI transfection (Figure 74). Results presented in the figure 75 shows the analysis of clearly detectable endogenous (figure 75-A) as well exogenous GFP-53BP1 (figure 75-B) foci formation in CHO clones harboring single-DSBs and DSB-clusters 12 h following transfection with I-SceI expressing plasmid. It indicates clones sustaining clustered-DSBs are able to elicit full foci development. It further support the notion that the persistence of 53BP1 (endo-53BP1 as well as GFP-53BP1) reflects the sustained 53BP1 signal generated by clustered-DSBs. In simple form of DSBs (CHO-1xS.D8), the number of foci scored is comparatively less. It suggests simple form of DSB clusters induces an attenuated downstream signaling that is manifested in their less 53BP1 foci formation. Of note, an overlap in the development of 53BP1 foci (endo and GFP-53BP1) was also noticed (figure 75-A and B). The level of IR induced GFP-53BP1 foci formation was not similar with that of the endogenous protein in both clonal cells but their magnitude at the DSB sites was comparable (figure 75-C).

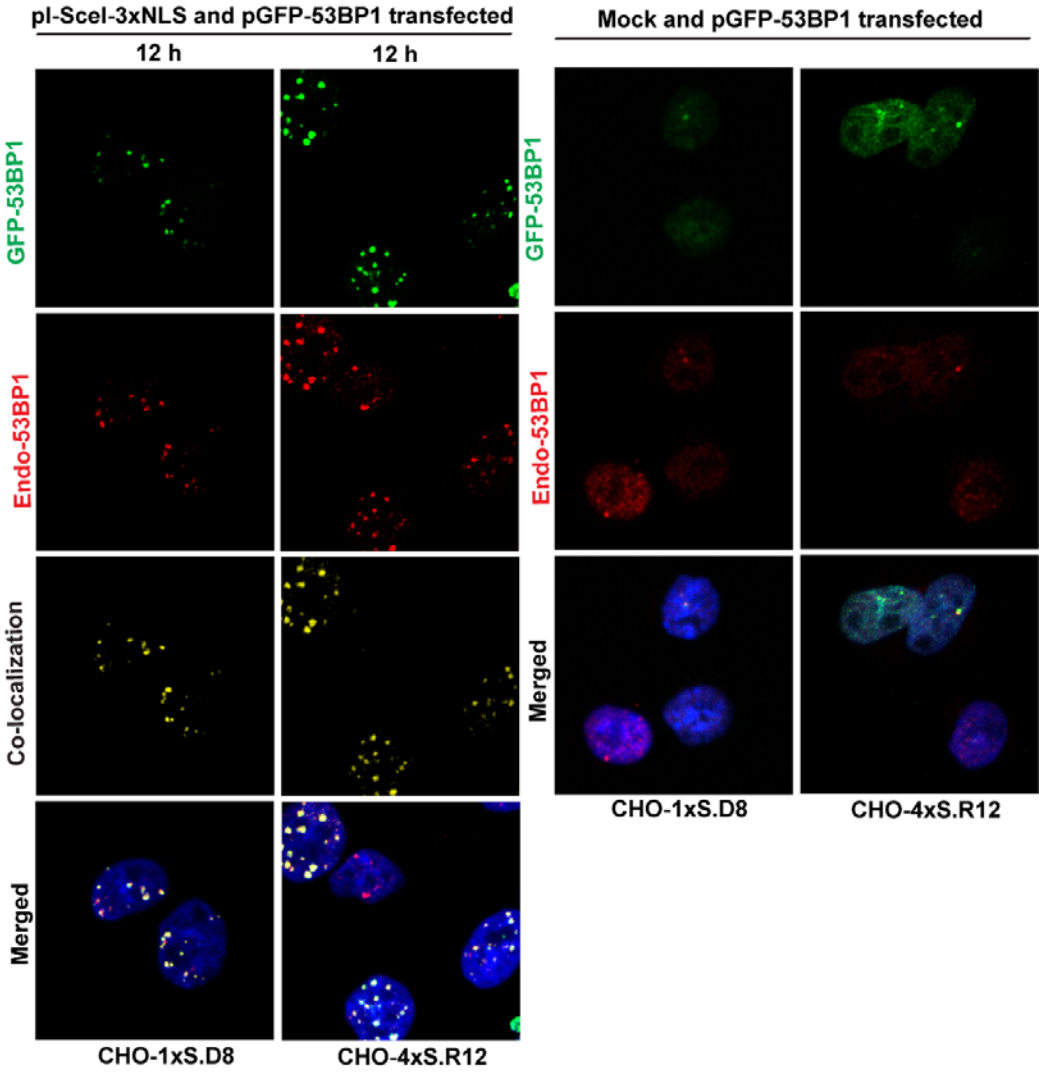

Figure 74 GFP-53BP1 fusion foci showed co-localization with endogenous 53BP1 foci in CHO cells. Representative IF images show I-SceI induced foci formation of endogenous 53BP1 (red), GFP-tagged GFP-53BP1 foci (green) and their co-localization (yellow) in simple and complex DSB harboring clones. Images were processed using Imaris software. Co-transfected cells with pI-SceI-3xNLS and pGFP-53BP1 were processed for immunofluorescence 12 h after transfection.

The enhanced engagement of 53BP1 in the repair of clustered DSBs clearly indicates an active downstream signaling thus discriminating clustered form of DSBs from simple-DSBs.

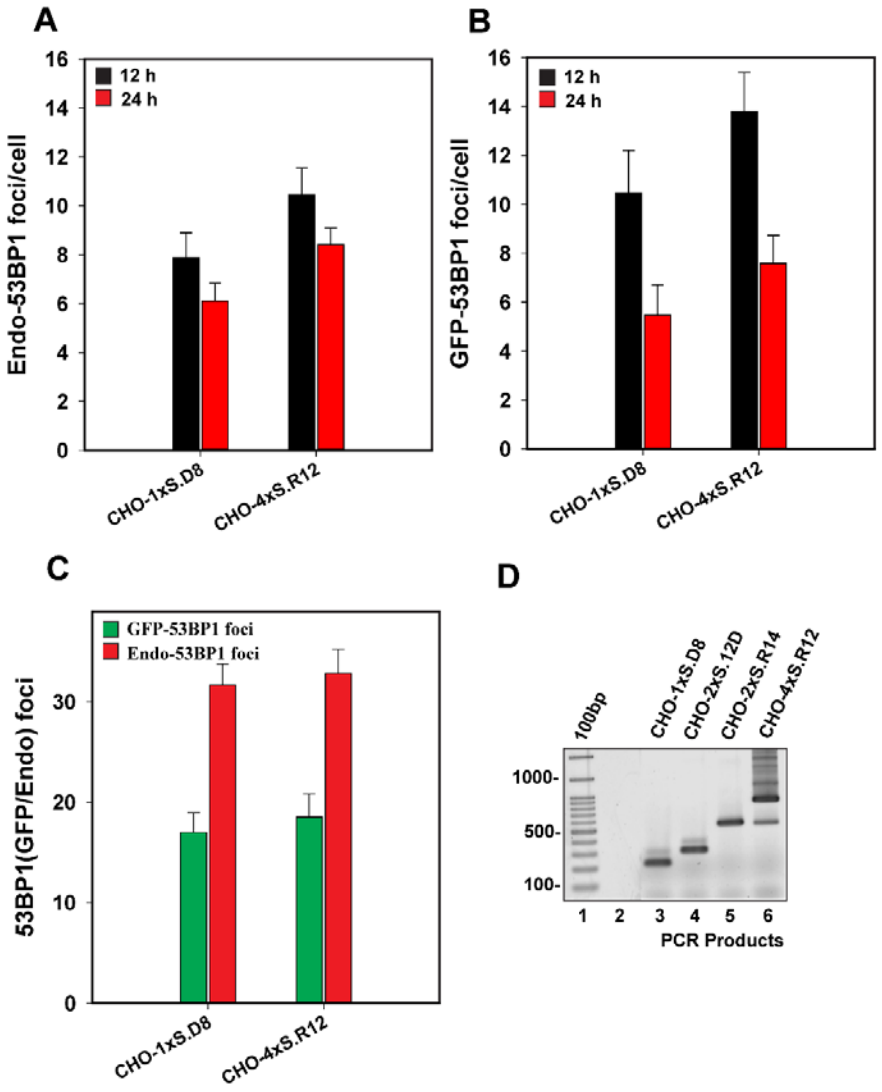

Figure 75 Persistent 53BP1 signaling is evident in clustered-DSBs (CHO-4xS.R12). (A) Quantitative analysis showing endogenous 53BP1 foci formation in both clones after transfection with I-SceI expressing plasmid at time point analyzed (12 and 24 h). **(B)** GFP-53BP1 foci formation same as in **(A)** but co-transfection with both I-SceI expressing and GFP-53BP1 fusion protein expressing plasmid. **(C)** Quantitative analysis of endogenous 53BP1 foci as well as GFP-53BP1 foci formation in both clones following only transfection with GFP-tagged 53BP1 plasmid and irradiation at 2Gy. **(D)** PCR-Genotyping based validation to confirm the retained I-SceI recognition sites during propagation in the clonal cell lines as described in detail in figure 1. Scored foci number is background subtracted. Results show the mean and standard deviation (SD) from two independent experiments.

2.13 Development of I-SceI based ligand-inducible model system: Difficulties and Future perspective

Many experimental systems based on I-SceI homing-endonuclease have been used widely to elucidate the ultimate cellular responses towards I-SceI-induced DSBs. However, this system is not a foolproof and has inherent limitations. One particular limitation is the restoration of I-SceI recognition site, which is mediated via c-NHEJ pathway. This c-NHEJ mediated restoration event will further lead to a recurring phenomenon of "cutting and sealing" as long as the endonuclease remains in the nucleus (Bennardo et al. 2009; Bindra et al. 2013; Honma et al. 2007; Mao et al. 2008). Such persistent DSBs may present a bias for data obtained with this system. Moreover, this system is based on the transfection efficiencies of *I-SceI*-expressing plasmid, which varies between cell lines. Most notably, expression of *I-SceI* enzyme following transfection takes several hours to manifest and the *I-SceI* exposure time varies between cells in a given population thus difficult to monitor or quantify.

In order to overcome these limitations, several laboratories developed stably integrated versions of an inducible *I-SceI* expression system, where the generation as well as repair of the *I-SceI* induced DSBs can be precisely controlled. The fundamental of this novel system is that it allows precise control of cleavage kinetics without the requirement of *I-SceI* plasmid transfection. It consists of a fusion between the I-SceI gene and the ligand-binding domain of the rat Glucocorticoid Receptor (GR) on the C-terminus, which is known as SceGR (Soutoglou et al. 2007). The ensuing fusion protein (I-SceI-GR) from *I-SceI* expression cassette is translocated into nucleus minutes after binding to synthetic GR ligand, Triamcinolone (TA) and thus DNA cleavage is induced. In the absence of TA, ISceGR is excluded from the nucleus such that DNA cleavage is limited. Addition in such constructs of a ligand-dependent destabilizing domain (DD) derived from FKBP12 (fused to N-terminus) to generate ddISceGR can provide an additional level of *I-SceI* control (Bindra et al. 2013). The destabilizing effect of DD in DD-tagged protein can be blocked by the addition of DD-specific and high affinity membrane-permeant ligand, Shield1, commercially available as the Proteo-Tuner system (Clontech Laboratories, Inc.). Thus, a 'two-tiered' control of *I-SceI* cleavage can be achieved. In the absence of any drug, stably transfected *I-SceI* is constitutively expressed but localizes in the cytoplasm where it is rapidly degraded by destabilizing degron (DD) motif. Administration of membrane-permeable ligand Shield1 stabilizes the fusion protein by binding to DD and is thus accumulated in the cytoplasm. Addition of TA mediates

the translocation into the nucleus of I-SceI enzyme, where it recognizes DSBs and cut the artificially integrated I-SceI recognition sites to generate DNA double strand breaks (DSBs). Upon ligand (Shield1) removal, cytoplasmic DD degradation is mediated via ubiquitin-proteasome pathway and thus stops the I-SceI induced DSBs generation in the genome (see figure 76-A). This system allows substantial control of I-SceI cleavage rates and exposure time.

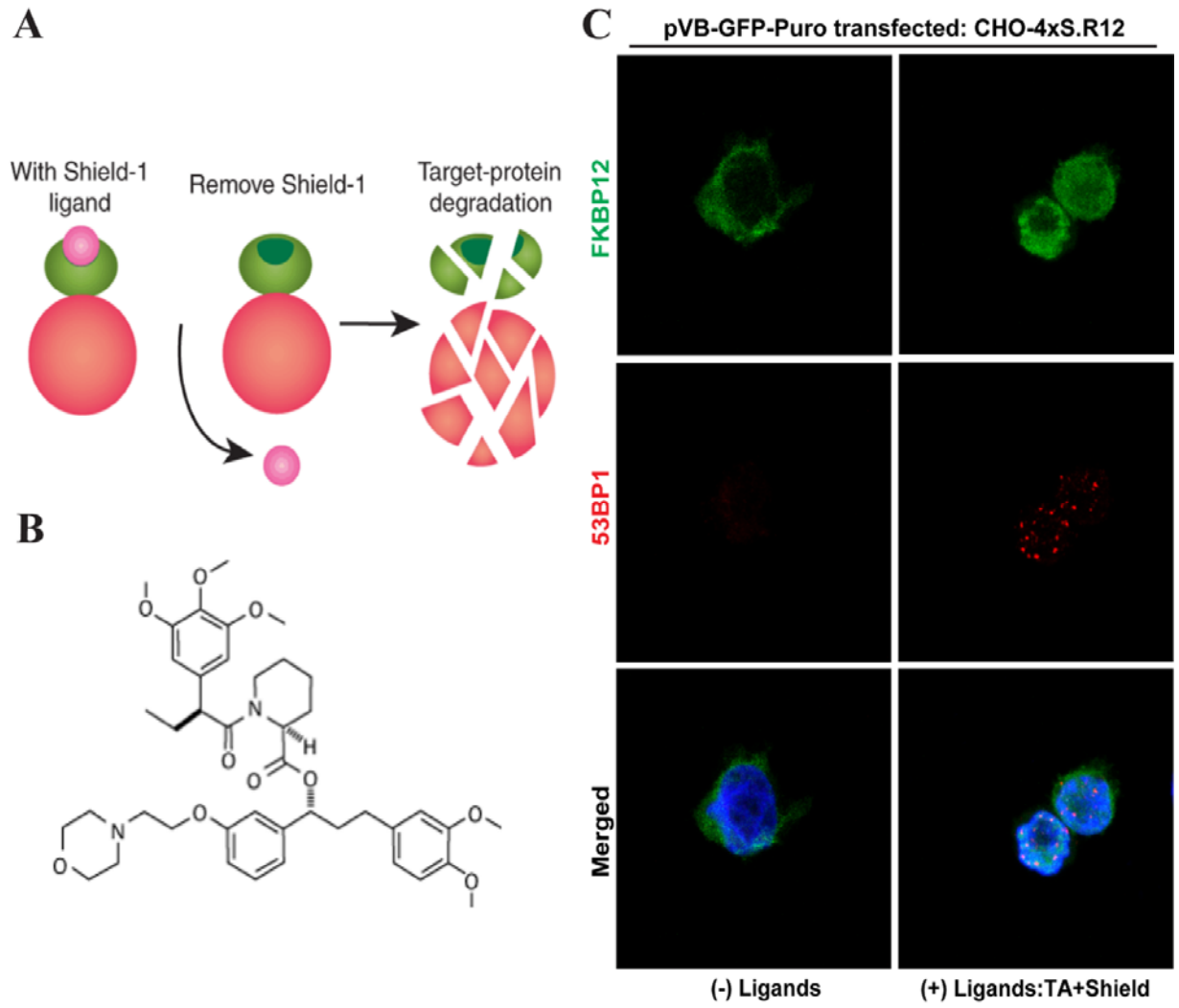

Figure 76 Schematic representation of ligand-dependent I-SceI inducible system (A) Ligand dependent I-SceI inducible system for control of I-SceI exposure time. In presence of ligand, Shield1, protein of interest will be stabilized and removal of ligand activates the destabilizing function of destabilizing domain (dd) and ultimately leads the fusion protein toward ubiquitin-proteasome pathway. **(B)** Chemical structure of the Shield1 ligand. **(C)** Immunofluorescence analysis of clonal cell harboring complex-DSBs with I-SceI semi-inducible system allowing regulated function of I-SceI. Images show translocation of FKBP12 (green) into nucleus from cytoplasm upon addition of ligands (TA and Shield) and I-SceI induced 53BP1 foci (red) formation in complex-DSBs harboring clone (CHO-4xS.R12). Twenty-four hour post-transfection with GFP-tagged I-SceI plasmid

(pVB-GFP-Puro), ligands were added and incubated for 4 h before fixation. Fixed cells were stained with indicated antibodies and subsequently analyzed by confocal microscopy.

To gain additional insight into this inducible degradation system, characterization of stable human (human retinal pigment epithelial-RPE1) and rodent (CHO10B4) clonal cell lines expressing *I-SceI* in an inducible manner is ongoing. Moreover, we have recently tested two newly designed plasmids allowing generation of cell lines stably expressing chimeric *I-SceI* expression cassette (DDSceGR) discussed above. We have validated the proper expression of the chimeric *I-SceI* in cells transfected with both plasmids and successfully confirmed that upon administration of ligands the fusion protein is translocated from cytoplasm into the nucleus.

In an effort to overcome the above-mentioned inherent limitations of our previously developed CHO model system we have been working exclusively on the development of an inducible system to express the I-SceI in a controlled manner. During the course of our experiments, we followed an alternative approach to test the selective activation of DDR following expression of chimeric I-SceI protein after transfection into clonal cells of GFP-fused I-SceI plasmid (pVB-GFP-Puro). Figure 70-C shows that upon administration of TA and Shield1, the DD-tagged stabilized fusion protein translocated into the nucleus from cytoplasm and efficiently cut the I-SceI recognition sites. I-SceI induced DSBs activated the DDR signaling in the form of 53BP1 foci in complex-DSBs harboring clonal cells following expression of chimeric I-SceI protein. Without the ligands, the fusion protein accumulated in the cytoplasm as its localization in cytoplasm is shown by staining with antibody against FKBP protein (the destabilization domain, DD). Since one of our focuses, as stated earlier, was to overcome transfection related stress, we therefore added Proteo-Tuner system based ligands (TA and Shield) 24 h after transient transfection of I-SceI expressing plasmid. Two limitations associated with transient transfections can thus be minimized. First of all, transiently transfected cells will overcome transfection related stress and secondly there will be significant ligand-induced DSB induction. As revealed in the IF image, addition of ligands successfully confirmed the proper induction of DSBs and thus activation of DNA damage response pathway. We therefore termed this system as a transient semi-inducible system to control I-SceI exposure and cleavage using ligands (TA and shield).

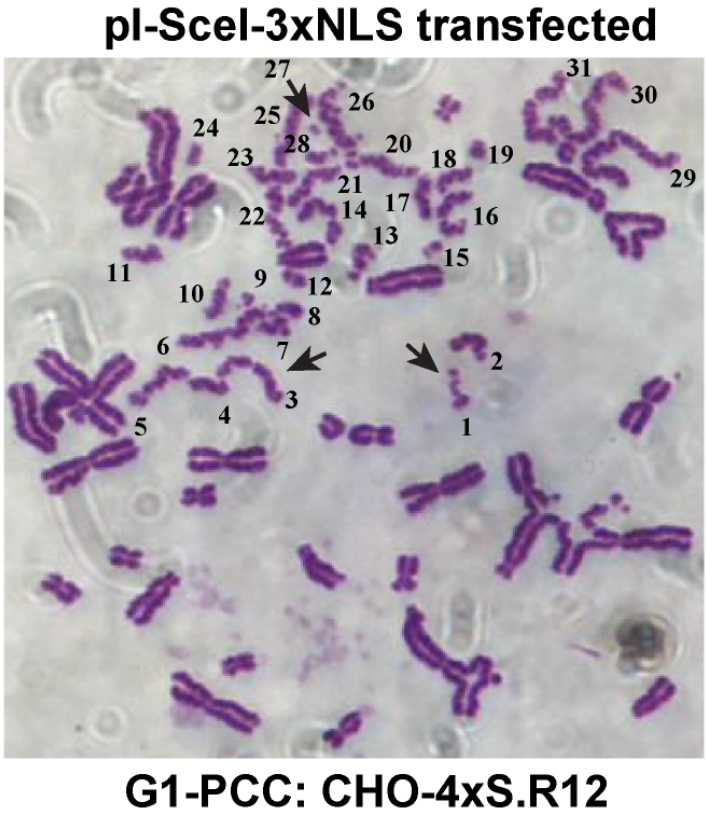

Figure 77 Representative image of I-SceI induced G1 chromosome breaks (more than 30 breaks) following transfection with I-SceI expressing plasmid in clone that harbors clustered DSBs. Indicated numericals show the total number of chromosomal breaks (light stained) in G1 phase of the cell cycle (single chromatid morphology).

During the analysis of metaphase in clonal cells following expression of I-SceI, we serendipitously noticed a G1-PCC in clone harboring complex types of DSBs. The PCC image shown in figure 77 indicates a significant number of G1 chromosome/PCC breaks (more than 30). It may therefore be worth investigating the effect of clustered lesions on chromosome level by looking at the formation of PCC breaks in these clonal cell lines following induction of DSB breaks in G1 phase of the cells. To induce breaks especially in this specific cell cycle phase, an inducible system would be an ideal approach. Inducible clonal cells synchronized in G1 phase by serum deprivation can easily be subjected to I-SceI-mediated DSB induction by simply adding Shield and TA. From present study and also based on ongoing experiments at our lab, we now have convincingly revealed CtIP as a major contributor in chromosomal breaks and translocation formations. Thus it will be an interesting area for further research to investigate cell cycle specific role of CtIP in mediating chromosomal rearrangements (CRs) with a particular focus on G1 phase of the cell cycle.

V Discussion

1 CtIP regulates DSB processing via alt-EJ

DNA double strand breaks (DSBs) are the most deleterious lesions owing to their inherent capability to distort the continuity of chromosomes. Illegitimate repair of DSBs may lead to genome instability and carcinogenesis. In eukaryotes, c-NHEJ and HRR predominantly process DSB within cells. C-NHEJ repairs the breaks by simply ligating the broken DNA ends, whereas HRR repairs by using the homologous sequence present in the sister chromatid. However, DSBs can also be processed by an alternative form of pathway termed as (alt-EJ), when both pathways are compromised. A common characteristic of alt-EJ is that it is micro-homology dependent and thus, it utilizes resection. Numerous previous studies have investigated the essential role of CtIP in DNA end resection and in DNA repair that is mediated via alt-EJ (Iliakis, Murmann, and Soni 2015). Alt-EJ in G1 phase operates when c-NHEJ is abrogated. In this present study, we investigated the functional role of CtIP and Mre11 in alt-EJ pathway in cells (G1-and -G2 phases) exposed to irradiation in rodent cells.

1.1 CtIP confers cellular survival in CHO cells and end resection in G1 phase

We measured the effect of CtIP depletion on cellular survival by clonogenic assays following exposure to irradiation. We show that CtIP depletion sensitizes the cells toward irradiation (Figure 24). We further showed that CtIP has a prominent role in the repair of DSBs in all phases of the cell cycle. Thus CtIP might be one of the factors for functional alt-EJ throughout the entire cell cycle. Using clonogenic survival experiment performed in HRR deficient cells, we noticed a moderate radio sensitization in cells depleted of CtIP via siRNA (figure 25). Using G1-phase cells, we found a limited radio sensitization of CtIP depleted cells, which is attributed to low expression level of CtIP in this phase of the cell cycle (figure 26). Thus we demonstrate that CtIP that is often considered as homologous recombination factor operates through alt-EJ in all cell cycle phases.

CtIP has also been shown to physically interact and stimulate the functional activity of MRN complex. These core resection components are conserved from yeast to human. Not long ago, it was thought that the function of CtIP is restricted to S/G2 phase of cells and in G1 phase, it is predominantly inhibited by a core c-NHEJ factor, Ku (Ku70/80). However, the end processing role of CtIP in alternative end joining (alt-EJ) has been implicated in previous reports (Bakr et al. 2016; Lee-Theilen et al. 2011; Liu and Huang 2016; Truong et al. 2013).

Several reports also highlighted the existence of G1 phase DNA end resection. A pioneer study reported resection in G1 cells for the first time with the observation that resection is required to repair complex lesions induced by high-LET irradiation (α-particles) (Averbeck et al. 2014). A later study from Löbrich lab points to that fact that not only complex lesions induced by high-LET but also complex lesions induced by high dose of low-LET (X-rays) can result in activation of resection in G1 phase (Barton et al. 2014). However, it is yet not clear which pathway would benefit from the resection process in G1 cells. Consistent with this, we also found that in CHO cells that CtIP depletion significantly reduced resection in all populations analyzed (G1 and G2) implying its role in DNA end processing (figures 27-29). Published results from our lab showed an elevated level of DNA end resection in c-NHEJ mutant cell lines (Mladenov, Fan, Paul-Konietzko, et al. 2019). In line with this, our present study also demonstrates an increase in resection in G2-phase DNA-PKcs deficient cell line (IRS-20) compared to DNA-PKcs proficient cell line (CHO10B4) (Figure 29).

1.2 DNA-PKcs deficient cells are independent of growth state

An inherent feature of alt-EJ is that it is growth state dependent and is compromised in cells entering a quiescence stage (G0) of growth. Interestingly, this compromised phenotype of alt-EJ in G0 is absent in DNA-PKcs deficient cells and is associated with elevated resection of DNA in G2 phase (Mladenov, Fan, Paul-Konietzko, et al. 2019; Satyendra K. Singh et al. 2011). In fact, our experimental results focused on G0 phase cells in wild type cells (CHO10B4) showed a marked reduction in the involvement of alt-EJ. Moreover, we showed a marked reduction of alt-EJ in other c-NHEJ mutant cell lines, for instance, XR-1; deficient in XRCC4 and XRS-6; lacking Ku80. The compromised repair phenotype in all tested cell lines is correlated with a corresponding reduced expression of CtIP (figure 30-C). Surprisingly, in the current study, no decrease in alt-EJ was noted in DNA-PKcs deficient cells and the efficiency in repairing residual DSBs is identical to their corresponding asynchronous cells (figure 30-D and E, figure 35-A). Interestingly, both in c-NHEJ mutants and parental CHO wild-type cells, the level of CtIP protein expression decreased very significantly (figure 30-C). This study thus reveals that the compromised alt-EJ activity in wild type plateau phase cells is likely to be associated with the reduction of resection factor, CtIP. Yet, the mechanisms by which DNA-PKcs cells show no dependence on alt-EJ remains speculative and require further investigation. However, the mechanism through which CtIP level is down regulated in cells during plateau phase of growth is associated with inhibitory function of ubiquitin ligase APC/C (Cdh1) (Lafranchi et al. 2014). Thus, a better

understanding of relationship between CtIP, DNA-PKcs and alt-EJ is necessary to elucidate the underlying regulatory mechanisms of alt-EJ independent DSB repair in DNA-PKcs-deficient cell lines. To confirm whether DNA-PKcs mutant cells somehow allow loading of long-range resection factors, it will be of prime importance to investigate how DSB processing is regulated in DNA-PKcs deficient cells following depletion of nuclease activity.

1.3 CtIP contributes to alt-EJ pathway in CHO cells

Based on previous and present studies in plateau phase cells, it is evident that cells lacking DNA-PKcs show alt-EJ independent repair phenotype (figure 30-D and E) (Satyendra K. Singh et al. 2011). Therefore, we additionally investigated if the depletion of CtIP in DNA-PKcs mutant cells can be substantiated with a concomitant reduction in their DSB repair proficiency following irradiation. We revealed in asynchronously growing wild type CHO cells, a significant CtIP dependent role of alt-EJ (figure 33-A). It hints to a previously unexplored role of CtIP in alt-EJ and further demonstrates that in absence of c-NHEJ, DSBs are repaired via CtIP-mediated alt-EJ. We tested in DNA-PKcs deficient cells the functional role of CtIP. Data from (Figure 35 and 36) revealed no change in the DSB repair kinetics. Akin to DNA-PK$^{-/-}$ cells, another cell line XR-1, mutant for an accessory c-NHEJ factor, XRCC4 showed also no detectable dependence on alt-EJ after CtIP knockdown (figure 38). Surprisingly, cells mutant for Ku80, a component of DNA-PK, showed involvement of CtIP-mediated alt-EJ as evident by a reduction in their repair efficiency (figure 37-A).

A compromised phenotype in alt-EJ in repairing PCC breaks (figure 42) corresponds not only to the defective DSB repair efficiency in XRS6 cells maintained in exponential state of growth after CtIP depletion (figure 37-A), but also to the cells maintained in plateau phase (figure 31). In each settings, DNA end resection either by RNAi of CtIP or by serum deprivation is restricted. This finding may suggest that the absence of DNA end tethering factor Ku70/80 allows the access of CtIP to process the DNA ends and promotes efficient alt-EJ.

Upon inhibition of catalytic function of DNA-PKcs, interestingly, a further accumulation of DSBs following DNA damage was noticed (figure 37-A, right panel. This repair defect manifests as a synergistic effect of CtIP on alt-EJ. This suggests, in the absence of DNA-PK holoenzyme, CtIP can be frequently recruited to DSB breaks to process their ends via Ku-independent pathway of end joining.

1.4 The endonuclease function of MRE11 promotes alt-EJ

DNA end processing is a critical determinant for pathway selection. Combined activities of nuclease ensemble that includes CtIP and MRN complex have been shown to promote HRR pathway and based on recent evidences also alt-EJ pathway. Stimulated by CtIP, MRE11 makes a nick in the vicinity of break with its intrinsic endonuclease activity and proceeds to the blocked end by chopping the DNA using its 3´-5´exonucelase function. Apart from its well-known role in HRR, the nuclease function of MRE11 has also been implicated in the regulation of alt-EJ, yet the underlying mechanism is not well known (J et al. 2011; Q et al. 2011; Truong et al. 2013; Xie, Kwok, and Scully 2009) .

In this study, we also examined how chemical inhibition of MRE11 nuclease function will affect the resection and consequently influence alt-EJ. We observed in wild type cells (CHO10B4: which is competent for DNA-PKcs), an increased accumulation of DSBs after inhibition of endo-nuclease function of MRE11 compared to DNA-PKcs mutant of CHO cells, IRS-20 (figure 48 and 49). This suggests that upon damage induction, DNA-PK complex bound DNA ends stimulate the endonuclease function of MRE11 and that is necessary to promote alt-EJ. A comparative repair proficient phenotype in DNA-PKcs mutant cells is reminiscent of what was observed in same mutant cell line after CtIP knockdown (Figure 35). However, the effect in DSBs rejoining after blocking its exonuclease activity remains unchanged both in wild type and DNA-PKcs deficient cells (figure 48 and 49). A study based on *in vitro* nuclease assay at Tanya Paul's lab showed that the efficiency in DNA end processing of MRE11 is enhanced when both DNA-PKcs and Ku are present. Consistent with this, despite detectable endonuclease activity of MRE11, we did not observe the sequential exonuclease activity. Nevertheless, we cannot also exclude the possibility of differential DSB response between *in vitro* and *in vivo* systems.

Notably, differential specificity of endo-nuclease specific small molecule inhibitor might result in divergent repair phenotype. Nuclease activity analysis showed that the inhibition of endonuclease activity caused by PFM03 was 98% compared to 60% by PFM01 - that was used in our current study (Deshpande et al. 2020). Not surprisingly, such widely divergent efficiency between two inhibitors would also contribute to the DSB repair outcome. It is highly likely that the reduced endonuclease activity of PFM01 would not be sufficient enough trigger the ensuing exonuclease activity of MRE11. As a consequence, efficient inhibition of endonuclease activity of MRE11 is thus required.

1.5 Alt-EJ of PCC breaks benefits from CtIP-dependent resection in CHO cells: a new finding

The functional role of CtIP in alt-EJ has previously been implicated in many studies including formation of chromosomal translocations and DNA end processing (Bennardo et al. 2008; Zhang and Jasin 2011). Experimental data from PFGE experiments converge on CtIP having functional roles in alt-EJ mediated DSBs repair and reveal that a substantial fraction of IR-induced DSBs is repaired with slow kinetics (figure 33-A). We anticipate that these residual DSBs result in the formation of chromosomal breaks. However, the functional interplay between CtIP and its role in repair of chromosomal breaks (PCC breaks) in G1 phase of cells is hitherto unknown. Using PCC assay, we documented a critical and yet previously overlooked end-processing function of CtIP in non-dividing G1 phase of the cell cycle in rodent cells. The relative low number of chromosomes (21), uniform analysis in G1, and most importantly, available derivative mutant cell lines make CHO an attractive tool for studying the chromosome breaks in any cell-cycle phase.

The results presented in figure 42 imply a substantial contribution of CtIP mediating alt-EJ pathway in chromosome break repair during interphase in c-NHEJ mutant cells. In wild type CHO cells, rejoining of chromosome breaks is efficient suggesting an equal contribution of both pathways (c-NHEJ and alt-EJ) and is independent of CtIP. It is, however, worth noting that cells deficient in c-NHEJ core factors remove most of their breaks albeit at a slower rate, which reflects the function of alt-EJ. It clearly demonstrates that the pathway in chromosome break repair is shunted from c-NHEJ to alt-EJ. The residual fraction in DNA-PKcs mutant cells of both DSBs and chromosome breaks is comparatively slower than that observed in DNA-PKcs proficient cell line (CHO10B4). Interestingly, the initial yield of chromosome breaks observed in DNA-PKcs cells is reminiscent of what was observed in DNA-PKcs inhibition condition in wild type cells suggesting DNA-PKcs inhibition exhibits equivalent c-NHEJ mutant phenotype. In support of this, we and others showed a significant contribution of c-NHEJ in chromosome breaks repair in a DNA-PKcs deficient mouse cell line (Evans et al. 1996; Terzoudi et al. 2008). In agreement with their alt-EJ dependent repair, rejoining in c-NHEJ mutant cells of IR-induced chromosomes strongly depends on CtIP. This indicates that resection is a decisive factor affecting the repair outcome of chromosomal breaks.

It is important to note that cells repair majority of IR-induced DSBs within 20-30 minutes using c-NHEJ, whereas the half time for chromosome repair is around 1-2 hours. Consequently, a subset of DSBs remained unrepaired, if they repair that is relatively with slow kinetics. It is

well considered that a subset of DSBs leads to chromosome breaks. Therefore it is considered that the fraction of slow repairing or sustained DSBs results in formation of chromosomal breaks. This comparative small fraction of persistent DSBs resulting in chromosome breaks might be associated with the nature of DSBs, for example, localization in chromatin (hetero or euchromatin) or in their genomic position (transcriptionally active or inactive region). A study focused on G1-cells convincingly showed that DSBs induced in transcriptionally active genes undergo DSB clustering and are associated with delayed repair. They further showed that this enhanced clustering is MRN complex dependent (Aymard et al. 2017). Yet the inherent nature, properties, functional consequences of DSBs leading to chromosomal breaks and pathways processing those breaks remained biochemically uncharacterized. However, the kinetics of chromosome break repair suggests that chromosome breaks arise from small amount of slow and persistent DSBs.

An intrinsic feature of alt-EJ is that it processes DSBs with slower kinetics. Importantly, the observations at the chromosome break level reveal that while breaks in wild type cells are mostly repaired by c-NHEJ, their repair in c-NHEJ mutant cells is dependent on CtIP and these breaks persist longer due to down-regulation of CtIP-mediated resection activity. Thus, in the context of slowly repairing DSBs in G1, earlier reports demonstrated that the fraction of DSBs rejoining with slow kinetics requires a coordinated end-processing activity of DNA-PKcs, Artemis and ATM thus raising the possibility of CtIP involvement (Aymard et al. 2017; Riballo et al. 2004). Given that DNA-PKcs stimulates the nuclease function of Artemis, its functional absence appears to allow resection to occur where this end-processing function is taken over by CtIP. Consistent with this, investigation of ATM phosphorylation sites of CtIP and independently of this, the proposed roles of ATM in the repair of a fraction of complex DSBs will be of particular importance, as slow repair process requires ATM.

Here, we report for the first time that PCC break repair in G1-arrested cells requires resection and that these breaks are processed by CtIP-dependent alt-EJ in cells deficient in core c-NHEJ factors such as DNA-PKcs and Ku80. Thus, chromosomal breaks following irradiation in G1 phase cells benefit from end processing factor CtIP in CHO cells. It is, however, important to characterize the properties of sustained DSBs, as well as the associated pathway that processes them. An interesting aspect for further investigation would be to elucidate the translocation formation by using a combination of both PCC assay and fluorescence *in situ* hybridization (FISH) method.

In addition, Parp is a DSB response factor that promotes alt-EJ to process DNA lesions and counteracts Ku binding to DSBs. Biochemical and genetic evidence implicates the

contribution of alt-EJ factors like ligase I, ligase III and Parp in DSB repair and is thought to operate as back-up for c-NHEJ. Alt-EJ is inherently mutagenic and chromosomal translocation formation is one of the manifestations of this pathway. It has previously been showed that both Parp and Ku compete for rapid binding to DNA ends. Other studies also demonstrated an enhanced translocation formation in irradiated c-NHEJ deficient G1 phase cells (Audebert, Salles, and Calsou 2004; Soni et al. 2014; Wang et al. 2005, 2006; Windhofer et al. 2007). To date, it is not clear how alt-EJ dependent Parp-1 and its involvement in alt-EJ contributes to chromosome break formation in G1 cells. Here we analyzed chromosome break formation in quiescent wild type and Ku80 mutant cells after CtIP depletion and observed a chromosome break repair deficient phenotype upon Parp inhibition. It further suggests that alt-EJ is backing up the predominantly active c-NHEJ pathway, but at the cost of chromosomal break formation. However, the observation of compromised chromosome break processing when resection is inhibited is independent of Parp. This suggests that the function of Parp in alt-EJ is likely to be resection independent and that the processing of breaks by Parp remains equally effective in wild type and c-NHEJ mutant cells.

Rad52 is another important factor during single strand annealing (SSA), a homology-directed pathway initiated when a DSB is generated between tandem repeat sequences. Due to deletion of the intervening sequence between the direct repeats, SSA generates large deletions and is thus highly erroneous (Haber n.d.). We enquired how in HRR deficient G1 phase, mutagenic Rad52-driven SSA pathway will be regulated in the context of processing of chromosome breaks. Analysis of Rad52 involvement in rejoining chromosomal breaks in CHO parental cells shows a Rad52 dependent repair of PCC breaks (figure 43-D). Interestingly, inhibition in Ku80 deficient cell line (XRS6) of Rad52 resulted in an increase in the numbers of chromosomal breaks (figure 44). It can be postulated that CtIP is associated with short range DNA end processing. However, if that process is somehow interrupted then long range resection apparatus takes over.

1.6 Bortezomib mediated ubiquitin-proteasome inhibition restrains DSB processing by CtIP

As outlined above, while majority of DSBs rejoining in G1 phase is mediated via fast-kinetics by c-NHEJ in wild type cells, a fraction of DSBs (~10-15%) is repaired with slow kinetics that results in chromosomal break formation. Thus, we attribute processing of this set of DSBs may be dependent on alt-EJ. Importantly and supporting previous findings, inhibition of c-NHEJ using DNA-PKcs inhibitor compromises the kinetics of DSB repair that is reflected by

an increase in the subset of unrepaired, persistent chromosome breaks - again hinting to alt-EJ pathway recruitment (Figure 45). Consistent with previous reports, we also demonstrate here that CtIP protein expression level is low in G1 phase compared to S/G2 phase and even lower in G0 cells. As such repair in G1-phase is compromised and mediated by alt-EJ. One possibility is that CtIP is ubiquitinated and degraded and thus no longer available to participate in DNA repair.

A study by Yu *et al,* demonstrated that CtIP is ubiquitinated by BRCA1 in a damage-induced manner, but is not degraded (Yu et al. 2006). Contrary to this, another study focused on ubiquitination and proteasome-dependent degradation of CtIP showed that SIAH-1, an E3 ligase family member, interacts with CtIP and mediates its degradation (Germani et al. 2003). Similarly, Sartori and co-workers revealed that prolyl isomerase PIN1 mediates CtIP ubiquitination and targets it for proteasomal degradation (Steger et al. 2013). However, how PIN1 isomerase in G1 is regulated has not been studied so far. We thus envision that chemical inhibition of ubiquitin-proteasome pathway will render repair efficient phenotype with a concomitant restoration of CtIP. To our surprise, despite its recuperation, the kinetics of DSB repair remained largely unaffected. Longer treatment with proteasome inhibitor bortezomib restores the CtIP protein expression to the level similar to that observed in exponentially growing cells (Figure 45-D and E), but show instead a compromised DSB repair identical to DNA-PKcs inhibited (single treatment) DSB repair phenotype in plateau phase cells (Figure 30-A and 45-A). This leads to a conundrum where rejoining of DSBs, as well as chromosome breaks are somehow inhibited in a CtIP independent manner and/or by nonproteasomal pathways which remain to be determined.

Due to its connection with ubiquitin mediated degradation, it is conceivable that CtIP might not be the only substrate of BRCA1 or SIAH-1 and may instead target other substrate proteins, which contain ubiquitin-binding domain (UBD). It is therefore intriguing to speculate that proteins other than BRCA1 negatively regulate and interact with ubiquitinated CtIP. An investigation linked with this aspect would provide insights into the functional role of CtIP ubiquitination of in repair of DSBs and chromosomal breaks in G1 phase of the cell cycle.

1.7 Processing of resected DSBs by alt-EJ in absence of Rad52

Despite the prominent homology-directed role of Rad52, it has been shown that cells with higher DSB loads require Rad52 for their processing (Mladenov, Staudt, et al. 2019). Since HR by default is suppressed at high doses of IR, the DSB repair is shunted to SSA. As such, either SSA or alt-EJ ultimately process resected DSBs generated at high dose that cannot

be processed by HRR. While alt-EJ requires short end resection, SSA profits from long-range resection. Thus, the length of homology functions as distinctive determinant between alt-EJ and SSA. We therefore investigated how these two pathways are regulated at high dose. It becomes evident that alt-EJ plays a prominent role in processing DSB loads in the absence of Rad52 (figure 50). We excluded the contribution of c-NHEJ at high dose by blocking the c-NHEJ pathway using NU7441. This suggests that at high DSB loads both SSA and alt-EJ process resected DSBs.

2 Investigation of differential 53BP1 signaling in clones sustaining simple and clustered-DSBs following expression of I-SceI

2.1 Gene silencing of RNF8/168 abrogates 53BP1 foci formation but not H2AX phosphorylation

53BP1's recruitment to sites of DSBs is dependent on two primary E3 ligases RNF8 and RNF168 in the DNA damage repair (DDR) pathway (Scheffner et al. 1995). In this study we used an RNAi-based approach to achieve an efficient knockdown of RNF8 and RNF168 that was manifested by absence of 53BP1 foci formation following ionizing radiation. Thus, we confirmed the efficiency and specificity of RNF8 and RNF168 targeting siRNA oligonucleotides by immunofluorescence staining of endogenous 53BP1 protein. Serendipitously, we achieved a highly efficient gene knockdown at 6 h which persisted till 48 h (figure 54 and 55). It has been shown that in response to IR or I-SceI induced DNA double strand breaks (DSBs), cells transiently transfected with the expression construct (GFP-fused to 53BP1 protein) also form GFP-tagged 53BP1 foci (GFP-53BP1) (Bekker-Jensen et al. 2005; Iliakis et al. 2018; Schipler et al. 2016). Consistent with this observation, we further showed that exogenous 53BP1 foci accrual to the sites of DSBs and is similar to endogenous 53BP1, and completely dependent on RNF8/RNF168 (figure 71-A). We confirmed previously published data that ring finger protein 8 and 168 function upstream of 53BP1 and their activity is required for IR-induced assembly of 53BP1 foci to the sites of DNA double strand breaks (DSBs). This further supports the notion that the presence of both E3 ligases is indispensable for efficient binding of downstream factor 53BP1.

DSB detection by MRN complex is followed first by ATM recruitment and then by the phosphorylation of H2AX in the DSB vicinity. These events promote the recruitment of 53BP1 (Bekker-Jensen et al. 2005; Lukas et al. 2004). To verify that endogenous 53BP1 knockout does not impair the initial DSB regulator γ-H2AX, we examined the IR-induced as well as I-

SceI induced phosphorylation of H2AX at the site of DSBs. Quantitative analysis of γ-H2AX foci formation showed that lack of endogenous 53BP1 or overexpression of 53BP1 in the form of GFP-53BP1 does not hinder prior formation of γ-H2AX foci (figure 61 and 63). Thus, we conclude that the ablation of RNF8/168 does not impair the initial recognition of DSBs by H2AX.

2.2 53BP1 ablation by siRNA of RNF8/168 is independent of the type of DSBs present

One focus of our study was to investigate the underpinning mechanism of DNA damage response towards simple DSBs and DSB clusters, and their differential regulation in DNA damage signaling. To gain more insights into the specific DNA damage response of either RNF8 or RNF168 depletion in clones following I-SceI expression, we monitored 53BP1 foci formation at different post-transfection times. It is important to mention that in this system continuous cutting and rejoining is possible whenever the I-SceI recognition site is restored after DSB rejoining. It is likely that repair mediated through c-NHEJ that synapses two broken ends can ultimately restore the I-SceI recognition site for a following DSB event to take place. This event is absent in the case of IR induced DSBs.

2.3 High-LET radiation modality shows low efficacy in killing RNF8/168-knockdown CHO cells

Ubiquitination, controlled by E3 ubiquitin ligases RNF8 and RNF168, plays a significant role in DDR. Upon damage induction, ubiquitination cascade regulated by E3 ligases triggers the localization of 53BP1 at DNA breaks. Consistent with previous study we here also showed that two E3 ubiquitin ligases are involved in DDR by recruiting a more downstream c-NHEJ component, 53BP1 (Bekker-Jensen and Mailand 2011). Previous research showed RNF8 as well as RNF168 knockdown sensitizes human cells to IR (Mailand et al. 2007; Stewart et al. 2009; Zhao et al. 2016). Here we explored and compared how these two RING finger proteins regulate the sensitivity of rodent CHO cells towards different radiation modalities (high-and low-LET) following their targeted gene knockdown by RNAi. CHO cells depleted in RNF8/168 exhibited higher radio sensitivity than their wild type counterparts. It suggests impairment of the ubiquitination pathway and thus deregulation in recruiting downstream DDR factors appears to be the underpinning mechanism of radio sensitization. Conversely, α-particles did not sensitize cells depleted for RNF8/168 suggesting that the quality of DSB lesions may affect the choice of repair pathway significantly (figure 57).

Indeed, previous work based on biological model from our lab demonstrated that the contribution of c-NHEJ pathway in repairing complex lesions (DSB-clusters) is less than in simple DSB lesions (Iliakis et al. 2018; Schipler et al. 2016). Although it is widely accepted that the ionization event along with the radiation track critically regulates the differential effect between high- and low-LET irradiation, clustered DNA lesions resulting from high-LET radiation pose more threats to cellular DSB repair systems compared to low-LET (Allen et al. 2011).

Correspondingly, our biological model system demonstrated an approach to mimic and analyze the physical characteristics of radiation-induced DSB clustering in a biologically controlled manner. We thus provided strong evidence supporting clustered-DSBs as a determinant of radiation-induced cell death and such event compromise the processing of DSBs by c-NHEJ pathway. Comparative genetic study based on transgenic mouse mutation assay showed that densely IR (high-LET) generated deletions which are more than 100bp in size, while sparsely IR by X-ray or γ-ray produced mostly short deletions. A mechanistic explanation for this is that mutation induced by low-LET is indirectly mediated through generation of reactive oxygen species (ROS), whereas in case of high-LET, mutations are induced by means of direct ionization event occurring at the DNA (Masumura et al. 2002).

Our findings altogether indicate that inhibition of ubiquitination process via silencing of RNF8 and RNF168 attenuated radio resistance and enhanced cell killing in CHO cells after exposure to low-LET but not to high-LET irradiation (figure 56). The underlying mechanism of c-NHEJ deficient cells lacking a high-LET mediated radio sensitization requires further investigation.

2.4 No increase in total residual DSB-loads following irradiation in clones already expressing I-SceI

The expressed I-SceI recognizes the genetically integrated 18bp recognition site of I-SceI enzyme thus generating DNA double strand breaks in a systematic manner. On the other hand, IR induces a wide variety of lesions including DSBs, SSBs and base damages. Thus, in our biological model system adverse consequences associated only with DSBs can be analyzed, thereby excluding largely the effects caused by single stranded breaks and base damages. Biological consequences associated with additional IR-induced DSBs in I-SceI site containing reporter cell lines have been studied in our very recent work (Mladenov, Staudt, et al. 2019). In the similar fashion, here we investigated whether I-SceI-induced DSBs confer any additional DSB-burden to irradiated cells. We demonstrated that DSBs generated at

integrated I-SceI meganuclease recognition sites do not elicit any additional detrimental cellular effects in the irradiated cells. IR-induced DSBs may not influence the enzymatic generation of DSBs, as it is unlikely that IR will hit such a small recognition site there in the genome. Even if there are direct hits by IR within I-SceI site, cells may take it as one break. We further explored the additional impacts of I-SceI induced DSBs in irradiated clonal cells already harboring DSBs of simple and complex type with a concomitant gene silencing of two E3 ligases (RNF8 and RNF168) (figure 58 and 59). Intriguing findings here, and previously published results indicate an engagement of c-NHEJ in the processing simple DSBs.
Thus, these results confirmed that DSBs induced in a combined RE-and-IR-induced manner did not increase the total yield of DSBs.

2.5 Ectopically expressed GFP-53BP1 foci co-localize with endogenous 53BP1 and γ-H2AX

IR-induced H2AX phosphorylation at serine 139 at sites of DNA damage is a very early step of DSB response. γ-H2AX staining has been reported to overlap with other critical DNA-damage response factors like MDC1, MRN complex, BRCA1,CHK2 and also to co-localize in ionizing radiation induced foci (IRIF) with 53BP1 (Lou et al. 2003; Rao et al. 2007; Wang et al. 2002). Consistently, we here demonstrated a co-existence of both DNA damage responders' γ-H2AX and 53BP1 (endogenous and exogenous) in the DSB-surrounded chromatin. This co-localization trend was observed in human (D-U2OS, U2OS-wt and A549) as well in CHO cells (parental and clonal cells) (figure 72 and 74).
It is also notable that upon exposure to IR, GFP-53BP1 foci always co-existed with those containing endogenous 53BP1, suggesting that ectopically expressed GFP-53BP1 foci recapitulates the DDR related physiological functions of endogenous 53BP1 protein. In addition, ectopic expression of GFP-53BP1 was carried out in cells lacking endogenous 53BP1 protein and thus, the relocation of exogenous GFP-53BP1 foci to the DSB sites reveals an essential role of 53BP1 in DNA damage response. Most importantly, visualization of the endogenous proteins at the same location as of the GFP-tagged protein re-confirms binding of the antibody with the specific target protein and shows that damage induced (by IR or I-SceI) relocation of GFP-53BP1 does not alter the distribution of the endogenous 53BP1 protein. Thus, our findings suggest that in rodent cells, identical to human cells, GFP-53BP1 foci have DNA damage regulatory function and this response is not distinct from I-SceI induced DSBs.

2.6 Disruption of ubiquitination results in compromised processing of simple DSBs by c-NHEJ

Supporting our previous finding, we also reconfirmed that complex-DSBs are more efficient in cell killing than simple-DSBs (Iliakis et al. 2018; Schipler et al. 2016). The induction of cell killing by single-DSBs increased three times following ubiquination cascade perturbation. Similarly, DSB-quadruplets also exhibited the same degree of increase in cytotoxicity. This finding illustrates that the tested E3 ligases play a critical role in regulating the effectiveness of ubiquitination. Our study entails the quantitative analysis of chromosomal translocation formation in clones harboring simple types, as well as complex types of DSBs (Iliakis et al. 2018; Schipler et al. 2016). Depletion in simple-DSBs of RNF8 had no apparent effect, while concomitant knockdown of RNF168 had additive effect on translocation formations. Notably, co-depletion of RNF8 and RNF168 increased the translocations almost by a factor of two (figure 65-A).

Processing of the lesions by an existing pathway with fast kinetics ensures suppression of chromosomal translocation formation. However, interference with 53BP1 recruitment or its upstream signaling machinery by gene silencing put this pathway on hold, thus increasing the incidence of chromosomal translocations with similar efficiency as in the cells harboring DSB-clusters. Conversely, combined knockdown of both ubiquitin ligases in complex-DSBs did not cause a substantial increase in translocations (figure 65-B). Supporting our previous observation, this result suggests that with increasing DSB-complexity the engagement of c-NHEJ is compromised and repair instead is mediated by an alternative form of DSB rejoining (alt-EJ). Altogether our study demonstrates that perturbation of key c-NHEJ factors, which function through the ubiquitination cascade, reduces the repair efficiency of simple DSBs and thus causes increase in translocation formation.

2.7 Simple types of DSBs rely on c-NHEJ for processing

A mechanistic explanation of the effects of DSB-related complexity: DSB-clusters, which especially occurs after exposure to high-LET radiation of cells has been offered recently (Iliakis et al. 2018, 2019; Schipler et al. 2016). When a particular DSB comprises additional lesions in the vicinity, it increases its complexity and shows more potential in destabilizing chromatin. Correspondingly, it has been shown also that clustered-DSBs have markedly more killing potential than simple-DSBs. Thus, this offers a plausible mechanistic explanation for the increased potential in killing of high-LET radiation. One of the important findings from

our previous study is that the contribution in processing DSBs of c-NHEJ is compromised within DSB-clusters. On the other hand, simple-DSB lesions rely more on c-NHEJ for their repair. As a result, we elucidated further the underpinning mechanism of simple DSBs and the relevance for their functional dependence on c-NHEJ by looking at more downstream repair factors.

DNA damage response (DDR) evoked by DSBs initiates a signaling cascade that begins with ATM dependent phosphorylation of H2AX (γ-H2AX) that facilitates subsequent recruitment of DNA damage response regulators Mdc1, RNF8, RNF168, 53BP1 and/or BRCA1. RNF8 and RNF168 mediated histone ubiquitination (K63-linked polyubiquitination) promotes assembly of c-NHEJ pathway decisive factor, 53BP1. Consistent with this, we further investigated the contribution of these two E3 ligase factors in the processing of simple DSBs and DSB clusters. Since single-DSBs rely on c-NHEJ, we considered that gene silencing of ubiquitin ligases would diminish the contribution of c-NHEJ. From the findings it became evident that ubiquitination plays a significant role in suppressing translocation formation. However, the ability to keep the formation of translocations in check is diminished when the ubiquitination process is impaired. Reduction of RNF8/168 impairs the 53BP1 activation, thus impeding the recruitment of 53BP1 to IRIF (figure 75-A and B). The sustained presence of 53BP1 in clones harboring complex-DSBs suggests a DSB-induced persistent 53BP1 signaling.

VI Summary

It is well known that classical non-homologous end joining (c-NHEJ) and homologous recombination repair (HRR) are the two main conserved pathways for DSB repair in higher eukaryotes. When compromised, cells employ an alternative end-joining (alt-EJ) mechanism to repair DSBs with slower kinetics. Contrary to the c-NHEJ, which is independent of cell growth state, alt-EJ shows dependence on growth state of the cells and is compromised in quiescent cells. Surprisingly, DNA-PKcs deficient cells maintained in plateau phase displayed active and functional alt-EJ. Recent studies focused on DNA-PKcs$^{-/-}$ cells revealed an active involvement of DNA end resection especially in quiescence stage (G0) of the cell cycle where alt-EJ is also functional. Therefore, the current study aimed at investigating the functional role of CtIP and DNA-PKcs in the regulation of alt-EJ mediated DSB repair.

The results obtained from our experiments demonstrated a significant suppression of alt-EJ upon depletion of CtIP in exponentially growing but also in serum deprived wild type cells suggesting CtIP plays a role in DNA-PKcs proficient cells. Intriguingly and contrary to DNA-PKcs proficient cells, DNA-PKcs deficient cells maintained in exponential as well as in plateaus phase showed efficient rejoining of DSBs suggesting an active involvement of alt-EJ. It is thus reasonable to deduce that DNA-PKcs proficient cells entering quiescent state of growth show marked dependence on alt-EJ while DNA-PKcs deficient cells fail. It further suggests activated DSB processing in wild type cells requires alt-EJ dependent resection and is mainly regulated by resection component like CtIP. However, DNA-PKcs deficient cells withstand alt-EJ and its requirement of limited DNA end resection in G1 cells entering plateau phase of growth, which requires further investigation.

Contrary to DNA-PKcs mutant cell lines, Ku80 mutant cells showed a marked reduction in their DSB rejoining capacity suggesting that the absence of DNA end tethering factor Ku70/80 may allow access for CtIP to resect the DNA ends thus facilitating alt-EJ mediated repair.

We also showed a marked sensitization of cells depleted in CtIP towards ionizing radiation. Furthermore, we demonstrated a moderate radio-sensitization of cells mutant in HRR suggesting that besides its involvement in HRR, CtIP can also operate in alt-EJ repair pathway in G2 phase of the cell cycle.

To investigate whether DNA end-processing is an essential requirement for alt-EJ in G1 phase cells, we investigated the requirement for CtIP in alt-EJ in G1 phase cells, which is

resection dependent albeit to a limited extent. Consistent with previous observations, we also found a significant resection activity in DNA-PKcs mutant cells.

Furthermore, we investigated the dependence of chromosome break repair on CtIP mediated resection in irradiated G0 wild type (CHO10B4) and c-NHEJ mutant cell lines (IRS-20 and XRS-6) derived from Chinese hamster ovary by examining premature chromosome condensation (PCC) breaks. In wild type cells, chromosome breaks are repaired effectively suggesting majority of IR-induced chromosome breaks are repaired through c-NHEJ. In contrast, a significant reduction is noted in c-NHEJ mutant cells suggesting a functional role of alt-EJ at the chromosome level. We thus revealed a hitherto unknown role of resection in repairing chromosomal breaks in G1 phase of the cell cycle and found that CtIP is indispensable for repair of G1-PCC breaks in CHO cells.

Taken together, our work demonstrated for the first time an important functional link between CtIP-mediated DNA end-resection and its role in repair of chromosome breaks in G1 phase of the cell cycle that is mediated by alt-EJ.

Previous findings from our laboratory demonstrated an association between persistent 53BP1 signaling and clustered-DNA damage, suggesting a compromised processing by c-NHEJ and thus shunting of DSBs towards error-prone alt-EJ at the cost of elevated chromosomal translocation formation. Consistent with this we investigated via indirect immunofluorescence the correlation between 53BP1 signaling and complex forms of DSBs It is widely accepted that the recruitment of 53BP1 to the sites of DSBs is dependent on sequential activation of two primary E3 ubiquitin ligases: RNF8 and RNF168. By RNA interference (RNAi) and subsequent immunofluorescence experiments we convincingly showed that these two ring finger E3 ligases act as a molecular linker between initial mark of DNA damage, γ-H2AX, and more downstream repair pathway choice with the help of 53BP1. In the present study, in line with previous findings, we also observed a sustained retention of 53BP1 foci in clones harboring complex-DSBs supporting again the notion that DSB-clustering is a relevant parameter of DSB complexity. Moreover, by employing cytogenetic methods, we analyzed chromosome aberration formation at metaphase in clones sustaining single DSBs or DSB clusters of increasing complexity following expression of I-SceI, with concomitant knockdown of RNF8/168. The results obtained showed that interference in ubiquitin signaling increases the degree of erroneous processing of simple DSBs that can be manifested with high yields of chromosomal translocation formation. It suggests that when c-NHEJ is compromised, simple lesions initiate DDR signaling which is in a way reminiscent of complex types of lesions.

In order to investigate the physiological relevant of ectopically expressed GFP-53BP1 foci with endogenous 53BP1 foci, we transiently expressed in cells of plasmid expressing a fusion protein containing GFP (GFP-53BP1). Transiently expressed green fluorescence protein (GFP) tagged with a truncated version of human 53BP1 protein in rodent cells (CHO), as well as in human cells (U2OS, D-U2OS, A549), showed its distribution as GFP-53BP1 foci in the DSB-flanking chromatin. As anticipated, endogenous 53BP1, as well as exogenous GFP-53BP1 overlapped with γ-H2AX decorated chromatin in both IR and I-SceI mediated DSBs.
Since our biological model system based on DSB clusters provided insights into the increased efficacy of high-LET radiation, we further studied how depletion of RNF8 and RNF168 is regulated between their exposures to high- and low-LET radiation. We observed that in the absence of RNF8/168, parental CHO cells exhibited elevated cellular sensitivity in response to IR, while the sensitivity remained almost unaffected following α-particle irradiation indicating that the ubiquitin ligase cascade responds differentially between sparsely ionizing radiation (low-LET) and densely ionizing radiation (high-LET).
Altogether, these findings suggest that the E3 ligase cascade consisting of RNF8 and RNF168 plays a critical role in DNA damage signaling.

VII Zusammenfassung

In höheren Eukaryoten sind die klassische nicht-homologe Endverknüpfung (c-NHEJ) und die homologe Rekombinationsreparatur (HRR) die beiden wichtigsten und lang bewährten Wege für die DSB-Reparatur. Wenn sie kompromittiert werden, verwenden Zellen einen alternativen Endverknüpfungsmechanismus (Alt-EJ), um DSBs mit langsamerer Kinetik zu reparieren. Im Gegensatz zum c-NHEJ, das unabhängig vom Zellwachstumszustand ist, zeigt alt-EJ eine Abhängigkeit von der Wachstumsphase der Zellen und ist vor allem in ruhenden Zellen stark beeinträchtigt. Überraschenderweise zeigten DNA-PKcs-defiziente Zellen in der Plateau-Phase funktionelle und aktive Alt-EJ. Jüngste Studien zeigten im Ruhezustand (G0) des Zellzyklus, in dem auch Alt-EJ funktionsfähig ist, eine aktive Beteiligung der DNA-Endresektion. Daher zielte die vorliegende Studie darauf ab, die funktionelle Rolle von CtIP und DNA-PKcs bei der Regulation der Alt-EJ-vermittelten DSB-Reparatur zu untersuchen. Die aus unseren Experimenten erhaltenen Ergebnisse zeigten nach Herunterregulierung von CtIP eine signifikante Unterdrückung von Alt-EJ in exponentiell wachsenden Wildtypzellen, aber auch unter Serumentzug, was darauf hindeutet, dass CtIP eine Rolle in DNA-PKcs-profizienten Zellen spielt. Interessanterweise und im Gegensatz zu DNA-PKcs-profizienten Zellen zeigten DNA-PKcs-Wildtyp-Zellen, die sowohl in der exponentiellen als auch in der Plateau-Phase gehalten wurden, eine effiziente Wiederverknüpfung von DSBs, was auf eine aktive Beteiligung von Alt-EJ hinweist. Es ist daher vernünftig zu folgern, dass DNA-PKcs-profiziente Zellen, die in den Ruhezustand eintreten, eine deutliche Abhängigkeit von Alt-EJ zeigen, während DNA-PKcs-defiziente Zellen hier versagen. Es legt nahe, dass die aktivierte DSB-Verarbeitung in Wildtyp-Zellen eine Alt-EJ-abhängige Resektion erfordert und hauptsächlich durch Resektionskomponenten wie CtIP reguliert wird. DNA-PKcs-defiziente Zellen widerstehen jedoch Alt-EJ und dessen Erfordernis einer begrenzten DNA-Endresektion in G1-Zellen, die in die Plateau-Wachstumsphase eintreten, was weitere Untersuchungen erfordert. Im Gegensatz dazu zeigten Ku80-Mutantenzellen eine deutliche Verringerung ihrer DSB-Wiederverknüpfungskapazität, was darauf hindeutet, dass das Fehlen des DNA-End-Verbindungsfaktors Ku70/80 CtIP den Zugang zur Resektion der DNA-Enden ermöglichen könnte, wodurch die Alt-EJ-vermittelte Reparatur erleichtert wird.

Wir zeigten auch eine deutliche Sensibilisierung von CtIP herunterregulierten Zellen gegenüber ionisierender Strahlung. Darüber hinaus zeigten wir eine moderate Radiosensibilisierung von Zellen, die in der HRR mutiert sind, was darauf hindeutet, dass

CtIP neben seiner Beteiligung an der HRR auch im Alt-EJ-Reparaturweg in der G2-Phase des Zellzyklus arbeiten kann.
Um zu untersuchen, ob die DNA-Endverarbeitung eine wesentliche Anforderung für Alt-EJ in G1-Phase-Zellen ist, haben wir die Anforderung für CtIP in Alt-EJ in G1-Phase-Zellen untersucht, die, wenn auch in begrenztem Umfang, resektionsabhängig ist. In Übereinstimmung mit früheren Beobachtungen fanden wir auch eine signifikante Resektionsaktivität in DNA-PKcs-Mutantenzellen. Bei der Untersuchung der Abhängigkeit der Reparatur von Chromosomenbrüchen von der CtIP-vermittelten Resektion stellten wir außerdem fest, dass ein erheblicher Teil der Wiederverknüpfungs-Ereignisse eine Endresektion erfordert, was auf eine funktionelle Rolle von Alt-EJ auf Chromosomenebene hindeutet. Wir haben daher eine bisher unbekannte Rolle der Resektion bei der Reparatur von Chromosomenbrüchen in der G1-Phase des Zellzyklus entdeckt und festgestellt, dass CtIP für die Reparatur von G1-PCC-Brüchen in CHO-Zellen unverzichtbar ist.
Zusammengenommen zeigten unsere Arbeiten zum ersten Mal einen wichtigen funktionellen Zusammenhang zwischen der CtIP-vermittelten DNA-Endresektion und ihrer Rolle bei der Reparatur von Chromosomenbrüchen in der G1-Phase des Zellzyklus, die durch alt-EJ vermittelt wird.
Frühere Ergebnisse aus unserem Labor zeigten einen Zusammenhang zwischen anhaltender 53BP1-Signalübertragung und DNA-Cluster-Schädigung, was auf eine beeinträchtigte Verarbeitung durch c-NHEJ und damit auf die Verlagerung von DSBs in Richtung fehleranfälliger Alt-EJ auf Kosten einer erhöhten chromosomalen Translokationsbildung hindeutet. In Übereinstimmung damit untersuchten wir mittels indirekter Immunfluoreszenz die Korrelation zwischen 53BP1-Signalen und komplexen Formen von DSBs. Es ist allgemein bekannt, dass die Rekrutierung von 53BP1 an die DSBs von der sequentiellen Aktivierung zweier primären E3-Ubiquitin-Ligasen abhängt: RNF8 und RNF168. Durch RNA-Interferenz (RNAi) und anschließende Immunfluoreszenz-Experimente konnten wir überzeugend zeigen, dass diese beiden Ringfinger-E3-Ligasen mit Hilfe von 53BP1 als molekularer Linker zwischen der anfänglichen Markierung der DNA-Schädigung (γ-H2AX) und einer nachgeschalteten Reparaturwegwahl fungieren. In der vorliegenden Studie beobachteten wir in Übereinstimmung mit früheren Befunden auch eine anhaltende Retention von 53BP1-Foki in Klonen mit komplexen DSBs, was wiederum die Annahme stützt, dass DSB-Clustering ein relevanter Parameter der DSB-Komplexität ist. Darüber hinaus analysierten wir mithilfe zytogenetischer Methoden die Bildung von Chromosomenaberrationen in der Metaphase in Klonen, die einzelne DSBs oder DSB-

Cluster mit zunehmender Komplexität nach Expression von I-SceI mit gleichzeitigem Abbau von RNF8/168 erhalten. Die erhaltenen Ergebnisse zeigten, dass eine Störung der Ubiquitin-Signalübertragung den Grad der fehlerhaften Verarbeitung einfacher DSBs erhöht, der sich mit hohen Ausbeuten in chromosomaler Translokationsbildung manifestieren kann. Es deutet darauf hin, dass bei einer Beeinträchtigung von c-NHEJ einfache Läsionen eine DDR-Signalübertragung auslösen, die in gewisser Weise an komplexe Arten von Läsionen erinnert.

Um die physiologische Relevanz von ektopisch exprimierten GFP-53BP1-Foki mit endogenen 53BP1-Foki zu untersuchen, exprimierten wir transient ein GFP enthaltendes Fusionsprotein (GFP-53BP1) in Zellen. Transient exprimiertes grün fluoreszierendes Protein (GFP), das mit einer verkürzten Version des menschlichen 53BP1-Proteins in Nagetierzellen (CHO) sowie in menschlichen Zellen (U2OS, D-U2OS, A549) markiert war, zeigte seine Verteilung als GFP-53BP1-Foki in DSB-flankierendem Chromatin. Wie erwartet überlappten endogenes 53BP1 sowie exogenes GFP-53BP1 mit γ-H2AX-dekoriertem Chromatin sowohl an IR- als auch in I-SceI-vermittelten DSBs.

Da unser auf DSB-Clustern basierendes biologisches Modellsystem Einblicke in die erhöhte Wirksamkeit von Strahlung mit hohem LET lieferte, haben wir weiter untersucht, wie die Herunterregulierung von RNF8 und RNF168 zwischen der Exposition gegenüber Strahlung mit hohem und niedrigem LET reguliert wird. Wir beobachteten, dass in Abwesenheit von RNF8/168 parentale CHO-Zellen eine erhöhte zelluläre Empfindlichkeit als Reaktion auf IR zeigten, während die Empfindlichkeit nach Bestrahlung mit α-Partikeln nahezu unbeeinflusst blieb, was darauf hinweist, dass die Ubiquitin-Ligase-Kaskade zwischen dünn ionisierender Strahlung (Niedrig-LET) und dicht ionisierende Strahlung (Hoch-LET) unterschiedlich reagiert. Insgesamt deuten diese Ergebnisse darauf hin, dass die aus RNF8 und RNF168 bestehende E3-Ligasekaskade eine entscheidende Rolle bei der Signalübertragung von DNA-Schäden spielt.

VIII References

Alberts, Bruce. n.d. *Molecular Biology of the Cell*.

Allen, Christopher, Thomas B. Borak, Hirohiko Tsujii, and Jac A. Nickoloff. 2011. “Heavy Charged Particle Radiobiology: Using Enhanced Biological Effectiveness and Improved Beam Focusing to Advance Cancer Therapy.” *Mutation Research* 711(1–2):150–57.

Alt, Frederick W., Yu Zhang, Fei-Long Meng, Chunguang Guo, and Bjoern Schwer. 2013. “Mechanisms of Programmed DNA Lesions and Genomic Instability in the Immune System.” *Cell* 152(3):417–29.

Anand, Roopesh, Lepakshi Ranjha, Elda Cannavo, and Petr Cejka. 2016. “Phosphorylated CtIP Functions as a Co-Factor of the MRE11-RAD50-NBS1 Endonuclease in DNA End Resection.” *Molecular Cell* 64(5):940–50.

Andres, Sara N. and R. Scott Williams. 2017. “CtIP/Ctp1/Sae2, Molecular Form Fit for Function.” *DNA Repair* 56:109–17.

Anon. n.d. “DEFINED BIOLOGICAL MODELS OF HIGH-LET RADIATION LESIONS.”

Audebert, Marc, Bernard Salles, and Patrick Calsou. 2004. “Involvement of Poly(ADP-Ribose) Polymerase-1 and XRCC1/DNA Ligase III in an Alternative Route for DNA Double-Strand Breaks Rejoining.” *The Journal of Biological Chemistry* 279(53):55117–26.

Averbeck, Nicole B., Oliver Ringel, Maren Herrlitz, Burkhard Jakob, Marco Durante, and Gisela Taucher-Scholz. 2014. “DNA End Resection Is Needed for the Repair of Complex Lesions in G1-Phase Human Cells.” *Cell Cycle* 13(16):2509–16.

Aymard, François, Marion Aguirrebengoa, Emmanuelle Guillou, Biola M. Javierre, Beatrix Bugler, Coline Arnould, Vincent Rocher, Jason S. Iacovoni, Anna Biernacka, Magdalena Skrzypczak, Krzysztof Ginalski, Maga Rowicka, Peter Fraser, and Gaëlle Legube. 2017. “Genome-Wide Mapping of Long-Range Contacts Unveils Clustering of DNA Double-Strand Breaks at Damaged Active Genes.” *Nature Structural & Molecular Biology* 24(4):353–61.

Bailey, Susan M. and Joel S. Bedford. 2006. “Studies on Chromosome Aberration Induction: What Can They Tell Us about DNA Repair?” *DNA Repair* 5(9–10):1171–81.

Bakr, Ali, Sabrina Köcher, Jennifer Volquardsen, Cordula Petersen, Kerstin Borgmann, Ekkehard Dikomey, Kai Rothkamm, and Wael Y. Mansour. 2016. “Impaired 53BP1/RIF1 DSB Mediated End-Protection Stimulates CtIP-Dependent End Resection and Switches the Repair to PARP1-Dependent End Joining in G1.” *Oncotarget* 7(36):57679–93.

Ball Jr., Alexander R. and Kyoko Yokomori. 2001. “The Structural Maintenance of Chromosomes (SMC) Family of Proteins in Mammals.” *Chromosome Research* 9(2):85–96.

Barton, Olivia, Steffen C. Naumann, Ronja Diemer-Biehs, Julia Künzel, Monika Steinlage, Sandro Conrad, Nodar Makharashvili, Jiadong Wang, Lin Feng, Bernard S. Lopez, Tanya T. Paull, Junjie Chen, Penny A. Jeggo, and Markus Löbrich. 2014. “Polo-like Kinase 3 Regulates CtIP during DNA Double-Strand Break Repair in G1.” *The Journal of Cell Biology* 206(7):877–94.

Beck, Carole, Isabelle Robert, Bernardo Reina-San-Martin, Valérie Schreiber, and Françoise Dantzer. 2014. “Poly(ADP-Ribose) Polymerases in Double-Strand Break Repair: Focus on PARP1, PARP2 and PARP3.” *Experimental Cell Research* 329(1):18–25.

Bekker-Jensen, Simon, Claudia Lukas, Fredrik Melander, Jiri Bartek, and Jiri Lukas. 2005. “Dynamic Assembly and Sustained Retention of 53BP1 at the Sites of DNA Damage Are Controlled by Mdc1/NFBD1.” *Journal of Cell Biology* 170(2):201–11.

Bekker-Jensen, Simon and Niels Mailand. 2011. “The Ubiquitin- and SUMO-Dependent Signaling Response to DNA Double-Strand Breaks.” *FEBS Letters* 585(18):2914–19.

Bekker-Jensen, Simon, Jannie Rendtlew Danielsen, Kasper Fugger, Irina Gromova, Annika Nerstedt, Claudia Lukas, Jiri Bartek, Jiri Lukas, and Niels Mailand. 2010. “HERC2 Coordinates Ubiquitin-Dependent Assembly of DNA Repair Factors on Damaged Chromosomes.” *Nature Cell Biology* 12(1):80–86; sup pp 1-12.

Bennardo, Nicole, Anita Cheng, Nick Huang, and Jeremy M. Stark. 2008. “Alternative-NHEJ Is a Mechanistically Distinct Pathway of Mammalian Chromosome Break Repair.” *PLoS Genetics* 4(6):e1000110.

Bennardo, Nicole, Amanda Gunn, Anita Cheng, Paul Hasty, and Jeremy M. Stark. 2009. “Limiting the Persistence of a Chromosome Break Diminishes Its Mutagenic Potential.” edited by G. P. Copenhaver. *PLoS Genetics* 5(10):e1000683.

Bhargava, Ragini, David O. Onyango, and Jeremy M. Stark. 2016. “Regulation of Single-Strand Annealing and Its Role in Genome Maintenance.” *Trends in Genetics* 32(9):566–75.

Bi, Baoyuan, Nataliya Rybalchenko, Efim I. Golub, and Charles M. Radding. 2004. “Human and Yeast Rad52 Proteins Promote DNA Strand Exchange.” *Proceedings of the National Academy of Sciences of the United States of America* 101(26):9568–72.

Bindra, Ranjit S., Alexander G. Goglia, Maria Jasin, and Simon N. Powell. 2013. “Development of an Assay to Measure Mutagenic Non-Homologous End-Joining Repair Activity in Mammalian Cells.” *Nucleic Acids Research* 41(11).

Blackford, Andrew N. and Stephen P. Jackson. 2017. “ATM, ATR, and DNA-PK: The Trinity at the Heart of the DNA Damage Response.” *Molecular Cell* 66(6):801–17.

Blier, P. R., A. J. Griffith, J. Craft, and J. A. Hardin. 1993. “Binding of Ku Protein to DNA. Measurement of Affinity for Ends and Demonstration of Binding to Nicks.” *The Journal of Biological Chemistry* 268(10):7594–7601.

Bohgaki, Toshiyuki, Miyuki Bohgaki, and Razqallah Hakem. 2010. “DNA Double-Strand Break Signaling and Human Disorders.” *Genome Integrity* 1(1):15.

Bryant, P. E. and P. J. Johnston. 1993. “Restriction-Endonuclease-Induced DNA Double-Strand Breaks and Chromosomal Aberrations in Mammalian Cells.” *Mutation Research* 299(3–4):289–96.

C, Richardson, Moynahan ME, and Jasin M. 1998. “Double-Strand Break Repair by Interchromosomal Recombination: Suppression of Chromosomal Translocations.” *Genes & Development* 12(24).

Cannan, Wendy J. and David S. Pederson. 2016. “Mechanisms and Consequences of Double-Strand DNA Break Formation in Chromatin.” *Journal of Cellular Physiology*

231(1):3.

Ceccaldi, Raphael, Beatrice Rondinelli, and Alan D. D'Andrea. 2016. "Repair Pathway Choices and Consequences at the Double-Strand Break." *Trends in Cell Biology* 26(1):52–64.

CH, Bassing, Suh H, Ferguson DO, Chua KF, Manis J, Eckersdorff M, Gleason M, Bronson R, Lee C, and Alt FW. 2003. "Histone H2AX: A Dosage-Dependent Suppressor of Oncogenic Translocations and Tumors." *Cell* 114(3).

Chang, Howard H. Y., Nicholas R. Pannunzio, Noritaka Adachi, and Michael R. Lieber. 2017. "Non-Homologous DNA End Joining and Alternative Pathways to Double-Strand Break Repair." *Nature Reviews. Molecular Cell Biology* 18(8):495–506.

Chapman, J. Ross, Patricia Barral, Jean-Baptiste Vannier, Valérie Borel, Martin Steger, Antonia Tomas-Loba, Alessandro A. Sartori, Ian R. Adams, Facundo D. Batista, and Simon J. Boulton. 2013. "RIF1 Is Essential for 53BP1-Dependent Nonhomologous End Joining and Suppression of DNA Double-Strand Break Resection." *Molecular Cell* 49(5):858–71.

Chen, Y., A. A. Farmer, C. F. Chen, D. C. Jones, P. L. Chen, and W. H. Lee. 1996. "BRCA1 Is a 220-KDa Nuclear Phosphoprotein That Is Expressed and Phosphorylated in a Cell Cycle-Dependent Manner." *Cancer Research* 56(14):3168–72.

Cheng, Yanlei, Fanghua Li, Emil Mladenov, and George Iliakis. 2015. "The Yield of DNA Double Strand Breaks Determined after Exclusion of Those Forming from Heat-Labile Lesions Predicts Tumor Cell Radiosensitivity to Killing." *Radiotherapy and Oncology* 116(3):366–73.

Chun, Jarin, Erika S. Buechelmaier, and Simon N. Powell. 2013. "Rad51 Paralog Complexes BCDX2 and CX3 Act at Different Stages in the BRCA1-BRCA2-Dependent Homologous Recombination Pathway." *Molecular and Cellular Biology* 33(2):387–95.

CJ, Bakkenist and Kastan MB. 2003. "DNA Damage Activates ATM Through Intermolecular Autophosphorylation and Dimer Dissociation." *Nature* 421(6922).

Cornforth, M. N. and J. S. Bedford. 1993. "Ionizing Radiation Damage and Its Early Development in Chromosomes." *Advances in Radiation Biology* 17:423–96.

D, Simsek, Brunet E, Wong SY, Katyal S, Gao Y, McKinnon PJ, Lou J, Zhang L, Li J, Rebar EJ, Gregory PD, Holmes MC, and Jasin M. 2011. "DNA Ligase III Promotes Alternative Nonhomologous End-Joining During Chromosomal Translocation Formation." *PLoS Genetics* 7(6).

Daley, James M. and Patrick Sung. 2014. "53BP1, BRCA1, and the Choice between Recombination and End Joining at DNA Double-Strand Breaks." *Molecular and Cellular Biology* 34(8):1380–88.

Deckbar, Dorothee, Penny A. Jeggo, and Markus Löbrich. 2011. "Understanding the Limitations of Radiation-Induced Cell Cycle Checkpoints." *Critical Reviews in Biochemistry and Molecular Biology* 46(4):271–83.

Deshpande, Rajashree A., Ji-Hoon Lee, Sucheta Arora, and Tanya T. Paull. 2016. "Nbs1 Converts the Human Mre11/Rad50 Nuclease Complex into an Endo/Exonuclease Machine Specific for Protein-DNA Adducts." *Molecular Cell* 64(3):593–606.

Deshpande, Rajashree A., Logan R. Myler, Michael M. Soniat, Nodar Makharashvili, Linda Lee, Susan P. Lees-Miller, Ilya J. Finkelstein, and Tanya T. Paull. 2020. “DNA-Dependent Protein Kinase Promotes DNA End Processing by MRN and CtIP.” *Science Advances* 6(2):eaay0922.

Deshpande, Rajashree, Logan Myler, Michael Soniat, Nodar Makharashvili, Linda Lee, Susan Lees-Miller, Ilya Finkelstein, and Tanya T. Paull. 2018. “DNA-PKcs Promotes DNA End Processing.” *BioRxiv* 395731.

DiBiase, S. J., Z. C. Zeng, R. Chen, T. Hyslop, W. J. Curran, and G. Iliakis. 2000. “DNA-Dependent Protein Kinase Stimulates an Independently Active, Nonhomologous, End-Joining Apparatus.” *Cancer Research* 60(5):1245–53.

Doil, Carsten, Niels Mailand, Simon Bekker-Jensen, Patrice Menard, Dorthe Helena Larsen, Rainer Pepperkok, Jan Ellenberg, Stephanie Panier, Daniel Durocher, Jiri Bartek, Jiri Lukas, and Claudia Lukas. 2009. “RNF168 Binds and Amplifies Ubiquitin Conjugates on Damaged Chromosomes to Allow Accumulation of Repair Proteins.” *Cell* 136(3):435–46.

Dorée, Marcel and Simon Galas. 1994. “The Cyclin-dependent Protein Kinases and the Control of Cell Division.” *The FASEB Journal* 8(14):1114–21.

Downs, Jessica A. and Stephen P. Jackson. 2004. “A Means to a DNA End: The Many Roles of Ku.” *Nature Reviews Molecular Cell Biology* 5(5):367–78.

Drouet, Jérôme, Philippe Frit, Christine Delteil, Jean-Pierre de Villartay, Bernard Salles, and Patrick Calsou. 2006. “Interplay between Ku, Artemis, and the DNA-Dependent Protein Kinase Catalytic Subunit at DNA Ends.” *Journal of Biological Chemistry* 281(38):27784–93.

Evans, J. W., X. F. Liu, C. U. Kirchgessner, and J. M. Brown. 1996. “Induction and Repair of Chromosome Aberrations in Scid Cells Measured by Premature Chromosome Condensation.” *Radiation Research* 145(1):39–46.

Fernandez-Capetillo, Oscar, Hua-Tang Chen, Arkady Celeste, Irene Ward, Peter J. Romanienko, Julio C. Morales, Kazuhito Naka, Zhenfang Xia, R. Daniel Camerini-Otero, Noboru Motoyama, Phillip B. Carpenter, William M. Bonner, Junjie Chen, and André Nussenzweig. 2002. “DNA Damage-Induced G2-M Checkpoint Activation by Histone H2AX and 53BP1.” *Nature Cell Biology* 4(12):993–97.

Fusco, Carlo, Alexandre Reymond, and Antonis S. Zervos. 1998. “Molecular Cloning and Characterization of a Novel Retinoblastoma-Binding Protein.” *Genomics* 51(3):351–58.

Germani, Antonia, Audrey Prabel, Samia Mourah, Marie-Pierre Podgorniak, Anna Di Carlo, Ricardo Ehrlich, Sylvie Gisselbrecht, Nadine Varin-Blank, Fabien Calvo, and Heriberto Bruzzoni-Giovanelli. 2003. “SIAH-1 Interacts with CtIP and Promotes Its Degradation by the Proteasome Pathway.” *Oncogene* 22(55):8845–51.

Goodarzi, Aaron A. and Penelope A. Jeggo. 2013. “The Repair and Signaling Responses to DNA Double-Strand Breaks.” *Advances in Genetics* 82:1–45.

Goodhead, Dudley T. and Hooshang Nikjoo. 1989. “Track Structure Analysis of Ultrasoft X-Rays Compared to High- and Low-LET Radiations.” *International Journal of Radiation Biology* 55(4):513–29.

Gotoh, Eisuke and Marco Durante. 2006. “Chromosome Condensation Outside of Mitosis:

Mechanisms and New Tools." *Journal of Cellular Physiology* 209(2):297–304.

Gunn, Amanda and Jeremy M. Stark. 2012. "I-SceI-Based Assays to Examine Distinct Repair Outcomes of Mammalian Chromosomal Double Strand Breaks." Pp. 379–91 in. Humana Press, Totowa, NJ.

H, Kato and Sandberg AA. 1967. "Chromosome Pulverization in Human Binucleate Cells Following Colcemid Treatment." *The Journal of Cell Biology* 34(1).

H, Wang, Zeng ZC, Perrault AR, Cheng X, Qin W, and Iliakis G. 2001. "Genetic Evidence for the Involvement of DNA Ligase IV in the DNA-PK-Dependent Pathway of Non-Homologous End Joining in Mammalian Cells." *Nucleic Acids Research* 29(8).

Haber, James E. n.d. *Genome Stability : DNA Repair and Recombination*.

Hada, Megumi and Betsy M. Sutherland. 2006. "Spectrum of Complex DNA Damages Depends on the Incident Radiation." *Radiation Research* 165(2):223–30.

Haince, Jean-François, Darin McDonald, Amélie Rodrigue, Ugo Déry, Jean-Yves Masson, Michael J. Hendzel, and Guy G. Poirier. 2008. "PARP1-Dependent Kinetics of Recruitment of MRE11 and NBS1 Proteins to Multiple DNA Damage Sites." *The Journal of Biological Chemistry* 283(2):1197–1208.

Hall, Eric J. and Amato J. Giaccia. n.d. *Radiobiology for the Radiologist*.

Hershko, A. and A. Ciechanover. 1998. "The Ubiquitin System." *Annual Review of Biochemistry* 67:425–79.

Hill, M. A. 1999. "Radiation Damage to DNA: The Importance of Track Structure." *Radiation Measurements* 31(1–6):15–23.

Hittelman, W. N. and P. N. Rao. 1975. "The Nature of Adriamycin-Induced Cytotoxicity in Chinese Hamster Cells as Revealed by Premature Chromosome Condensation." *Cancer Research* 35(11 Pt 1):30-27–35.

Honma, Masamitsu, Mayumi Sakuraba, Tomoko Koizumi, Yoshio Takashima, Hiroko Sakamoto, and Makoto Hayashi. 2007. "Non-Homologous End-Joining for Repairing I-SceI-Induced DNA Double Strand Breaks in Human Cells." *DNA Repair* 6(6):781–88.

Humphrey, Tim and Gavin Brooks. 2004. *Cell Cycle Control*. Vol. 296. New Jersey: Humana Press.

Hustedt, Nicole and Daniel Durocher. 2017. "The Control of DNA Repair by the Cell Cycle." *Nature Cell Biology* 19(1):1–9.

Hydbring, Per, Marcos Malumbres, and Piotr Sicinski. 2016. "Non-Canonical Functions of Cell Cycle Cyclins and Cyclin-Dependent Kinases." *Nature Reviews Molecular Cell Biology* 17(5):280–92.

Iliakis, G. E., L. Metzger, N. Denko, and T. D. Stamato. 1991. "Detection of DNA Double-Strand Breaks in Synchronous Cultures of CHO Cells by Means of Asymmetric Field Inversion Gel Electrophoresis." *International Journal of Radiation Biology* 59(2):321–41.

Iliakis, G., H. Wang, A. R. Perrault, W. Boecker, B. Rosidi, F. Windhofer, W. Wu, J. Guan, G. Terzoudi, and G. Pantelias. 2004. "Mechanisms of DNA Double Strand Break Repair and Chromosome Aberration Formation." *Cytogenetic and Genome Research* 104(1–4):14–20.

Iliakis, George, Emil Mladenov, and Veronika Mladenova. 2019. “Necessities in the Processing of DNA Double Strand Breaks and Their Effects on Genomic Instability and Cancer.” *Cancers* 11(11):1671.

Iliakis, George, Veronika Mladenova, Mortoga Sharif, Shipra Chaudhary, Ifigenea Mavragani, Aashish Soni, Janapriya Saha, Agnes Schipler, and Emil Mladenov. 2018. *Defined Biological Models of High LET Radiation Lesions*.

Iliakis, George, Tamara Murmann, and Aashish Soni. 2015. “Alternative End-Joining Repair Pathways Are the Ultimate Backup for Abrogated Classical Non-Homologous End-Joining and Homologous Recombination Repair: Implications for the Formation of Chromosome Translocations.” *Mutation Research. Genetic Toxicology and Environmental Mutagenesis* 793:166–75.

Ip, Stephen C. Y., Ulrich Rass, Miguel G. Blanco, Helen R. Flynn, J. Mark Skehel, and Stephen C. West. 2008. “Identification of Holliday Junction Resolvases from Humans and Yeast.” *Nature* 456(7220):357–61.

J, Della-Maria, Zhou Y, Tsai MS, Kuhnlein J, Carney JP, Paull TT, and Tomkinson AE. 2011. “Human Mre11/Human Rad50/Nbs1 and DNA Ligase IIIalpha/XRCC1 Protein Complexes Act Together in an Alternative Nonhomologous End Joining Pathway.” *The Journal of Biological Chemistry* 286(39).

Jackson, Stephen P. and Jiri Bartek. 2009. “The DNA-Damage Response in Human Biology and Disease.” *Nature* 461(7267):1071–78.

Jette, Nicholas and Susan P. Lees-Miller. 2015. “The DNA-Dependent Protein Kinase: A Multifunctional Protein Kinase with Roles in DNA Double Strand Break Repair and Mitosis.” *Progress in Biophysics and Molecular Biology* 117(2–3):194–205.

JOHNSON, R. T. and P. N. RAO. 1970. “Mammalian Cell Fusion : Induction of Premature Chromosome Condensation in Interphase Nuclei.” *Nature* 226(5247):717–22.

JR, Chapman, Taylor MR, and Boulton SJ. 2012. “Playing the End Game: DNA Double-Strand Break Repair Pathway Choice.” *Molecular Cell* 47(4).

K, Kostyrko, Bosshard S, Urban Z, and Mermod N. 2015. “A Role for Homologous Recombination Proteins in Cell Cycle Regulation.” *Cell Cycle (Georgetown, Tex.)* 14(17).

Kinoshita, N., H. Yamano, H. Niwa, T. Yoshida, and M. Yanagida. 1993. “Negative Regulation of Mitosis by the Fission Yeast Protein Phosphatase Ppa2.” *Genes & Development* 7(6):1059–71.

Kumagai, Akiko and William G. Dunphy. 1992. “Regulation of the Cdc25 Protein during the Cell Cycle in Xenopus Extracts.” *Cell* 70(1):139–51.

Lafranchi, Lorenzo, Harmen R. Boer, Elisabeth GE Vries, Shao-En Ong, Alessandro A. Sartori, and Marcel ATM Vugt. 2014. “APC / C ^{C} ^{Dh1} Controls Ct IP Stability during the Cell Cycle and in Response to DNA Damage.” *The EMBO Journal* 33(23):2860–79.

Lanz, Michael Charles, Diego Dibitetto, and Marcus Bustamante Smolka. 2019. “DNA Damage Kinase Signaling: Checkpoint and Repair at 30 Years.” *The EMBO Journal* 38(18):e101801.

Lee-Theilen, Mieun, Allysia J. Matthews, Dierdre Kelly, Simin Zheng, and Jayanta Chaudhuri. 2011. “CtIP Promotes Microhomology-Mediated Alternative End Joining during Class-

Switch Recombination." *Nature Structural & Molecular Biology* 18(1):75–79.

Liang, L., L. Deng, S. C. Nguyen, X. Zhao, C. D. Maulion, C. Shao, and J. A. Tischfield. 2008. "Human DNA Ligases I and III, but Not Ligase IV, Are Required for Microhomology-Mediated End Joining of DNA Double-Strand Breaks." *Nucleic Acids Research* 36(10):3297–3310.

Lieber, Michael R. 2008. "The Mechanism of Human Nonhomologous DNA End Joining." *The Journal of Biological Chemistry* 283(1):1–5.

Lieber, Michael R. 2010. "NHEJ and Its Backup Pathways in Chromosomal Translocations." *Nature Structural & Molecular Biology* 17(4):393–95.

Liu, Feng and Wen-Hwa Lee. 2006. "CtIP Activates Its Own and Cyclin D1 Promoters via the E2F/RB Pathway during G1/S Progression." *Molecular and Cellular Biology* 26(8):3124–34.

Liu, Ting and Jun Huang. 2016. "DNA End Resection: Facts and Mechanisms." *Genomics, Proteomics & Bioinformatics* 14(3):126–30.

Liu, Xiangyu, Xiaobin S. Wang, Brian J. Lee, Foon K. Wu-Baer, Xiaohui Lin, Zhengping Shao, Verna M. Estes, Jean Gautier, Richard Baer, and Shan Zha. 2019. "CtIP Is Essential for Early B Cell Proliferation and Development in Mice." *The Journal of Experimental Medicine* 216(7):1648–63.

Lou, Zhenkun, Claudia Christiano, Silva Chini, Katherine Minter-Dykhouse, and Junjie Chen. 2003. "Mediator of DNA Damage Checkpoint Protein 1 Regulates BRCA1 Localization and Phosphorylation in DNA Damage Checkpoint Control* Downloaded From." *Accelerated Publication THE JOURNAL OF BIOLOGICAL CHEMISTRY* 278(16):13599–602.

Luijsterburg, Martijn S. and Haico van Attikum. 2012. "Close Encounters of the RNF8th Kind: When Chromatin Meets DNA Repair." *Current Opinion in Cell Biology* 24(3):439–47.

Lukas, Claudia, Fredrik Melander, Manuel Stucki, Jacob Falck, Simon Bekker-Jensen, Michal Goldberg, Yaniv Lerenthal, Stephen P. Jackson, Jiri Bartek, and Jiri Lukas. 2004. "Mdc1 Couples DNA Double-Strand Break Recognition by Nbs1 with Its H2AX-Dependent Chromatin Retention." *EMBO Journal* 23(13):2674–83.

Mailand, Niels, Simon Bekker-Jensen, Helene Faustrup, Fredrik Melander, Jiri Bartek, Claudia Lukas, and Jiri Lukas. 2007. "RNF8 Ubiquitylates Histones at DNA Double-Strand Breaks and Promotes Assembly of Repair Proteins." *Cell* 131(5):887–900.

Makharashvili, Nodar and Tanya T. Paull. 2015. "CtIP: A DNA Damage Response Protein at the Intersection of DNA Metabolism." *DNA Repair* 32:75–81.

Mao, Zhiyong, Michael Bozzella, Andrei Seluanov, and Vera Gorbunova. 2008. "DNA Repair by Nonhomologous End Joining and Homologous Recombination during Cell Cycle in Human Cells." *Cell Cycle* 7(18):2902–6.

Masumura, Ken-ichi, Kensuke Kuniya, Toshihiro Kurobe, Masamichi Fukuoka, Fumio Yatagai, and Takehiko Nohmi. 2002. "Heavy-Ion-Induced Mutations in Thegpt Delta Transgenic Mouse: Comparison of Mutation Spectra Induced by Heavy-Ion, X-Ray, and ?-Ray Radiation." *Environmental and Molecular Mutagenesis* 40(3):207–15.

Maton, Gilliane, Thierry Lorca, Jean-Antoine Girault, René Ozon, and Catherine Jessus.

2005. “Differential Regulation of Cdc2 and Aurora-A in Xenopus Oocytes: A Crucial Role of Phosphatase 2A.” *Journal of Cell Science* 118(11):2485–94.

MB, Kastan and Bartek J. 2004. “Cell-Cycle Checkpoints and Cancer.” *Nature* 432(7015).

Meek, K., P. Douglas, X. Cui, Q. Ding, and S. P. Lees-Miller. 2007. “Trans Autophosphorylation at DNA-Dependent Protein Kinase’s Two Major Autophosphorylation Site Clusters Facilitates End Processing but Not End Joining.” *Molecular and Cellular Biology* 27(10):3881–90.

Mehta, A. and J. E. Haber. 2014. “Sources of DNA Double-Strand Breaks and Models of Recombinational DNA Repair.” *Cold Spring Harbor Perspectives in Biology* 6(9):a016428–a016428.

Mirman, Zachary and Titia de Lange. 2020. “53BP1: A DSB Escort.” *Genes & Development* 34(1–2):7–23.

Mitchell, S., P. Abel, M. Ware, G. Stamp, and E. N. Lalani. 2001. “Phenotypic and Genotypic Characterization of Commonly Used Human Prostatic Cell Lines.” *BJU International* 85(7):932–44.

Mladenov, Emil, Xiaoxiang Fan, Rositsa Dueva, Aashish Soni, and George Iliakis. 2019. “Radiation-Dose-Dependent Functional Synergisms between ATM, ATR and DNA-PKcs in Checkpoint Control and Resection in G2-Phase.” *Scientific Reports* 9(1):8255.

Mladenov, Emil, Xiaoxiang Fan, Katja Paul-Konietzko, Aashish Soni, and George Iliakis. 2019. “DNA-PKcs and ATM Epistatically Suppress DNA End Resection and Hyperactivation of ATR-Dependent G2-Checkpoint in S-Phase Irradiated Cells.” *Scientific Reports* 9(1):14597.

Mladenov, Emil, Simon Magin, Aashish Soni, and George Iliakis. 2016. “DNA Double-Strand-Break Repair in Higher Eukaryotes and Its Role in Genomic Instability and Cancer: Cell Cycle and Proliferation-Dependent Regulation.” *Seminars in Cancer Biology* 37–38:51–64.

Mladenov, Emil, Janapriya Saha, and George Iliakis. 2018. “Processing-Challenges Generated by Clusters of DNA Double-Strand Breaks Underpin Increased Effectiveness of High-LET Radiation and Chromothripsis.” Pp. 149–68 in.

Mladenov, Emil, Christian Staudt, Aashish Soni, Tamara Murmann-Konda, Maria Siemann-Loekes, and George Iliakis. 2019. “Strong Suppression of Gene Conversion with Increasing DNA Double-Strand Break Load Delimited by 53BP1 and RAD52.” *Nucleic Acids Research*.

Mladenova, Veronika, Emil Mladenov, and George Iliakis. 2016. “Novel Biological Approaches for Testing the Contributions of Single DSBs and DSB Clusters to the Biological Effects of High LET Radiation.” *Frontiers in Oncology* 6:163.

Morrical, Scott W. 2015. “DNA-Pairing and Annealing Processes in Homologous Recombination and Homology-Directed Repair.” *Cold Spring Harbor Perspectives in Biology* 7(2):a016444.

Mortensen, U. H., C. Bendixen, I. Sunjevaric, and R. Rothstein. 1996. “DNA Strand Annealing Is Promoted by the Yeast Rad52 Protein.” *Proceedings of the National Academy of Sciences* 93(20):10729–34.

Nevaldine, B., J. A. Longo, and P. J. Hahn. 1997. “The Scid Defect Results in Much Slower Repair of DNA Double-Strand Breaks but Not High Levels of Residual Breaks.” *Radiation Research* 147(5):535–40.

Nowsheen, Somaira, Khaled Aziz, Asef Aziz, Min Deng, Bo Qin, Kuntian Luo, Karthik B. Jeganathan, Henan Zhang, Tongzheng Liu, Jia Yu, Yibin Deng, Jian Yuan, Wei Ding, Jan M. van Deursen, and Zhenkun Lou. 2018. “L3MBTL2 Orchestrates Ubiquitin Signalling by Dictating the Sequential Recruitment of RNF8 and RNF168 after DNA Damage.” *Nature Cell Biology* 20(4):455–64.

Nowsheen, Somaira, Min Deng, and Zhenkun Lou. 2019. “Ubiquitin and the DNA Double-Strand Break Repair Pathway.” *Genome Instability & Disease* 1–12.

Obe, G. and A. T. Natarajan. 1985. “Chromosomal Aberrations Induced by the Restriction Endonuclease Alu I in Chinese Hamster Ovary Cells: Influence of Duration of Treatment and Potentiation by Cytosine Arabinoside.” *Mutation Research/Fundamental and Molecular Mechanisms of Mutagenesis* 152(2–3):205–10.

Orthwein, Alexandre, Amélie Fradet-Turcotte, Sylvie M. Noordermeer, Marella D. Canny, Catherine M. Brun, Jonathan Strecker, Cristina Escribano-Diaz, and Daniel Durocher. 2014. “Mitosis Inhibits DNA Double-Strand Break Repair to Guard against Telomere Fusions.” *Science (New York, N.Y.)* 344(6180):189–93.

Pantelias, G. E. and H. D. Maillie. 1983. “A Simple Method for Premature Chromosome Condensation Induction in Primary Human and Rodent Cells Using Polyethylene Glycol.” *Somatic Cell Genetics* 9(5):533–47.

Paul, Katja, Minli Wang, Emil Mladenov, Alena Bencsik-Theilen, Theresa Bednar, Wenqi Wu, Hiroshi Arakawa, and George Iliakis. 2013. “DNA Ligases I and III Cooperate in Alternative Non-Homologous End-Joining in Vertebrates” edited by A. J. Lustig. *PLoS ONE* 8(3):e59505.

Paull, Tanya T. 2015. “Mechanisms of ATM Activation.” *Annual Review of Biochemistry* 84(1):711–38.

Peng, C. Y., P. R. Graves, R. S. Thoma, Z. Wu, A. S. Shaw, and H. Piwnica-Worms. 1997. “Mitotic and G2 Checkpoint Control: Regulation of 14-3-3 Protein Binding by Phosphorylation of Cdc25C on Serine-216.” *Science (New York, N.Y.)* 277(5331):1501–5.

Peterson, Shaun E., Yinyin Li, Foon Wu-Baer, Brian T. Chait, Richard Baer, Hong Yan, Max E. Gottesman, and Jean Gautier. 2013. “Activation of DSB Processing Requires Phosphorylation of CtIP by ATR.” *Molecular Cell* 49(4):657–67.

Polo, Sophie E. and Stephen P. Jackson. 2011. “Dynamics of DNA Damage Response Proteins at DNA Breaks: A Focus on Protein Modifications.” *Genes & Development* 25(5):409.

Povirk, Lawrence F. 2006. “Biochemical Mechanisms of Chromosomal Translocations Resulting from DNA Double-Strand Breaks.” *DNA Repair* 5(9–10):1199–1212.

Q, Cheng, Barboule N, Frit P, Gomez D, Bombarde O, Couderc B, Ren GS, Salles B, and Calsou P. 2011. “Ku Counteracts Mobilization of PARP1 and MRN in Chromatin Damaged With DNA Double-Strand Breaks.” *Nucleic Acids Research* 39(22).

Radford, I. R. 1985. “The Level of Induced DNA Double-Strand Breakage Correlates with Cell

Killing after X-Irradiation." *International Journal of Radiation Biology and Related Studies in Physics, Chemistry, and Medicine* 48(1):45–54.

Rao, V. Ashutosh, Chiara Conti, Josee Guirouilh-Barbat, Asako Nakamura, Ze Hong Miao, Sally L. Davies, Barbara Saccá, Ian D. Hickson, Aaron Bensimon, and Yves Pommier. 2007. "Endogenous γ-H2AX-ATM-Chk2 Checkpoint Activation in Bloom's Syndrome Helicase-Deficient Cells Is Related to DNA Replication Arrested Forks." *Molecular Cancer Research* 5(7):713–24.

RD, Johnson and Jasin M. 2000. "Sister Chromatid Gene Conversion Is a Prominent Double-Strand Break Repair Pathway in Mammalian Cells." *The EMBO Journal* 19(13).

Reddy, Gurucharan, Efim I. Golub, and Charles M. Radding. 1997. "Human Rad52 Protein Promotes Single-Strand DNA Annealing Followed by Branch Migration." *Mutation Research/Fundamental and Molecular Mechanisms of Mutagenesis* 377(1):53–59.

Reynolds, Richard J. and Jay A. Schecker. 1999. "Radiation , Cell Cycle , and Cancer We Have Seen the Enemy , and He Is Us ! —."

Riballo, Enriqueta, Martin Kühne, Nicole Rief, Aidan Doherty, Graeme C. M. Smith, María-José Recio, Caroline Reis, Kirsten Dahm, Andreas Fricke, Andrea Krempler, Antony R. Parker, Stephen P. Jackson, Andrew Gennery, Penny A. Jeggo, and Markus Löbrich. 2004. "A Pathway of Double-Strand Break Rejoining Dependent upon ATM, Artemis, and Proteins Locating to Gamma-H2AX Foci." *Molecular Cell* 16(5):715–24.

Rogakou, E. P., D. R. Pilch, A. H. Orr, V. S. Ivanova, and W. M. Bonner. 1998. "DNA Double-Stranded Breaks Induce Histone H2AX Phosphorylation on Serine 139." *The Journal of Biological Chemistry* 273(10):5858–68.

RS, Williams, Moncalian G, Williams JS, Yamada Y, Limbo O, Shin DS, Groocock LM, Cahill D, Hitomi C, Guenther G, Moiani D, Carney JP, Russell P, and Tainer JA. 2008. "Mre11 Dimers Coordinate DNA End Bridging and Nuclease Processing in Double-Strand-Break Repair." *Cell* 135(1).

Sartori, Alessandro A., Claudia Lukas, Julia Coates, Martin Mistrik, Shuang Fu, Jiri Bartek, Richard Baer, Jiri Lukas, and Stephen P. Jackson. 2007. "Human CtIP Promotes DNA End Resection." 450.

Scheffner, Martin, Ulrike Nuber, and Jon M. Huibregtse. 1995. "Protein Ubiquitination Involving an E1–E2–E3 Enzyme Ubiquitin Thioester Cascade." *Nature* 373(6509):81–83.

Schipler, Agnes and George Iliakis. 2013. "DNA Double-Strand-Break Complexity Levels and Their Possible Contributions to the Probability for Error-Prone Processing and Repair Pathway Choice." *Nucleic Acids Research* 41(16):7589–7605.

Schipler, Agnes, Veronika Mladenova, Aashish Soni, Vladimir Nikolov, Janapriya Saha, Emil Mladenov, and George Iliakis. 2016. "Chromosome Thripsis by DNA Double Strand Break Clusters Causes Enhanced Cell Lethality, Chromosomal Translocations and 53BP1-Recruitment." *Nucleic Acids Research* 44(16):7673–90.

Shibata, Atsushi, Davide Moiani, Andrew S. Arvai, Jefferson Perry, Shane M. Harding, Marie-Michelle Genois, Ranjan Maity, Sari van Rossum-Fikkert, Aryandi Kertokalio, Filippo Romoli, Amani Ismail, Ermal Ismalaj, Elena Petricci, Matthew J. Neale, Robert G. Bristow, Jean-Yves Masson, Claire Wyman, Penny A. Jeggo, and John A. Tainer. 2014.

"DNA Double-Strand Break Repair Pathway Choice Is Directed by Distinct MRE11 Nuclease Activities." *Molecular Cell* 53(1):7–18.

Sibanda, Bancinyane L., Dimitri Y. Chirgadze, David B. Ascher, and Tom L. Blundell. 2017. "DNA-PKcs Structure Suggests an Allosteric Mechanism Modulating DNA Double-Strand Break Repair." *Science (New York, N.Y.)* 355(6324):520–24.

Singh, Satyendra K., Theresa Bednar, Lihua Zhang, Wenqi Wu, Emil Mladenov, and George Iliakis. 2012. "Inhibition of B-NHEJ in Plateau-Phase Cells Is Not a Direct Consequence of Suppressed Growth Factor Signaling." *International Journal of Radiation Oncology*Biology*Physics* 84(2):e237–43.

Singh, Satyendra K, Minli Wang, Christian Staudt, and George Iliakis. 2011. "Post-Irradiation Chemical Processing of DNA Damage Generates Double-Strand Breaks in Cells Already Engaged in Repair." *Nucleic Acids Research* 39(19):8416–29.

Singh, Satyendra K., Wenqi Wu, Lihua Zhang, Holger Klammer, Minli Wang, and George Iliakis. 2011. "Widespread Dependence of Backup NHEJ on Growth State: Ramifications for the Use of DNA-PK Inhibitors." *International Journal of Radiation Oncology*Biology*Physics* 79(2):540–48.

Smeenk, Godelieve and Niels Mailand. 2016. "Writers, Readers, and Erasers of Histone Ubiquitylation in DNA Double-Strand Break Repair." *Frontiers in Genetics* 7:122.

Soni, Aashish, Maria Siemann, Martha Grabos, Tamara Murmann, Gabriel E. Pantelias, and George Iliakis. 2014. "Requirement for Parp-1 and DNA Ligases 1 or 3 but Not of Xrcc1 in Chromosomal Translocation Formation by Backup End Joining." *Nucleic Acids Research* 42(10):6380–92.

Soutoglou, Evi, Jonas F. Dorn, Kundan Sengupta, Maria Jasin, Andre Nussenzweig, Thomas Ried, Gaudenz Danuser, and Tom Misteli. 2007. "Positional Stability of Single Double-Strand Breaks in Mammalian Cells." *Nature Cell Biology* 9(6):675–82.

Stark, Jeremy M., Andrew J. Pierce, Jin Oh, Albert Pastink, and Maria Jasin. 2004. "Genetic Steps of Mammalian Homologous Repair with Distinct Mutagenic Consequences." *Molecular and Cellular Biology* 24(21):9305–16.

Steger, Martin, Olga Murina, Daniela Hühn, Lorenza P. Ferretti, Reto Walser, Kay Hänggi, Lorenzo Lafranchi, Christine Neugebauer, Shreya Paliwal, Pavel Janscak, Bertran Gerrits, Giannino Del Sal, Oliver Zerbe, and Alessandro A. Sartori. 2013. "Prolyl Isomerase PIN1 Regulates DNA Double-Strand Break Repair by Counteracting DNA End Resection." *Molecular Cell* 50(3):333–43.

Stewart, Grant S., Stephanie Panier, Kelly Townsend, Abdallah K. Al-Hakim, Nadine K. Kolas, Edward S. Miller, Shinichiro Nakada, Jarkko Ylanko, Signe Olivarius, Megan Mendez, Ceri Oldreive, Jan Wildenhain, Andrea Tagliaferro, Laurence Pelletier, Nadine Taubenheim, Anne Durandy, Philip J. Byrd, Tatjana Stankovic, A. Malcolm R. Taylor, and Daniel Durocher. 2009. "The RIDDLE Syndrome Protein Mediates a Ubiquitin-Dependent Signaling Cascade at Sites of DNA Damage." *Cell* 136(3):420–34.

Stiff, Tom, Mark O'Driscoll, Nicole Rief, Kuniyoshi Iwabuchi, Markus Löbrich, and Penny A. Jeggo. 2004. "ATM and DNA-PK Function Redundantly to Phosphorylate H2AX after Exposure to Ionizing Radiation." *Cancer Research* 64(7):2390–96.

Suryadinata, Randy, Martin Sadowski, and Boris Sarcevic. 2010. "Control of Cell Cycle

Progression by Phosphorylation of Cyclin-Dependent Kinase (CDK) Substrates." *Bioscience Reports* 30(4):243–55.

Syljuåsen, Randi G., Sanne Jensen, Jiri Bartek, and Jiri Lukas. 2006. "Adaptation to the Ionizing Radiation-Induced G2 Checkpoint Occurs in Human Cells and Depends on Checkpoint Kinase 1 and Polo-like Kinase 1 Kinases." *Cancer Research* 66(21):10253–57.

Symington, Lorraine S. 2016. "Mechanism and Regulation of DNA End Resection in Eukaryotes." *Critical Reviews in Biochemistry and Molecular Biology* 51(3):195–212.

Terzoudi, Georgia I., Satyendra Kumar Singh, Gabriel E. Pantelias, and George Iliakis. 2008. "Premature Chromosome Condensation Reveals DNA-PK Independent Pathways of Chromosome Break Repair." *International Journal of Oncology* 33(4):871–79.

Thorslund, Tina, Anita Ripplinger, Saskia Hoffmann, Thomas Wild, Michael Uckelmann, Bine Villumsen, Takeo Narita, Titia K. Sixma, Chunaram Choudhary, Simon Bekker-Jensen, and Niels Mailand. 2015. "Histone H1 Couples Initiation and Amplification of Ubiquitin Signalling after DNA Damage." *Nature* 527(7578):389–93.

Truong, L. N., Y. Li, L. Z. Shi, P. Y. H. Hwang, J. He, H. Wang, N. Razavian, M. W. Berns, and X. Wu. 2013. "Microhomology-Mediated End Joining and Homologous Recombination Share the Initial End Resection Step to Repair DNA Double-Strand Breaks in Mammalian Cells." *Proceedings of the National Academy of Sciences* 110(19):7720–25.

Uematsu, Naoya, Eric Weterings, Ken-ichi Yano, Keiko Morotomi-Yano, Burkhard Jakob, Gisela Taucher-Scholz, Pierre-Olivier Mari, Dik C. van Gent, Benjamin P. C. Chen, and David J. Chen. 2007. "Autophosphorylation of DNA-PKCS Regulates Its Dynamics at DNA Double-Strand Breaks." *The Journal of Cell Biology* 177(2):219–29.

Wang, Bin, Shuhei Matsuoka, Phillip B. Carpenter, and Stephen J. Elledge. 2002. "53BP1, a Mediator of the DNA Damage Checkpoint." *Science* 298(5597):1435–38.

Wang, Huichen, Bustanur Rosidi, Ronel Perrault, Minli Wang, Lihua Zhang, Frank Windhofer, and George Iliakis. 2005. "DNA Ligase III as a Candidate Component of Backup Pathways of Nonhomologous End Joining." *Cancer Research* 65(10):4020–30.

Wang, Minli, Weizhong Wu, Wenqi Wu, Bustanur Rosidi, Lihua Zhang, Huichen Wang, and George Iliakis. 2006. "PARP-1 and Ku Compete for Repair of DNA Double Strand Breaks by Distinct NHEJ Pathways." *Nucleic Acids Research* 34(21):6170–82.

Ward, J. F. 1985. "Biochemistry of DNA Lesions." *Radiation Research. Supplement* 8:S103-11.

Windhofer, Frank, Wenqi Wu, and George Iliakis. 2007. "Low Levels of DNA Ligases III and IV Sufficient for Effective NHEJ." *Journal of Cellular Physiology* 213(2):475–83.

Wong, Alexander KC, Patricia A. Ormonde, Ralph Pero, Yuan Chen, Lubing Lian, Grant Salada, Simin Berry, Quentin Lawrence, Priya Dayananth, Phuong Ha, Sean V Tavtigian, David H. F. Teng, and Paul L. Bartel. 1998. "Characterization of a Carboxy-Terminal BRCA1 Interacting Protein." *Oncogene* 17(18):2279–85.

Wu, Wenqi, Minli Wang, Tamara Mussfeldt, and George Iliakis. 2008. "Enhanced Use of Backup Pathways of NHEJ in G2 in Chinese Hamster Mutant Cells with Defects in the Classical Pathway of NHEJ." *Radiation Research* 170(4):512–20.

Wu, Wenqi, Minli Wang, Weizhong Wu, Satyendra K. Singh, Tamara Mussfeldt, and George Iliakis. 2008. “Repair of Radiation Induced DNA Double Strand Breaks by Backup NHEJ Is Enhanced in G2.” *DNA Repair* 7(2):329–38.

Xiao, Z., John Xue, Thomas J. Sowin, and Haiying Zhang. 2006. “Differential Roles of Checkpoint Kinase 1, Checkpoint Kinase 2, and Mitogen-Activated Protein Kinase-Activated Protein Kinase 2 in Mediating DNA Damage-Induced Cell Cycle Arrest: Implications for Cancer Therapy.” *Molecular Cancer Therapeutics* 5(8):1935–43.

Xie, Anyong, Amy Kwok, and Ralph Scully. 2009. “Role of Mammalian Mre11 in Classical and Alternative Non-Homologous End Joining.” *Nature Structural & Molecular Biology* 16(8):814.

Y, Shiloh. 2003. “ATM and Related Protein Kinases: Safeguarding Genome Integrity.” *Nature Reviews. Cancer* 3(3).

Yan, Catherine T., Cristian Boboila, Ellen Kris Souza, Sonia Franco, Thomas R. Hickernell, Michael Murphy, Sunil Gumaste, Mark Geyer, Ali A. Zarrin, John P. Manis, Klaus Rajewsky, and Frederick W. Alt. 2007. “IgH Class Switching and Translocations Use a Robust Non-Classical End-Joining Pathway.” *Nature* 449(7161):478–82.

Yannone, Steven M., Imran S. Khan, Rui-Zhe Zhou, Tong Zhou, Kristoffer Valerie, and Lawrence F. Povirk. 2008. “Coordinate 5’ and 3’ Endonucleolytic Trimming of Terminally Blocked Blunt DNA Double-Strand Break Ends by Artemis Nuclease and DNA-Dependent Protein Kinase.” *Nucleic Acids Research* 36(10):3354–65.

You, Zhongsheng and Julie M. Bailis. 2010. “DNA Damage and Decisions: CtIP Coordinates DNA Repair and Cell Cycle Checkpoints.” *Trends in Cell Biology* 20(7):402–9.

Yu, X. and R. Baer. 2000. “Nuclear Localization and Cell Cycle-Specific Expression of CtIP, a Protein That Associates with the BRCA1 Tumor Suppressor.” *The Journal of Biological Chemistry* 275(24):18541–49.

Yu, Xiaochun, Shuang Fu, Maoyi Lai, Richard Baer, and Junjie Chen. 2006. “BRCA1 Ubiquitinates Its Phosphorylation-Dependent Binding Partner CtIP.” *Genes & Development* 20(13):1721–26.

Yun, Maximina H. and Kevin Hiom. 2009. “CtIP-BRCA1 Modulates the Choice of DNA Double-Strand-Break Repair Pathway throughout the Cell Cycle.” *Nature* 459(7245):460–63.

Zhang, Yu and Maria Jasin. 2011. “An Essential Role for CtIP in Chromosomal Translocation Formation through an Alternative End-Joining Pathway.” *Nature Structural & Molecular Biology* 18(1):80–84.

Zhao, Mei Jun, Yan Feng Song, Hai Tao Niu, Ying Xia Tian, Xu Guang Yang, Kun Xie, Yu Hong Jing, and De Gui Wang. 2016. “Adenovirus-Mediated Downregulation of the Ubiquitin Ligase RNF8 Sensitizes Bladder Cancer to Radiotherapy.” *Oncotarget* 7(8):8956–67.

Zhao, Weixing, Sivaraja Vaithiyalingam, Joseph San Filippo, David G. Maranon, Judit Jimenez-Sainz, Gerald V. Fontenay, Youngho Kwon, Stanley G. Leung, Lucy Lu, Ryan B. Jensen, Walter J. Chazin, Claudia Wiese, and Patrick Sung. 2015. “Promotion of BRCA2-Dependent Homologous Recombination by DSS1 via RPA Targeting and DNA Mimicry.” *Molecular Cell* 59(2):176–87.

Zhou, Yi and Tanya T. Paull. 2013. “DNA-Dependent Protein Kinase Regulates DNA End Resection in Concert with Mre11-Rad50-Nbs1 (MRN) and Ataxia Telangiectasia-Mutated (ATM).” *The Journal of Biological Chemistry* 288(52):37112–25.

IX Supplementary Data

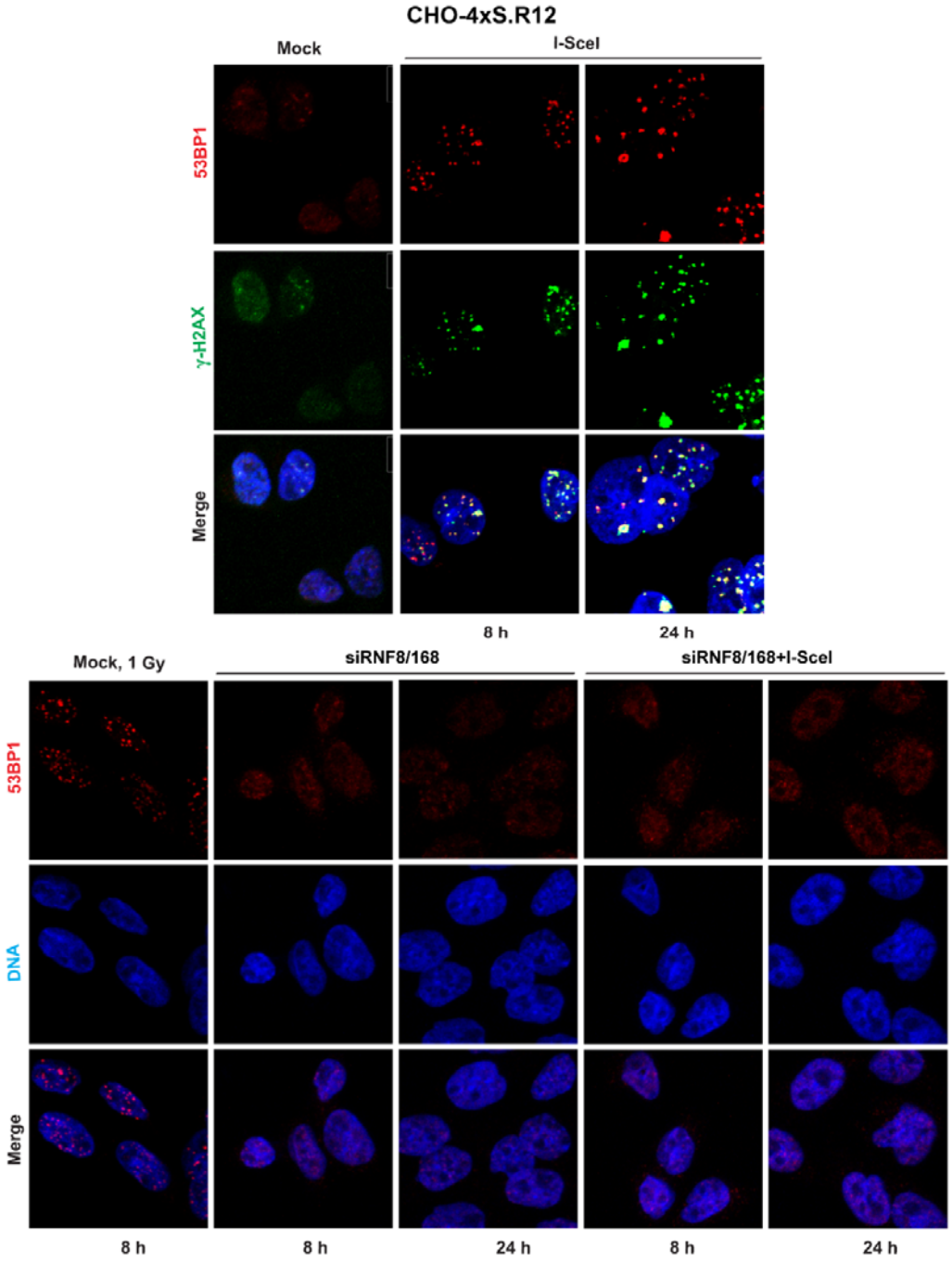

Abbildung 1

Supplementary Figure 1 RNAi mediated depletion of RNF8/168 restrains 53BP1 recruitment to the sites of DSBs generated by I-SceI. Representative images obtained with confocal fluorescence microscope show γ-H2AX (green) and 53BP1 foci (red) in simple DSB clone harboring a single I-SceI recognition site (CHO-4xS.R12) transfected with plasmid expressing I-SceI (pI-SceI-3xNLS). In contrast, 53BP1 foci formation was inhibited in I-SceI transfected as well as in corresponding irradiated cells (1 Gy) upon RNF8/168 knockdown. Corresponding mock-transfected cells instead show IR induced 53BP1 foci retention following their exposure to 1 Gy of irradiation.

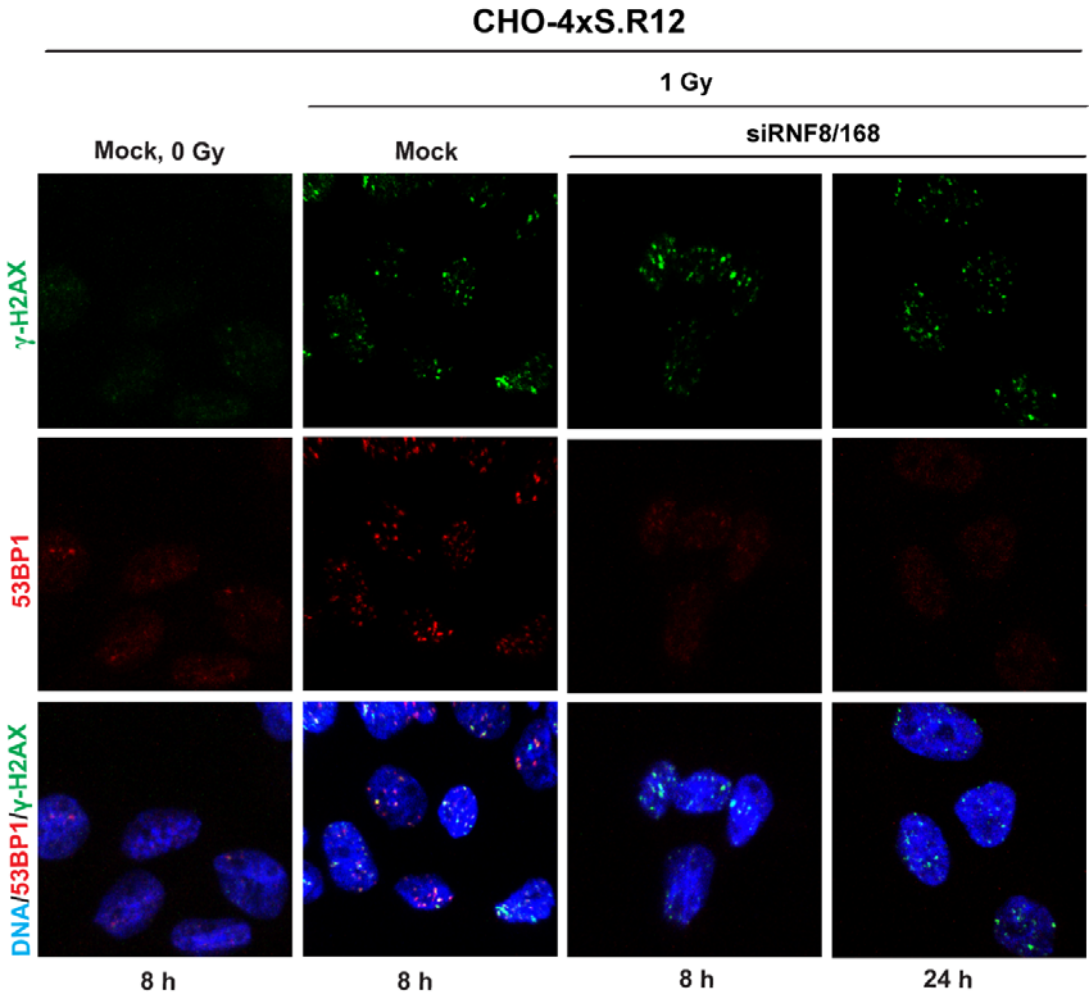

Supplementary Figure 2 Knockdown of E3 ligases RNF8 and RNF168 does not affect the IR- induced γ-H2AX foci formation at DSB sites. Representative γ-H2AX foci (green) and 53BP1 foci (red) formation at indicated times (8 and 24 h) in cells harboring DSBs of simple type (CHO-1xS.D8). RNF8/168 specific siRNAs abrogated the retention of IRIFs (ionizing radiation induced foci) at damaged chromatin. Twenty-four after transfection with siRNF8/168, cells were irradiated with 1 Gy of dose and were fixed after one hour before staining with indicated antibodies. DNA was counterstained with DAPI (blue).

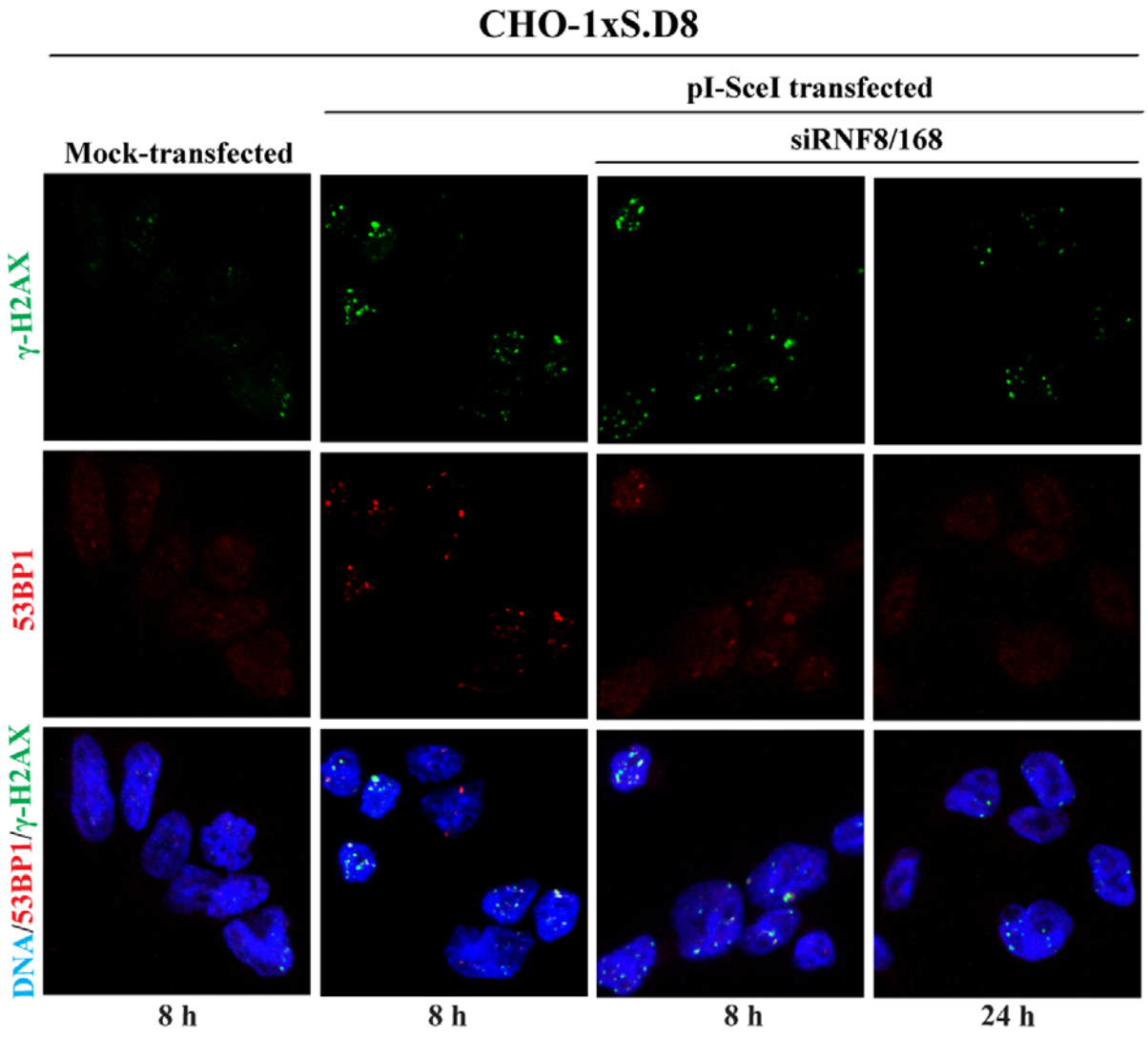

Supplementary Figure 3 knockdown of RNF8 and RNF168 does not affect I-SceI generated γ-H2AX foci formation at damaged chromatin. IF shows images of γ-H2AX (green) and 53BP1 (red) foci formation at indicated times (8 and 24 h) in CHO clones harboring clustered DSBs (CHO-1xS.D8). Cells co-transfected with siRNF8/168 and pI-SceI were fixed at indicated times (8 and 24 h) and were processed for immunofluorescence with indicated antibodies. DNA was counterstained with DAPI (blue).

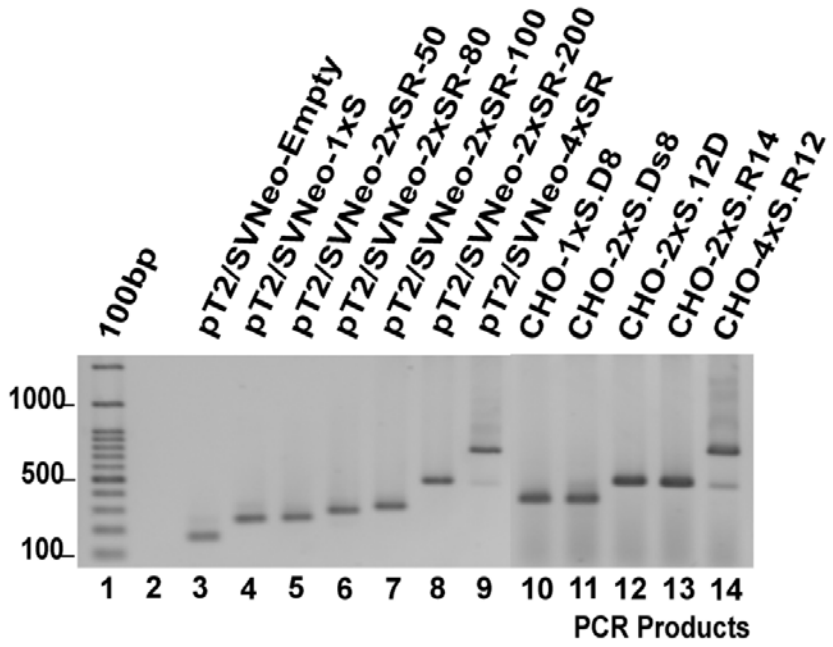

Supplementary Figure 4 PCR-Genotyping based validation to confirm the retained I-SceI recognition sites during propagation in the clonal cell lines as described in detail in figure 65.

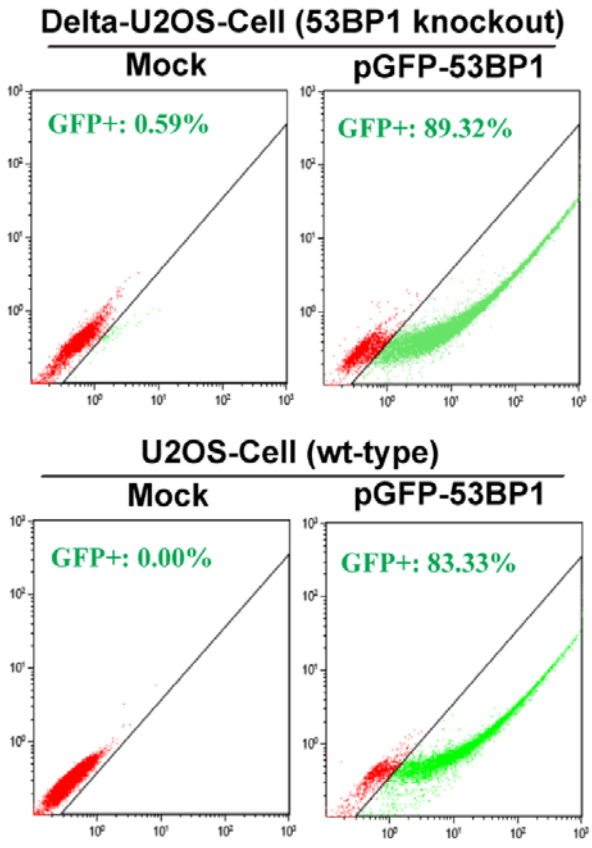

Supplementary Figure 5 Representative histogram shows the transfection efficiency (GFP+ cells) measured after 24 h using GFP expressing plasmid, pEGFP-53BP1 (upper panel).

X Acknowledgements

I offer my gratitude to my supervisor Prof. Dr. George Iliakis, of all people, without whose constant supervision, support and timely advices, this work would not have been materialized. I, to be honest, have never seen a person having such enthusiasm and generosity towards science. I wish I could take a bit of this along into my future research life.

I would also like to extend my gratitude to the scientific staffs at the Institute of Medical radiation biology especially, Dr. Emil Mladenov and Dr. Fanghua Li for their constant guidance and numerous stimulating discussions. I cannot thank them enough for their unexpected help during that long and bumpy way. I am truly grateful to Dr. Aashish Soni, Dr. Simon Magin, Dr. Veronika Mladenova, Dr. Mohd Yasser and Dr. Prabodha Kumar Meher for their kind scientific support when I needed. A special thanks to Dr. Rositsa Dueva for final proofreading of my thesis and providing me with very useful suggestions at that moment.

Being supported every now and then for anything and everything while I was at lab, I would like to sincerely thank Malihe Mesbah, Tamara Mußfeldt and Christian Möllers. Special appreciation goes to Dr. Lisa Krieger not only for being colleague but also for helping with administrative matters, and to write the summary (Zussamenfassung) part in German language. And thanks goes to our present and previous members of this institute. Some names are worth mentioning here: Dr. Yanlei Cheng; who helped me in the beginning to get hands-on in PFGE technique, Dr. Qiong Yang, Dr. Xiao Huaping, Daxian Luo, Gerasimos Pollakis, Michael Piel, Sun Yanjie, Bing Pan and Xiaolou Duan. Very very special thanks to Shipra Chaudhary, Pelin Kucuk and Vasiliki Tasiou for not being colleagues but being friends during the time.

I extend thanks to Prof. Dr. Gabriel Pantellias who helped to get my expertise in cytogenetics especially in G1 PCC technique. At the last phase of my PhD, his significant help gave me a good finishing of my work. Much kudos to you!

I am grateful to the University hospital Essen and University of Duisburg-Essen for providing me the opportunity to perform my work. Moreover, I would also like to thank DFG funded Graduate school; GRK1739 to permit me to be an associated member for my dissertation.
Lastly, I want to express my cordial love to my beloved parents and to all my family members for their support by being distantly located.

Last but not least, the scientific work presented in this doctoral thesis was funded and supported by Bundesministerium für Bildung und Forschung BMBF [02NUK043B-COLLAR] and the DFG [GRK1739] and I am indebted to them for their financial assistance for this project. Finally I, without doubt, thank each and every one of you who helped me in every bit to come where I am today.

Sharif Mortoga

"The curriculum vitae is not included in the online version for data protection reasons."

"The curriculum vitae is not included in the online version for data protection reasons."

XII Publications

1. SCF^{SKP2} regulates APC/C^{CDH1}-mediated degradation of CtIP to adjust DNA-end resection in G2-phase. Fanghua Li, Emil Mladenov, **Sharif Mortoga**, George Iliakis. ***Cell Death Dis. 2020 Jul.*** PMID: 32683422.
2. Defined Biological Models of High LET Radiation Lesions. Iliakis G, Mladenova V, **Sharif Mortoga,** Chaudhary S, Mavragani IV, Soni A, Saha J, Schipler A, Mladenov E. ***Radiat Prot Dosimetry. 2019 May.*** PMID: 30566664.
3. Inhibition of Parp1 by BMN673 effectively sensitizes cells to radiotherapy by upsetting the balance of repair pathways processing DNA double-strand breaks. Soni A, Li F, Wang Y, Grabos M, Krieger LM, Chaudhary S, **Hasan Mohammad Sharif Mortoga**, Ahmed M, Coleman CN, Teicher BA, Piekarz RL, Wang D, Iliakis GE. ***Mol Cancer Ther. 2018 Oct.*** PMID: 29970481.

XIII Declaration

Erklärung:

Hiermit erkläre ich, gem. § 6 Abs. (2) g) der Promotionsordnung der Fakultät für Biologie zur Erlangung der Dr. *rer. nat.*, dass ich das Arbeitsgebiet, dem das Thema „***Regulated systems of I-SceI expression for in-depth studies of the biological effects of DSBs and DSB clusters***“ zuzuordnen ist, in Forschung und Lehre vertrete und den Antrag von Herr **Mohammad Sharif Mortoga Hasan** befürworte und die Betreuung auch im Falle eines Weggangs, wenn nicht wichtige Gründe dem entgegenstehen, weiterführen werde.

Essen, den _____ _____

Unterschrift eines Mitglieds der Universität Duisburg-Essen

Erklärung:

Hiermit erkläre ich, gem. § 7 Abs. (2) d) + f) der Promotionsordnung der Fakultät für Biologie zur Erlangung des Dr. *rer. nat.*, dass ich die vorliegende Dissertation selbständig verfasst und mich keiner anderen als der angegebenen Hilfsmittel bedient, bei der Abfassung der Dissertation nur die angegeben Hilfsmittel benutzt und alle wörtlich oder inhaltlich übernommenen Stellen als solche gekennzeichnet habe.

Essen, den _____ _____

Unterschrift des Doktoranden

Erklärung:

Hiermit erkläre ich, gem. § 7 Abs. (2) e) + g) der Promotionsordnung der Fakultät für Biologie zur Erlangung des Dr. *rer. nat.*, dass ich keine anderen Promotionen bzw. Promotionsversuche in der Vergangenheit durchgeführt habe und dass diese Arbeit von keiner anderen Fakultät/Fachbereich abgelehnt worden ist.

Essen, den _____ _____

Unterschrift des Doktoranden